FEDERAL UNIVERSITY OF MINAS GERAIS
School of Engineering
Graduate Program in Mechanical Engineering

Osvaldo Manuel Nuñez Bosch

THERMODYNAMIC AND ECONOMIC ASSESSMENT OF CRYOGENIC ENERGY STORAGE (CES) SYSTEMS OPERATING IN COGENERATION REGIME

Belo Horizonte
2021

Osvaldo Manuel Nuñez Bosch

THERMODYNAMIC AND ECONOMIC ASSESSMENT OF CRYOGENIC ENERGY STORAGE (CES) SYSTEMS OPERATING IN COGENERATION REGIME

Final Version

Doctoral thesis presented to the Graduate Program in Mechanical Engineering from the Federal University of Minas Gerais as a partial requirement for obtaining the title of Doctor in Mechanical Engineering.

Advisor: Prof. Dr. Matheus Pereira Porto

Belo Horizonte
2021

Nuñez Bosch, Osvaldo Manuel.
N972t Thermodynamic and economic assessment of cryogenic energy storage (CES) systems operating in cogeneration regime [recurso eletrônico] / Osvaldo Manuel Nuñez Bosch. - 2021.
1 recurso online (179 f. : il., color.) : pdf.

Orientador: Matheus Pereira Porto.

Tese (doutorado) - Universidade Federal de Minas Gerais, Escola de Engenharia.

Apêndices: f. 166-179.

Bibliografia: f. 146-165.
Exigências do sistema: Adobe Acrobat Reader.

1. Engenharia mecânica - Teses. 2. Energia - Armazenamento - Teses. 3. Energia elétrica e calor - Cogeração - Teses. 4. Exergia - Teses. I. Porto, Matheus Pereira. II. Universidade Federal de Minas Gerais. Escola de Engenharia. III. Título.

CDU: 621(043)

Ficha catalográfica elaborada pelo bibliotecário Reginaldo Cesar Vital dos Santos CRB/6 2165
Biblioteca Prof. Mário Werneck, Escola de Engenharia da UFMG

UNIVERSIDADE FEDERAL DE MINAS GERAIS
ESCOLA DE ENGENHARIA
PROGRAMA DE PÓS-GRADUAÇÃO EM ENGENHARIA MECÂNICA

FOLHA DE APROVAÇÃO

AVALIAÇÃO TERMODINÂMICA E ECONÔMICA DE SISTEMAS DE ARMAZENAMENTO DE ENERGIA CRIOGÊNICA (CES) OPERANDO EM REGIME DE COGERAÇÃO

OSVALDO MANUEL NUÑEZ BOSCH

Tese submetida à Banca Examinadora designada pelo Colegiado do Programa de Pós-Graduação em Engenharia Mecânica da Universidade Federal de Minas Gerais, constituída pelos Professores: Dr. Matheus Pereira Porto (Orientador - Departamento de Engenharia Mecânica/UFMG), Dr. Paulo Alexandre Costa Rocha (Universidade Federal do Ceará/UFC), Dr. Felipe Raul Ponce Arrieta (Pontifícia Universidade Católica de Minas Gerais/PUC-Minas), Dr. Paulo Vinicius Trevizoli (Departamento de Engenharia Mecânica/UFMG) e Dr. Rafael Augusto Magalhães Ferreira (Departamento de Engenharia Mecânica/UFMG), como parte dos requisitos necessários à obtenção do título de **"Doutor em Engenharia Mecânica"**, na área de concentração de "Energia e Sustentabilidade**".**

Tese aprovada no dia 10 de setembro de 2021.

Documento assinado eletronicamente por **Matheus Pereira Porto**, **Servidor(a)**, em 17/09/2021, às 08:59, conforme horário oficial de Brasília, com fundamento no art. 5º do Decreto nº 10.543, de 13 de novembro de 2020.

Documento assinado eletronicamente por **Paulo Alexandre Costa Rocha**, **Usuário Externo**, em 17/09/2021, às 10:29, conforme horário oficial de Brasília, com fundamento no art. 5º do Decreto nº 10.543, de 13 de novembro de 2020.

Documento assinado eletronicamente por **Rafael Augusto Magalhães Ferreira**, **Professor do Magistério Superior**, em 17/09/2021, às 14:39, conforme horário oficial de Brasília, com fundamento no art. 5º do Decreto nº 10.543, de 13 de novembro de 2020.

Documento assinado eletronicamente por **Felipe Raul Ponce Arieta**, **Usuário Externo**, em 17/09/2021, às 14:55, conforme horário oficial de Brasília, com fundamento no art. 5º do Decreto nº 10.543, de 13 de novembro de 2020.

Documento assinado eletronicamente por **Paulo Vinicius Trevizoli**, **Professor do Magistério Superior**, em 19/09/2021, às 13:56, conforme horário oficial de Brasília, com fundamento no art. 5º do Decreto nº 10.543, de 13 de novembro de 2020.

A autenticidade deste documento pode ser conferida no site https://sei.ufmg.br/sei/controlador_externo.php?acao=documento_conferir&id_orgao_acesso_externo=0, informando o código verificador **0964388** e o código CRC **83A0E31B**.

Referência: Processo nº 23072.248531/2021-76 SEI nº 0964388

Acknowledgements

Education is a powerful tool that helps us grow up, develop, and create a better society in harmony with nature and human beings. My education started at home and later deeply strengthened at school by consecrated educators. Furthermore, during the last few years, I have had the great fortune to know new persons, to whom I am sincerely thankful for helping me to keep going in my academic preparation.

First of all, I would like to dedicate this thesis to the memory of my dear mother Noelia Erlinda Bosch Centeno, who taught me through her personal example the importance and relevance of the study, moral values, and commitment to noble causes.

I would like to express my profound gratitude to Renata Siviero Martins, my wife, who encouraged me to continue with the graduate studies. Thanks for all the support, complicity, love, and understanding.

I am very grateful to my dear friend, Prof. Carlucia for her valuable support, remarkable encouragement at every stage of this research, generosity, and for being there with us.

A special thanks to Prof. Sãozinha and Prof. Antônio Julio for their selfless help and devotion to education.

I acknowledge, with appreciation, the guidance given to me by my thesis advisor, Prof. Matheus Pereira Porto.

I am very thankful to my dear friends Bianca, Marcio, Patricia, Eliete, Icaro and Marcelo for all the afforded support and permanent interest on my studies.

My appreciation also extends to Dr. Gilvander for all of his valuable support and commitment.

I wish to express my profound gratitude to Prof. Jorge Posada, who rendered important support and significant incentive to enroll in graduate studies.

My sincere thanks also go to Maria Cristina and Prof. José for their invaluable help and for taking care of my mental and physical health.

I would like also to acknowledge Maria do Rosario for her remarkable help and time dedicated to legal advice.

I wish to express my gratitude and deep appreciation to Deusmar for her prayers and generosity. Thanks for every good morning, sense of humor, and expressions of friendship.

I gratefully acknowledge Juciane, my sister-in-law, for her permanent interest and good thoughts on my research.

I express my deep gratitude to Prof. Gustavo E. Fernandez Salva for his moral support and permanent interest in my studies.

Thank you to Prof. Fábio for his encouragement and solidarity rendered to me in the last part of this work.

My profound gratitude to Fran and Hugo for their kindness, generosity, and friendship. I would also like to convey my thanks to the staff of graduate studies of the Mechanical Engineering Department from the Federal University of Minas Gerais for providing me invaluable assistance on my preparation.
Special thanks to the Cuban educational system and all the educators who have contributed with my education and for providing me the scientific and educational bases to face this research.
I would like to acknowledge CAPES for the four years of financial support given to me to develop this study.
I am also thankful to all my colleagues from the labTerm laboratory.
Thanks to my family, my dear sisters Idania, Isis and Xiomara, for their unconditional support, encouragement, and understanding. I also pay tribute to the memory of my dear sister Tatiana who was an inspiration and support for a long time. A big thank to my nephews Harold, Henry and Chapo for maintaining the communication and wishing me success in my studies.
Finally, I would like to thank my daughter Laura, my sons Obed and Alejandro for their understanding and for bringing happiness to me.

"Culture, which makes talent shine, is not completely ours either, nor can we place it solely at our disposal. Rather, it belongs mainly to our country, which gave it to us, and to humanity, from which we receive it as a birthright."
(José Julián Martí Pérez (28 January 1853 – 19 May 1895))

Resumo

O sistema de armazenamento de energia criogênica (CES) é uma tecnologia emergente que pode melhorar a estabilidade da rede elétrica respondendo aos desequilíbrios na produção e no consumo de energia elétrica e, consequentemente, contribuir para aumentar a participação de fontes de energia renováveis intermitentes conectadas à rede. Além disso, os sistemas CES podem ser integrados à indústria, usinas de energia e setores de serviços, fornecendo capacidade e energia após uma falha do sistema (blackout). No entanto, a eficiência do ciclo CES, sua integração e os modos de operação dos processos de carga e descarga requerem investigações adicionais.

Esta pesquisa visa aprimorar o desempenho da tecnologia CES por meio da operação simultânea dos processos de carga e descarga, explorando seu potencial de co-geração e adotando algumas modificações no layout do ciclo para aumentar a produção de energia. Além disso, a tese propõe uma metodologia sistemática para projeto e avaliação de sistemas CES. É demonstrada a superioridade da modificação conceitual referente à simultaneidade dos processos de armazenamento e descarga em relação a tecnologias semelhantes. Para isso, três alternativas principais com diferentes modos de operação são projetadas, simuladas e avaliadas usando critérios termodinâmicos e econômicos. Primeiramente, uma análise termodinâmica e um modelo matemático detalhado baseado em balanços de massa, energia e exergia são desenvolvidos. Além disso, os principais métodos econômicos, como valor presente líquido (VPL), taxa interna de retorno (TIR), período de retorno (PBP), relação benefício-custo (B/C) e custos nivelados são avaliados. Um procedimento de otimização e uma análise de sensibilidade utilizando o software Engineering Equation Solver (EES) são realizados para investigar a influência de alguns parâmetros nos principais índices e indicadores.

Com base nas premissas estabelecidas, verifica-se que a operação simultânea dos processos de carga e descarga e a modificação do layout do sistema CES produzem uma redução no consumo de energia durante o processo de armazenamento de 19,9 % e um aumento na produção de energia de 59,6 % durante o processo de descarregamento, levando a uma melhoria significativa da eficiência de ida e volta em comparação com o caso base. Para o calor residual disponível a 600 K, uma pressão da bomba de saída de 20 MPa e uma capacidade do tanque criogênico de 200 t, a eficiência de ciclo completo atinge entre 38,5 e 46,8 %. Os resultados também mostraram que o rendimento líquido específico encontrado é de 0,412 kg_L/kg_a, resultando em 39,3 % maior do que na investigação anterior em que este estudo se baseia. As análises termodinâmicas e a otimização mostram que a densidade de exergia e o fator de utilização de exergia no regime de descarga são determinados como 133,5 kWh/m^3 e 89,2 %, respectivamente. A densidade exergética é comparativamente maior do que a de outras tecnologias, como armazenamento de energia hidroelétrica

bombeada (PHES) e armazenamento de energia por ar comprimido (CAES). A análise econômica sugere que o sistema CES de cogeração é altamente competitivo com outras tecnologias de armazenamento. O custo de investimento específico do sistema CES ótimo resultou de 1301,4 a 782,3 $\$US/kW$ e o período de retorno variou entre 20,9 e 15,2 anos, dependendo da escala do sistema CES. Por fim, o estudo revela que a rentabilidade do sistema CES de cogeração é altamente sensível à temperatura do calor residual, ou seja, quanto maior a temperatura de reaquecimento, maior o valor presente líquido.

Palavras-chaves: armazenamento de energia criogênica, cogeração, exergia, ciclo de Claude, análise econômica.

Abstract

Cryogenic energy storage (CES) system is an emerging technology that can improve the stability of the power grid by responding to imbalances in electrical energy production and consumption, and consequently, contribute to enhancing the participation of grid-connected intermittent renewable energy sources. Additionally, CES systems can be integrated into the industry, power plants and service sectors, providing capacity and energy after a system failure (blackout). Nevertheless, the CES cycle efficiency, its integration and the operation modes of charging and discharging processes require further investigations.

This research aims to enhance the performance of the CES technology through the simultaneous operation of the charging and discharging processes, exploring its potential for cogeneration and adopting some modifications in the cycle layout to increase energy production. Moreover, the thesis proposes a systematic methodology for CES systems design and evaluation. The superiority of the conceptual modification referred to the simultaneity of storage and discharge processes with respect to similar technologies is demonstrated. For this, three main alternatives with different operation modes are designed, simulated and evaluated using both thermodynamic and economic criteria. First of all, a thermodynamic analysis and a detailed mathematical model based on mass, energy and exergy balances are developed. Additionally, the main economic methods, such as net present value (NPV), internal rate of return (IRR), payback period (PBP), benefit cost ratio (B/C) and levelized costs are assessed. An optimization procedure and a sensitivity analysis using the Engineering Equation Solver (EES) software are conducted in order to investigate the influence of some parameters on the main indexes and indicators.

Based on the established assumptions, it is found that the simultaneous operation of the charging and discharging processes and the layout modification of the CES system produce a reduction in power consumption during the storage process of 19.9 % and an increase in the power production of 59.6 % during the discharging process, leading to a significant improvement of the round-trip efficiency compared to the base case. For waste heat available at 600 K, an outlet pump pressure of 20 MPa and a cryogenic tank capacity of 200 t, the round-trip efficiency attains to be between 38.5 and 46.8 %. The results also showed that specific liquid air yield is found to be 0.412 kg_L/kg_a, resulting in 39.3 % higher than that of the previous investigation this study is based on. Thermodynamic analyses and optimization show that the exergy density and exergy utilization factor in discharging regime are determined as 133.5 kWh/m^3 and 89.2 %, respectively. The exergy density is comparatively higher than that of other technologies, such as pumped hydroelectric energy storage (PHES) and compressed air energy storage (CAES). The economic analysis suggests that the cogeneration CES system is highly competitive with others storage technologies. The specific investment cost of the optimal CES system resulted from 1301.4

to 782.3 $\$US/kW$ and the payback period ranged from 20.9 to 15.2 years, depending on the CES system scale. Finally, the study reveals that the profitability of the cogeneration CES system is highly sensitive to the waste heat temperature, that is, the higher the reheat temperature, the greater the net present value.

Key-words: cryogenic energy storage, cogeneration, exergy, Claude cycle, economic analysis.

List of Figures

Figure 1.1 – Prediction of the evolution of total power generation around the world [1]. 27
Figure 1.2 – Wind and solar renewable energy sources penetration across all regions [2]. 28
Figure 1.3 – Mode of operation of a cryogenic energy storage system [3]. 29
Figure 1.4 – Representation of the power rating and discharge time of current energy storage technologies [4]. 31
Figure 2.1 – Cryogenic energy storage development over time. Adapted from [5]. . . 35
Figure 2.2 – Temperature and entropy diagram for nitrogen [6]. 36
Figure 2.3 – Pressure and enthalpy diagram for nitrogen [6]. 36
Figure 2.4 – (a) A simple Linde–Hampson high pressure and (b) T–s diagram liquefaction system. Adapted from [7]. 40
Figure 2.5 – (a) A precooled Linde–Hampson high pressure liquefaction system, and (b) T–s diagram. Adapted from [7]. 41
Figure 2.6 – (a) A Claude low-pressure process cycle using an expansion machine and (b) T–s diagram. Adapted from [7]. 42
Figure 2.7 – (a) A Collins process liquefaction cycle using two expansion machines and (b) its representation on the T–s diagram.Adapted from [8]. 43
Figure 2.8 – (a) A Kapitza process liquefaction cycle and (b) T–s diagram. 44
Figure 2.9 – (a) A Heylandt process liquefaction cycle and (b) its representation on the T–s diagram. 45
Figure 3.1 – Schematic of a conventional stand-alone CES system with heat and cold storage. 64
Figure 3.2 – Schematic of the modified Claude liquefaction cycle studied in [9] . . . 64
Figure 3.3 – Proposed CES system. The system is divided in liquefaction, cooling and power circuits. During discharging regime, section 19 to 21 is bypassed (HE-1 and HE-2 are not used) 65
Figure 3.4 – Schematic of the modified Claude liquefaction cycle for cogeneration regime with a hydraulic expansion turbine (operation mode A) 67
Figure 3.5 – Schematic of the proposed CES system with a hydraulic cryogenic turbine (operation mode B and C) 68
Figure 3.6 – Temperature and entropy diagram of the Claude cycle during charging regime 68
Figure 3.7 – Temperature and entropy diagram of the Claude cycle during discharging regime 69
Figure 3.8 – Temperature and entropy diagram of the Claude cycle during charging regime with a hydraulic cryogenic turbine 69

Figure 3.9 – Flow chart of the general methodology for cogeneration CES cycle analysis. 71
Figure 3.10–Flow chart pattern of the applied general mathematical model for the CES systems. 72
Figure 3.11–Flow chart layout for the iterative method applied for heat exchangers modeling. 74
Figure 3.12–Discretization diagram for heat exchanger modeling. 75
Figure 3.13–Cryogenic tank during (a) charging and (b) discharging regimes. Adapted from [10]. 78
Figure 3.14–Procedure of the optimization algorithm. 93
Figure 3.15–Frequency histogram and probability function for the electricity tariff on peak time (Dollar trading on March, 22nd 2021. $\$USD$ 1.00 = $R\$$ 5.53). 99
Figure 3.16–Frequency histogram and probability function for the electricity tariff in off-peak time (Dollar trading on March, 22nd 2021. $\$USD$ 1.00 = $R\$$ 5.53).100
Figure 4.1 – Variation of the specific exergy consumption with diverted air mass fraction for $\varepsilon = 0.8$. 102
Figure 4.2 – Effect of diverted air mass fraction 103
Figure 4.3 – Effect of diverted air mass fraction and effectiveness of the heat exchangers on specific liquid yield during charging regime for operation modes B and C. 104
Figure 4.4 – Influence of compressor pressure and effectiveness of the heat exchangers on specific liquid yield during charging regime for α=0.60 (Fig. 3.3). . . 105
Figure 4.5 – Dependence of the charging time respect to compressor pressure and effectiveness of the heat exchangers, for $\dot{m}_c$=18.0 kg/s, α=0.60 and C_t=50 t (Fig. 3.3). 105
Figure 4.6 – Effect of compressor pressure and effectiveness of the heat exchangers on exergy efficiency during charging process, for $\dot{m}_c$=6.0 kg/s, α=0.60 and P_p=20.0 MPa (Fig. 3.3). 106
Figure 4.7 – Effect of compressor pressure and effectiveness of the heat exchangers on exergy efficiency for operation modes B and C during charging process, for $\dot{m}_c$=6.0 kg/s, α=0.60 and P_p=20.0 MPa. 106
Figure 4.8 – Influence of pump pressure and inlet turbine temperature on exergy efficiency during discharging process, with compressor pressure of 5.0 MPa, α=0.60 and ε=0.95. 107
Figure 4.9 – Dependence of the exergy efficiency respect to air mass flow rate and effectiveness of the heat exchangers during charging process (Fig. 3.3). 108
Figure 4.10–Influence of the air mass flow rate and effectiveness of the heat exchangers on exergy efficiency during charging process for operation modes B and C (Fig. 3.5). 108

Figure 4.11–Exergy destruction distribution for charging process, following the thermodynamic states given in Table A.1. 109
Figure 4.12–Exergy destruction distribution for discharging process, following the thermodynamic states given in Table A.2. 109
Figure 4.13–Exergy destruction distribution for charging process. 110
Figure 4.14–Exergy destruction distribution for discharging process. 110
Figure 4.15–Effect of diverted air mass fraction and effectiveness of the heat exchangers on specific exergy consumption during charging regime (Fig. 3.3). . 112
Figure 4.16–Influence of compressor pressure and effectiveness of the heat exchangers on specific exergy consumption during charging regime (Fig. 3.3). . . . 113
Figure 4.17–Effect of air mass flow rate and effectiveness of the heat exchangers on specific exergy consumption during charging regime (Fig. 3.3). 113
Figure 4.18–Dependence of the net specific exergy consumption and liquid yield respect to effectiveness of the heat exchangers and compressor pressure (Fig. 3.3). 114
Figure 4.19–Influence of compressor pressure and effectiveness of the heat exchangers on specific exergy consumption during charging regime, for α=0.6. . . . 115
Figure 4.20–Enlargement of the region for the overlapped curves in graph 4.19. . . . 115
Figure 4.21–Influence of pump pressure and turbine inlet temperature on exergy density during discharging process (Fig. 3.3). 116
Figure 4.22–Influence of pump outlet pressure and turbine inlet temperature on exergy density during discharging process for operation modes A and C. 117
Figure 4.23–Exergy efficiency and exergy stored at the cryogenic tank vs charging time. 117
Figure 4.24–Exergy efficiency and exergy stored at the cryogenic tank vs discharging time. 118
Figure 4.25–Round-trip efficiency vs diverted air mass fraction and turbine inlet reheat temperature (Fig. 3.3). 118
Figure 4.26–Influence of compressor pressure and turbine inlet reheat temperature on round-trip efficiency (Fig. 3.3). 119
Figure 4.27–Distribution of power, cooling and heat loads for operation mode A. . . 120
Figure 4.28–Distribution of power, cooling and heat loads for operation mode B. . . 120
Figure 4.29–Distribution of power, cooling and heat loads for operation mode C. . . 121
Figure 4.30–Effect of compressor pressure and effectiveness of the heat exchangers on exergy utilization factor during the charging regime (Fig. 3.3). . . . 121
Figure 4.31–Effect of compressor outlet pressure and effectiveness of the heat exchangers on exergy utilization factor during the charging regime (for operation modes B and C from Fig. 3.5). 122

Figure 4.32–Influence of air mass flow rate and effectiveness of the heat exchangers on exergy utilization factor during the charging regime (Fig. 3.3). . . . 122
Figure 4.33–Effect of pump pressure and turbine reheat inlet temperature on exergy utilization factor during the discharging process (Fig. 3.3). 123
Figure 4.34–Effect of pump discharge pressure and turbine inlet temperature on exergy utilization factor during the discharging process (operation modes A and C). 124
Figure 4.35–Effect of pump pressure and inlet turbine temperature on electrical and thermal efficiency for discharging regime (Fig. 3.3). 124
Figure 4.36–Influence of liquid air mass flow rate and turbine inlet temperature on electrical and thermal efficiency for discharging regime (Fig. 3.3). . . . 125
Figure 4.37–Round-trip efficiency vs diverted air mass fraction and reheat turbine inlet temperature for cogeneration regime (Fig. 3.3). 125
Figure 4.38–Influence of compressor pressure and turbine inlet temperature on round-trip efficiency for cogeneration regime (Fig. 3.3). 126
Figure 4.39–Effect of diverted air mass fraction and operation modes on round trip efficiency for cogeneration regime at 600 K of reheat temperature. . . . 126
Figure 4.40–Influence of compressor pressure and operation modes on round trip efficiency for cogeneration regime at 600 K of reheat temperature. . . . 127
Figure 4.41–Average annual revenue accounting for selling electricity and cooling load. 129
Figure 4.42–Average annual revenue accounting for selling electricity, liquid air and cooling load. 130
Figure 4.43–Effect of cryogenic tank capacity on NPV for every operation mode accounting for selling electricity and cooling load. 130
Figure 4.44–Variation of NPV with cryogenic tank capacity for every operation mode accounting for selling electricity, liquid air and cooling load. 131
Figure 4.45–Effect of interest rate on NPV for each operation mode accounting for selling electricity and cooling load. 131
Figure 4.46–Influence of reheat air temperature on NPV for every operation mode accounting for selling electricity and cooling load. 132
Figure 4.47–Variation of benefit to cost ratio (B/C) with reheat temperature for every operation mode accounting for selling electricity and cooling load. 132
Figure 4.48–Variation of payback period with cryogenic tank capacity for each operation mode accounting for selling electricity and cooling load. . . . 133
Figure 4.49–Levelized cost of liquid air and specific exergy consumption as a function of cryogenic tank capacity for every operation mode. 134
Figure 4.50–Influence of electricity tariff in off-peak time and round-trip efficiency on levelized cost of electricity storage for operation mode A ($i = 6$ % and $c_y = 4$ $cycles/day$). 136

Figure 4.51–Effect of electricity tariff in off-peak time and cogeneration round-trip efficiency on levelized cost of electricity and cooling for operation mode A ($i = 6$ % and $c_y = 4$ $cycles/day$). 136
Figure 4.52–Influence of electricity tariff in off-peak time and round-trip efficiency on levelized cost of electricity storage for operation mode B ($i = 6$ % and $c_y = 4$ $cycles/day$). 137
Figure 4.53–Effect of electricity tariff in off-peak time and cogeneration round-trip efficiency on levelized cost of electricity and cooling for operation mode B ($i = 6$ % and $c_y = 4$ $cycles/day$). 137
Figure 4.54–Influence of electricity tariff in off-peak time and round-trip efficiency on levelized cost of electricity storage for operation mode C ($i = 6$ % and $c_y = 4$ $cycles/day$). 138
Figure 4.55–Effect of electricity tariff in off-peak time and cogeneration round-trip efficiency on levelized cost of electricity and cooling for operation mode C ($i = 6$ % and $c_y = 4$ $cycles/day$). 138
Figure 4.56–Sensitivity analysis for the NPV varying the main parameters by ±50 % for operation mode C, accounting for selling electricity and cooling income. 139
Figure 4.57–Sensitivity analysis for the NPV varying the main parameters by ±50 % for operation mode C, accounting for selling electricity, liquid air and cooling income. 140

List of Tables

Table 2.1 – Properties of cryogenic fluids [11]. 37
Table 2.2 – Specific work of liquefaction for cryogenic fluids [7]. 37
Table 2.3 – Characteristics of stand-alone CES systems and main parameters. . . . 48
Table 2.4 – Characteristics of Hybrid CES systems and main parameters. 53
Table 2.5 – Summary of the main patents on CES systems from 1992 to 2021. . . . 62
Table 3.1 – Data and assumptions for thermodynamic analysis of the CES systems. 70
Table 3.2 – Data and assumptions for economic analysis of the CES systems. 70
Table 3.3 – Designation of exergy of Fuel ($\dot{E}_{xF}$) and exergy of Product ($\dot{E}_{xP}$) of the CES systems for charging regime. 88
Table 3.4 – Designation of exergy of Fuel ($\dot{E}_{xF}$) and exergy of Product ($\dot{E}_{xP}$) of the CES systems for discharging regime. 89
Table 3.5 – Capital cost equations of the CES system equipment, ($USD). 94
Table 3.6 – Main cost elements for the CES systems ($USD) [12]. 95
Table 4.1 – Comparison of the relative exergy destruction for different CES systems researches (%). 111
Table 4.2 – Optimization results for charging regime for different capacities of the cryogenic tank. 128
Table 4.3 – Optimization results for discharging regime for different capacities of the cryogenic tank. 128
Table 4.4 – Specific investment cost ($\$/kW$), IRR (%) and PBP (year) for different capacities of the cryogenic tank. 133
Table 4.5 – Indexes and indicators for the reference scenario. 139
Table A.1 – Thermodynamics properties and parameters for charging regime. 168
Table A.2 – Thermodynamics properties and parameters for discharging regime. . . 169
Table B.1 – Mass, energy and exergy balance equations for modeling and optimization. 171
Table C.1 – Exergy performance results for CES system components for charging regime. 173
Table C.2 – Exergy performance results for CES system components for discharging regime. 173
Table C.3 – Exergy performance results for CES system components in operating mode A for charging regime. 174
Table C.4 – Exergy performance results for CES system components in operating mode A for discharging regime. 174
Table C.5 – Exergy performance results for CES system components in operating mode B for charging regime. 175

Table C.6 – Exergy performance results for CES system components in operating mode B for discharging regime. 175
Table C.7 – Exergy performance results for CES system components in operating mode C for charging regime. 176
Table C.8 – Exergy performance results for CES system components in operating mode C for discharging regime. 176
Table D.1 – Optimization results for charging regime for different capacities of the cryogenic tank. 178
Table D.2 – Optimization results for discharging regime for different capacities of the cryogenic tank. 179

List of abbreviations and acronyms

ARC	Absorption Refrigeration Cycle
BOG	Board Boil-off gas
B/C	Benefit cost ratio
CAES	Compressed Air Energy Storage
CCCPP	Cryogenic Combined Cycle Power Plant
CEPCI	Chemical Engineering Plant Cost Index
CES	Cryogenic Energy Storage
CF	Cash flow
DC	Direct Cost
E_xUF	Exergy Utilization Factor
FCI	Fixed Capital Investment
HE	Heat Exchanger
IC	Indirect Cost
IRR	Internal Rate of Return
LAES	Liquid Air Energy Storage
LCOC	Livelized Cost of Cogeneration
LCOL	Livelized Cost of Liquid Air
LCOS	Livelized Cost of Storage
LNG	Liquefied Natural Gas
NPP	Nuclear Power Plant
NPV	Net Present Value
NTU	Number of Transfer Unit
OL	Other Outlays

ORC	Organic Rankine Cycle
PBP	Payback Period
PEC	Purchased Equipment Cost
PHES	Pumped Hydroelectric Energy Storage
SHTES	Sensible Heat Thermal Storage
SIR	Savings to Investment Ratio
SPP	Simple Payback Period
TCI	Total Capital Investment
TSOD	Thermal System Optimal Designer
VCRC	Vapor Compression Refrigeration Cycle

List of symbols

A	Heat transfer area $[m^2]$
C	Capacitance $[kW/K]$
C_T	Cryogenic tank capacity $[t]$
c_p	Specific heat at constant pressure $[kJ/kgK]$
d	Diameter $[m]$
E	Energy $[kWh]$ or electricity tariff $[\$/kWh]$
$\dot{E}$	Exergy rate $[kW]$
E_{xD}	Exergy destruction rate $[kW]$
e	Specific exergy $[kJ/kg]$
e_n	Specific exergy consumption $[kWh/kg_L]$
F_{BM}	Bare-module factor
F_M	Material factor
f_q	Quantity factor
g	Acceleration of gravity $[m/s^2]$
h	Specific enthalpy $[kJ/kg]$
I	Inflation rate [%] or cost index
i	Interest rate [%]
L	Length $[m]$
m	Mass $[kg]$
$\dot{m}$	Mass flow rate $[kg/s]$
N	Number of nodes or trays
n	Useful life of the technology $[years]$
P	Pressure $[MPa]$

$\dot{Q}$	Heat transfer rate $[kW]$
q	Specific heat transfer $[kJ/kg]$
r	Time ratio or Relative cost difference
S_v	Salvage value $[\$USD]$
s	Specific entropy $[kJ/kgK]$
T	Temperature $[K]$
t	Time $[h]$
U	Internal energy $[kJ/K]$ or Overall heat transfer coefficient $[kW/m^2K]$
u	Specific internal energy $[kJ/kg]$
v	Specific volume $[m^3/kg]$
v_i	Velocity $[m/s]$
$\dot{V}$	Volume displacement $[m^3/s]$
V_{st}	Storage volume $[m^3]$
$\dot{W}_C$	Compressor power $[kW]$
$\dot{W}_P$	Pump power $[kW]$
$\dot{W}_t$	Turbine power $[kW]$
x	Quality
y	Liquid yield $[kg_L/kg_a]$
y_k	Fraction of exergy destroyed
y^*	Overall fraction of exergy destroyed
Z	Capital cost of a component $[\$USD]$
Z_i	Height $[m]$
$\dot{Z}$	Capital cost rate $[\$/h]$

Greek symbols

α	Diverted air mass fraction
β	Exponent

γ	Dislodge factor
Δ	Change in parameter or difference
ε	Effectiveness of the heat exchangers
η_C	Compressor isentropic efficiency
η_P	Pump isentropic efficiency
η_T	Turbine isentropic efficiency
λ	Electric to thermal ratio
ρ	Density $[kg/m^3]$
τ	Charging or discharging time $[h]$

Subscripts and superscripts

0	Reference condition (environment)
1, 2, 3 ..	State points
a	Air or actual
act	Actual
C, c	Compressor
CI	Capital investment
ch	Charging
co	Crossover
cog	Cogeneration
cv	Control volume
D	Destruction or density
dis	Discharging
E	Evaporator
g	Gas or saturated vapor
H	Heater
in	Inlet

k	Element
L	Loss
L, l	Liquid
m	Mean or mutation
max	Maximum
min	Minimum
N	Net
rt	Round-trip
out	Outlet
OM	Operation and maintenance
P, p	Pump
$\dot{Q}_E$	Evaporator load
r	Reheat
T, t	Turbine or time
TO	Off-peak time
TP	Peak time
th	Thermal
w	Weighted

Contents

1 INTRODUCTION . . . 27
1.1 Research objectives. . . . 30
1.2 Contribution of the research. . . . 31
1.3 Thesis outline. . . . 32

2 LITERATURE REVIEW . . . 33
2.1 History of cryogenics. . . . 33
2.2 Thermodynamics properties of cryogenic fluids. . . . 35
2.3 Cycles for cryogenic energy storage. . . . 39
2.4 Hybrid CES technologies. . . . 49
2.5 Poly-generation CES systems. . . . 54
2.6 Economic assessment of the cryogenic energy storage systems. . . . 55
2.7 Summary of literature review. . . . 60

3 RESEARCH METHODS . . . 63
3.1 System description. . . . 63
3.2 Mathematical model and assumptions. . . . 69
3.3 Thermodynamic modeling. . . . 71
3.3.1 Heat exchangers. . . . 71
3.3.2 Evaporator model. . . . 76
3.3.3 Expansion valve model. . . . 78
3.3.4 Cryogenic tank. . . . 78
3.3.5 Liquid yield. . . . 80
3.3.6 Charging and discharging time. . . . 83
3.3.7 Power consumption. . . . 83
3.3.8 Power production. . . . 84
3.3.9 Exergy analysis. . . . 85
3.3.10 Cycle performance indexes and indicators. . . . 89
3.3.11 Cycle based on combined cooling and power. . . . 90
3.3.12 Multi-objective optimization procedure. . . . 91
3.4 Economic analysis. . . . 92
3.4.1 Capital investment. . . . 94
3.4.2 Cash flow or annual revenue. . . . 95
3.4.3 Net Present Value (NPV). . . . 96
3.4.4 Internal Rate of Return (IRR). . . . 97
3.4.5 Payback Period (PBP). . . . 97

3.4.6 Benefit to cost ratio (B/C). 97
3.4.7 Levelized costs of products. 97
3.4.8 Uncertainty analysis. 98

4 RESULTS AND DISCUSSION. 101
4.1 Mathematical model verification 101
4.2 Liquid yield and charging time. 102
4.3 Exergy analysis. 105
4.4 Sensitivity analysis of performance indexes and indicators. 111
4.5 Cogeneration. 119
4.6 Optimization results. 127
4.7 Results of economic analysis. 128

5 CONCLUSION, LIMITATIONS AND SUGGESTIONS FOR FURTHER RESEARCH 141
5.1 Conclusions. 141
5.2 Limitations of this research. 143
5.3 Suggestions for further research. 144

BIBLIOGRAPHY 146

APPENDIX 166

APPENDIX A – THERMODYNAMIC PROPERTIES. 167

APPENDIX B – SUMMARY OF MODELING EQUATIONS. . . . 170

APPENDIX C – EXERGY PERFORMANCE RESULTS FOR THE COMPONENTS. 172

APPENDIX D – OPTIMIZATION RESULTS. 177

1 Introduction

The concern about global warming due to greenhouse gases emissions caused by prolonged use of fossil fuels has led to the increasing application of renewable energy sources for electricity generation. As a result of this trend, fossil fuels demand is falling down around the world while renewable energy sources are experienced an annual growing rate of about 7 % [1]. Figure 1.1 shows the predicted evolution of the total power generation up to 2040. The combination of energy sources used for electricity generation will substantially shift over the coming years, with renewables increasing in importance. The main reduction of fossil fuel consumption will be experienced by oil and coal. Even so, coal will remain the largest primary source of power production in 2040, with a share of around 30 %. That is, the world energy consumption is moving to the use of clean, affordable and sustainable energy sources. For example, solar photovoltaic electricity production increased from 4 TWh to 554 TWh over a period of 13 years, that is, from 2005 to 2018, whereas in the same period, wind electricity production grew up from 104 TWh to 1273 TWh [13]. Brazil also experienced an increasing trend from 2017 to 2018, where photovoltaic and wind electricity generation increased from 0.8 GWh and 42.4 GWh to 3.5 GWh and 48.5 GWh, respectively [14].

Globally, among the renewable energy sources, wind and solar will experience a significant growth across all regions around the world, as illustrated in Fig. 1.2, which illustrates the penetration in the power grid of the installed capacity for solar and wind renewable energy sources in 2016 for different regions around the world and their previsions

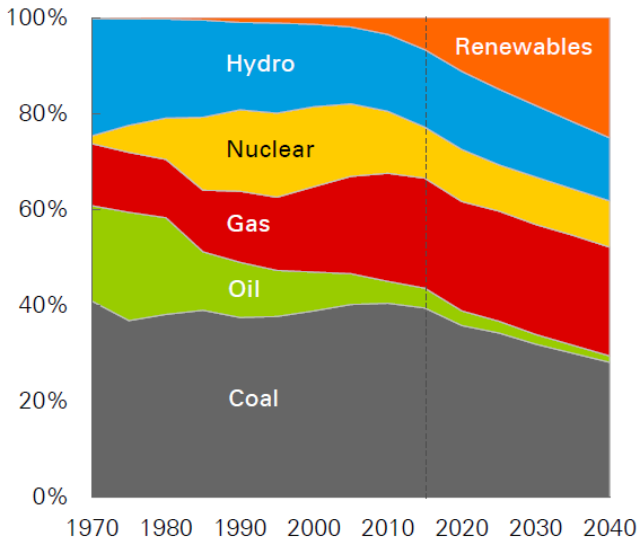

Figure 1.1 – Prediction of the evolution of total power generation around the world [1].

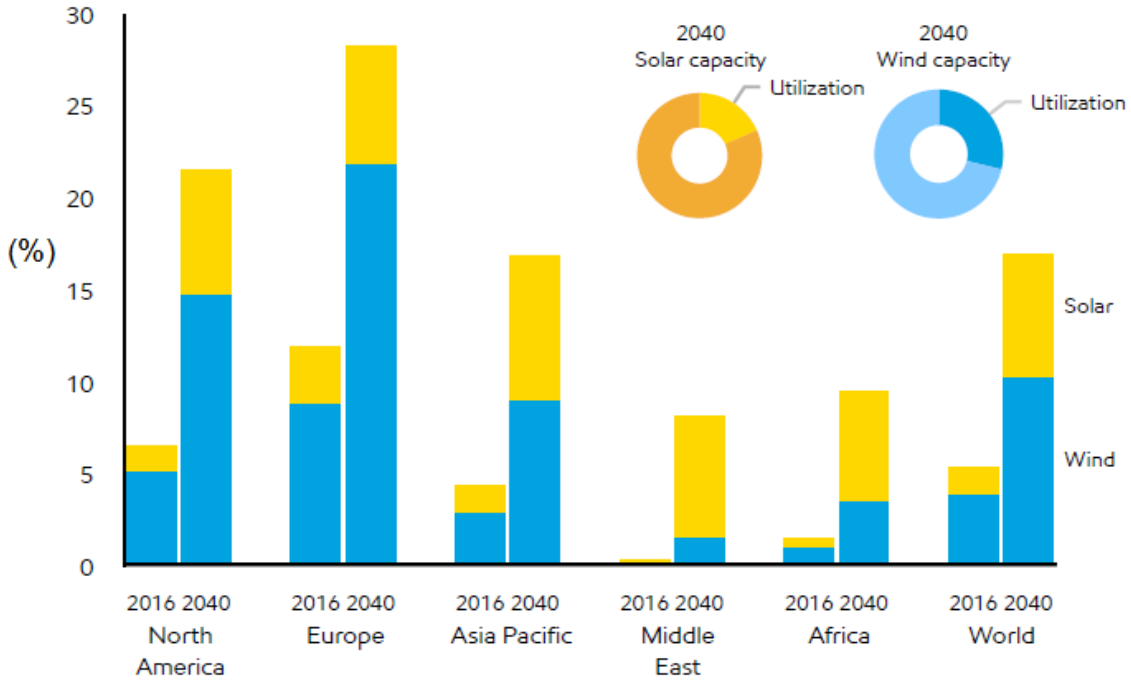

Figure 1.2 – Wind and solar renewable energy sources penetration across all regions [2].

for 2040. It is expected that more than 20 % of the electricity delivered in North America and Europe will come from wind and solar in 2040. Nevertheless, the increased penetration of renewable energy sources into the power network faces nowadays significant challenges. For instance, the natural intermittence of renewable energy sources causes severe difficulties to the electrical grid, increasing the challenge of balancing power supply and demand [15]. Moreover, when the penetration of the fluctuating renewables exceeds 20 %, the voltage and frequency stability of the power grid can be seriously affected without an available reserve capacity [16]. Forecasts suggest that intermittency will still limit the utilization to around 30 % for wind and 20 % for solar energy in 2040, as shown in Fig. 1.2.

The aforementioned issues can be addressed by Electrical Energy Storage (EES) technologies, which are recognized as valuable alternatives to improve the power grid flexibility. The EES systems absorb excess electricity generation when demand is very low [17, 18, 19].When power is needed, the stored energy is recovered by conventional power cycles, which contributes to reducing the use of fossil fuel generators and consequently the CO_2 emissions. Pumped hydroelectric energy storage (PHES) and compressed air energy storage (CAES) technologies are considered to be the most mature and widespread procedures for large-scale applications. The PHES technology accounts for more than 99% of the storage systems used worldwide [20], achieves specific cost of 600 - 2000 $\$US/kW$, operational life time of 40 - 60 years and its round-trip efficiency varies in practice between 65 - 87% [5]. However, PHES systems have geographical restrictions, low energy density of 0.5 - 1.5 kWh/m^3 and the environmental concern is a critical point. For instance, this

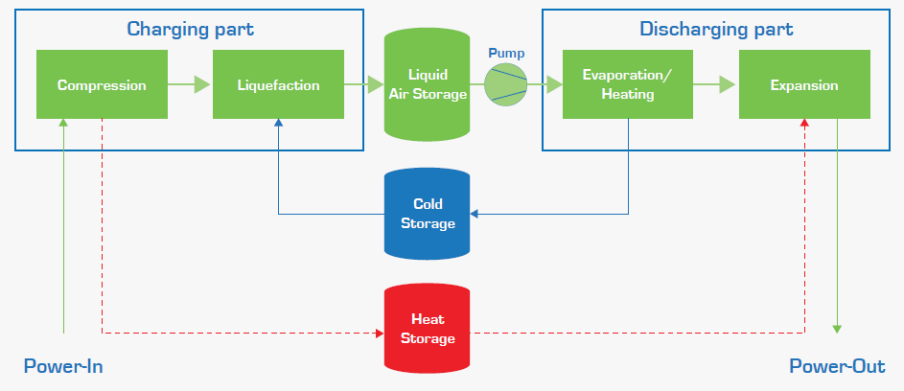

Figure 1.3 – Mode of operation of a cryogenic energy storage system [3].

technology requires large-scale water reservoirs, which have reached their limits in some developed countries [21]. In addition, for large-scale water reservoirs, the environmental impacts are significant in terms of soil, water quality and biodiversity. These impacts bring about socioeconomic issues, such as, displacement and loss of source of revenue for population living around the lock away area, prevalence of diseases in neighboring communities and loss of resources to support traditional ways of life [22]. Regarding to CAES system, it is the second most applied technology for energy storage in the world. There are currently two grid-scale CAES plants, in Alabama, a 110 MW plant and a 290 MW plant in Huntorf, Germany [23]. The main advantage of CAES systems is that they have acceptable capital cost (970 - 5000 $\$US/kW$), long operational lifetime (20 - 40 years), are based on well established technologies and their round-trip efficiency can reach between 38 - 60% [5]. However, CAES systems also have geographical restrictions, since they require large-scale underground caverns to storage the compressed air and low energy density of 3 - 20 kWh/m^3. In general, the storage technology required to overcome the challenges of the penetration of renewables into the power grid should present an integral solution in terms of technical, environmental and economic feasibility.

In this scenario, cryogenic energy storage (CES) systems can provide a suitable solution, acting as bulk electricity storage and back-up power generation. During off-peak, CES systems can be able to absorb and store in a cryogenic fluid excess renewables power when the grid demand is very low. The cryogenic liquid produced in the liquefaction process is stored in an insulated tank at low pressure, which performs as an energy store, as illustrated in Fig. 1.3. At peak times or when the power demand and electricity prices are high, cryogenic liquid is pumped to high pressure and converted in a high pressure gas through heat exchangers and supplied in expansion turbine to generate electricity, thus, fossil fuel generators can be displaced and CO_2 emissions reduced. Consequently, the use of CES systems can turn the intermittent renewables to be a dispatched and controlled power sources.

The CES systems do not use toxic materials like battery energy storage (BES) systems and can develop a power rate comparable with PHES and CAES technologies, as shown in Fig. 1.4, with the advantages of having no geographical restrictions and achieve high round trip efficiency when they are integrated to renewables and conventional power plants [24]. In addition, CES technology presents high energy density (120 - 200 kWh/m^3), most of the components are available in the market and it has long useful life (>30 years) [5]. All of these explain why CES power plants have received increasing attention from several researchers. However, none of these studies has brought up the simultaneous operation of the charging and discharging processes for CES systems operating in a cogeneration regime, and neither have they quantitatively evaluated the application of the first and second laws of thermodynamics of this simultaneous operation on the main indexes and indicators. Moreover, the economic analysis of CES systems, which is an important criterion for technology selection, is limited in the current literature and there are no detailed feasibility analyses. The current study, based on Abdo *et al.* [10] and [9], covers these knowledge gaps and addresses the aforementioned drawbacks of other technologies by proposing a novel cogeneration CES system with the simultaneous operation of the charging and discharging processes and using only air as working fluid. The main modifications incorporated into the proposed cogeneration CES system are summarized as follows: (i) it liquefies a minor amount of fluid during the power generation regime, and generates a minor amount of power during the liquefaction regime; (ii) it uses a multi-expansion turbine with re-heaters fed by an external source of energy [25, 26, 27]; (iii) it uses an expander split into two sections, employing the environment as a heat source before the second expansion.

1.1 Research objectives.

The present thesis investigates the thermodynamic and economic viability of a novel cogeneration CES system based on the Claude cycle. Then, the general objective aims to enhance the performance of the base case CES system proposed in [9] by employing cogeneration, a new layout architecture for power production and the simultaneous operation of the charging and discharging circuits using external sources of thermal energy.

The specific objectives of this research include:

1. To develop mathematical models to perform the thermodynamic and economic analyses of cogeneration CES systems in order to find out the influence of the main parameters on the indexes and indicators;

2. To verify the mathematical models throughout a systematic comparison of the performance characteristics of CES cycles with those stated in the literature;

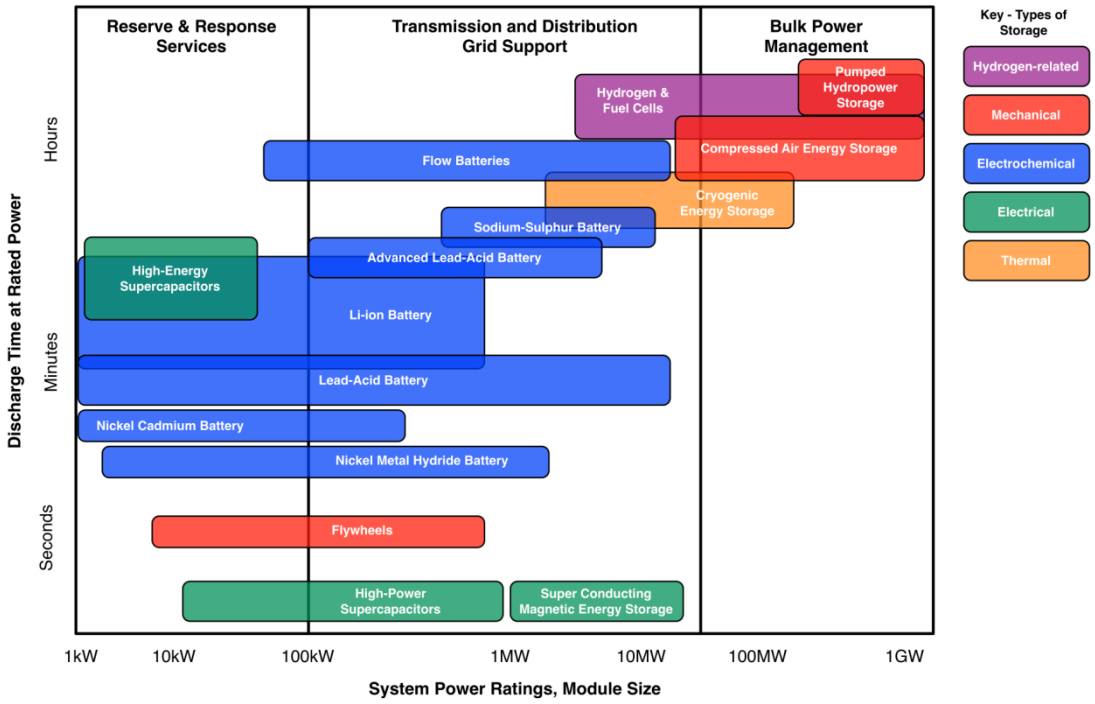

Figure 1.4 – Representation of the power rating and discharge time of current energy storage technologies [4].

3. To design, through thermodynamic principles, cryogenic energy storage systems that operate under a cogeneration regime in order to improve their performance;

4. To quantify the impact of the simultaneous operation of the charging and discharging processes and the new layout architecture for power generation on the thermodynamic performance of the cogeneration CES systems;

5. To evaluate the economic feasibility of the simultaneous operation of the charging and discharging processes of the cogeneration CES systems through sensitivity analysis of the main economic selection criteria, such as net present value (NPV), internal rate of return (IRR), benefit cost ratio (B/C) and payback period (PB).

1.2 Contribution of the research.

The most important contributions of this research can be summarized as follows:

1. The fundamental principles and thermodynamic characteristics of the simultaneous operation of the charging and discharging processes and its effect on the performance of cogeneration CES systems;

2. A systematic methodology based on thermodynamic and economic models, which will help in the understanding of the CES systems behavior and improve the accuracy of the results during the design, evaluation and selection of this storage technology;

3. Improved CES system performance through the use of the simultaneous operation of the charging and discharging processes, cogeneration, waste heat recovery and a different layout topology for power production employing only air as working fluid.

1.3 Thesis outline.

This thesis is structured in five chapters. Chapter one focuses on the background and motivation, the main objectives of the thesis, the contribution of the research and the structure of the whole thesis.

Chapter two reviews the most important technologies related to CES systems. The history of cryogenics is briefly reviewed, presenting the technology evolution up to nowadays. After that, the basic concepts of cryogenic, advantages and applications are presented. A number of scientific researches concerning of hybrid CES systems, cryogenic cycles, poly-generation in CES technology and economic feasibility analysis are discussed. Finally, a summary of the chapter is given. The literature review aims to uncover the research gaps and opportunities to improve the CES systems performance.

Chapter three provides the thermodynamic and economic methodology to model the CES cycles. The considered CES systems topologies are presented, the design modifications, the cogeneration proposal and the simultaneous operation of the charging and discharging processes are justified, the main assumptions adopted for simulation are introduced and a general procedure combining exergy analysis, genetic algorithms optimization and uncertainty assessment is proposed. The aim of this chapter is to develop thermodynamic and economic models in order to investigate the CES systems performance by parametric studies.

Chapter four analyses the enhancement of the CES systems performance and establishes comparison between their operation modes from thermodynamic and economic point of views. The main results from the analysis of CES systems performance, the sensitivity of the indexes and indicators, the optimization outcomes and the verification of the mathematical model are discussed. This chapter aims to find out the impact of the simultaneous operation of the charging and discharging processes and the design modifications on the performance of the CES systems.

Chapter five summaries the key conclusions of the research work and the most important achievements, as well as the main limitations. Recommendations for future investigations are also provided.

2 Literature review

The literature review of cryogenic energy storage systems is focused on a brief history about the emergence and development of cryogenic science, remarking the successes for the liquefaction of cryogenic fluids by the most relevant scientists involved in this area of knowledge. In addition, the development of CES technology is also presented. As an important element to assess the design and operation of CES systems, the thermodynamic properties of cryogenic fluids are approached. This chapter also highlights the main types of stand-alone CES cycles. The efforts of some researchers to raise the overall efficiency of CES systems by their integration with renewable energy sources and conventional power plants is presented. Next, some relevant investigations about the polygeneration of CES systems are analyzed. For the introduction of any technology to the global market must be proved its economic viability, that is why the economic assessment to CES systems is additionally examined. Finally, the most remarkable contributions and gaps in the current knowledge about the enhancement of cryogenic energy storage technologies are summarized.

2.1 History of cryogenics.

Cryogenics is the science and technology concerned with the low temperature processes and techniques. The word comes from the Greek word "kryo" meaning "cold" and "genic" meaning "to produce or generate" [11, 7]. The term "cryogenic" was first used in 1894, in a paper titled “On the cryogenic laboratory at Leiden and on the production of very low temperatures” [28]. It was in 1950s when engineers and scientists at the National Bureau of Standards (NIST) suggested to establish the field of cryogenics at temperature below 123 K (–150 °C). This temperature was selected because the domestic refrigerants boil at temperature above 123 K [29].

Among others, permanent gases, such as oxygen, nitrogen, hydrogen, and helium are used as cryogenic fluids, so they become liquid at temperature below 123 K [7, 29]. For many years scientists from different countries tried to liquefy air and others permanent gases, but it was in 1877 that Louis Cailletet in France and Raoul Pictet in Switzerland were successful in producing liquid air [28]. In 1895 air was liquefied at industrial scale by Linde. He compressed air from 2 to 6 MPa and cooled to ambient temperature, then fed in to a counter flow heat exchanger and expanded using the Joule-Thomson effect, thereby lowering its temperature up to obtain the liquid air [30]. Then, in 1883, Simon von Wroblewski and K. Olszewski in Cracow, Poland, produced liquid oxygen [30].

Louis Cailletet in 1877 claimed to see hydrogen mist, and other scientist, Maunier,

confirmed him. Later, Cailletet admitted he had not seen any mist during the first test. The liquefaction of hydrogen was succeeded for the first time by Sir James Dewar in 1898, pressurizing gaseous hydrogen at 180 bar and pre-cooling it at 23 K with carbonic acid and liquid air, and expanded up to atmosphere, Dewar found the boiling point of hydrogen at 20 K and obtained 4 cc/min of liquid hydrogen flow rate [28]. Helium gas was the last element to be liquefy. It was first discovered in 1868 by Lockyer and Frankland, later found in earth mineral and finally in natural gas and air. The physicist Heike Kamerlingh Onnes liquefied helium in 1908, at a temperature of 4.2 K. To do this, helium gas was compressed to 40 bar, cooled in heat exchangers and throttle to ambient temperature, thereby being partially liquefied [30].

Liquefaction of gases can be produced by heat conduction and cooling by fast expansion (the Joule-Thomson effect). In conduction process, the gas to be liquefied is immersed in a cryogenic liquid or cooled by cryogenic refrigeration until condensation takes place, for this, a heat exchanger is used. The Joule-Thomson effect was discovered by William Thomson, Lord Kelvin, and James Prescott Joule in 1852 [30, 11, 7]. They found that when a gas is rapidly expanded, its temperature dramatically drops and certain amount of liquid is produced.

In 1977 the University of Newcastle (UK) proposed a liquid air energy storage (LAES) technology concept for peak shaving of electricity grids [24]. Subsequent development of the technology has been carried out by Mitsubishi Heavy Industries and Hitachi (Japan) and Highview Power Storage in collaboration with the University of Leeds (UK) [31, 32]. The first pilot plant around the world was built by Highview Storage and is at present located at the University of Birmingham, School of Chemical Engineering, UK. Chengdu Air Separation Corporation supplied the liquefaction unit. The pilot plant has a power rate of 350 kW with integration of waste heat at 60 °C. A 60 ton capacity cryogenic tank, which is able to store 2.5 MWh of energy. Meanwhile, the maximum liquid air production rate and specific liquefaction work are 1.44 t/h and 0.73 MWh/t respectively. All the components of the plant are commercially available, except the high grade cold thermal storage [31, 24]. In recent June 5, 2018, Highview Power officially launched the world's first grid-scale cryogenic energy storage (CES) plant. The 5 MW/15 MWh LAES plant is located close to Manchester, United Kingdom and has a lifespan of between 30 and 40 years. Furthermore, the plant that is able to deliver electricity to power about 5000 homes for three hours, will provide grid balancing, reserve and regulation services. According to Highview Power, world energy storage market is expected to grow by 2030 to a cumulative of 125 GW/305 GWh. The historical development of CES technology is illustrated in Fig. 2.1.

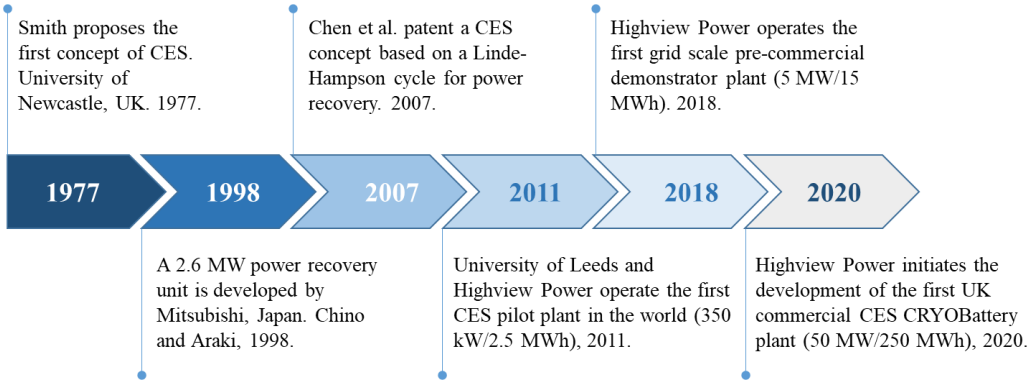

Figure 2.1 – Cryogenic energy storage development over time. Adapted from [5].

2.2 Thermodynamics properties of cryogenic fluids.

An accurate thermal analysis for CES systems could be well performed when the thermodynamic properties of the working fluids can be established. Thus, the design and evaluation performance of thermodynamic processes are thermal and transport properties dependent. A series of diagrams and tables (Figures 2.2 and 2.3) have been prepared over the years to represent the thermodynamic properties and facilitate the engineering calculation [33, 34, 35]. The diagrams involve the different relationship among properties, that is, temperature-entropy, pressure-temperature, pressure-enthalpy and others [36, 37, 38]. With the develop of computer programming, many engineering softwares have included in their database the thermodynamic and transport properties calculation. Engineering Equation Solver (EES) software is an example. For this research, the EES software (64-bit Academic professional license) is used to determine the working fluid properties for the real gas.

Air is composed by various gases, of which nitrogen (N_2) and oxygen (0_2) together account for approximately 99.03 % of the total sample volume. For practical purposes, it is considered, by mole fraction and excluding water vapor, as a mixture of 78.084 % N_2, 20.946 % 0_2, 0.934 % Ar, 0.033 % CO_2, and 0.003 % of other gases, such as Ne, He, Kr and Xe [39, 40]. Air has a boiling point of 78.78 K and 867.7 kg/m^3 as density, as shown in Table 2.1. Liquid air is principally used in the production of pure nitrogen, oxygen, and other gases for their application in the steel, petrochemical and metal industries where large amounts of oxygen and nitrogen are required. Lately, air is being studied as a working fluid in different cryogenic energy storage systems [41, 42, 10], that is, it has become a new energy vector for electricity production as atmosphere air is broadly available without limit for the energy storage power plants. Nitrogen is another important cryogenic fluid, it boils at 77.33 K, freezes at 63.22 K and in liquid state has a density of 800.9 kg/m^3, as illustrated in Table 2.1. This cryogenic fluid is produced by distillation of liquid air. It has wide range of application, it is used to provide an inert atmosphere in chemical and metallurgical processes, for magnet refrigeration, food and blood preservation, among

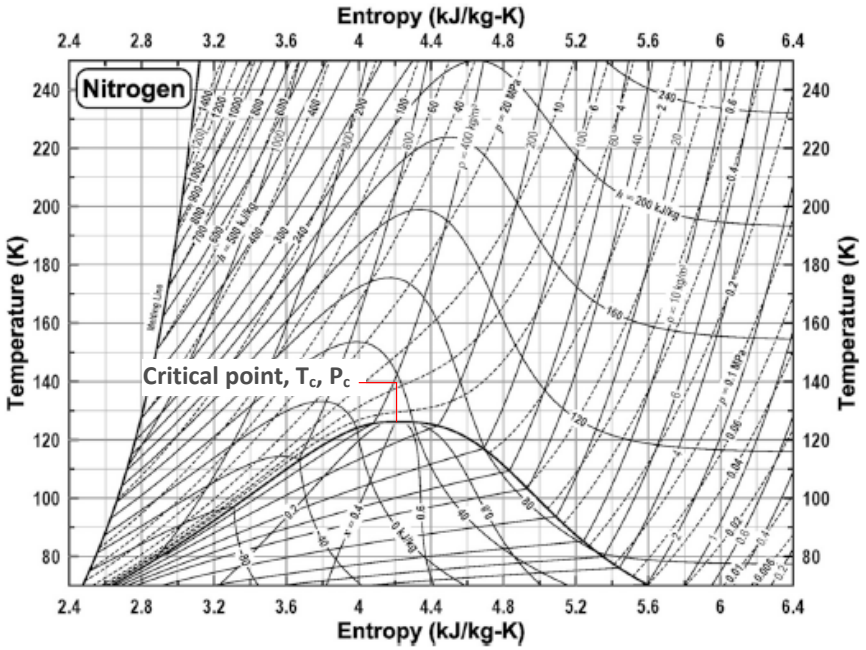

Figure 2.2 – Temperature and entropy diagram for nitrogen [6].

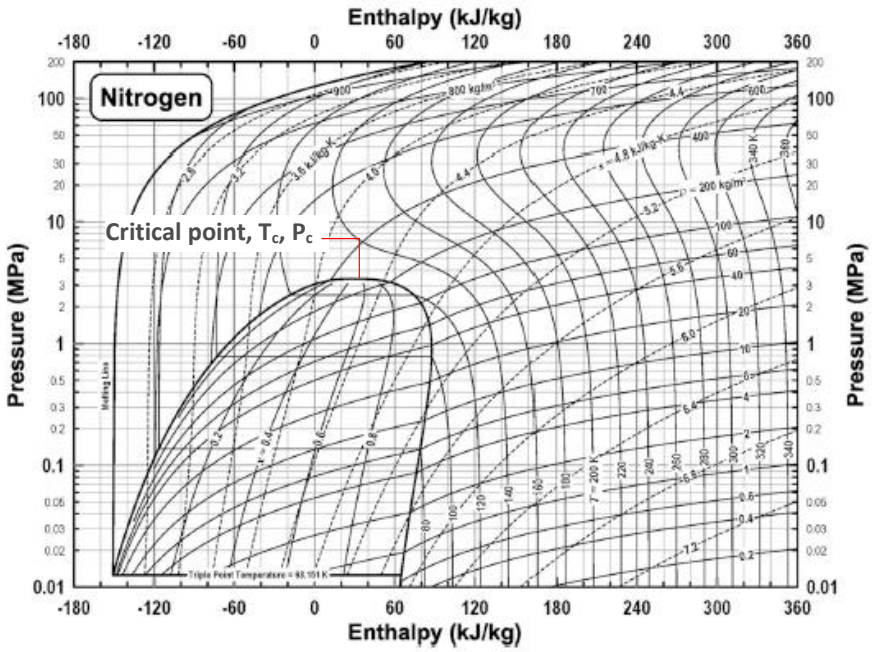

Figure 2.3 – Pressure and enthalpy diagram for nitrogen [6].

others [37]. The large amount of nitrogen production, as a waste product from oxygen separation, transforms this cryogen in a promising energy vector [43].

The cryogenic fluids (Table 2.1) at ambient conditions are highly superheated, but their pressure are well bellow critical pressures. When the temperature and pressure of a certain gas are brought into the region between the saturated liquid and saturated vapor,

Table 2.1 – Properties of cryogenic fluids [11].

	Normal Boiling Point			Critical Point		Triple Point	
Name	T (K)	Liquid Density (kg/m^3)	Latent Heat (J/kg·mole)	T (K)	P (kPa)	T (K)	P (kPa)
Helium	4.22	123.9	91,860	5.28	227		
Hydrogen	20.39	70.40	902,300	33.28	1296	14.00	7.20
Deuterium	23.56	170.0	1,253,000	38.28	1648	18.72	17.10
Neon	27.22	1188.7	1,737,000	44.44	2723	26.28	43.23
Nitrogen	77.33	800.9	5,579,000	126.17	3385	63.22	12.55
Air	78.78	867.7	5,929,000				
Carbon monoxide	82.11	783.5	6,024,000	132.9	3502	68.11	15.38
Fluorine	85.06	1490.6	6,530,000	144.2	5571		
Argon	87.28	1390.5	6,504,000	151.2	4861	83.78	
Oxygen	90.22	1131.5	6,801,000	154.8	5081	54.39	0.14
Methane	111.72	421.1	8,163,000	190.61	4619	90.67	11.65
Krypton	119.83	2145.4	9,009,000	209.4	5488	116.00	73.22
Nitric oxide	121.50	1260.2	13,809,000	179.2	6516	108.94	
Nitrogen trifluoride	144.72	1525.6	11,561,000	233.9	4530		
Refrigerant-14	145.11	1945.1	11,969,000	227.7	3737	89.17	0.12
Ozone	161.28	1617.8	14,321,000	261.1	5454		
Xenon	164.83	3035.3	12,609,000	289.8	5840	161.39	81.50
Ethylene	169.39	559.4	13,514,000	282.7	5068	104.00	0.12

Table 2.2 – Specific work of liquefaction for cryogenic fluids [7].

Gas	Normal Boiling Point (K)	Ideal Work of Liquefaction (W_i/m_i) (kJ/kg)
Helium-3	3.19	8178
Helium-4	4.21	6819
Hydrogen, H_2	20.27	12019
Neon, Ne	27.09	1335
Nitrogen, N_2	77.36	768.1
Air	78.8	738.9
Carbon monoxide, CO	81.6	768.6
Argon, A	87.28	478.6
Oxygen, O_2	90.18	635.6
Methane, CH_4	111.7	1091
Ethane, C_2H_6	184.5	353.1
Propane, C_3H_8	231.1	140.4
Ammonia, NH_3	239.8	359.1

as depicted in Figures 2.2 and 2.3, a portion of gas becomes liquid or condensate, verifying the liquefaction process. For instance, if a gas at P_1 pressure and T temperature, where $T > T_c$ (Fig. 2.2) is desired to be liquefied, it is necessary to increase its pressure and reduce temperature to take the final thermodynamic state into the liquid-vapor region. Thus, heat must be taken from the gas to be liquefied. Liquefaction by cooling or expanding the gas in a reversible way are the two common procedures to liquefy cryogenic fluids [44]. Butane, propane and mixtures of hydrocarbons can be obtained as liquids by cooling. The Joule-Thomson effect is another method to obtain liquid from gases [45, 37]. The procedure consists of driving gas through a porous plug or expansion valve, initially, as a result of a pressure drop through the device, the temperature increases up to a certain value, then, the continuous decrease in pressure produces a drop or decrease in temperature. During

this process, the enthalpy remains constant and a fraction of liquid from gas is obtained, it can be easily verified by the application of the first law of thermodynamics [7, 46, 47].

How it has been said before, to bring the cryogenic gases to liquid, the pressure must be increased and temperature reduced. The work of liquefaction is the parameter used to compute the energy required to produce the unit of liquid mass. For air, the ideal work of liquefaction is 738.9 kJ/kg, 3.8 % lower than that of nitrogen, as illustrated in Table 2.2. Hydrogen gas requires a minimum work of 12019 kJ per kilogram of liquid yield, it is the gas that requires more energy to be liquefied. The selection of the working fluid for the CES systems must be done by observing, from a critical point of view, the most relevant thermodynamic properties to help in the design and optimization of these promising technologies. The use of the cold exergy during the air distillation and liquefaction of natural gas can bring substantial benefits to recover low grade heat in those thermal processes [48, 49, 26].

The CES system is often called LAES (Liquid Air Energy Storage) system, because air is generally used as the working fluid. However, in this thesis CES is used instead, because this system can be adapted for other alternative cryogenic fluids such as carbon dioxide (CO_2) [50], hydrogen (H_2) [51, 52], nitrogen (N_2) [25, 53], helium (H_e) [54, 55, 56], and methane (CH_4) [43], just to mention the most relevant cryogenic fluids. For other interests, it can also be checked Ref. [6]. The use of different working fluids to improve the liquefaction and expansion processes performance has been studied by several authors. Khalil *et al.* [57] thermodynamically evaluated a CES system integrated into a Rankine cycle using liquid nitrogen and liquid air as cryogenic working fluids. The results showed that the use of liquid air as the working fluid significantly improved the performance of the plant compared to nitrogen. The study reported a round-trip efficiency of 84.15 % for the liquid air system and 63.27 % for nitrogen. In other research, Zhang *et al.* [50] compared a compressed CO_2 energy storage (CCES), an adiabatic CAES (AA-CAES) and a CO_2 CES system. The results indicated that CCES presented a round-trip efficiency 4.05 % higher than CO_2 CES system, and also found an energy density for CCES 2.8 times greater than AA-CAES.

In [43], authors evaluated a Joule-Thomson cryogenic cycle for five cryogenic fluids (Air, Nitrogen, Oxygen, Argon and Methane) and found, by thermodynamic comparison, that methane presented the highest liquefaction efficiency and recovery efficiency with approximated values of 30 % and 38 %, respectively. The liquefaction and recovery efficiencies reached, respectively, their maximum values for a compressor discharge pressure of 35 MPa and a turbine inlet pressure of 10 MPa. For the other analyzed cryogenic fluids, the liquefaction efficiency varied in the range of 12 % to 22 %, whereas for that of recovery efficiency, the other four cryogenic fluids performed in the range of 31 % to 34 %. Wang *et al.* [17] studied a CO_2 CES system integrated into an organic Rankine cycle

(ORC) and powered by wind energy. The results showed that round-trip efficiency and energy density reached 56.64 % and 36.12 kWh/m^3, respectively. Comparing to AA-CAES, round-trip efficiency showed lower results, but energy density was favorable for the hybrid CES system (2.91 kWh/m^3 < 36.12 kWh/m^3). The authors in [58] proposed the use of propane and methanol as cold fluids for a CES system. The thermodynamic analysis indicated a round-trip efficiency in a range of 54 % to 55 %, and the highest irreversibilities located in the air compression process and heat exchangers. The right selection of the cryogenic working fluid is crucial to obtain optimum performance in CES systems. The most significant features of an appropriated cryogenic working fluid are low flammability and toxicity, availability, compatibility and stability with others materials and properties. For instance, the lower the boiling point the higher the specific liquefaction work, which leads to decreasing performance of cryogenic power generation cycles. All of these explain why air has become the most used cryogenic fluid.

2.3 Cycles for cryogenic energy storage.

The liquefaction of gases is applied to increase the density and reduce the volume to be stored and transported, in this way the commercialization of such products becomes cost effective and highly efficient. In the industry there are many liquefaction cycles, the most well known are Linde-Hampson, Claude and Collins cycles. The simplest cryogenic cycle is Linde-Hampson cycle patented by William Hampson and Carl von Linde in 1895 [59], it is also known as the Joule-Thomson cycle. Figure 2.4 shows the Linde-Hampson cycle and its ideal representation in the temperature and entropy (T-s) diagram. The uncondensed gas from the cycle is mixed with a gas for replacement (make up) at state 1, as shown in Fig. 2.4b. The gas is compressed isothermally (process 1-2) up to the condition 2 increasing the pressure of the gas. The heat produced during the compression process is absorbed by an external heat exchanger using a cooling fluid with a low boiling point. The high pressure gas at state 2 enters the heat exchanger and cooled (2-3) by the uncondensed gas leaving from the cryogenic storage tank (g-1). At the exit of the heat exchanger, the gas is throttled through an expansion valve (3-4), reducing its pressure and temperature, in this way a fraction of gas is condensed. The resulting vapor-liquid mixture (4) enters the reservoir where liquid is removed (f) and the vapor phase is recycled (g). The exergy efficiency of the Linde-Hampson cycle is very low, approximately 3.1 % for air liquefaction and a reported specific liquid yield of 0.0866 kg_L/kg_a [9]. This low efficiency is due to the high irreversibilities during the isenthalpic expansion in the valve (3-4) and the irreversible process of heat transfer between the cryogenic heat exchanger and the surroundings.

A modified Linde-Hampson cycle is illustrated in Fig. 2.5. The high pressure gas is successively cooled in two heat exchangers (2-3 and 3-4). First, heat is removed for the gas returning from the storage tank (6-1) and also for the refrigeration cycle (d-a), as

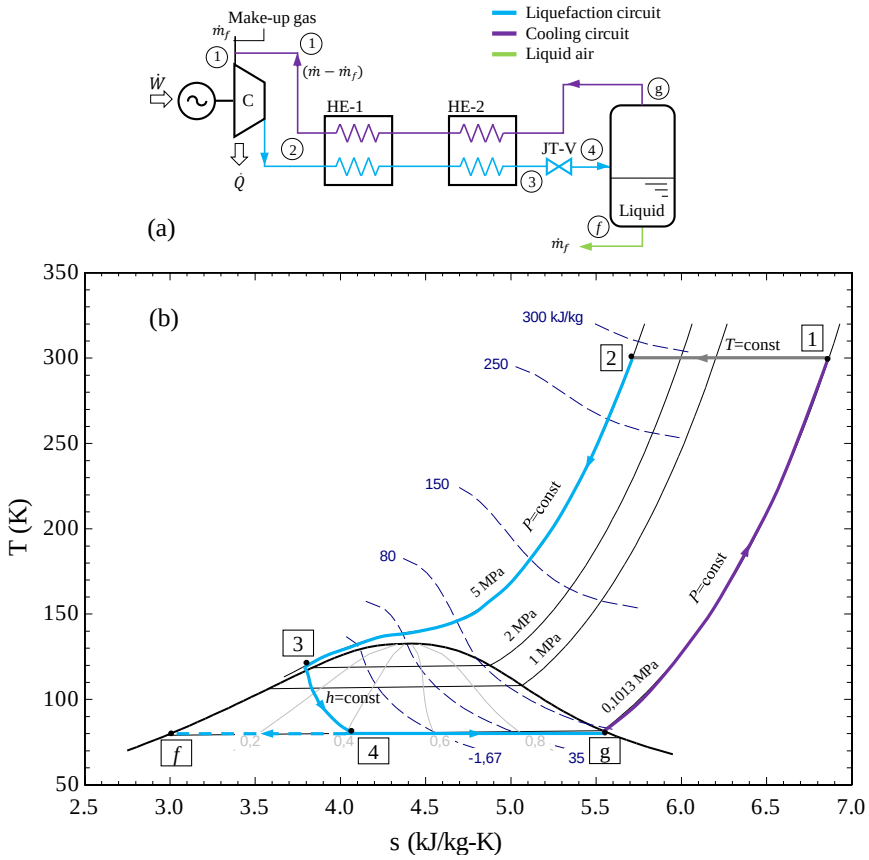

Figure 2.4 – (a) A simple Linde–Hampson high pressure and (b) T–s diagram liquefaction system. Adapted from [7].

illustrated in Fig. 2.5b. At the second heat exchanger, the gas is cooled by the recycled vapor (g-6). The high pressure gas temperature (4) could be lower than that of basic Linde-Hampson cycle, increasing the liquid yield. For a Van der Waals gas, the maximum pressure at which the gas can be liquefied by the Joule-Thomson effect is nine times the critical pressure [44]. The exergy efficiency of the Linde-Hampson cycle can be significantly improved when the precooled process is integrated. For instance, Lim et al. [60] found an exergy efficiency of 27.8 % for a Linde-Hampson cycle.

The Claude and Collins cycles are modifications of the Linde-Hampson cycle. Figure 2.6 illustrates the Claude cycle and an ideal representation on the T-s diagram. In 1902, George Claude proposed using two expansions instead of one like the Linde-Hampson cycle has. One expansion with the Joule-Thomson valve (JT-V) and a second one through a turbine located along a fraction of the high and low pressure streams. A fraction of the high pressure gas (3) is drawn in to the expansion turbine to produce work (3-e), the exhausted gas is mixed with the recycled vapor coming from the third heat exchanger (7). Consequently, the work of the compressor is significantly reduced by the work produced by the turbine and simultaneously a lower temperature of the working fluid is obtained. Hence, the work of the expansion turbine makes the cycle more efficient by improving the

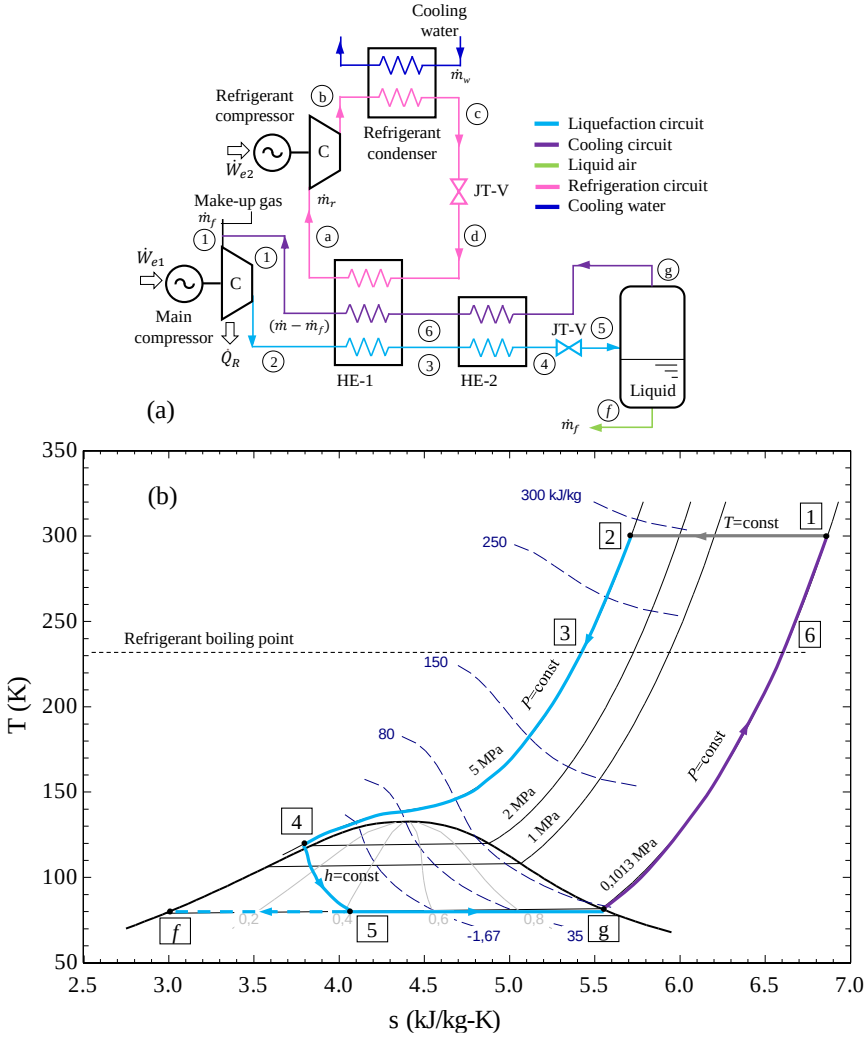

Figure 2.5 – (a) A precooled Linde–Hampson high pressure liquefaction system, and (b) T–s diagram. Adapted from [7].

overall efficiency of the system. Claude cycle can achieve exergy efficiency greater than 60 % and liquid yield higher than that of the Linde-Hampson cycle [60, 52]. Abdo [9] reported a exergy efficiency and specific liquid yield of 44.8 % and 0.305 kg_L/kg_a, respectively.

In 1947, Collins designed the helium liquefaction cycle [61], which uses two expansion turbines, unlike the Claude cycle which uses only one. The Collins cycle is normally used for helium liquefaction, which is a gas with the lowest boiling point (4.22 K, Table 2.1) among the cryogenic fluids, and also for refrigeration at temperature below 20 K [9]. Fig. 2.7 depicts a schematic outline of the Collins cycle and its representation on the T-s diagram. The cycle has six heat exchangers and two fractions of air (α_1 and α_2) are diverted through the expansion turbine 1 and 2, respectively. Abdo [9] investigated the performance of the Collins cycle for air liquefaction and found an exergy efficiency of 44.68 % and an optimal liquid yield of 0.303 kg_L/kg_a. Additionally, the author reported an optimum diverted fraction through turbines 1 and 2 of 0.59 and 0.10, respectively.

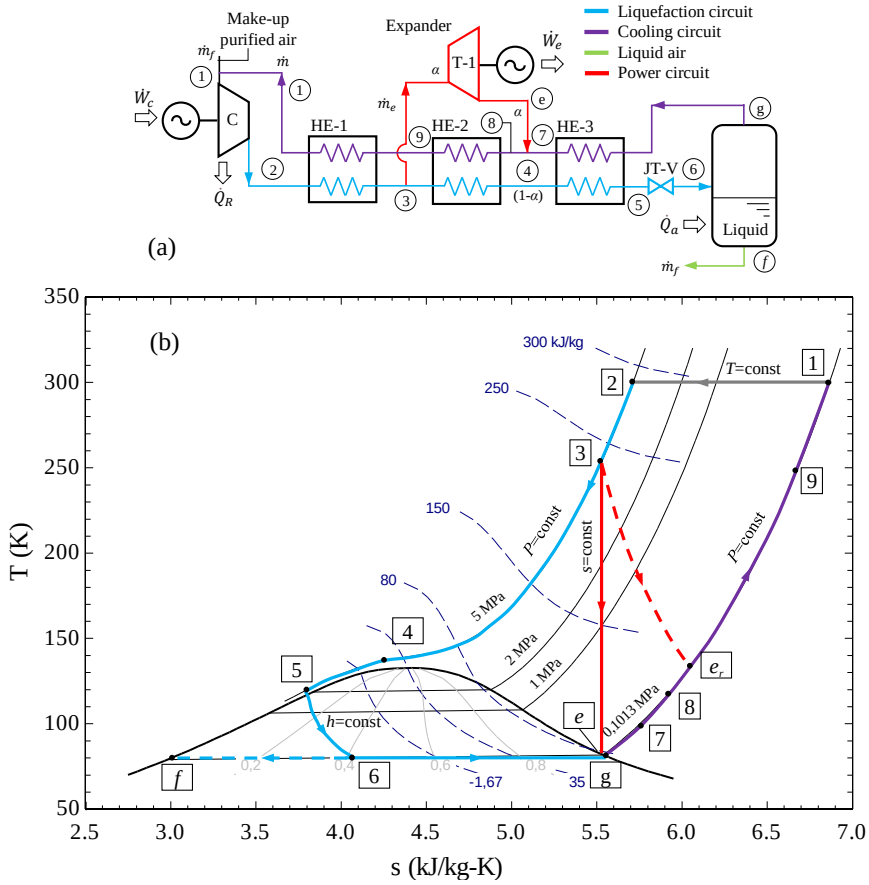

Figure 2.6 – (a) A Claude low-pressure process cycle using an expansion machine and (b) T–s diagram. Adapted from [7].

Atrey [54] evaluated and optimized a helium liquefaction cycle and found respectively optimum mass flow rate fractions through turbines 1 and 2 of 0.45 and 0.35. These results suggest that the mass flow rate ratio diverted through turbines must range between 0.60 and 0.80 to obtain the best performance during the liquefaction process.

Peter Kapitza patented in 1939 a liquefaction cycle based on the Claude cycle by eliminating the third heat exchanger and introducing a rotary expansion engine instead of the reciprocating expander [59]. Fig. 2.8 presents the Kapitza cycle and its representation on the T-s diagram.

The Heylandt liquefaction process is also a modification of the Claude cycle or a conversion of the precooled Linde-Hampson cycle with an expansion turbine and using air as a refrigerant. Fig. 2.9 shows the Heylandt liquefaction cycle and its representation on the T-s diagram. Hamdy *et al.* [62] thermodynamically evaluated both Kapitza and Heylandt liquefaction cycles. The results showed that when the Kapitza and Heylandt cycles use cold storage their exergy efficiency is 76.6 and 76.7 %, respectively. Moreover, both cycles presented specific liquid yield greater than 0.60 kg_L/kg_a.

Over the last ten years, there has been an increasing number of researches on

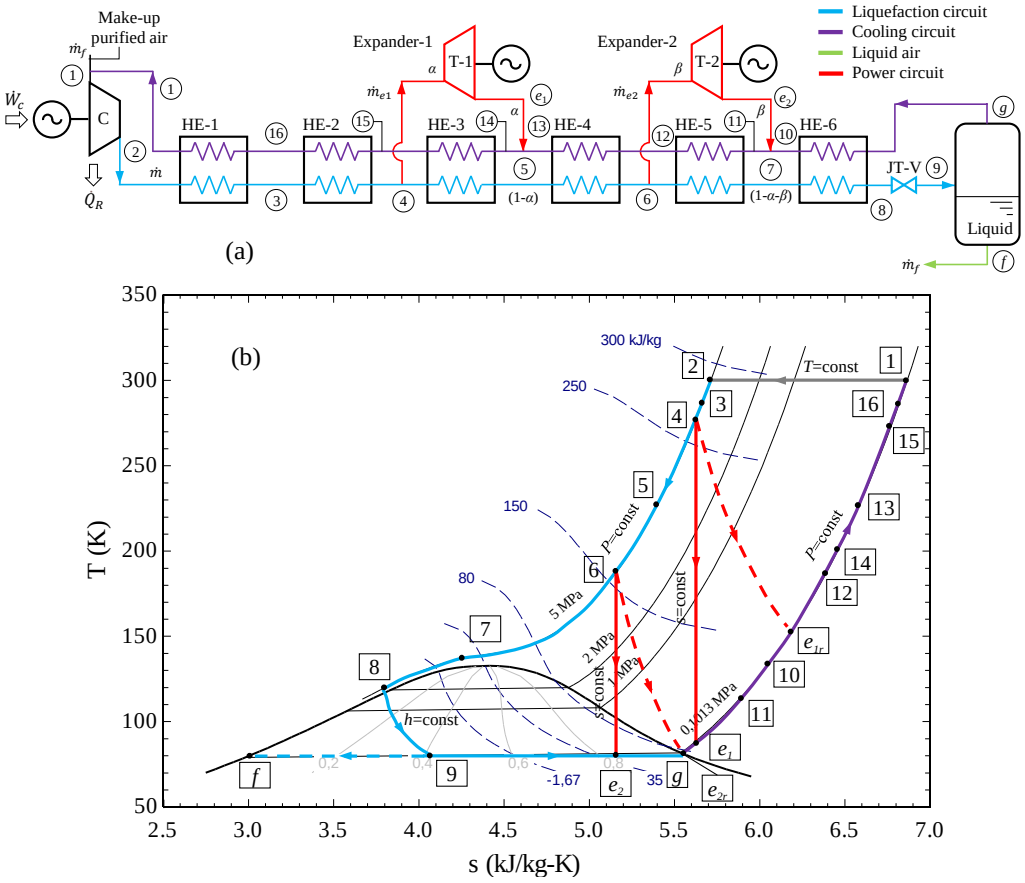

Figure 2.7 – (a) A Collins process liquefaction cycle using two expansion machines and (b) its representation on the T–s diagram.Adapted from [8].

cryogenic energy storage system for power production. Smith [63] was the first author to propose using the CES system in 1977. The author claimed an energy recovery efficiency of 72 %. Chen *et al.* [64] conceived in 2009 a CES system as a power generation plant with separated liquefaction and power generation circuits. According to the authors, cycle efficiency varies from 77.7 % to 172.3 %. The fundamental reason of this high efficiency lies in non-consideration, by the authors, of the input heat. In 2011 the first CES pilot plant is built by Highview Power and successfully tested [65]. However, the reported gross round-trip efficiency reached around 8 % for a specific cold recycle greater than 150 kWh/kg_L. A comparison between Linde-Hapmson, Claude and Collins cycles was presented by Abdo *et al.* [10]. The authors' most important legacy was to suggest the integration of charging/discharging circuits in the same system, which created opportunities for cogeneration by taking advantages of the exergy of the liquid air in an evaporator before its expansion in the turbine, this was not demonstrated. The conclusions showed that Claude and Collins cycles are more effective for power generation and liquid production than Linde-Hapmson cycle. A demonstrator CES plant in Greater Manchester started operation in April 2018, and researchers reported a round-trip efficiency of around 60 % [66]. In another research, [67], the authors reported an energy efficiency of 49 %, using hot

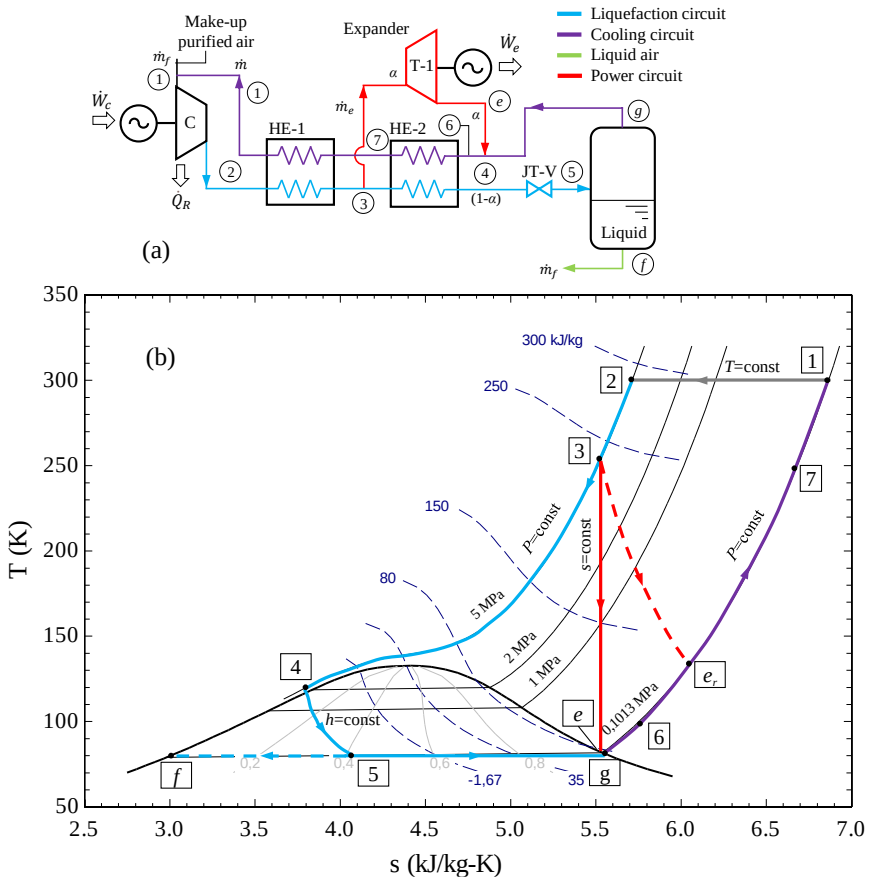

Figure 2.8 – (a) A Kapitza process liquefaction cycle and (b) T–s diagram.

and cold regenerators with thermal fluid as a storage medium and ideal air as cryogenic working fluid. The effectiveness for regenerators has a strong influence on round-trip efficiency for energy storage cycles, and it is common to be assumed as 100 %. Regarding this, the authors in [68] found storage efficiency in the range of 21.13 - 33.74 % for nine storage materials with heat capacity between 1.131 and 3.332 $MJ/(m^3K)$.

A thermodynamic analysis of a compressed air energy storage (CAES) and a liquid air energy storage (LAES) was conducted by Krawczyk *et al.* [69]. LAES consists of a liquefaction cycle and a gas turbine for power generation. Using Ansys Aspen software the CAES and LAES power plants were simulated in a dynamic mode. The authors found that both cycles are characterized by high storage efficiency, favorable for LAES with 55 %, while CAES achieved 40 %. An experimental study of the first LAES pilot plant in the world and currently installed at University of Birmingham was conducted by Sciacovelli *et al.* [70]. In the study, the influence of operational parameters, technology reliability, operation principles and star-up/shut down performance were analyzed. The study demonstrated that the liquefier from the industry can be used for the LAES charging process. The authors highlighted the rapid reaction of the system during the discharging process, where 80 % of the power load was reached in two minutes. They also emphasized

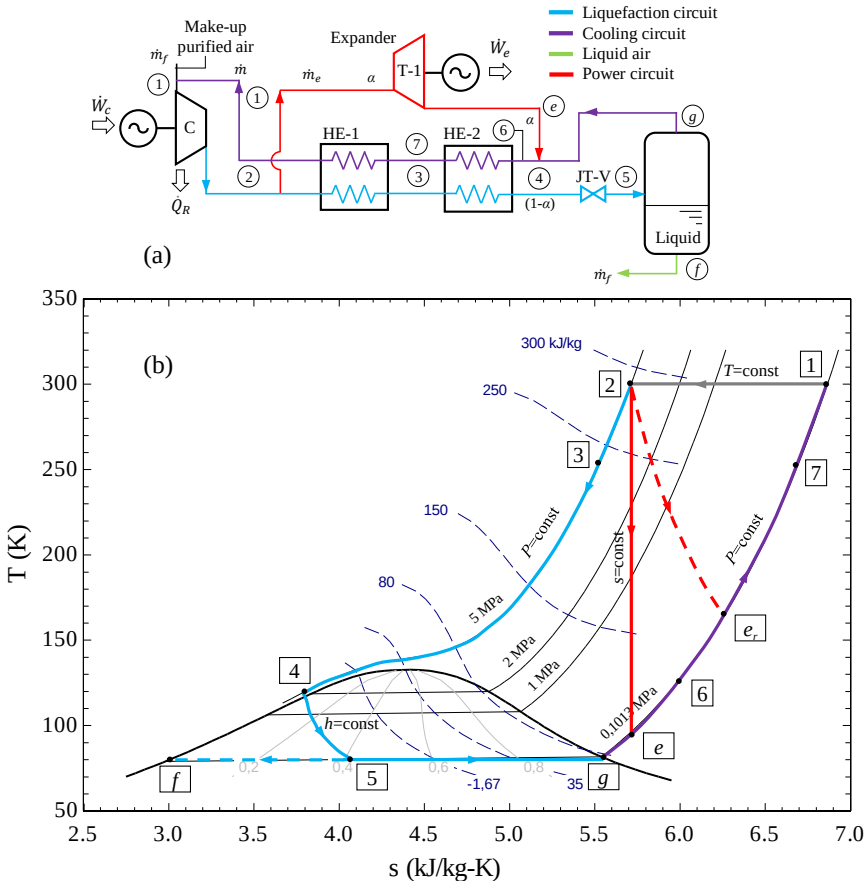

Figure 2.9 – (a) A Heylandt process liquefaction cycle and (b) its representation on the T–s diagram.

on the necessity to recycle cold thermal energy from discharge to charge process to achieve high overall efficiency.

An exergy analysis of a modified Claude cycle was performed by Thomas *et al.* [71]. The helium liquefaction system with two expanders was evaluated using the simulator Aspen HYSYS. The influence of compressor pressure ratio and expander flow fraction on the exergetic efficiency of the cycle was studied. The research concluded that increasing the pressure ratio produces an improvement on exergetic efficiency. Other results show that there is an optimum flow fraction to be passed through the expanders to get the maximum efficiency of the cycle. A laboratory scale CES with 5 kW of power capacity and based on Rankine cycle using carbon dioxide as working fluid was studied in [72]. The results showed that the small scale CES was able to consume during off-peak hours between 3.2 and 4.8 kWh to generate cold energy in a temperature range of -50 to -40 °C. Based on the experimental measurements the CES efficiency achieved values between 24 and 44 %. The effects of heat exchanger variables on the performance of a helium liquefier using Collins cycle was studied in [73], the authors simulated the operation of the heat exchangers taking the product overall heat transfer coefficient and heat transfer area (UA)

and deterioration factor (F) as independent parameters to compute the behaviour of the helium liquefaction rate. They also studied the influence of the inlet turbine temperatures on the helium liquid production. The study was performed on the basis to assume steady state conditions, negligible pressure drops through out the heat exchangers and pipelines, the effective product UA considers axial heat conduction, heat in-leak, flow maldistribution and specific heat variation in fluids, other assumption stated that component efficiencies do not depend on temperature, pressure and mass flow rate. Researchers concluded that the effectiveness of the heat exchangers varies linearly in respect to helium liquid yield and their performance have an important influence on liquid production. According with the authors, when the additional heat transfer area is distributed in proportion of UA in the heat exchangers, the maximum helium liquid yield is obtained. When the effectiveness values of the heat exchangers keep above 0.95, only with degradation beyond 50 % of limiting UAs, the losses in the heat exchangers sharply increase and the decrease in liquid production becomes more significant. The authors also asserted that the optimal re-circulation fraction through out the turbines was not influenced by the variation of the heat exchangers effectiveness.

In other study [21], a liquid air Rankine cycle is operated as part of a cryogenic energy storage system. The effect of the compressor pressure, fraction of air and effectiveness of the heat exchanger on specific net power output and liquid yield are analyzed. The results showed that recovery efficiency in the Rankine cycle is 36.8 %. But, when heat waste at 300 K is used in a combined cycle the efficiency resulted in 43.3 %. The authors also found that the combined cycle efficiency is very sensitive to the heat exchanger effectiveness. A method to improve the round trip efficiency of a liquid nitrogen energy storage cycle was proposed by Dutta *et al.* [25]. The technique consists of applying multiple stages of reheat and expansion using an available waste of heat. The research concluded that the maximum round trip efficiency for a single stage was found to be 28 %, meanwhile using four stages the efficiency was increased up to 47 %. Borri *et al.* [74] studied three air liquefaction plants for liquid air energy storage. A parametric analysis of Linde-Hampson, Claude and Kapitza (Collins) cycles was carried out with the help of Aspen HYSYS software. The results show that Claude and Kapitza cycles presented the lowest specific power consumption and the application of the double stage of compression may be possible to increase the performance in 25 %. According with the authors, Kapitza cycle presented the best performance and the optimal two stage compressor pressure resulted in 40 bar with a specific energy consumption of 700 kWh/t.

A study about the influence of expanders in the helium liquefaction process using Collins cycle was carried out in [55]. Authors used Aspen HYSYS software to simulate Collins cycle under different operating conditions. The main assumptions assumed to perform the parametric study were focused on steady state regime, no heat in-leak into the system, efficiencies of compressor and expander or effectiveness of the heat exchangers

remain constant and negligible pressure drops in heat exchangers and pipes. The study points out that the optimal liquid yield was obtained when the re-circulation fraction through out the expanders was of 80 % of the compressor flow. Another result suggests that the flow through out the expanders has more influence on the performance of the heat exchangers than the expanders efficiency.

M. Sadaghiani and M. Mehrpooya [75] proposed a novel hydrogen liquefaction process configuration with two independent refrigeration cycles. According with the results, the exergetic efficiency and coefficient of performance reached their peak values at an operating pressure of the first refrigeration cycle of 16 bar. The research concludes that the specific energy consumption of the first and second refrigeration cycles consume 1.102 and 3.258 kWh/kg_{LH_2} respectively to cool hydrogen from 25 °C to −195 °C. Finally, the exergetic efficiency of the first and second refrigeration cycles were of 67.53 % and 52.24 % respectively, while the whole system achieved 55.47 %. Table 2.3 summarizes the characteristics of some CES system technologies and the main results of their performance.

In general, the studies adopted different assumptions for simulating the CES systems. Moreover, the working fluid parameters for the charging and discharging processes vary in a wide range, even for similar CES cycles. Another relevant characteristic in the reviewed research works was the use of more than one working fluid to recover cold and heat. The second law analysis was applied in a few number of publications. This limits the possibility of identifying the origin of irreversibilities and their magnitude, which is crucial for the optimization process. Finally, some relevant parameters, such as effectiveness of the heat exchangers and air diverted air mass fraction, were not studied during the simulation procedure considering the simultaneous operation of charging and discharging processes. In this research, the aforementioned drawbacks are overcome. Additionally, this study demonstrates the feasibility of the simultaneous operation of the charging and discharging processes in CES systems.

Table 2.3 – Characteristics of stand-alone CES systems and main parameters.

Authors	Objective of the study	Type of CES	P_{ch}/P_{dis} (MPa)	Storage & Fluid	y (kg_L/kg_a)	η_{rt} (%)
Nandi-Sarangi, 1993 [52]	Thermodynamic analysis of hydrogen liquefier	Linde-Hampson (LH) and Claude (C) cycles	LH: 6.0-10.0/C: 1.0-3.0	Hydrogen	LH: 0.12-0.17, C: 0.16-0.20	-
Atrey, 1998 [54]	Thermodynamic analysis of helium liquefier	Collins cycle	1.5/-	Helium	0.065 for ε=0.97	-
Li., 2011 [76]	Thermodynamic analysis	Linde-Hampson cycle	13.7/11.2	Cryo-turbine and storage tank (Air)	0.74	37.0
Ameel *et al.*, 2013 [21]	Thermodynamic analysis	Linde-Hampson-Rankine cycle	2.0/10.0	Cryogenic storage tank (Air)	0.36	43.3
Abdo *et al.*, 2015 [10]	Thermodynamic analysis	Linde-Hampson, Claude and Collins cycles	4.0-20.0/20.0	Storage tank (Air)	0.08-0.30	-
Guizzi *et al.*, 2015 [58]	Thermodynamic second law analysis	Linde-Hampson cycle	18.0/6.5	Six regenerators (Oil, Methane and Propane)	0.84	54.0 - 55.0
Xue *et al.*, 2015 [67]	Thermodynamic analysis	Linde-Hampson cycle	11.5-16.0/4.0-10.0	Two regenerators and Packed bed (Air)	-	49.0
Krawczyk *et al.*, 2016 [77]	Thermodynamic analysis	Linde-Hampson cycle	2.0-14.0/10.0	Two tanks (Air, Oil, Methanol and Propane)	-	57.0
Sciacovelli *et al.*, 2017 [70]	Thermodynamic analysis and dynamic modelling	Claude cycle	18.1/7.5	Two regenerators (Air, Oil, Packed bed rocks)	0.78	50.0
Peng *et al.*, 2018 [78]	Thermodynamic second analysis	Linde-Hampson cycle	12.1/5.0	Two regenerators (Air, Oil, Methane, Propane and Packed bed rocks)	0.75 - 0.87	50.0-62.0
Hamdy *et al.*, 2019 [62]	Thermodynamic second law analysis and economic evaluation	Linde, Claude, Heylandt and Kapitza cycles	8.0-20.0/20.0	Storage tanks (Air, Methanol, Propane, Oil and R32)	0.33-0.62	46.9-50.0
Lars and Span, 2019 [68]	Thermodynamic analysis of storage material properties	Modified Claude cycle	-	Packed bed, storage efficiency 21.13% - 33.74%	-	-
Tafone *et al.*, 2019 [79]	Thermodynamic analysis and performance maps	Kapitza cycle	4.0-9.0/6.0-16.0	Two tanks (Air, Oil)	-	-
Xu *et al.*, 2020 [80]	Thermodynamic analysis	Linde-Hampson cycle	12.0/25.0	Two tanks (Air, Methanol and Propane)	-	37.8
Sun *et al.*, 2021 [81]	Thermodynamic second law analysis	Linde-Hampson cycle	15.0/14.7	Two tanks (CO_2, Methanol and Water)	-	51.4

2.4 Hybrid CES technologies.

The round-trip efficiency for the CES systems can be appreciably improved by integrating them with other technologies, such as conventional power plants, refrigeration cycles, renewables energy sources, Liquefied Natural Gas (LNG) waste cold recovery and also with the use of external thermal energy sources (waste heat recovery) from industrial processes. In the last decade, many researchers dedicated efforts to improving the CES system's round-trip efficiency, integrating it with other technologies and using different operation strategies.

A study about hybrid power plants was presented in [82], the research assessed three examples involving liquid air storage, process air expansion with combustion, an organic Rankine cycle and a Brayton cycle. The hybrid power plants were compared against a baseline configuration. The best predicted round trip efficiencies for the hybrid systems were estimated in 76 % for air expansion with combustion, 77 % for organic Rankine cycle and 90 % for the cold Brayton cycle, much higher than that of baseline, which registered a value of 18 %. An analytical study was conducted by Guo *et al.* [83] about a hybrid compressed air energy storage systems (SC-CAES) and a cryogenic energy storage. The effect of key parameters of the plant on the round trip efficiency, liquefaction ratio and exergy destruction were analyzed. The results point out that exergy destruction in heat storage is the main factor of total exergy destruction in the system. Another research [27] presents different concepts of CES and a evaluation of two exergy recovery cycles, the first one a direct expansion of liquid air and the second one an expansion of liquid air combined with a organic Rankine cycle (ORC). The results show that the energy densities of the proposed systems were found to be between 120 and 150 kWh/kg and the round trip efficiency reached 40 %.

The CES systems can provide cold exergy for refrigeration cycles and consequently improve their performance. A proposed liquid hydrogen production plant to provide the required liquid H_2 for a large urban area is analyzed in [84]. The plant consists of a pre-cooling section, cryogenic section with six simple Linde-Hampson cascade cycles and a Joule-Brayton refrigeration cycle. The second law of thermodynamic was applied to assess the performance of the system. The effect of hydrogen pressure and heat flow on the exergy efficiency, temperature difference at the heat exchangers, coefficient of performance and specific energy consumption are analyzed. The specific energy consumption to cool hydrogen from 25 °C to -198.2 °C in the pre-cooling section resulted in 1.589 kWh/kg_{LH_2}. The total energy consumption of the plant was 7.69 kWh/kg_{LH_2}. Another result showed that the heat exchangers had the highest exergy destruction. She *et al.* [85] proposed a hybrid CES system, wherein the heat released from the compression process is used to power an Organic Rankine Cycle (ORC), whereas the heat sink is a Vapor Compression Refrigeration Cycle (VCRC). The authors performed a thermodynamic analysis to compute

the influence of charging pressure, stages of expansion, discharging pressure, type of organic working fluid and turbine inlet pressure of ORC on the round trip efficiency, excess heat of compression stored in thermal oil, exergy efficiency and liquid yield. The results show that the higher the charging pressure, the higher the exergetic and round trip efficiency, a similar behaviour is also achieved by the liquid yield parameter. In the discharging cycle, the hybrid CES round trip efficiency is approximately 10-12 % higher than the baseline cycle and the best performance of exergetic efficiencies is achieved for discharging pressure of 13 MPa. Another result shows that increasing stages of expansion produces an increasing of the round trip efficiency and a reduction of the excess heat of compression for a range of charging pressure between 10 and 14 MPa. The authors concluded that the round-trip efficiency of the hybrid CES system could be higher than 60 % and R32, R502 and R134a working fluids are favorable candidates for the ORC, which optimal turbine inlet pressure was found at 11 MPa. A hybrid system, integrated by a liquid energy storage plant, an Organic Rankine Cycle and an Absorption Refrigeration Cycle (ARC) was presented by Peng *et al.* [86]. The investigation shows that the excessive compression heat can be used to drive the ARC reducing the temperature environment for the ORC, and working at the same time as heat source of the ORC. According with the authors, the enhancement of the round trip efficiency ranged from 3 to 9 %.

The integration of CES systems to renewables energy sources has been studied by some authors. For example, Wang *et al.* [17] proposed different schemes of a liquid carbon dioxide storage system powered by wind energy. A parametric analysis was applied to examine the influence of some thermodynamic parameters on the performance of each proposed scheme.The optimal value of the round trip efficiency resulted in 56.67 %. A solar cryogenic hybrid power system, using nitrogen as cryogenic fluid, was proposed by Li *et al.* [87]. The hybrid system consists on a closed loop Brayton cycle and an open cryogenic cycle with direct expansion. The system is fed by solar thermal and cryogenic fueled power. The sequential quadratic programming (SQP) method was applied to optimize the system. The total irradiance of the collector and the usable process heat were modeled to predict the thermal and exergetic efficiencies of the solar collector. The cryogenic cycle and hybrid system efficiencies were also estimated to evaluate the performance of the proposed solar cryogenic hybrid power system. The authors concluded that the hybrid system was able to provide about 30 % more power than the sum of the power generated by the other two systems if they were operating independently. The exergetic efficiency of the hybrid system resulted in 27.55 %, higher in 3.66 % and 9.45 % than that of solar thermal and cryogenic fueled power systems. Other finding from the research suggests that the optimal hot end temperature of the heat carrier heated by the solar collector must be approximately to removed 600 K considering hybrid system operation.

Some authors have undertaken different analyses of cryogenic energy storage hybrid cycles with geothermal power plant. A hybrid geothermal energy plant and a

Claude hydrogen liquefaction cycle was thermodynamically evaluated by Kanoglu *et al.* [88] applying the first and second laws of thermodynamic. The influence of compressor pressure, geothermal temperature and cooled hydrogen gas temperature on coefficient of performance (COP), figure of merit (FOM), exergy efficiency, liquefaction work and liquefied mass fraction were analyzed. For the absorption refrigeration cycle and the Claude cycle the COP resulted in 0.556 and 0.0120, respectively. Based on the fuel and product approach the exergy efficiency of every system was estimated in 67.0 % and 67.3 %, respectively. The overall system reached an exergy efficiency of 67.9 %. A hybrid system, composed by a supercritical CO_2 power generation system fueled by geothermal source and a cold LNG power plant used as heat sink, was investigated by Wang *et al.* [89]. The mathematical models of the hybrid system were established to simulate and optimize the main thermodynamic parameters, for this, multi-objective optimization method was carried out. The authors assumed steady state regime, negligible pressure drop in the pipes, adiabatic condition for every component and CO_2 saturated liquid at the condenser outlet. The influence of CO_2 turbine inlet pressure, temperature and CO_2 turbine back pressure on the net power output, total heat transfer area and exergetic efficiency were analyzed. An increase of CO_2 turbine inlet pressure results in an increase in the exergetic efficiency and the net power output, the optimal values were obtained at 13 MPa. Meanwhile, the total heat transfer area decreases with the increase of CO_2 turbine inlet pressure. The authors found that the transcritical CO_2 geothermal power system increases its energy production as a result of the back pressure reduction due to the use of the cold LNG as heat sink on the condenser. They also suggested to take advantage of the exergy flow leaving from the natural gas (NG) turbine.

The cold exergy from LNG re-gasification process may be also used for the liquefaction process in CES systems. An efficient cryogenic energy storage (CES) process to harness the wasted exergy from liquefied natural gas (LNG) re-gasification process is presented by Lee *et al.* [90]. The performance of the system was evaluated by the second law of thermodynamics. The air storage section achieved an exergy efficiency of 94.2 % while the release or expansion section was of 61.1 %. A double stage Rankine cycle using binary and ternary mixtures as working fluids to harness the cold exergy from liquefied natural gas for power production was analyzed in [91]. An optimization procedure based on genetic algorithm was performed. The results showed a significant increasing of the thermal and exergy efficiencies from the baseline scheme to the optimal case. Kim *et al.* 2018 [92] conducted a thermodynamic, environmental and economic investigation of a distributed energy generation hybrid plant using liquid air combined with liquefied natural gas (LNG). A sensitivity analysis proved the influence of liquid air storage pressure, turbine inlet pressure and compressor pressure on round trip efficiency, renewable (or grid) energy-source penetration ratio and storage efficiency. The researchers found round trip and storage efficiencies to be 64.2 % and 73.4 %, respectively. Another result showed

that the exergy efficiency of the storage-site, generation-site and the system was 70.2 %, 75.1 %, and 62.1 %, respectively. Depending on the storage time, the levelized cost of energy (LCOE) ranged from 142.5 to 190.0 $/MWh. The exergy recovery technology from a liquefied natural gas system for transportation was presented in [93]. The authors evaluated four exergy recovery systems, consisting of a single-stage and two-stage direct expansion systems, an ORC (Organic Rankine Cycle) system, and a combined system (ORC + direct expansion). An exergy analysis and optimization procedure were applied to assess the performance of the proposed schemes. According with the results, the exergy recovered ranged 20-36 %. The direct and two-stage expansion systems were able to recover 24 and 30 % of LNG exergy.

Li *et al.* [94] proposed the integration of a nuclear power plant (NPP) with a cryogenic energy storage technology. The main purpose of this particular hybrid system was to attain an efficient time shift of the electrical power output. The proposed CES system stores the excess electricity by liquefaction of air at off-peak hours and recover the energy by expanding the working fluid at peak hours. The results showed that during charging regime compressor units presented the highest exergy destruction, achieving a ratio of 20 % from total, while heat exchangers placed second with 16 %. In the generating mode, heat exchangers were responsible of an exergy destruction of 40 % and 30 % for the cryogenic pump. The study also showed that the higher ambient temperature, the lower round trip efficiency, meanwhile net output power in generating mode remains almost constant and liquid air mass flow rate, in the same mode, slightly drops. The authors found that the round trip efficiency linearly increased with liquid air storage pressure, while for both net output power and liquid air mass flow rate, in generating regime, experienced a slightly reduction. Additionally, round trip efficiency linear increased respect to secondary loop topping pressure. Opposite to the influence of this parameter on net output power and liquid air mass flow rate, where both slightly decreased. The main remarks of this investigation indicated that the round trip efficiency was about 71 % while the net output power in the energy release mode represented 2.7 times that in a nuclear power plant alone.

Table 2.4 illustrates a summary of the main characteristics of CES systems and results of different studies on their integration with other technologies. Overall, it is observed in the literature reviews that the influence of CES system integration with other technologies or the use of waste heat recovery on specific liquid yield, specific exergy consumption and exergy density was infrequently evaluated. Moreover, the round-trip efficiency varies over a wide range and some studies reported values greater than 100 %, this occurs when some energy inputs are not accounted, which makes comparison impossible. In this research, the influence of the waste heat recovery temperature on the main indexes and indicators of the proposed cogeneration CES systems with the simultaneous operation of the charging and discharging processes is analyzed.

Table 2.4 – Characteristics of Hybrid CES systems and main parameters.

Authors	Objective of the study	Type of CES	P_{ch}/P_{dis} (MPa)	Storage & Fluid	y (kg_L/kg_a)	η_{rt} (%)
Kantharaj *et al.*, 2015 [95]	Thermodynamic first law analysis	CAES-CES	5.0/5.0	Cryogenic storage tank (Air)	-	-
Kanoglu *et al.*, 2016 [88]	Thermodynamic second law analysis	Geothermal, Absorption refrigeration and Claude cycle	5.0/-	Cryogenic storage tank (H_2, N_2, NH_3+water)	0.15-0.23	-
Farres *et al.*, 2018 [96]	Thermodynamic analysis	Hybrid CES-PTES system	15.0/-	Ten storage tanks (Air, Helium, Oil, Molten salt, Ethanol)	-	70.0
Tafone *et al.*, 2018 [97]	Thermodynamic analysis	Hybrid CES-ORC-trigeneration	11.0/18.0	Two tanks (N_2, Therminol 66, Air)	-	55.7
Barsali *et al.*, 2018 [98]	Thermodynamic analysis	Hybrid CES-LNG	-/14.9	Two tanks (O_2, Methane, Water)	-	82.0-104.0
She *et al.*, 2019 [99]	Thermodynamic second law analysis	Hybrid CES-Brayton-LNG system	12.0/12.0	Eight regenerators (Air, N_2, Propane, Methanol, Thermal oil)	0.71	70.6
Peng *et al.*, 2019 [66]	Thermodynamic second law analysis	Hybrid CES-LNG-CS system	7.6/8.0	Four regenerators (Air, Oil, Propane and Methane)	0.87	88.0
Cetin *et al.*, 2019 [100]	Thermodynamic analysis	Hybrid CES-Geothermal system	20.0/18.0	Four regenerators (Water, Air, Methanol and Propane)	0.58	46.6
Lee and You 2019 [101]	Thermodynamic first and second law analysis	Hybrid CES-LNG and CES-LNG-ORC	4.4/21.0	One tank (Air, LNG and Seawater)	-	105.6/122.8
Xu *et al.*, 2020 [80]	Thermodynamic second law analysis	Hybrid Rankine cycle, Solar and LCES	12.0/2.2	Four storage tanks (CO_2, Propane and Methanol)	-	45.3
Briola *et al.*, 2020 [102]	Thermodynamic and economic analysis	Hybrid CES-AGTC-NGCC	4/1.2-2.4	Two tanks (Air, Methanol and Propane)	-	-
Qi *et al.*, 2020 [103]	Thermodynamic and economic analysis	LNG-CES system	3.5/21.0	Two storage tanks (Air, Propane)	-	129.2
Ebrahimi *et al.*, 2021 [104]	Thermodynamic second law analysis	Hybrid CES-Kalina CHP-SPC	6.6/8.8	Three storage tanks (Air, Propane, NH_3-water, Oil, LNG, Water)	-	45.4

2.5 Poly-generation CES systems.

Some investigations about CES systems have also focused on evaluating their poly-generation potential in order to meet the heating, cooling and electricity demands. That is, the cogeneration and trigeneration capability of CES systems have been assessed by some authors. Ahmad *et al.* [53] presented a new approach for providing cooling and power from a CES system operating only in discharging regime and using liquid nitrogen as a cryogenic working fluid. Authors reported saving up to 28 % in residential buildings, compared to conventional air conditioning systems and considering the local liquid nitrogen prices; it concluded that 85 % of the energy stored can be recovered by using two closed cascade Rankine cycles. In another study, Tafone *et al.* [97] investigated the integration of a CES system with organic Rankine cycle (ORC) and/or absorption chiller and found, with respect to a stand-alone CES system, an improvement of the round-trip efficiency of 30 % when the three systems were integrated. The study reported an overall efficiency of 55.7 % (trigeneration) and both the cogeneration and trigeneration configurations worked only in discharging regime. Moreover, the authors also found a specific energy consumption of 0.232 kWh/kg_L for the integration of the CES system to the absorption chiller, which represented a reduction of 4.5 % respect to the stand-alone CES system. The performance of a CES system with district heating and cooling capabilities was proposed by Al Zareer *et al.* [105], the CES system was integrated to a Rankine cycle, a gas turbine and a solid-gas sorption cycle. Considering the cooling and heating capabilities of the integrated system, the overall energy and exergy efficiencies resulted in 72.1 % and 53.7 %, respectively. Additionally, the combustion chamber and the second intercooler carried the highest irreversibilities.

A quantitative and qualitative analysis of different energy storage technologies was presented by Comodi *et al.* [106]. The authors evaluated a Linde-Hampson CES system operating in a cogeneration regime for two different scenarios. A scenario of medium scale with the daily cooling energy demand of 10 MWh and a large scale scenario with the cooling demand of 500 MWh. According to the authors, for the medium scale scenario, the total efficiency for cogeneration and full electric modes resulted in 17 % and 25 %, respectively, while for large scale mode, the efficiency respectively increased in 13 % and 35 %. Vecchi *et al.* [107] proposed a multi-CES system for the provision of heat, cold and electricity in districts with cooling and heating networks. A reduced thermodynamic model was developed to evaluate the performance of the CES system and according to the authors multi-CES system may provide multiple energy vectors to support district operation contributing to about 5 % and 10 % of district power and thermal demand. However, they found some constraints, for example, the electrical efficiency reduced when increasing heat provision, while cooling provision decreased electrical efficiency but increased heating output. The authors also referred that energy efficiency was improved from 47 % to 72.8 %

when the multi-CES system capability of multi-generation was harnessed.

Even though there are some studies on poly-generation in CES systems, the potential of this storage technology for that purpose has not been deeply surveyed. In general, the studies only conceived the cogeneration during the discharging process, which limits the multi-generation capability of the CES technologies. In addition, the investigations about the cogeneration potential of the CES systems rarely considered the sensitivity analysis of the main indexes and indicators on cryogenic storage capacity and charging and discharging times. In order to cover the aforesaid gaps, the simultaneous operation of the charging and discharging regimes is applied as an alternative operation mode that can contribute to improve the indexes and indicators of the CES systems considering the scale of the plant. In this work, the advantages of using this operation mode in cogeneration CES systems are also presented.

2.6 Economic assessment of the cryogenic energy storage systems.

At present, most studies about CES systems have been focused on the thermodynamic evaluation, aimed at determining the influence of some parameters on the main indexes and indicators, such as specific liquid yield, specific consumption, round-trip efficiency, among others. However, the economic evaluation on CES systems is significantly limited in the literature and only a few articles provide in-depth economic analysis, but in quite different contexts from this study. Additionally, the economic benefit from the CES systems is generally restricted to electricity selling in most of the studies and others marketable products that can be obtained from this technology.

Xie *et al.* [108] provided an economic feasibility of decoupled energy storage technologies, considering as example a CES system. A methodology to optimize the size of the main components for charging, storing and discharging energy was proposed. According to the authors, the profitability of the CES system was improved by both the increasing the waste heat temperature and the system scale. The study also concluded that for a 200 MW CES system, the payback period varied from 25.7 to 5.6 years for waste heat temperature ranged from 0 to 250 °C. A methodology to evaluate the economic viability of CES system was proposed by Lin *et al.* [109] as part of the resumption of the previous study. The authors designed an arbitrage algorithm to determine price thresholds every half hour under different operation strategies. The study found that the viability of a CES plant was affected by both the system scale and the waste heat temperature. For instance, in order to be profitable, a 100 MW CES system should use waste heat at temperature greater than 150 °C considering an interest rate of 6 %. Moreover, a positive net present value (NPV) of £43.8 million was obtained for a 200 MW CES plant for an operational strategy where the price thresholds were determined using 12 historical prices and 12 future

prices. The payback period was found to be as long as 36.9 to 39.4 years for a 200 MW CES plant without using waste heat. Nevertheless, using waste heat, the payback period was shortened to 8.7-9.4 years. Pimm *et al.* [110] presented a techno-economic analysis for a hybrid energy storage system, comprising CAES and CES systems. The authors developed an algorithm that can be used to obtain the maximum profits from the hybrid system from a set of electricity prices. Under certain conditions, the hybrid storage energy system was found to be more profitable than the respective standalone CAES and CES systems. In another investigation, Vecchi *et al.* [111] presented a technical and economic evaluation of a 100 MW CES standalone plant. The authors developed and validated a model, which was applied to assess the CES system performance when arbitrage, short term operating reserve and fast reserve were provided. The study demonstrated that, during off-design operation, round-trip efficiency and liquid air consumption could vary by up to 30 %, causing a loss of revenue of 10 thousand £/MW. Mazzoni *et al.* [112] evaluated the economic feasibility of the integration of a CES system and an Electrochemical Energy Storage technology as a polygeneration plant to satisfy the cooling and electric load from an Eco-building. The authors found that the 300 kWh capacity CES system, after 20 years of operation and prioritizing electrical power over heating and cooling power output, achieved a NPV of more than 2 million Singapore dollars and a payback period shorter than 7 years. Briola *et al.* [102] proposed a novel integration of a CES plant and a gas turbine cycle with an existing large-scale Natural Gas Combined Cycle (NGCC). The authors performed a thermodynamic evaluation and an economic uncertainty analysis through six uncertainty variables to assess the profitability of the stand-alone and integrated plant in three alternatives scenarios. The authors found that during the charging regime, the highest irreversibility took place in the compressor, while for discharging, the combustion chamber from the additional gas turbine resulted the most irreversible component. Another result showed that the integrated plant afforded profitability in the expected scenario in the specified range of discharge pressure. Gao *et al.* [113] proposed a CES system integrated into a combined cycle power plant with recovering of the waste heat and cold energy. The economic analysis showed that the NPV was $ 13.4 million for service life of 30 years and air turbine temperature of 373.15 K. The authors found that the lower the compressor and turbine inlet temperature, the better the economic feasibility of the system. For instance, for the turbine inlet air temperature of 373.15 K and the default compressor inlet temperature, the dynamic payback period and internal rate of return were 4.07 years and 39.4 %, respectively.

An economic analysis of three hydrogen liquefaction systems was presented in [114]. The operation, investment and maintenance costs were considered. The effect of liquid production rate and liquefier efficiency on electric power cost, operation and maintenance cost, effective cost of components and cost of liquid hydrogen were analyzed. The results showed that liquefaction cost was 0.63 $/kg for the optimized option when the liquid

production rate was of 30 t/h and electricity price of 0.04 $/kWh. An economic analysis of a hybrid CES system was presented in [85], the investigation pointed out to evaluate the benefits of the integration of an Organic Rankine Cycle and a vapor refrigeration compression cycle applying the annualized cash flow method. The influence of the discount and inflation rates on the Net Present Value (NPV), simple payback period (SPP) and savings to investment ratio (SIR) were analyzed. According to the authors, the combination of the ORC and VCRC leads up to a payback period of 2.7 years assuming a project useful life of 15 years and generates a saving to investment ratio of 3.08. The optimal NPV for this combination was about 3.5 million dollars, higher in 0.9 million respect to the ORC alone. The researchers also found that the discount rate has a higher significant effect on the economic parameters (NPV, SPP and SIR) than the inflation rate. They conclude that the proposed hybrid CES could be technically and economically feasible. A techno-economic comparison among the energy storage technologies in cooling applications to show their suitability at different scales was presented by Comodi *et al.* 2017 [106]. The authors focused on Li-Ion batteries (Li-Ion EES), sensible heat thermal energy storage (SHTES); phase change material (PCM-TES), compressed air energy storage (CAES) and cryogenic energy storage (CES) technologies. Levelized cost of energy, Pay-back period and savings per energy unit were the parameters used to analyze and compare the technologies in different scenarios. The authors described the technical and economical characteristics of CES systems collected from others researches, for instance, the specific installation cost and specific generation cost were ranged 900-2000 $/kW and 260-530 $/kWh, respectively. The useful life was estimated between 20 and 40 years, while the round trip efficiency was of 60-90 %. The article also referred to the pilot plant test results performed by researchers from Birmingham University. A cost effective solution of a liquefied natural gas (LNG) boil-off re-liquefaction plant and an on-board boil-off gas (BOG) re-liquefaction system as a cryogenic refrigeration cycle was conducted in [115]. A thermoeconomic optimization procedure to assess the LNG-BOG liquefaction system performance was applied. Using the genetic algorithm method, the minimization of the unit cost of the refrigeration effect as a product of BOG was implemented. A sensitivity analysis to study the effect of compressor pressure ratio and suction compressor pressure on total cost product rate was carried out. The results show that by increasing the pressure ratio, the total product cost rate is decreased.

The levelized cost of storage (LCOS) has been increasingly used by researchers in order to compare different types of storage technologies with different scales, investment and operating time periods. It is a useful metric that accounts for all technical and economic variables (efficiency, capital cost, operation and maintenance costs, replacement costs, among others) which affect the lifetime cost of the storage technology [116]. LCOS can be compared to the levelized cost of electricity (LCOE)[117], which is the price of electricity at which the energy is produced by the storage technology must be sold to

break even over the lifetime technology [118]. Hamdy *et al.* [119] carried out an economic sensitivity analysis of seven CES systems by evaluating the effect of price of electricity, specific investment cost, annual operation hours and economic life on the CES levelized cost of discharged electricity. The results revealed that the integration of waste heat reduced the specific energy cost from 1400 €/kWh to 1100 €/kWh. In addition, the diabatic CES system with combustion of natural gas reached the lowest levelized cost of electricity with 161 €/MWh followed by CES system with waste heat integration, which registered 171 €/MWh. In [120], the authors proposed a transient model to assess the performance of a 100 MW CES power plant with packed-bed cold-storage system. The economic study consisted of evaluating different scenarios of penetration of the photovoltaic and wind energy systems into the power grid with the integration of the CES plant. The results indicated the convenience to store photovoltaic energy during peak hours and release energy during the night-time to maximize the use of the storage plant. Additionally, the levelized cost of energy estimated for the CES system integrated into the power network was 150 €/MWh. A techno-economic feasibility study of a CES system integrated with ORC technology, based on LCOS methodology, was proposed by Tafone *et al.* [121]. The results showed the feasibility of recovering the low-grade heat discharged by the CES system with the use of an Organic Rankine Cycle. For a 100 MW/400 MWh CES plant operating 365 cycles per year and an electricity price of 0.15 €/kWh, the levelized cost of storage for full electric configuration registered a value of 0.385 €/kWh, whilst for cogenerative regime was 0.437 €/kWh. These results are comparatively lower than that of the LCOS values for stand-alone CES system, respectively. In addition, the authors found that LCOS is highly sensitive to the number of cycles per year, electricity price, CES plant integration and round-trip efficiency. Kim *et al.* [92] investigated a storage generation system using liquid air combined with liquefied natural gas (LNG). According to the results and depending on the size and the storage time, the levelized cost of energy (LCOE) ranged from 142.5 to 190.0 $/MWh, which is competitive with others storage technologies. In another research, Georgiou *et al.* [122] provided a thermo-economic analysis of two large-scale electricity storage technologies, Pumped Thermal Electricity Storage (PTES) and CES. The study focused on system efficiency, power capital cost ($/kW) and energy capital cost ($/kWh). The authors found that the CES technology enhanced significantly its performance through the integration and utilization of waste heat and cold streams. The comparison of the CES and PTES technologies at the same capacities (2 MW/11.5 MWh) showed that power capital cost, energy capital cost and LCOS for CES system were slightly higher than PTES system. The financial feasibility of the storage systems over their lifetimes also indicated the advantage for the PTES system when considering the buy price of the electricity (peak-times) above of removed 0.15 $/kWh. Moreover, the authors introduced a level of uncertainty for the maintenance costs, discount rate and energy cost (off-peak electricity cost) parameters. For this analysis, CES system presented

higher vulnerability to the market fluctuations electricity prices than PTES system, due to the low round-trip efficiency and the high energy consumption during the compression process.

The economic evaluation of the integration of CES technology into geothermal power plants has received the attention of some researchers. For example, a thermoeconomic optimization applying genetic algorithm of a hydrogen liquefaction system assisted by geothermal power plant was conducted in [123]. The author performed the study to minimize the unit cost of hydrogen liquefaction. The optimization results demonstrated that the specific energy consumption was found to be 10.06 kWh/kg of liquid hydrogen. The exergetic cost of liquid hydrogen resulted in 1.114 $/kg. Yilmaz and Kaska 2018 [124] presented a study of a hybrid system integrated by a hydrogen liquefaction Claude cycle and an absorption pre-cooling refrigeration process assisted by geothermal heat. The authors applied thermoeconomic optimization procedure using genetic algorithm method to minimize the unit cost of the liquefied hydrogen. They found that cooling down hydrogen gas to -30 °C the exergetic cost was reduced 2.42 $/kg of liquid hydrogen. The optimized exergetic cost was found in 1.349 $/kg of liquid hydrogen. Kaska *et al.* 2018 [125] carried out a thermodynamic assessment of a Organic Rankine Cycle (ORC) using a geothermal source of energy and a Claude cycle for hydrogen liquefaction. Applying the first and second laws of Thermodynamics the exergetic cost of the liquid hydrogen and electricity produced were calculated. The study showed that the electricity cost was found to be 0.025 $/kWh and that of liquefaction was about 39.7 % lower than direct value (1.650 $/kg) given in the literature.

The previous literature reviews show the variety of scientific researches about the economic analysis of CES systems and their integration with other technologies. However, the number of studies with a detailed economic analysis and relevant information about cost structure is limited. Most economic studies are conducted using specific costs ($/kW or $/kWh) as the basis for calculation. This procedure can lead to underestimating some elements of investment costs and distorting the results of the economic indicators. Additionally, the marketable product is generally directed to electricity, but other commercialization options must be added, such as cold and heat loads for external users, which some investigations have already been considered previously [121, 107]. Another marketable final product is the cryogenic fluid, whose commercialization can contribute to the economic feasibility of the CES technology, to the expansion of the small scale cryogenic generators and reduce fuel consumption in the transport sector [15]. To fill these gaps, this research assesses the economic feasibility of cogeneration CES systems with different operation modes and highlights the economic viability of the simultaneous operation of the charging and discharging processes, which has not been presented and demonstrated before, as a novel contribution to improve the performance of this technology.

2.7 Summary of literature review.

It is clear, from the above-mentioned literature reviews, that there are several researches on proposing and evaluating both stand-alone and integrated CES systems for the electricity generation only or poly-generation (cogeneration and trigenration). Despite this, some limitations have been identified in the current researches, which opens a door of opportunities for further investigations in the identified areas of interest.

Simultaneity for storage and discharge processes. None of these studies has brought up the simultaneous operation of the charging and discharging processes for CES systems operating in a cogeneration regime, and neither have they quantitatively evaluated the effect of this simultaneous operation on the main indexes and indicators. The advantages of the simultaneous operation of the charging and discharging processes lie on the increase of the exergy utilization factor through the production of an extra cooling load from an evaporator, the reduction of the power demand during the charging process through the additional power generation in the expansion section of the cycle, and the possibility of reducing the operating costs. Furthermore, this operation mode constitutes a novelty for CES systems, which may potentially be registered as an invention according to the overall literature review. Table 2.5 summarizes the main patents registered on CES systems from 1992 to 2021.

Transient regime for the storage tank. For an obvious simplification, the charging regime at the cryogenic tank is frequently treated as a steady state process in order to estimate the specific liquid yield. In the author's knowledge, the evaluation of the charging process in the cryogenic tank considering transient regime in order to obtain both the specific liquid yield and charging time has not been performed before.

The integration of heat source. The integration of waste heat from an industrial process or a power plant into CES systems has been suggested and evaluated for some authors in order to improve the round-trip efficiency, but no studies have quantified the effect of this integration on cogeneration CES systems thermodynamic and economic performance when both storage and discharge processes are simultaneously executed.

Specific costs for economic evaluation. The economic evaluation for CES systems is generally conducted by using of power and energy specific costs as the calculation base. Taking into account that CES system is a new technology in development and that the specific costs in literature vary significantly, the above assumptions can lead to inaccurate results.

Poly-generation and economic feasibility. The researches about CES systems have been focused on electricity generation and its commercialization in order to demonstrate the economic viability of this technology. However, besides producing electricity, the CES systems can also provide cooling load and cryogenic fluids to external users. This

potential of CES technology has not been thoroughly studied. Furthermore, the economic evaluation results for this emerging technology changes from one region to another, that is why, case studies are essential to be applied. The cryogenic fluids are widely used in the health, livestock, food and research (physics of the condensed matter and solid state) sectors. Moreover, cryogenic fluids could also be integrated into a transport, distribution and storage network for power generation and refrigeration in lorries [15]. The diversity of possibilities of use of cryogenic fluids in the economic and service sectors in Brazil would create opportunities for the expansion of CES systems, for example, at the LNG regasification terminals [126], where the waste cold exergy from the regasification process can be used for air liquefaction [26, 127]. Additionally, emergency power systems using cryogenset (storage tank, heat exchanger, turbine and generator) [15] could be widely applied into the service sector in order to replace the diesel generators and reduce the green house gas emissions.

The conducted literature reviews also identified some drawbacks for CES systems, specifically: (i) environmental issue when CES systems are integrated to combustion technologies based on fossil fuels; (ii) geographical restriction for CES systems with external heat source coming from geothermal cycles; (iii) low energy density which increases the volume of the storage tank and consequently the investment cost; and (iv) overestimation of the storage efficiency of regenerators using liquid or solid substances as storage media.

In order to cover the knowledge gaps as well as to address the aforementioned drawbacks, a novel cogeneration CES system based on Claude cycle from [9] is proposed, using only air as working fluid. The main modifications incorporated into the proposed cogeneration CES system are summarized as follows: (i) it liquefies a minor amount of fluid during the power generation regime, and generates a minor amount of power during the liquefaction regime; (ii) it uses a multi-expansion turbine with re-heaters fed by an external source of energy [25, 26, 27]; (iii) it uses an expander split into two sections, employing the environment as a heat source before the second expansion, a technique that increases power production and improves the liquefaction process. The proposed CES system does not have any environmental issue associated with the use of fossil fuels or toxic substances. Furthermore, it is geographically unconstrained due to the use of a simple cryogenic fluid (air) and easily adapted to consume electricity and heat from renewables or conventional power plants. In order to conceive a simple cycle without the presence of regenerators with low efficiency, the only way of storing energy for the cogeneration CES system is in the form of liquid air in the cryogenic tank whose storage capacity can be selected to meet the external demands of electricity and cooling loads. The present work aims to enhance the performance of the base case CES system by employing cogeneration, a new layout architecture for power production and the simultaneous operation of the charging and discharging circuits.

Table 2.5 – Summary of the main patents on CES systems from 1992 to 2021.

Authors	Type of CES	$\eta_{rt}(\%)$
Ha, 1992 [128]	Air Separation Unit (ASU)-Expander	-
Atsumi, 1996 [129]	Gas turbine-Storage tank	-
Wakana *et al.*, 2001 [130]	Gas turbine-Storage tank	-
Chino *et al.*, 2003 [131]	Gas turbine-Storage tank	-
Shirk *et al.*, 2005 [132]	Rankine-Cryogenic storage tank	-
Claire, 2006 [133]	Cryogenic storage tank-propeller	21.0
Chen *et al.*, 2007 [134]	Linde-Hampson-ASU-Storage tank	172.3
Chen *et al.*, 2009 [64]	Linde-Hampson-ASU-Storage tank	172.3
Vandor, 2011 [135]	Kapitza, Linde-Hampson Storage	108.5
Morgan *et al.*, 2013 [136]	Claude-Storage tank	-
Cook *et al.*, 2015 [137]	Simple expansion Cryogenic tank	-
Alekseev, 2015 [138]	Linde-Hampson (L-H) Cryogenic tank	-
Porto *et al.*, 2016 [139]	L-H, Claude and Collins Cryogenic tank	-
Chen *et al.*, 2016 [140]	Linde-Hampson-ASU Storage tank	172.3
Chen *et al.*, 2016 [141]	Linde-Hampson Storage tank	-
Naumovitz *et al.*, 2017 [142]	Cold storage-Heat pipes	-
Morgan *et al.*, 2018 [143]	Claude, Kapitza, Cryogenic storage tank	-
Ding *et al.*, 2018 [144]	CES-Battery-Cryogenic storage tank	-
She *et al.*, 2018 [145]	Hybrid-Linde-Hampson Storage tank	-
Upperman *et al.*, 2019 [146]	Heylandt Cryogenic storage tank	-
Conlon, 2019 [147]	Heat engine-CES Cryogenic tank	46.9
Upperman *et al.*, 2020 [148]	Heylandt Cryogenic storage tank	-
Conlon, 2020 [149]	Gas turbine-CES Cryogenic tank	69.5
Sinatov, 2020 [150]	CHP: Gas turbine-CES	79.3
Conlon, 2021 [151]	CCCPP: ORC-Gas turbine-CES	144.4

3 Research methods

This chapter provides the research methods associated with the thermodynamic and economic analysis of cogeneration CES systems with the simultaneous operation of the charging and discharging processes to achieve the objectives of the present work. The main characteristics of the CES cycles are described. The energy and exergy analyses based on mathematical models to assess the thermodynamic performance of the CES systems are applied. Additionally, economic analysis for three alternatives of cogeneration CES systems is carried out. Likewise, optimization and uncertainty tools are applied to come up with the optimal parameters and indicators of the proposed CES systems and, respectively, prove the accuracy of the economic results. In this work, the metric system of measurement used is the International System of Units established in 1960 [152].

3.1 System description.

A simplified schematic diagram of a conventional stand−alone CES system is shown in Fig. 3.1. Off−peak or renewable electricity is used to drive the compressor (C) and a fraction of air mass flow rate ($\dot{m}_c$) is liquefied by expansion in the Joule-Thomson valve (JT-V) and stored in the cryogenic tank, which must be well insulated to reduce heat leak [153]. On peak time or when power is required, liquid air is pumped through a cryogenic pump (CP) and evaporate in a heat exchanger, then gas mass flow rate ($\dot{m}_p$) at high pressure runs the turbine (T) to produce electricity. Cold from the evaporation process is recycled and waste heat from the charging section or external source can be used to improve the performance of the cycle. The air flow throughout the recycling circuit is promoted by a flow machine. The traditional form to operate CES system has been established by means of the separation of the charging and discharging processes. This thesis proposes an alternative of operation for CES systems combining or running simultaneously the liquefaction and expansion processes. For this, during charging regime, a low liquid air mass flow rate ($\dot{m}_p << \dot{m}_c$) is evaporated and then expansioned in the turbine to produce power, and at the same time reduce the required liquefaction work. Whilst for discharging process, a reduced air mass flow rate ($\dot{m}_c << \dot{m}_p$) is liquefied in order to extent the electricity generation, guarantee the steady state operation and enhance the thermal inertia during the inversion process.

Claude cycle has been studied by many researches [10, 52, 55, 88, 70, 154], and results reveal that it performs an efficient liquefaction process. Abdo *et al.* [9] proposed the schematic of Figure 3.2 to be compared with Linde-Hampson and Collins liquefaction cycles. In this cycle, for charging process, the air ($\dot{m}_c$) is compressed (1-2) at high pressure,

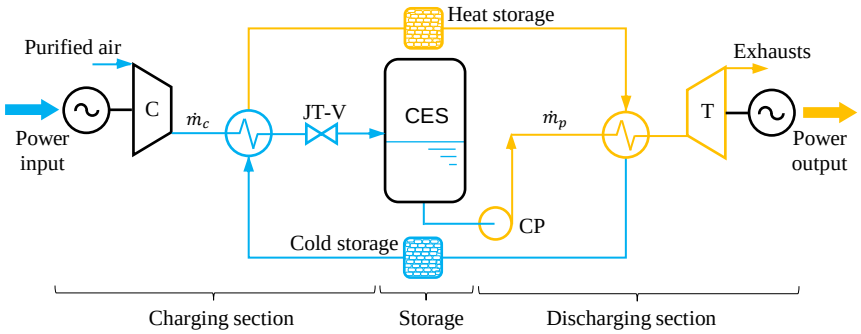

Figure 3.1 – Schematic of a conventional stand-alone CES system with heat and cold storage.

and then is cooled through the heat exchangers (2-6), and expanded through an expansion valve (6-7) to the storage of liquid air. After the first heat exchanger, a fraction of air is diverted (13) and expanded (13-14) in a single expansion turbine (T-1), which reduces the power required by the compressor. The return air gas ($\dot{m}_g$, state 8) flows through the three heat exchangers (8-12) to cool the high pressure air. Similarly, a reduced liquid air mass flow rate ($\dot{m}_p$) serves as a second cooling circuit (17-19), which is expanded for power production (19-20). For discharging process, the cycle operates in a similar way, but with a reduced air mass flow rate ($\dot{m}_c$) through the liquefaction circuit. The main limitations of this cycle are found in the reduced harness of the exergy from the cooling circuit 2 for both charging and discharging processes (possibility of using an evaporator), the low use of electricity generation potential from T-2 (possibility of using a multiexpansion turbine), and the insufficient use of the electricity generation potential at the expander (T-1) without compromise the cold production (use of double expansion). Based on this study, the present work proposes alternative conceptual changes in the operation mode and the topology of the cycle, as shown in Fig. 3.3.

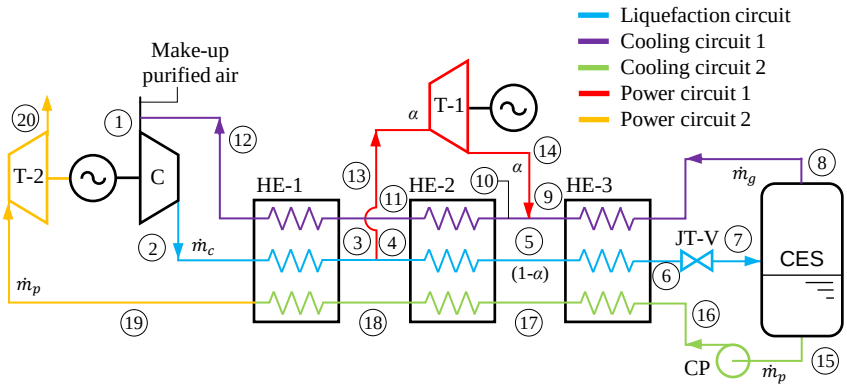

Figure 3.2 – Schematic of the modified Claude liquefaction cycle studied in [9]

.

The selection of the Claude cycle in this research obeys its appropriate technical

characteristics and advantages with respect to other liquefaction cycles. For instance, for the same working fluid, Claude cycle presents higher specific liquid yield and efficiency than Linde-Hampson cycle [52, 155] and slightly higher figures to Collins cycle [9]. Another advantage is the basic layout of the components. In this regard, Claude cycle has three heat exchangers and an expander, which are useful to reduce the power consumption from the compressor. While Linde-Hampson cycle does not have expander, Collins cycle has two and six heat exchangers [54, 73], which represent the double of the elements in the liquefaction section compared to Claude cycle. In spite of the number of expanders in the Collins cycle, the required specific work to produce the unit of liquid air is higher than Claude cycle [9]. Additionally, Claude cycle can be more easily integrated to other storage technologies, conventional or renewable power plants [28, 88], modified [156, 157, 158] and uses different working fluids [18, 51]. These aforementioned advantages of Claude cycle make it suitable for cogeneration purposes.

Figure 3.3 depicts the proposed cycle with the main modifications. The liquefaction process is represented by the sequence of thermodynamic states 2-7. This is the path followed by the air up to the cryogenic tank. The secondary circuits responsible for cooling are: Cooling circuit 1 (8-12) and Cooling circuit 2 (18-21). Also, power is produced from: Power circuit 1 (13-16) and Power circuit 3 (22-30). The non-consecutive numbering of power circuits obeys the order that the three turbines (Figures 3.4 and 3.5) would finally have when replacing the expansion valve with a cryogenic hydraulic turbine.

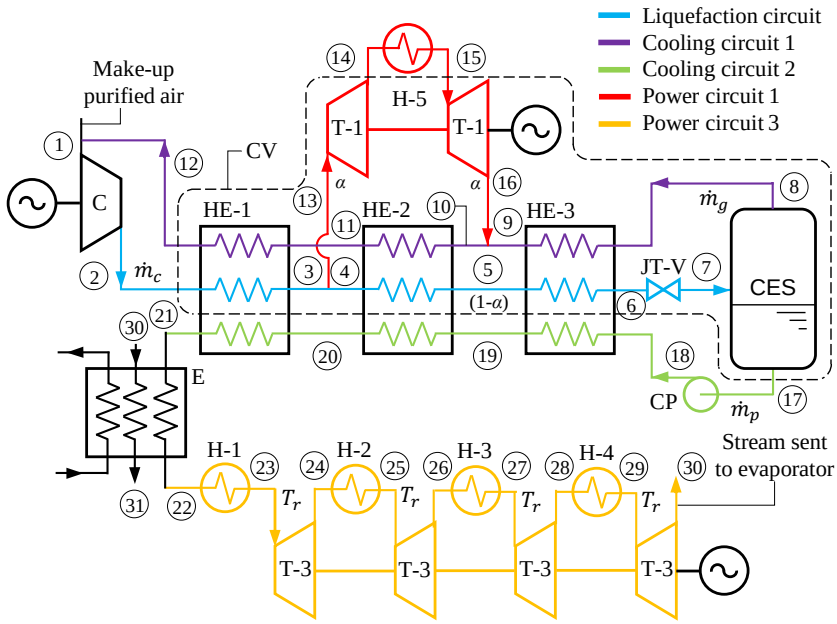

Figure 3.3 – Proposed CES system. The system is divided in liquefaction, cooling and power circuits. During discharging regime, section 19 to 21 is bypassed (HE-1 and HE-2 are not used)

.

The main cooling section is the Cooling circuit 1 (8-12). Part of the fluid from the Liquefaction circuit (2-7) is bypassed to the two section cryogenic turbine through the Power circuit 1 (13-16) with intermediate reheat (14-15) up to environment temperature, which increases the cooling effect of sections 8-12, and at the same time, more power is produced, and consequently, less work is needed by the cycle. Additionally, cooling is provided to section 2-7 coming from Cooling circuit 2 (18-21). In section 21-22 and 30-31, the cycle serves as a cooling source for an external load at the evaporator (E), turning the cycle in a cogeneration system. In the previous research [10], this available exergy cooling load was not utilized. An additional power circuit is also proposed in Power circuit 3 (22-30), using the multi-expansion turbine (T-3) with reheat temperature (T_r) at every stage. For turbines, the power changes with the number of expansion stages. The higher the turbine stages, the higher power generation when the inlet pressure of the working fluid gradually increases [159]. Likewise, the increase of power generation with the number of expansion sections is meaningful in the first three or four stages. For five or six expansion sections, the trend of power gain is reduced and the power plant becomes more complex, which can led to increase the irreversibilities. Consequently, the use of four section expansion turbine is generally recommended [70, 79].

The main proposed operation modes for CES systems are explained as follows. In the charging mode, mass flow rate of sections 18-21, which is driven by a cryogenic pump, is much lesser than the one coming from the compressor ($\dot{m}_p << \dot{m}_c$). Under this condition, cooling load is provided to an external user through the evaporator and the additional power generated at the multi-expansion turbine further reduces the power required for the liquefaction process. During the discharging mode, the system remains operating with the same components, with the exception that: (i) $\dot{m}_c << \dot{m}_p$; and (ii) HE-1 and HE-2 in the Cooling circuit 2 are bypassed, due to the lower required cooling load. Figures 3.6 and 3.7 show the temperature and entropy diagrams for the cycle in charging and discharging regime, respectively.

In order to assess the thermodynamic and economic performance of the proposed alternatives, based on the conventional cycle shown in Fig. 3.2, three operation modes and modifications in the topology have been also considered. For operation mode A is used the Fig. 3.4. For this, the expansion valve (Fig. 3.2), which executes a highly irreversible process, is substituted by a hydraulic cryogenic turbine (T-2). An evaporator (E) is added to provide cooling load to an external user. Moreover, the single expansion turbine in Fig. 3.2 is replaced by the four section expansion turbine (T-3) and the air stream from the final expansion (Fig. 3.4) is returned to the evaporator to increase the cooling load and turn the cycle more efficient. For the operation mode A, the charging and discharging processes are performed as usual, that is, separately.

Figure 3.5 illustrates the proposed CES system to evaluate its performance for

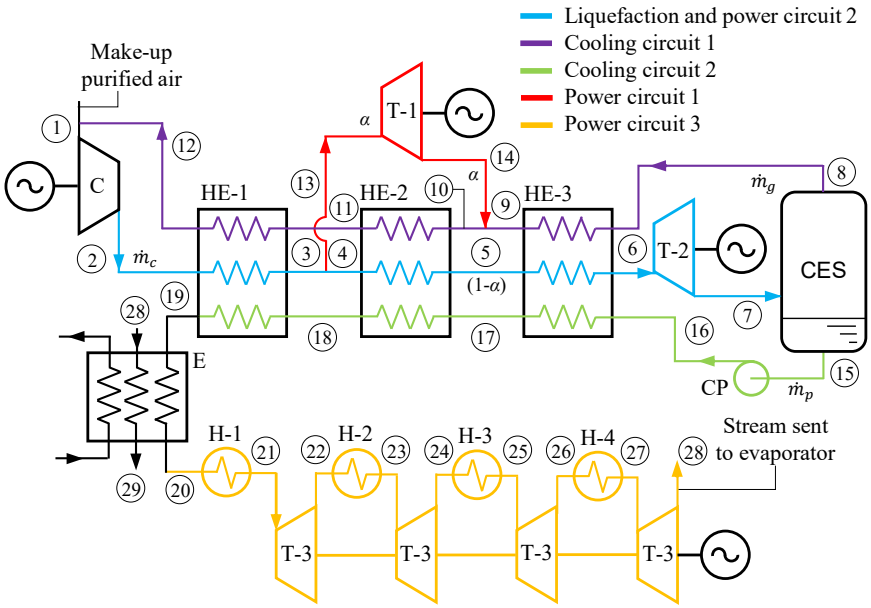

Figure 3.4 – Schematic of the modified Claude liquefaction cycle for cogeneration regime with a hydraulic expansion turbine (operation mode A)

.

two operation modes, that is, B and C. The liquefaction process is represented by the sequence of thermodynamic states 2-7. For this, three heat exchangers are used, identified as HE-1, HE-2 and HE-3. This is the path followed by the air up to the cryogenic tank. At the cryogenic turbine (T-2), the air is expanded (6-7) from the compressed liquid region to the liquid-gas region, then the phases are separated in the cryogenic storage tank. The secondary circuits responsible for cooling are: Cooling circuit 1 (8-12) and Cooling circuit 2 (18-21). Also, power is produced from: Power circuit 1 (13-16), where a two section expansion turbine is used rather than the single expansion turbine from Fig. 3.2; Power circuit 2 (6-7); and Power circuit 3 (22-30). At the turbine T-3, the air is reheated in every stage up to T_r temperature.

The main differences between the operation modes B and C are explained as follows. For mode B, during charging process, the air mass flow rate through the compressor is greater than the expansion section ($\dot{m}_c >> \dot{m}_p$). Under this condition, the liquid air mass flow rate ($\dot{m}_p$) does not surpass the liquefaction rate (dm/dt) in the storage tank, also a cooling load is served to an external user through the evaporator and an additional power generated at T-3, reducing the required power for the liquefaction process. During the discharging process, the CES system remains operating in the same way, with the exception that: (i) $\dot{m}_c << \dot{m}_p$, in contrast to what happens in the charging regime; and (ii) HE-1 and HE-2 in the Cooling circuit 2 are disabled to exchange heat, due to the lower load necessary to liquefy the air. For mode C, the charging process is identical to the operation mode B. Whilst for discharging process, only the equipment from the

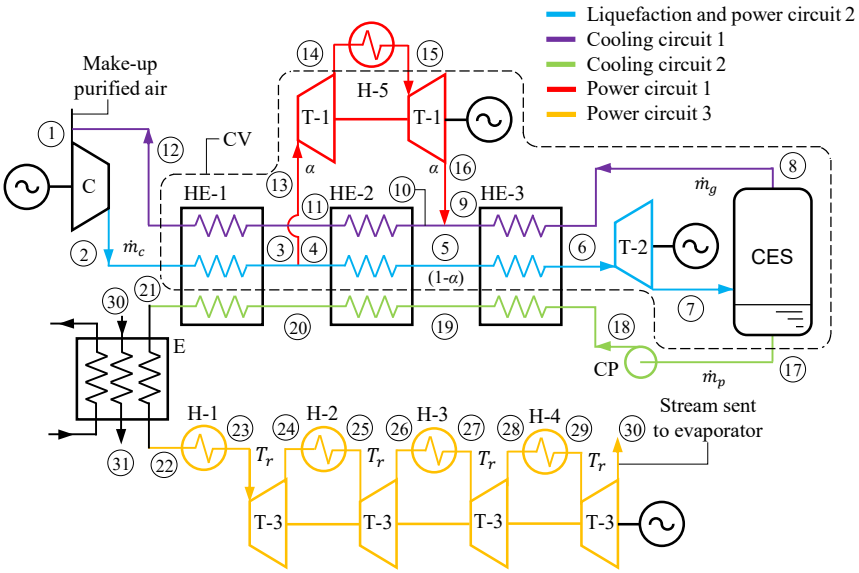

Figure 3.5 – Schematic of the proposed CES system with a hydraulic cryogenic turbine (operation mode B and C)

.

expansion section operates, that is, the cryogenic pump (CP), the evaporator (E) and the four sections expansion turbine (T-3). Figures 3.8 and 3.7 show the temperature and entropy diagrams for the cycles in the charging and discharging regime, respectively.

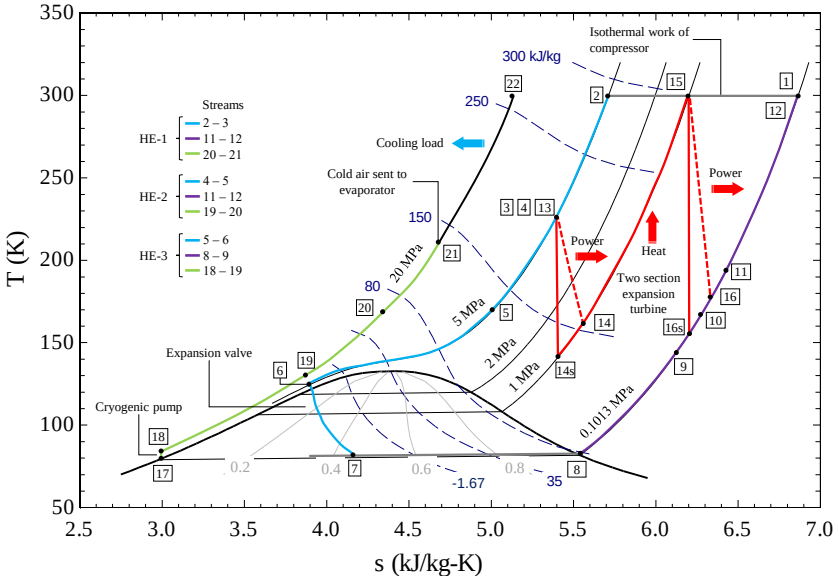

Figure 3.6 – Temperature and entropy diagram of the Claude cycle during charging regime

.

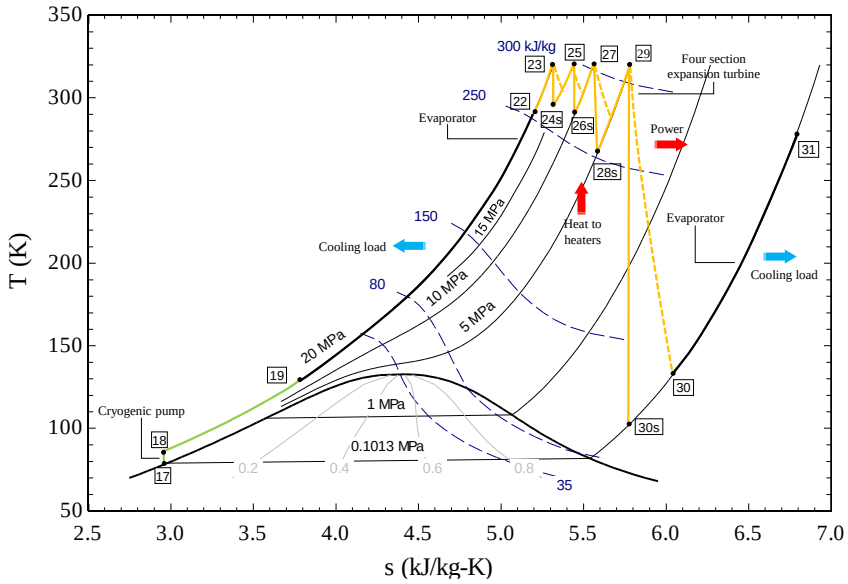

Figure 3.7 – Temperature and entropy diagram of the Claude cycle during discharging regime

.

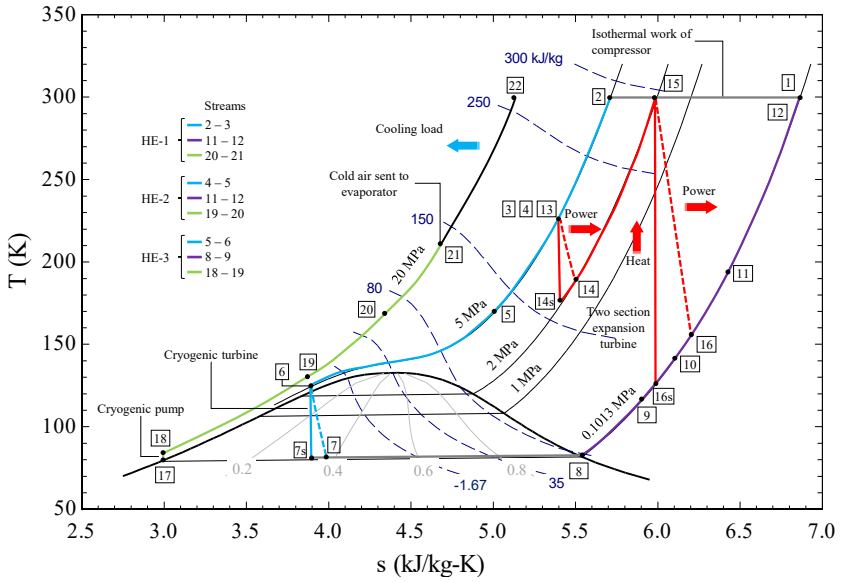

Figure 3.8 – Temperature and entropy diagram of the Claude cycle during charging regime with a hydraulic cryogenic turbine

.

3.2 Mathematical model and assumptions.

The general methodology applied for thermodynamic and economic evaluations of the cogeneration CES systems is illustrated in Fig. 3.9. Similarly, the general mathematical model algorithm applied in this study is shown in Fig. 3.10. In order to define the most feasible alternative among CES systems from a thermodynamic and economic point of view, the assumptions for the simulation procedure are assumed as follows: (i) the cryogenic

Table 3.1 – Data and assumptions for thermodynamic analysis of the CES systems.

Parameter	Unit	Value	Ref.
Ambient pressure	MPa	0.1013	[161]
Ambient temperature	K	298.15	[161]
Outlet compressor pressure	MPa	5.0	[10]
Outlet pump pressure	MPa	20.0	[10]
Compressor isothermal efficiency	-	0.87	[10, 92]
Turbine isentropic efficiency	-	0.90	[86, 65, 162]
Pump isentropic efficiency	-	0.78	[10, 76]

Table 3.2 – Data and assumptions for economic analysis of the CES systems.

Parameter	Unit	Value	Ref.
Cycles per year, c_y	c/y	730 - 2190	[121, 119]
Economic life, n	years	30	[92, 163]
Interest rate, i	%	6.0	[109]
Inflation rate, I	%	1.5	
Peak electricity price, E_T	$\$/kWh$	0.2249	[164]
Off-peak electricity price, E_T	$\$/kWh$	0.0897	[164]
Price of heat, C_H	$\$/kWh$	0.0098	[163]
Price of cooling, C_C	$\$/kWh$	0.059	[163]
Price of liquid air, C_L	$\$/kg$	0.324	[165]

tank operates at transient regime and constant pressure of 0.1 MPa. The rest of the thermodynamic states are assumed to be at steady state; (ii) changes on potential and kinetic energy are neglected; (iii) compressor, pump and turbine efficiency does not depend on pressure, temperature or mass flow rate; (iv) negligible pressure drop in heat exchangers and pipelines; (v) thermodynamic properties of the working fluid are evaluated using the EES software as a real gas; (vi) the electrical efficiency of the generator is 100 %; (vii) the heat transfer (heat leak) between the subsystems and the surroundings is only considered at the heat exchangers; and (viii) the throttling process in the expansion valve is isenthalpic. The heat leaks by volume per day in low-pressure cryogenic tanks reported in literature oscillate from 0.05 % to 0.2 % decreasing with cryogenic tank size [65, 160, 76, 110]. That is why the heat leaks at the cryogenic tank are considered negligible. The general assumptions made for thermodynamic and economic simulations are summarized in Tables 3.1 and 3.2, respectively.

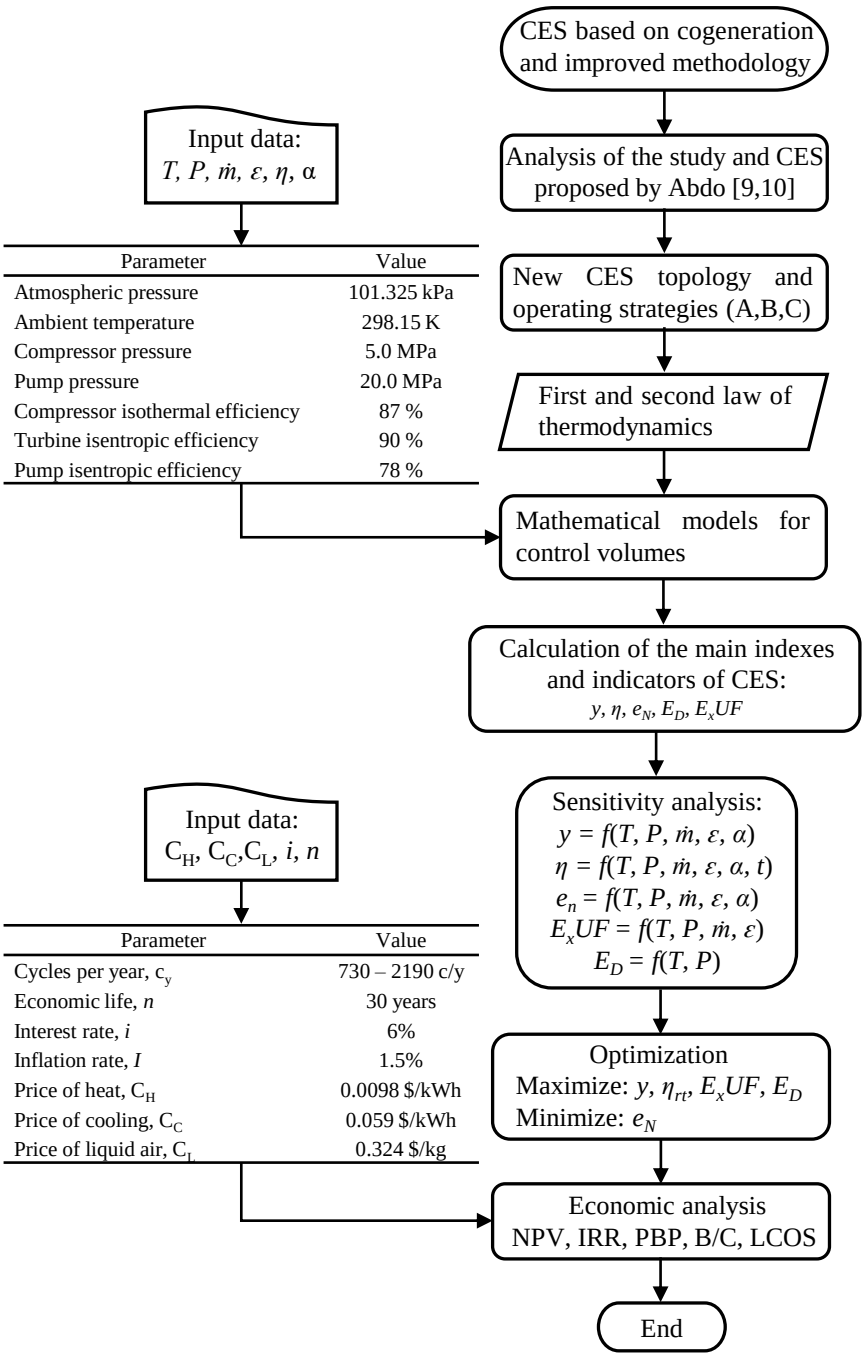

Figure 3.9 – Flow chart of the general methodology for cogeneration CES cycle analysis.

3.3 Thermodynamic modeling.

3.3.1 Heat exchangers.

The three-fluid counter flow heat exchangers are modeled by NTU method [166, 167, 168] to find the inlet and outlet temperatures by iterative procedure as shown in Fig. 3.11. The heat exchanger effectiveness (ε) is defined as the ratio of the actual heat transfer rate to the maximum possible heat transfer rate. For each heat exchanger, the

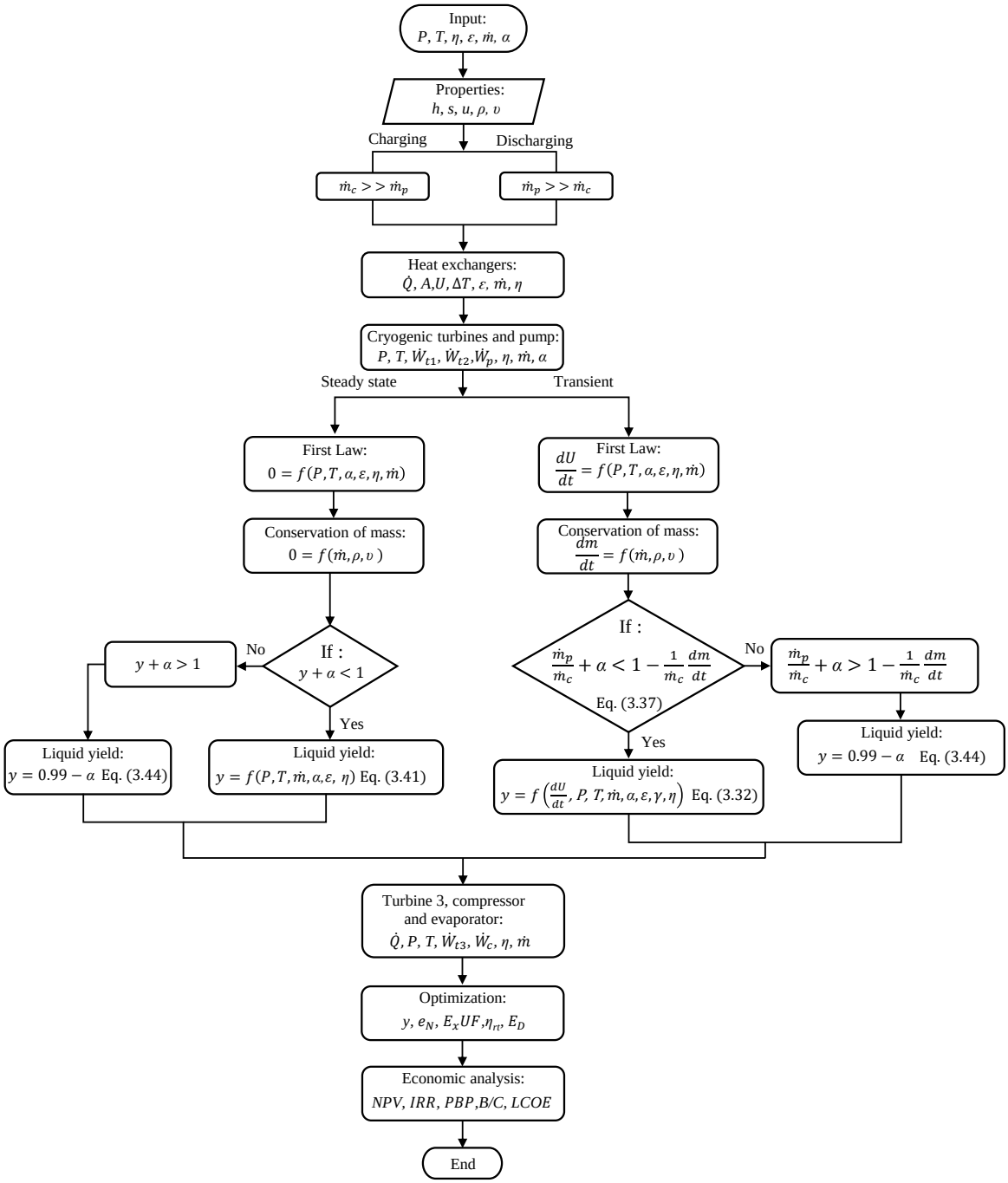

Figure 3.10 – Flow chart pattern of the applied general mathematical model for the CES systems.

effectiveness and energy balance equations are applied.

$$\varepsilon_k = \frac{\dot{Q}_{a,k}}{\dot{Q}_{max,k}} = \frac{C_h(T_{h,i} - T_{h,o})}{C_{in}(T_{h,i} - T_{in,i}) + C_c(T_{h,i} - T_{c,i})} \tag{3.1}$$

where, C_h, C_{in} and C_c are the capacity rates of the hot, intermediate and cold fluids, respectively. The capacity rate is the product of mass flow rate and specific heat capacity

for every stream. $T_{h,i}$, $T_{in,i}$ and $T_{c,i}$ represent the inlet temperature of hot, intermediate and cold fluids, respectively. The outlet temperature have been set with the subscript o. For the study, the hot fluid is identified by stream 2-6, which flows counter-current in respect to intermediate (8-12) and cold (18-21) streams as illustrated in Figs. 3.3, 3.4 and 3.5, respectively.

The critical part for heat exchangers analysis is that only T_2, T_8 and T_{18} temperatures are known. The T_8 and T_{17} values, which represent respectively the saturated vapor and liquid, are set by the cryogenic tank pressure. All the intermediate temperatures ($T_3 = T_4$, T_5, T_6, T_9, T_{10}, T_{11}, T_{19} and T_{20}) are unknown variables. Based on the fact that the effectiveness of the heat exchangers must be high enough to achieve high liquefaction rates [52] and in the light of increasing effectiveness with decreasing liquefaction air temperature [54], it is set to be $\varepsilon_1 = 0.96$, $\varepsilon_2 = 0.97$ and $\varepsilon_3 = 0.98$, respectively. As the air compression in the compressor is considered as isothermal, $T_2 = T_{12i}$ for ideal conditions. When the effectiveness concept of HE-1 is considered for one stream, $\varepsilon_1 = (h_{12} - h_{11})/(h_{12i} - h_{11})$, the actual intermediate outlet temperature (T_{12}) is lower than the ideal one ($T_{12} < T_{12i}$). The previous procedure is also applied to HE-2. Considering that the heat absorbed in the cold box takes place by the heat transfer process between the intermediate and cold fluids with the surroundings, the heat lost at every heat exchanger is given by Eq. 3.2.

$$\dot{Q}_{0,k} = (1 - \varepsilon_k)[\dot{m}_i(h_{in,o} - h_{in,i}) + \dot{m}_p(h_{c,o} - h_{c,i})] \tag{3.2}$$

The equivalent effectiveness (ε) can be deduced considering that the total heat transferred in the cold box is the sum of the heat transferred by each heat exchanger, that is:

$$\begin{aligned}\varepsilon = \varepsilon_1 \frac{(h_2 - h_{11})}{(h_2 - h_8) + (h_2 - h_{18})} + \varepsilon_2 \frac{(h_4 - h_{10})}{(h_2 - h_8) + (h_2 - h_{18})} \\ + \varepsilon_3 \frac{(h_5 - h_8)}{(h_2 - h_8) + (h_2 - h_{18})}\end{aligned} \tag{3.3}$$

The specific heat capacity of cryogenic fluids (Air, N_2, CO_2, and others) vary dramatically with temperature as the pressure approaches the critical point (pseudocritical region), this characteristic must be considered when cryogenic heat exchangers are evaluated. For this reason, every heat exchanger is discretized into N elements or nodes (N=150) in order to take into account the variation of fluid properties with temperature. By iterative procedure, the N value was chosen according to the minimum difference (absolute convergence error) between the heat transfer areas obtained for N and N+1, respectively [169, 170]. Fig. 3.12 shows the discretization scheme for the heat exchangers modeling. For every node j, the heat capacity rate of the hot, cold and intermediate fluid are given by equations Eqs. 3.4, 3.5 and 3.6, respectively.

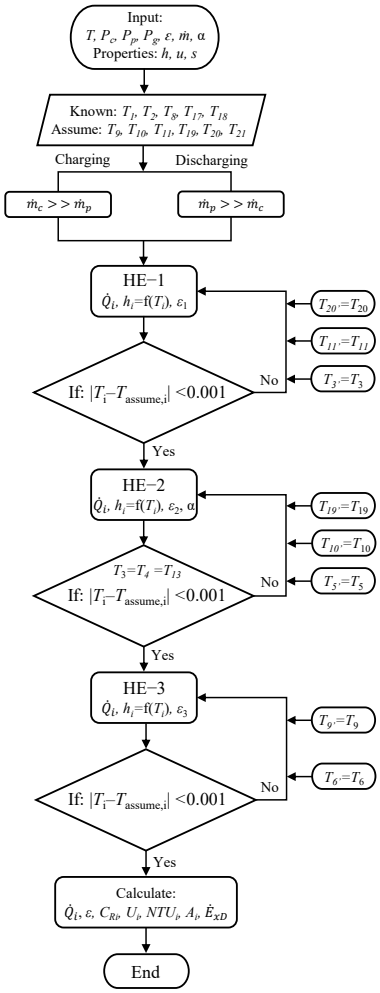

Figure 3.11 – Flow chart layout for the iterative method applied for heat exchangers modeling.

$$C_{h,j} = \dot{m}_h \frac{h_{h,j} - h_{h,j+1}}{T_{h,j} - T_{h,j+1}} \tag{3.4}$$

$$C_{c,j} = \dot{m}_c \frac{h_{c,j} - h_{c,j+1}}{T_{c,j} - T_{c,j+1}} \tag{3.5}$$

$$C_{in,j} = \dot{m}_{in} \frac{h_{in,j} - h_{in,j+1}}{T_{in,j} - T_{in,j+1}} \tag{3.6}$$

Where, the subscripts j and j+1 represent respectively the fluid outlet and inlet at every node. $\dot{m}_h$, $\dot{m}_c$ and $\dot{m}_{in}$ are the air mass flow rate for the hot, cold and intermediate stream, respectively. In the application of this procedure, the temperatures and enthalpies are firstly updated, and then the heat capacity rate. The actual heat transfer rate at every node ($Q_{ak,j}$) and the heat leak ($Q_{0k,j}$) are defined by the discretization of the heat balance equations (Table B.1 from Appendix B) for each heat exchanger and Eq. 3.2, respectively.

Then, the heat capacity ratio for every node of the heat exchanger is calculated when $C_{min,j}$ and $C_{max,j}$ are identified.

$$C_{R,j} = \frac{C_{min,j}}{C_{max,j}} \tag{3.7}$$

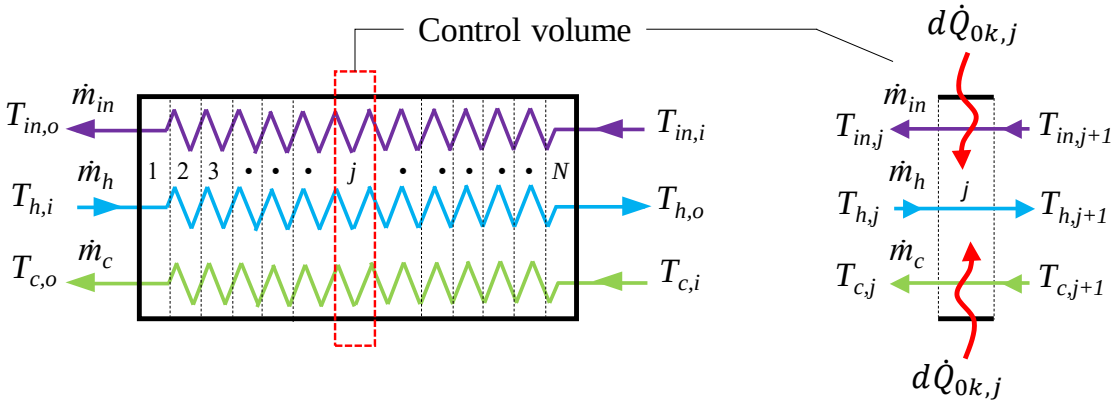

Figure 3.12 – Discretization diagram for heat exchanger modeling.

For the mixing point, located between HE-2 and HE-3, Fig. 3.3, the heat and mass balance equations are applied: $\dot{m}_9 h_9 + \dot{m}_{16} h_{16} = \dot{m}_{10} h_{10}$ and $\dot{m}_9 + \dot{m}_{16} = \dot{m}_{10}$, respectively. The resultant state (10) at the mixer point will depend on temperature and mass flow rate coming from the HE-3 (9) and the second stage of the cryogenic turbine (16). The actual condition at state 16 is obtained by considering the isentropic efficiency of the turbine given in Fig. 3.9, that is, $\eta_t = (h_{15} - h_{16})/(h_{15} - h_{16s})$. All the early assumed temperatures are corrected by using the convergence criteria for every heat exchanger as indicated in Fig. 3.11. The subscript s at η_t equation represents an ideal isentropic expansion process.

For design conditions, the product of the overall heat transfer coefficient and reference surface area (UA) for the entire heat exchanger is essential [171, 172]. Therefore, in order to determine the heat transfer area for every heat exchanger, the overall heat transfer coefficient (U_k) at off-design condition is chosen according to fluids phases interaction [37] and varying in respect to air mass flow rate at every heat exchanger [111] according with Eq. 3.8.

$$U_k = U_0 \left(\frac{\dot{m}_k}{\dot{m}_0} \right)^{\beta} \tag{3.8}$$

where U_0 and $\dot{m}_0$ are respectively the overall heat transfer coefficient and air mass flow rate for design conditions. In particular, U_0 is assumed to be 0.9 kW/m^2K [173, 174] and $\dot{m}_0$ is selected according to the cryogenic tank capacity. β is an exponent that depends on the heat exchanger configuration, for this study is taken as β=0.66 [175].

The number of transfer unit ($NTU_{k,j}$) within each node is modelled by Eq. 3.46 [37].

$$NTU_{k,j} = \frac{1}{1 - C_{R,j}} ln\left(\frac{1 - C_{R,j}\varepsilon_k}{1 - \varepsilon_k}\right) \tag{3.9}$$

The heat transfer area of each element and the total area of every heat exchanger are calculated by Eqs. 3.47 and 3.66, respectively.

$$A_{k,j} = \frac{NTU_{k,j} C_{min,j}}{U_k} \tag{3.10}$$

$$A_k = \sum_{i=1}^{N} A_{k,j} \tag{3.11}$$

3.3.2 Evaporator model.

The cooling thermal exergy generate by the CES, which turns it in a cogeneration plant, is supplied to the external consumer through the evaporator by means of two streams, the first one coming from HE-1 (21) and the second one (30) from the last expansion of turbine three (T-3) as shown in Figure 3.3. The cooling exergy is the product of the heat transfer rate and the Carnot efficiency [176], where T_w is taken as the weighted average temperature between the streams. For the evaporator, the energy and exergy balance equations for steady state conditions are given in Table B.1. Other approaches with different model propositions for exergy evaluation can be seen in [177, 178]. In order to predict the evaporator performance, three alternatives of modeling can be applied: (i) node lump modeling method, (ii) distributed modeling method, and (iii) zone modeling method [166, 37]. During the charging regime, the evaporator operates in the supercritical region (Figs. 3.6 and 3.8) where phase changes do not occur. For this, the first modeling method can be applied. However, during the discharging regime, the evaporator operates in the sub-cooled and superheated regions as illustrated in Fig. 3.7. Therefore, the zone modeling method should be considered. Consequently, the evaporator is divided into two regions, sub-cooled region and superheated region. Then the discretization for each region is applied dividing the evaporator into segments along the flow direction [179] in a similar way to that carried out for the heat exchangers. Considering adiabatic external surface along the evaporator and charging regime, the heat absorbed in every node is given by Eq. 3.12.

$$\dot{Q}_{E,k} = \dot{m}_p[(h_{1,k} - h_{1,k+1}) + (h_{2,k} - h_{2,k+1})] \tag{3.12}$$

Where, k and k+1 are the fluid outlet and inlet at each node, respectively. h_1 and h_2 represent the specific enthalpy of streams 21-22 and 30-31, respectively. For N=150 nodes, the total heat transfer rate or cooling load for the external user is estimated as:

$$\dot{Q}_{E,t} = \sum_{k=1}^{N} \dot{Q}_{E,k} \tag{3.13}$$

In order to consider the variation of fluid properties with respect to temperature, for every node k, the heat capacity for the streams are calculated as:

$$C_{1,k} = \dot{m}_p \frac{h_{1,k} - h_{1,k+1}}{T_{1,k} - T_{1,k+1}} \tag{3.14}$$

$$C_{2,k} = \dot{m}_p \frac{h_{2,k} - h_{2,k+1}}{T_{2,k} - T_{2,k+1}} \tag{3.15}$$

During discharging regime, the stream 19-22 undergoes a phase change, whilst stream 30-31 remains in gas state (superheated region) during the heat transfer process (Fig. 3.7). For low cooling demand at the heat exchangers, the state 19 can be defined at a lower temperature. The heat transfer rate in every node is determined by Eq. 3.16

$$\dot{Q}_{E,k} = \dot{m}_p[(h_{1a,k} - h_{1a,k+1}) + (h_{1b,k} - h_{1b,k+1}) + (h_{2,k} - h_{2,k+1})] \tag{3.16}$$

In above equation, h_{1a} and h_{1b} represent the specific enthalpy of fluid for the sub-cooled and superheated region, respectively. The total heat transfer rate is determined by Eq. 3.13 and the heat capacity in every node for liquid and gas regions are calculated by Eqs. 3.17 and 3.18, respectively.

$$C_{1a,k} = \dot{m}_p \frac{h_{1a,k} - h_{1a,k+1}}{T_{1a,k} - T_{1a,k+1}} \tag{3.17}$$

$$C_{1b,k} = \dot{m}_p \frac{h_{1b,k} - h_{1b,k+1}}{T_{1b,k} - T_{1b,k+1}} \tag{3.18}$$

For stream 30-31, the heat capacity in every node is determined by Eq. 3.15. In the previous methodology, the critical temperature of air is used to separate the sub-cooled region from superheated region.

The local heat transfer unit for every node can be expressed as [180].

$$NTU_{E,k} = \frac{ln\left[\frac{(1-\varepsilon_k)}{(1-C_{R,k}\varepsilon_k)}\right]}{C_{R,k} - 1} \tag{3.19}$$

The heat capacity ratio for every section of the evaporator is given by Eq. 3.20.

$$C_{R,k} = \frac{C_{min,k}}{C_{max,k}} \tag{3.20}$$

For each section of the evaporator, the heat transfer area can be obtained by Eq. 3.21 and the total area is calculated by Eq. 3.22, respectively [181].

$$A_{E,k} = \frac{NTU_{E,k} C_{min,k}}{U_k} \tag{3.21}$$

$$A_E = \sum_{i=1}^{N} A_{E,k} \tag{3.22}$$

3.3.3 Expansion valve model.

An expansion valve is approximated as an isenthalpic and dissipative device with negligible heat transfer and no work interaction. For the throttle valve, the model proposed in [182] is applied. Other approaches can be seen in [178, 177]. The study presents a detailed analysis to deal with dissipative devices to avoid conflicting results regarding the application of the Second Law of Thermodynamics.

3.3.4 Cryogenic tank.

The cryogenic tank (Fig. 3.13) separates the liquid and vapor phases and stores liquid air by reducing evaporation for a long time with the use of a suitable insulation material.

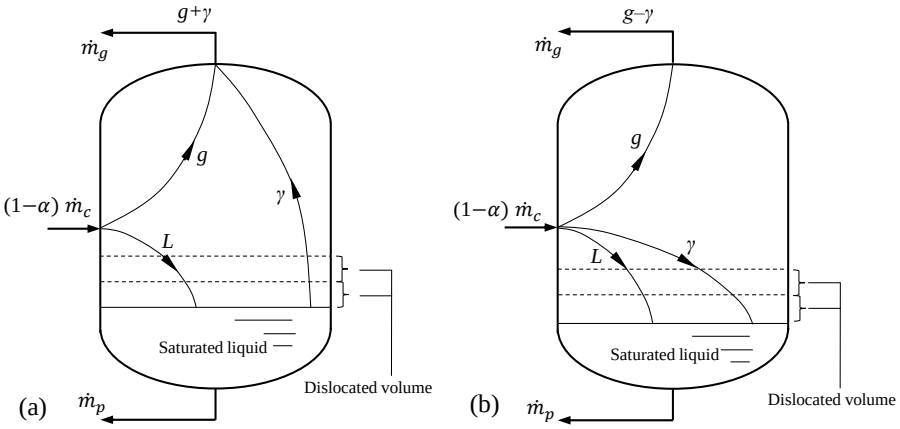

Figure 3.13 – Cryogenic tank during (a) charging and (b) discharging regimes. Adapted from [10].

The increase or decrease of liquid level inside the tank produces a dislodgement of the gaseous phase, increasing the gas mass flow rate leaving from the tank during

charging regime as shown Fig. 3.13a, and reducing it for discharging regime as indicated in Fig. 3.13b. The liquid level movement produces a volume displacement given by Eq. 3.23.

$$\dot{V}_l = v_l[(1-\alpha)y\dot{m}_c - \dot{m}_p] \tag{3.23}$$

where v_l is the specific volume of saturated liquid going out the tank, m^3/kg. Knowing that $\gamma = \dot{m}_g/(1-\alpha)\dot{m}_c$, equation 3.24 can be deduced.

$$\gamma = \frac{\rho_g \dot{V}_l}{(1-\alpha)\dot{m}_c} = \rho_g v_l \left[y - \frac{1}{(1-\alpha)} \frac{\dot{m}_p}{\dot{m}_c} \right] \tag{3.24}$$

where ρ_g is the gas density, kg/m^3. The term γ represents the variation of the mass of liquid air per unit of air mass entering the tank and characterizes the transient process inside it. The mass balance equation for cryogenic tank control volume is expressed by Eq. 3.25.

$$\frac{dm}{dt} = [(1-y)(1-\alpha)\dot{m}_c(t) + (1-\alpha)y\dot{m}_c(t)] - \dot{m}_p(t) - [(1-y)(1-\alpha)\dot{m}_c(t) + \dot{m}_g(t)] \tag{3.25}$$

Substituting Eq. 3.24 and simplifying, the mass balance equation for the transient regime in the tank is stated by 3.26.

$$\frac{dm}{dt} = [(1-\alpha)y\dot{m}_c(t) - \dot{m}_p(t)](1-\rho_g v_l) \tag{3.26}$$

For the cryogenic tank control volume, the heat balance equation for transient regime is stated by 3.27.

$$\frac{dU}{dt} = [(1-y)(1-\alpha)\dot{m}_c(t)h_g + (1-\alpha)y\dot{m}_c(t)h_l] - \dot{m}_p(t)h_p - [(1-y)(1-\alpha)\dot{m}_c(t) + \dot{m}_g(t)]h_g \tag{3.27}$$

The previous equation establishes that the stored energy is proportional to the energy entering the tank, reduced in the energy leaving the tank to the expansion section for power production and also reduced by the energy used in the liquefaction heat exchangers. Knowing that the enthalpy of saturated liquid entering the tank is equal to the liquid enthalpy leaving the tank ($h_l = h_p$), also $h = u + pv$ and reducing terms, the heat balance equation is simplified to 3.28.

$$\frac{dU}{dt} = [(1-\alpha)y\dot{m}_c(t) - \dot{m}_p(t)]u_l - (1-\alpha)\dot{m}_c(t)u_g\gamma \tag{3.28}$$

The thermodynamic models for predicting the transient variations of mass and internal energy in the cryogenic tank are given by Eqs. 3.26 and 3.28. Internal energy and exergy vary mainly by air mass flow rates and internal pressure in the tank, then by means of pressure the properties of gas and liquid are determined for saturated conditions. During charging and discharging regimes, for this study, the pressure in the cryogenic tank is considered to remain constant (0.1 MPa). Therefore, the liquid air mass variation drives the storage of internal energy and exergy inside the cryogenic tank.

After every discharging process, certain amount of liquid air remains inside the tank to ensure the steady state conditions. Moreover, during the charging process, the liquid air mass increases with time according to the mass balance equation given in Eq. 3.26, even though the liquid air mass flow rate through the pump ($\dot{m}_p$), the air gas stream used for cooling at the heat exchangers ($\dot{m}_g$) and the mixture entering the storage tank all remain at steady state conditions, the liquid phase inside the tank increases whilst the gas phase decreases by the fact of having a liquefaction rate greater than the liquid leaving the tank.

3.3.5 Liquid yield.

For the cryogenic energy storage (CES) systems liquid yield (kg_L/kg_a) is a very important energy vector. In order to obtain the liquid yield mathematical model, for discharging regime, the First Law of Thermodynamics is applied throughout heat exchangers, turbines one and two, throttle valve and cryogenic tank control volume as illustrated in Figs. 3.3 and 3.5, respectively. For this, internal energy are considered at certain rate of accumulation and kinetic and potential energy are neglected. The equation 3.29 is obtained.

$$\frac{dU}{dt} = \dot{Q}_0 - \alpha\dot{m}_c[(h_{13} - h_{14s}) + (h_{15} - h_{16s})]\eta_T - (1-\alpha)\dot{m}_c(h_6 - h_{7s})\eta_T + \dot{m}_c h_2 - \dot{m}_g h_{12} - \dot{m}_p h_{17} \quad (3.29)$$

In the liquefaction of air and other gases, heat exchangers must offer an efficient method of heat transfer to enhance the liquid yield. Then, heat transfer ($\dot{Q}_0$) with the surroundings must be minimal. The heat absorbed by the heat exchangers is evaluated by Eq. 3.2 and the methodology used in Subsection 3.3.1 is also considered to obtain the liquid yield mathematical model.

Applying mass balance equation for the cryogenic tank control volume (Fig. 3.13) and considering the meaning of γ expressed before, the equation 3.30 is obtained.

$$\dot{m}_g = \dot{m}_c - \dot{m}_l \pm \dot{m}_\gamma \quad (3.30)$$

In the previous equation, the positive (+) sign is used for charging regime and negative (-) sign for discharging. Dividing equation 3.30 by $\dot{m}_c$, the following relationship is obtained:

$$\frac{\dot{m}_g}{\dot{m}_c} = 1 - y \pm \gamma \tag{3.31}$$

Where, y is the specific liquid yield in the cryogenic tank, expressed in kilogram of liquid per kilogram of air. Substituting 3.31 and 3.2 on equation 3.29, also dividing it by $\dot{m}_c$ and solving for the specific liquid yield indicator, the equation 3.32 is inferred.

$$\begin{aligned} y = \frac{[(h_{12} - h_2)(1-\varepsilon)(h_{12} - h_8)] + \frac{\dot{m}_p}{\dot{m}_c} h_{17} + \frac{1}{\dot{m}_c}\frac{dU}{dt} \pm \gamma h_{12}}{h_{12} - (1-\varepsilon)(h_{12} - h_8)} \\ + \frac{\alpha[(h_{13} - h_{14s}) + (h_{15} - h_{16s})]\eta_T}{h_{12} - (1-\varepsilon)(h_{12} - h_8)} + \frac{(1-\alpha)(h_6 - h_{7s})\eta_T}{h_{12} - (1-\varepsilon)(h_{12} - h_8)} \end{aligned} \tag{3.32}$$

The previous equation models the specific liquid yield when a cryogenic hydraulic turbine is used before the storage tank (Fig. 3.5). When the expansion valve is used for liquefaction purposes (Fig. 3.3) and transient condition is considered, the liquid yield function is given by Eq. 3.33.

$$\begin{aligned} y = \frac{[(h_{12} - h_2)(1-\varepsilon)(h_{12} - h_8)] + \frac{\dot{m}_p}{\dot{m}_c} h_{17} + \frac{1}{\dot{m}_c}\frac{dU}{dt} \pm \gamma h_{12}}{h_{12} - (1-\varepsilon)(h_{12} - h_8)} \\ + \frac{\alpha[(h_{13} - h_{14s}) + (h_{15} - h_{16s})]\eta_T}{h_{12} - (1-\varepsilon)(h_{12} - h_8)} \end{aligned} \tag{3.33}$$

To find the domain or limits in which the above function is valid, a mass balance is applied for the cryogenic tank. For this case, the conservation of mass principle takes the general form:

$$\frac{dm_{cv}}{dt} = \sum_{i=1}^{n} \dot{m}_i - \sum_{j=1}^{n} \dot{m}_e \tag{3.34}$$

For the cryogenic tank control volume (Fig. 3.13), the mass balance equation for transient condition is stated as:

$$\frac{dm_{cv}}{dt} = (\dot{m}_c - \dot{m}_\alpha) - \dot{m}_g - \dot{m}_p \tag{3.35}$$

where $\dot{m}_g$ and m_p are the saturated vapor and liquid mass flow rates leaving the tank, kg/s; $\dot{m}_\alpha$ is the re-circulation mass flow rate through the turbine, kg/s.

To achieve an effective production of liquid, m_g must be greater than zero ($\dot{m}_g > 0$). Under this condition Eq. 3.35 adopts the following form:

$$-\frac{dm_{cv}}{dt} + \dot{m}_c - \dot{m}_\alpha - \dot{m}_p > 0 \tag{3.36}$$

Dividing equation 3.36 by $\dot{m}_c$, the validity of function 3.32 for transient condition is obtained, that is:

$$\frac{\dot{m}_p}{\dot{m}_c} + \alpha < 1 - \frac{1}{\dot{m}_c}\frac{dm}{dt} \tag{3.37}$$

When the inequality of the previous inequation is the opposite, for instance, the condition in equation 3.38 is met, the limit of liquid yield is stated by equation 3.39 and the liquid yield estimated by Eq. 3.40.

$$\frac{\dot{m}_p}{\dot{m}_c} + \alpha > 1 - \frac{1}{\dot{m}_c}\frac{dm}{dt} \tag{3.38}$$

$$y = \lim_{\frac{\dot{m}_p}{\dot{m}_c}+\alpha \to\ 1-\frac{1}{\dot{m}_c}\frac{dm}{dt}} = y(\alpha) \tag{3.39}$$

$$y(\alpha) = 0.99 - \alpha \tag{3.40}$$

For steady state condition and using a cryogenic hydraulic turbine before the storage tank (Fig. 3.5), the liquid yield is given by Eq. 3.41.

$$y = \frac{[(h_{12} - h_2)(1-\varepsilon)(h_{12} - h_8)]}{h_{12} - (1-\varepsilon)(h_{12} - h_8)} + \frac{\alpha[(h_{13} - h_{14s}) + (h_{15} - h_{16s})]\eta_T}{h_{12} - (1-\varepsilon)(h_{12} - h_8)} + \frac{(1-\alpha)(h_6 - h_{7s})\eta_T}{h_{12} - (1-\varepsilon)(h_{12} - h_8)} \tag{3.41}$$

Equation 3.41 is valid for the following condition [10]:

$$y + \alpha < 1 \tag{3.42}$$

When the condition is given by the inequality 3.43, the liquid yield should be calculated by Eq. 3.44 [10].

$$y + \alpha > 1 \tag{3.43}$$

$$y = 0.99 - \alpha \tag{3.44}$$

For an expansion valve as a device for liquefaction process (Fig. 3.3), the Eq. 3.41 becomes Eq. 3.45. The conditions 3.42 and 3.43 must be considered to apply Eq. 3.45.

$$y = \frac{[(h_{12} - h_2)(1-\varepsilon)(h_{12} - h_8)]}{h_{12} - (1-\varepsilon)(h_{12} - h_8)} + \frac{\alpha[(h_{13} - h_{14s}) + (h_{15} - h_{16s})]\eta_T}{h_{12} - (1-\varepsilon)(h_{12} - h_8)} \tag{3.45}$$

3.3.6 Charging and discharging time.

The cryogenic storage tank operates in transient regime. The storage capacity will determine the cooling and electrical production during discharging regime. By applying the mass balance equation around the cryogenic tank control volume (Fig. 3.13a), the charging time can be estimated by Eq. 3.46 assuming that the tank is being charged from 5 % of its total capacity. The remaining air liquid (5 %) at the cryogenic tank ensures the steady state operation of the rest of the components, that is, at the beginning of the charging regime there is air liquid to be used for cooling and power production (cogeneration) in the evaporator and four section expansion turbine, respectively. Since $\dot{m}_p << \dot{m}_c$, the cryogenic tank will be charged up to its maximum capacity.

$$\Delta\tau_{ch} = \frac{0.95 C_t 10^3}{[(1-\alpha)y\dot{m}_c - \dot{m}_p]\,(1-\rho_g \upsilon_l)3600} \tag{3.46}$$

where C_t is the cryogenic tank capacity in t, $\dot{m}_c$ is the air mass flow rate through the compressor in kg/s, $\dot{m}_p$ is the liquid air mass flow rate through the cryogenic pump in kg/s, ρ_g is the air gas density in kg/m^3, and υ_l is the specific volume of liquid air in m^3/kg. During discharging regime ($\dot{m}_p >> \dot{m}_c$) the liquid yield, stated by $(1-\alpha)y\dot{m}_c$, at the cryogenic tank, helps to extent the power production. Under this condition, the discharging time is also obtained by the mass balance equation in transient regime applied to the storage tank control volume (Fig. 3.13). At this point, the discharging process must be carried out until 95 % of the total cryogenic tank capacity is used.

$$\Delta\tau_{dis} = \frac{0.95 C_t 10^3}{\dot{m}_p(1+\rho_g \upsilon_l)3600} \tag{3.47}$$

where C_t is the cryogenic tank capacity in t, $\dot{m}_p$ is the liquid air mass flow rate through the cryogenic pump in kg/s, ρ_g is the air gas density in kg/m^3, and υ_l is the specific volume of liquid air in m^3/kg.

3.3.7 Power consumption.

The power required by the compressor (process 1-2, Figs. 3.3, 3.4 and 3.5) during the charging and discharging processes is expressed by the isothermal reversible work and determined by Eq. 3.48 [7, 76].

$$-\frac{\dot{W}_c}{\dot{m}_c} = \frac{T_1(s_1 - s_2) - (h_1 - h_2)}{\eta_C} \tag{3.48}$$

Where $\dot{W}_c$ is the total power required by the compressor, kW. T_1 is the absolute inlet temperature, K. s_1 and s_2 are the inlet and outlet specific entropies of air, kJ/kgK. h_1 and h_2 are the inlet and outlet enthalpies of air, kJ/kg. η_C is the dimensionless isoentropy efficiency of compressor. The previous equation (Eq. 3.48) is obtained by applying the First Law of Thermodynamics [47] to compressor control volume, where the heat rejected in order to obtain an isothermal process is taken as the absolute temperature and entropy difference product. In practice, it is difficult to achieve an isothermal compression process, so the expression is divided by the isentropic efficiency of the compressor. For the optimization procedure, this efficiency is considered to vary in 17 % respect to the assumed value given in Table 3.1. Additionally, for the economic analysis, the global efficiency of the cycles is regarded to vary ±50 %.

The cryogenic pump is used to supply the liquid air through out the second cooling circuit and the expansion section (process 15-16 in Fig. 3.4 and process 17-18 in Figs. 3.3 and 3.5). The power required by the pump is calculated by Eq. 3.49.

$$-\frac{\dot{W}_p}{\dot{m}_p} = \frac{v_l(P_d - P_i)10^3}{\eta_P} = (h_d - h_i) \tag{3.49}$$

Where $\dot{W}_p$ is the total power required by the pump, kW. v_l is the specific volume of saturated liquid at the inlet of the pump, m^3/kg. P_d and P_i are the discharge and suction pressures respectively, MPa. h_d and h_i are the discharge of the real process and inlet enthalpies of liquid air, kJ/kg. η_P is the dimensionless isentropic efficiency of the pump.

3.3.8 Power production.

The power generation by the two sections expansion turbine from power circuit 1 (Figs. 3.3 and 3.5) is expressed by Eq. 3.50.

$$\dot{W}_{t1} = \alpha\dot{m}_c[(h_{13} - h_{14s}) + (h_{15} - h_{16s})]\eta_T \tag{3.50}$$

In a similar way, the single expansion turbine located in the liquefaction section (Fig. 3.4 for operation mode A) is modelled by Eq. 3.51.

$$\dot{W}_{t1} = \alpha\dot{m}_c[(h_{13} - h_{14s})]\eta_T \tag{3.51}$$

In the case of the cryogenic hydraulic turbine (Figs. 3.4 and 3.5), which substitutes the expansion valve, the power generation is calculated by Eq. 3.52.

$$\dot{W}_{t2} = (1-\alpha)\dot{m}_c[(h_6 - h_{7s})]\eta_T \tag{3.52}$$

The power produced by the four sections expansion turbine from Fig. 3.4 is determined by Eq. 3.53 whilst for Figs. 3.3 and 3.5 the Eq. 3.54 is applied.

$$\dot{W}_{t3} = \dot{m}_p[(h_{21} - h_{22s}) + (h_{23} - h_{24s}) + (h_{25} - h_{26s}) + (h_{27} - h_{28s})]\eta_T \tag{3.53}$$

$$\dot{W}_{t3} = \dot{m}_p[(h_{23} - h_{24s}) + (h_{25} - h_{26s}) + (h_{27} - h_{28s}) + (h_{29} - h_{30s})]\eta_T \tag{3.54}$$

3.3.9 Exergy analysis.

The main purposes of the exergy analysis are to find out the causes of the irreversibilities, quantitatively estimate them and locate the subsystems with the worst thermodynamic performance. This powerful tool, used in the evaluation and design of thermal systems, shows the way to a better understanding of the transformation processes and can also be used to determine the most suitable solution in order to improve the performance of the CES systems.

The exergy analysis is carried out in order to evaluate the exergy efficiency of each component of the CES systems and also for the plant. This study provides relevant information about the CES's thermodynamic behaviour during charging and discharging regimes by means of the exergy destruction calculation. Exergy can be understood as the amount of work obtainable when a substance is brought to the state of thermodynamic equilibrium with the surroundings through reversible processes where the interaction, for instance, heat transfer, mass transfer, magnetic energy transfer and other forms of interactions occur only with the environment [183]. The rate of exergy through a control volume operating in transient regime is obtained and expressed by Eq. 3.55 [184, 185, 44].

$$\frac{dE_{cv}}{dt} = \sum_{i=1}^{n}\left(1 - \frac{T_0}{T_i}\right)\dot{Q}_i - \left(\dot{W}_{cv} - p_0\frac{dV_{cv}}{dt}\right) + \sum_{i=1}^{n}(\dot{m}_i e_{xi})_{in} - \sum_{i=1}^{n}(\dot{m}_i e_{xi})_{out} - \dot{E}_{xD} \tag{3.55}$$

The second term of the right hand side represents the useful work, and it is defined as the difference between the work done by the system and the work done by the environment at pressure p_0, assuming that the boundary of the system can be expanded or contracted. Next, the third and fourth terms represent the rate of exergy entering and leaving the control volume and the last one, the exergy destruction or irreversibility. For every component of the CES systems, the exergy destruction at steady state condition can be expressed in a general form as:

$$\dot{E}_{xD} = \sum_{i=1}^{n} \left(1 - \frac{T_0}{T_i}\right) \dot{Q}_i - \left(\dot{W}_{cv} - p_0 \frac{dV_{cv}}{dt}\right) + \sum_{i=1}^{n} (\dot{m}_i e_{xi})_{in} - \sum_{i=1}^{n} (\dot{m}_i e_{xi})_{out} \tag{3.56}$$

The liquefaction section for the CES systems is mainly composed by heat exchangers (Figs. 3.3, 3.4 and 3.5). For these subsystems the main sources of irreversibility is caused by the temperature difference between the fluids, heat transfer to the surrounding and pressure drop. Neglecting the last cause of exergy destruction and considering the fact that exergy loss direction is opposite to heat transfer direction, the mathematical equation for the rate of exergy destruction at the heat exchanger control volume, for steady state condition, is expressed by Eq. 3.57.

$$\dot{E}_{xD} = \sum_{i=1}^{n} \left(\frac{T_0}{T_i} - 1\right) \dot{Q}_i + \sum_{i=1}^{n} (\dot{m}_i e_{xi})_{in} - \sum_{i=1}^{n} (\dot{m}_i e_{xi})_{out} \tag{3.57}$$

Considering that the cryogenic tank has an excellent insulating material, the exergy loss by heat transfer with the surrounding can be neglected and the viscous effect of the liquid air and the internal surface of the cryogenic tank is assumed inappreciable. Then, the only source of irreversibility generation is the phase separation process. As the phase separation (L-g, Fig. 3.13) occurs due to the effect of the force of gravity, the cryogenic tank control volume is considered free of exergy destruction. Applying the Eq. 3.55 to the cryogenic tank control volume the rate of exergy stored can be expressed by Eq. 3.58.

$$\frac{dE_x}{dt} = \sum_{i=1}^{n} (\dot{m}_i e_{xi})_{in} - \sum_{i=1}^{n} (\dot{m}_i e_{xi})_{out} \tag{3.58}$$

By substituting the corresponding terms in the previous equation, the final expression for modeling the rate of exergy stored in the cryogenic tank for transient regime is given by Eq. 3.59.

$$\frac{dE_x}{dt} = [(1-\alpha) y \dot{m}_c(t) - \dot{m}_p(t)](e_{xl} - \rho_g v_l e_{xg}) \tag{3.59}$$

Exergy can be divided into four components: physical, chemical, kinetic and potential [176]. Therefore, the general expression to obtain the exergy of a stream is given by Eq. 3.60.

$$\dot{E}_{xi} = \dot{E}_x^{ph} + \dot{E}_x^{ch} + \dot{E}_x^{k} + \dot{E}_x^{p} \tag{3.60}$$

The latter two terms are assumed negligible in this study, since changes in elevation and velocity are very small. Since there is not change in chemical composition and chemical reactions in the cryogenic working fluids do not exist, the chemical exergy can be also

neglected. Therefore, the physical exergy, defined as the work obtainable by taking the working fluid through reversible physical processes from a initial state of pressure P and temperature T, to the state determined by pressure P_0 and temperature T_0 of the surroundings[183, 186] is expressed by Eq. 3.61 [176, 187, 182].

$$\dot{E}_{xi} = \dot{m}_i \left[(h_i - h_0) - T_0(s_i - s_0)\right] = \dot{m}_i \left[(u_i - u_0) + (P_i \upsilon_i - P_0 \upsilon_0) - T_0(s_i - s_0)\right] \quad (3.61)$$

Where, $\dot{m}_i$ is the mass flow rate of stream ith, kg/s. h_i and s_i are the specific enthalpy and entropy of the i-th stream, kJ/kg and kJ/kgK, respectively. u_i and υ_i are the specific internal energy and specific volume of the stream ith, kJ/kg and m^3/kg. h_0 and s_0 are the same properties of the working fluid at the surroundings condition (reference level). For the study the reference level is adopted at $T_0 = 298.15\ K$ and $p_0 = 101.325\ kPa$.

The exergy efficiency and exergy destruction of every subsystem are obtained applying the "Fuel" and "Product" rules [188, 176, 8, 182]. The Tables 3.3 and 3.4 define the "Fuel" and "Product" for each component of the CES systems for charging and discharging regimes, respectively.

The most typical irreversibilities associated with thermal systems are irreversible heat transfer, diffusion, friction and throttling. The rate of exergy loss ($\dot{E}_{xL}$) must be understood as the available exergy from a stream or the exergy related with a heat flow that is wasted or rejected to the environment. Table B.1 summarizes the exergy destruction equation for every component of the CES systems. The exergy balance equation for the overall CES system can be expressed by Eq. 3.62.

$$\dot{E}_{xF,t} = \dot{E}_{xP,t} + \dot{E}_{xD,t} + \dot{E}_{xL,t} \quad (3.62)$$

Where, $\dot{E}_{xF,t}$ is the exergy rate input to the CES system, $\dot{E}_{xP,t}$ is the product exergy of the system, $\dot{E}_{xD,t}$ is the total exergy destruction of the system and $\dot{E}_{xL,t}$ is the rate of exergy loss in the system.

For the exergy evaluation of the CES systems the concepts of exergy efficiency and the exergy destruction ratio of each sub-component are applied. The exergy efficiency of a subsystem can be written as:

$$\eta_{exe,k} = \frac{\dot{E}_{xP,k}}{\dot{E}_{xF,k}} = 1 - \frac{\dot{E}_{xD,k}}{\dot{E}_{xF,k}} \quad (3.63)$$

The exergy destruction ratio compares the exergy destruction of a component with respect to the total exergy of fuel of the overall CES system and it is given by Eq. 3.64, which is a measure of the inefficiency of a system component [12].

Table 3.3 – Designation of exergy of Fuel ($\dot{E}_{xF}$) and exergy of Product ($\dot{E}_{xP}$) of the CES systems for charging regime.

Components	Fuel (kW)	Product (kW)
Compressor	$\dot{W}_c$	$(\dot{E}_2 - \dot{E}_1)$
Heat exchanger 1	$\dot{m}_{in}T_0(s_{12}-s_{11})-\dot{m}_h(h_3-h_2)+\dot{m}_cT_0(s_{21}-s_{20})+(1-\varepsilon_1)\left(\frac{T_0}{T_m}-1\right)\dot{Q}_{a,1}$	$\dot{m}_hT_0(s_3-s_2)-\dot{m}_{in}(h_{12}-h_{11})-\dot{m}_c(h_{21}-h_{20})$
Heat exchanger 2	$\dot{m}_{in}T_0(s_{11}-s_{10})-\dot{m}_h(h_5-h_4)+\dot{m}_cT_0(s_{20}-s_{19})+(1-\varepsilon_2)\left(\frac{T_0}{T_m}-1\right)\dot{Q}_{a,2}$	$\dot{m}_hT_0(s_5-s_4)-\dot{m}_{in}(h_{11}-h_{10})-\dot{m}_c(h_{20}-h_{19})$
Heat exchanger 3	$\dot{m}_{in}T_0(s_9-s_8)-\dot{m}_h(h_6-h_5)+\dot{m}_cT_0(s_{19}-s_{18})+(1-\varepsilon_3)\left(\frac{T_0}{T_m}-1\right)\dot{Q}_{a,3}$	$\dot{m}_hT_0(s_6-s_5)-\dot{m}_{in}(h_9-h_8)-\dot{m}_c(h_{19}-h_{18})$
Turbine 1	$(\dot{E}_{13}-\dot{E}_{14})+(\dot{E}_{15}-\dot{E}_{16})$	$\dot{W}_{t1}$
Turbine 2	$(\dot{E}_6-\dot{E}_7)$	$\dot{W}_{t2}$
Turbine 3	$(\dot{E}_{23}-\dot{E}_{24})+(\dot{E}_{25}-\dot{E}_{26})+(\dot{E}_{27}-\dot{E}_{28})+(\dot{E}_{29}-\dot{E}_{30})$	$\dot{W}_{t3}$
Expansion valve	$(1-\alpha)\dot{m}_c)[(p_7\upsilon_7-p_6\upsilon_6)-T_0(s_7-s_6)]$	$(1-\alpha)\dot{m}_c(u_7-u_6)$
Cryogenic pump	$\dot{W}_P$	$(\dot{E}_{18}-\dot{E}_{17})$
Evaporator	$(\dot{E}_{22}-\dot{E}_{21})+(\dot{E}_{31}-\dot{E}_{30})$	$\left(\frac{T_0}{T_w}-1\right)\dot{Q}_E$
Heater 1	$\left(1-\frac{T_0}{T_r}\right)\dot{Q}_{H1}$	$(\dot{E}_{23}-\dot{E}_{22})$
Heater 2	$\left(1-\frac{T_0}{T_r}\right)\dot{Q}_{H2}$	$(\dot{E}_{25}-\dot{E}_{24})$
Heater 3	$\left(1-\frac{T_0}{T_r}\right)\dot{Q}_{H3}$	$(\dot{E}_{27}-\dot{E}_{26})$
Heater 4	$\left(1-\frac{T_0}{T_r}\right)\dot{Q}_{H4}$	$(\dot{E}_{29}-\dot{E}_{28})$
Heater 5	$\left(\frac{T_0}{T_m}-1\right)\dot{Q}_{H5}$	$(\dot{E}_{15}-\dot{E}_{14})$

$$y_{D,k} = \frac{\dot{E}_{xD,k}}{\dot{E}_{xF,t}} \tag{3.64}$$

The subsystem exergy destruction can be also compared with respect to the total exergy destruction of the overall plant. This ratio can be expressed by Eq. 3.65 and it is a useful indicator to compare the components of a system.

$$y^*_{D,k} = \frac{\dot{E}_{xD,k}}{\dot{E}_{xD,t}} \tag{3.65}$$

The exergy efficiency for charging and discharging regimes are estimated by Eqs. 3.66 and 3.67, respectively. For charging regime is the ratio between the exergy stored in the cryogenic tank and the overall net rate of exergy used in the cycle. Whereas for the discharging process is the ratio between the net rate of work exergy produced by the cycle

Table 3.4 – Designation of exergy of Fuel ($\dot{E}_{xF}$) and exergy of Product ($\dot{E}_{xP}$) of the CES systems for discharging regime.

Components	Fuel (kW)	Product (kW)
Compressor	$\dot{W}_c$	$(\dot{E}_2 - \dot{E}_1)$
Heat exchanger 1	$\dot{m}_{in}T_0(s_{12} - s_{11}) - \dot{m}_h(h_3 - h_2) + (1 - \varepsilon_1)\left(\frac{T_0}{T_m} - 1\right)\dot{Q}_{a,1}$	$\dot{m}_hT_0(s_3 - s_2) - \dot{m}_{in}(h_{12} - h_{11})$
Heat exchanger 2	$\dot{m}_{in}T_0(s_{11} - s_{10}) - \dot{m}_h(h_5 - h_4) + (1 - \varepsilon_2)\left(\frac{T_0}{T_m} - 1\right)\dot{Q}_{a,2}$	$\dot{m}_hT_0(s_5 - s_4) - \dot{m}_{in}(h_{11} - h_{10})$
Heat exchanger 3	$\dot{m}_{in}T_0(s_9 - s_8) - \dot{m}_h(h_6 - h_5) + \dot{m}_cT_0(s_{19} - s_{18}) + (1 - \varepsilon_3)\left(\frac{T_0}{T_m} - 1\right)\dot{Q}_{a,3}$	$\dot{m}_hT_0(s_6 - s_5) - \dot{m}_{in}(h_9 - h_8) - \dot{m}_c(h_{19} - h_{18})$
Turbine 1	$(\dot{E}_{13} - \dot{E}_{14}) + (\dot{E}_{15} - \dot{E}_{16})$	$\dot{W}_{t1}$
Turbine 2	$(\dot{E}_6 - \dot{E}_7)$	$\dot{W}_{t2}$
Turbine 3	$(\dot{E}_{23} - \dot{E}_{24}) + (\dot{E}_{25} - \dot{E}_{26}) + (\dot{E}_{27} - \dot{E}_{28}) + (\dot{E}_{29} - \dot{E}_{30})$	$\dot{W}_{t3}$
Expansion valve	$(1 - \alpha)\dot{m}_c)[(p_7\upsilon_7 - p_6\upsilon_6) - T_0(s_7 - s_6)]$	$(1 - \alpha)\dot{m}_c(u_7 - u_6)$
Cryogenic pump	$\dot{W}_P$	$(\dot{E}_{18} - \dot{E}_{17})$
Evaporator	$(\dot{E}_{22} - \dot{E}_{21}) + (\dot{E}_{31} - \dot{E}_{30})$	$\left(\frac{T_0}{T_w} - 1\right)\dot{Q}_E$
Heater 1	$\left(1 - \frac{T_0}{T_r}\right)\dot{Q}_{H1}$	$(\dot{E}_{23} - \dot{E}_{22})$
Heater 2	$\left(1 - \frac{T_0}{T_r}\right)\dot{Q}_{H2}$	$(\dot{E}_{25} - \dot{E}_{24})$
Heater 3	$\left(1 - \frac{T_0}{T_r}\right)\dot{Q}_{H3}$	$(\dot{E}_{27} - \dot{E}_{26})$
Heater 4	$\left(1 - \frac{T_0}{T_r}\right)\dot{Q}_{H4}$	$(\dot{E}_{29} - \dot{E}_{28})$
Heater 5	$\left(\frac{T_0}{T_m} - 1\right)\dot{Q}_{H5}$	$(\dot{E}_{15} - \dot{E}_{14})$

and the sum of the stored exergy at the cryogenic tank and the exergy of heat employed in the heaters.

$$\eta_{exe}^{ch} = \frac{\frac{dE_x}{dt}}{\dot{W}_c + \dot{W}_p - \dot{W}_{t1} - \dot{W}_{t2} - \dot{W}_{t3} + \sum_{i=1}^{n}\left(1 - \frac{T_0}{T_i}\right)\dot{Q}_{Hi}} \tag{3.66}$$

$$\eta_{exe}^{dis} = \frac{\dot{W}_{t1} + \dot{W}_{t2} + \dot{W}_{t3} - \dot{W}_c - \dot{W}_p}{\dot{m}_p\left[(h_{17} - h_0) - T_0(s_{17} - s_0)\right] + \sum_{i=1}^{n}\left(1 - \frac{T_0}{T_i}\right)\dot{Q}_{Hi}} \tag{3.67}$$

3.3.10 Cycle performance indexes and indicators.

The net specific exergy consumption (kWh/kg_L) is calculated by Eq. 3.68. It represents the exergy required to produce the unit of liquid or to liquefy a kg of air

$$e_N = \frac{\int_0^{\Delta\tau_{ch}} (\dot{W}_c + \dot{W}_p - \dot{W}_{t1} - \dot{W}_{t2} - \dot{W}_{t3}) dt}{\int_0^{\Delta\tau_{ch}} [(1-\alpha) y \dot{m}_c] \, dt} \tag{3.68}$$

Exergy density (kWh/m^3) is an useful and important indicator that states the net exergy generated during discharging regime per unit volume of the cryogenic tank.

$$E_D = \frac{\int_0^{\Delta\tau_{dis}} (\dot{W}_{t1} + \dot{W}_{t2} + \dot{W}_{t3} - \dot{W}_c - \dot{W}_p) dt}{V_t} \tag{3.69}$$

The round trip efficiency is one of the most important indexes to evaluate the performance of electricity storage technologies. It is defined as the ratio of the net electrical energy output in the discharging cycle to the net electrical energy input in the charging cycle [76, 189, 190].

$$\eta_{rt} = \frac{E_n^{dis}}{E_n^{ch}} = \frac{\int_0^{\Delta\tau_{dis}} \left[(\dot{W}_{t1} + \dot{W}_{t2} + \dot{W}_{t3} - \dot{W}_c - \dot{W}_p) - \sum_{i=1}^{n} \left(1 - \frac{T_0}{T_i}\right) \dot{Q}_{Hi} \right] dt}{\int_0^{\Delta\tau_{ch}} \left[(\dot{W}_c + \dot{W}_p - \dot{W}_{t1} - \dot{W}_{t2} - \dot{W}_{t3}) + \sum_{i=1}^{n} \left(1 - \frac{T_0}{T_i}\right) \dot{Q}_{Hi} \right] dt} \tag{3.70}$$

3.3.11 Cycle based on combined cooling and power.

The efficiency of the Second Law of Thermodynamics to evaluate the performance of the CES system is the exergy utilization factor (E_xUF). It is expressed by the ratio between the overall useful exergy generated in the form of power and thermal energy (cooling and/or heat) and the total input exergy. For charging process the input exergies are the compressor and pump powers and the amount supplied by heaters, whilst the output exergies are represented by the power of turbines, cooling load at the evaporator and the exergy stored in the cryogenic tank. During discharging regime, the input exergies are given by the sum of the exergy rate leaving from the cryogenic tank and the heaters exergy, while the output exergies are the net power and the cooling load exergy. Eqs. 3.71 and 3.72 state the exergy utilization factor for charging and discharging regimes, respectively.

$$E_xUF^{ch} = \frac{\sum_{i=1}^{n} \dot{W}_{ti} + \dot{E}_{xQ} + \frac{dE_x}{dt}}{\dot{W}_c + \dot{W}_p + \sum_{i=1}^{n} \left(1 - \frac{T_0}{T_i}\right) \dot{Q}_{Hi}} \tag{3.71}$$

$$E_xUF^{dis} = \frac{\sum_{i=1}^{n} \dot{W}_{ti} + \dot{E}_{xQ} - \dot{W}_c - \dot{W}_p}{\dot{m}_p e_{x17} + \sum_{i=1}^{n} \left(1 - \frac{T_0}{T_i}\right) \dot{Q}_{Hi}} \tag{3.72}$$

Another important index for cogeneration plants is the ratio between electric and thermal (cooling) power [191], for discharging regime is given by:

$$\lambda = \frac{\dot{W}_{t1} + \dot{W}_{t2} + \dot{W}_{t3} - \dot{W}_c - \dot{W}_p}{\dot{E}_{xQ}} \tag{3.73}$$

Using the previous index, the electrical and thermal efficiency are defined by Eqs. 3.74 and 3.75, respectively [191, 192].

$$\eta_{el} = E_x UF \left(\frac{\lambda}{1+\lambda} \right) \tag{3.74}$$

$$\eta_{th} = E_x UF \left(\frac{1}{1+\lambda} \right) \tag{3.75}$$

For one operation cycle, the round-trip efficiency, considering cogeneration regime (Eq. 3.78), can be stated as the ratio between both net electrical and thermal energy produced (Eq. 3.76) to the net consumed (Eq. 3.77), that is:

$$\begin{aligned} E_{dis}^{cog} = & \int_0^{\Delta\tau_{dis}} (\dot{W}_{t1} + \dot{W}_{t2} + \dot{W}_{t3} - \dot{W}_c - \dot{W}_p) dt + \int_0^{\Delta\tau_{dis}} \left[\left(\frac{T_0}{T_w} - 1 \right) \dot{Q}_E \right] dt \\ & - \int_0^{\Delta\tau_{dis}} \left[\sum_{i=1}^{n} \left(1 - \frac{T_0}{T_i} \right) \dot{Q}_{Hi} \right] dt \end{aligned} \tag{3.76}$$

$$\begin{aligned} E_{ch}^{cog} = & \int_0^{\Delta\tau_{ch}} (\dot{W}_c + \dot{W}_p - \dot{W}_{t1} - \dot{W}_{t2} - \dot{W}_{t3}) dt + \int_0^{\Delta\tau_{ch}} \left[\sum_{i=1}^{n} \left(1 - \frac{T_0}{T_i} \right) \dot{Q}_{Hi} \right] dt \\ & - \int_0^{\Delta\tau_{ch}} \left[\left(\frac{T_0}{T_w} - 1 \right) \dot{Q}_E \right] dt \end{aligned} \tag{3.77}$$

$$\eta_{rt}^{cog} = \frac{E_{dis}^{cog}}{E_{ch}^{cog}} \tag{3.78}$$

3.3.12 Multi-objective optimization procedure.

Liquefaction of air is considered as an energy-intensive process. Several parameters, such as the compressor pressure (P_c), effectiveness of the heat exchangers (ε), diverted air mass fraction (α), equipment efficiencies (η_k) and air mass flow rate ($\dot{m}_c$) affect the process performance, specifically, indicators like specific liquid yield (y) and specific exergy consumption (e_n). Likewise, during energy recovery, pump pressure (P_p), reheat temperature (T_r) and liquid air mass flow rate ($\dot{m}_p$) have a direct influence on energy production, electrical efficiency (η_{el}), exergy utilization factor ($E_x UF$) and round-trip efficiency (η_{rt}). Thermodynamic optimization is performed by genetic algorithm (GA)

method using EES software for charging and discharging regimes. The GA method is suitable for solving multi-objective optimization problems and is based on evolutionary techniques that simulate biology processes [193, 194]. The Darwing theory, about survival of fittest principle, supports the base of genetic algorithm [195].

The optimization process begins with a random selection of a population of individuals from the specified constraints of the independent variables [196]. Moreover, the fitness (value of the objective function) of each individual of the population is evaluated [197]. Then several individuals are selected from the actual population according to their fitness to form the new generation. Those selected individuals make up the new population with a better association respect to the objective functions [198, 199]. An iterative process is executed continuously until the algorithm tends up to the desired optimal value [200]. Generally, the multi-objective optimization method involves two or more objective functions [201, 202]. The selected objective functions to be maximized are specific liquid yield (Eq. 3.32), exergy efficiency (Eqs. 3.66 and 3.67), exergy density (Eq. 3.69), exergy utilization factor (Eqs. 3.71 and 3.72), electrical efficiency (Eq. 3.74) and round-trip efficiency (Eq. 3.70 and 3.78). To find the maximum round-trip efficiency, the maximum values of electricity generation for discharging regime and the minimum values of electricity consumption during charging are obtained. In addition, for the cogeneration regime, the maximum cooling load for charging and discharging regimes are also determined. Whereas, specific exergy consumption (Eq. 3.68) that involves minimization of this indicator is transformed into a maximization problem of $E_i = 1/(1 + e_{ni})$, where the minimum of e_{ni} tends to be the maximum of E_i [193]. Similar procedure is applied for the electricity consumption during charging regime. The decision variables are chosen from the sensitivity analysis, considering their significant influence on the performance of the CES systems.

The genetic algorithm method is selected from the dialog box of EES software and the number of individuals, generations, crossover and mutation probability are respectively chosen as 100, 100, 0.85 and 0.01 [18, 203, 204]. The genetic algorithm routine takes between 15 and 18 minutes to rin in EES. The flow chart for the multi-objective optimization procedure is illustrated in Fig. 3.14. The decision variables and constrains to be satisfied, selected according to the simulation results, are also summarized in Fig. 3.14. Furthermore, four options of optimization for both charging and discharging regimes are applied by selecting, respectively, cryogenic tank capacity of 50, 100, 150 and 200 t.

3.4 Economic analysis.

Additionally to the technical evaluation of the thermal engineering systems, the economic analysis represents the completion of the design project, because from its results, the feasibility and main decisions for investments can be established. In order to evaluate

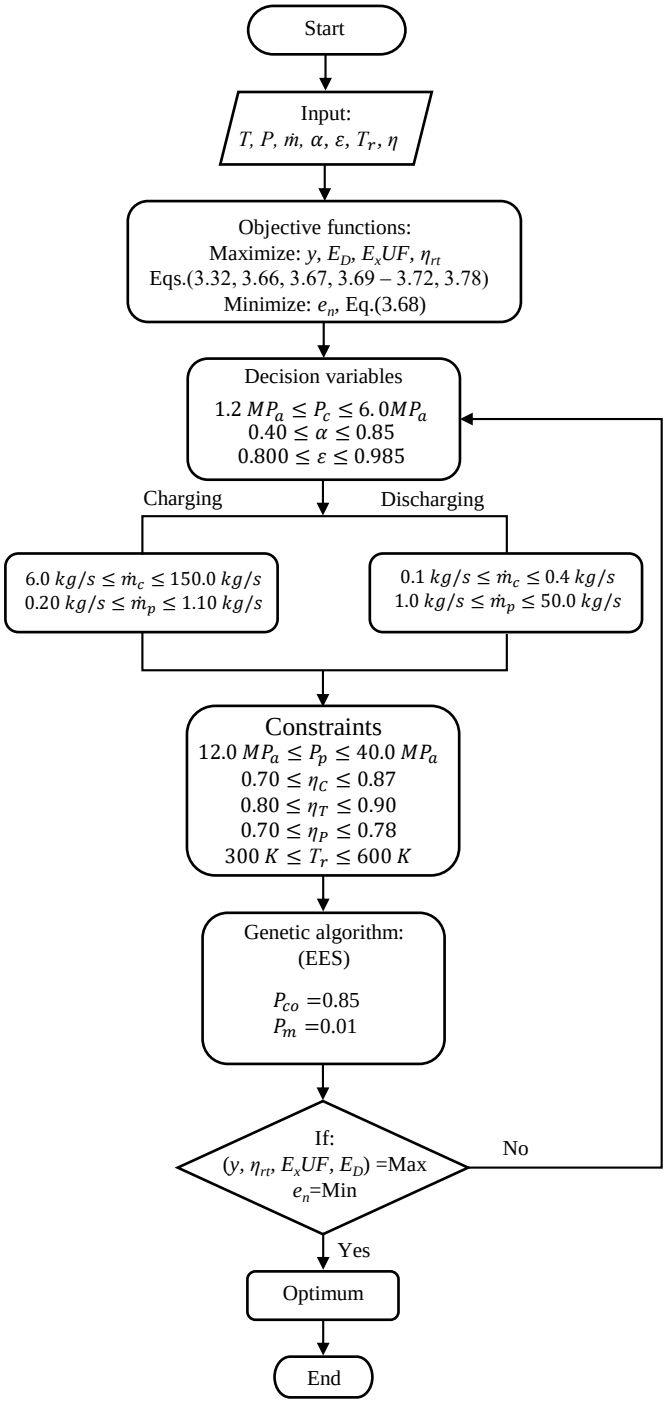

Figure 3.14 – Procedure of the optimization algorithm.

the economic feasibility of the proposed CES cogeneration plant, a life-cost analysis is accomplished by using methods based on rational criteria. Net present value (NPV), Internal rate of return (IRR), Payback period (PBP), Benefit cost ratio (B/C), and Levelized product costs methods are introduced in this study in order to compare the economic performance of the proposed CES systems.

Table 3.5 – Capital cost equations of the CES system equipment, ($USD).

Components	Functions	Reference
Compressor	$Z_{k,c} = \left(\frac{39.5\dot{m}_c}{0.9-\eta_c}\right)\left(\frac{P_2}{P_1}\right) ln\left(\frac{P_2}{P_1}\right)$	[76]
Heat exchangers	$Z_{k,he} = 130\left(\frac{A_{HE}}{0.093}\right)^{0.78}$	[76]
Turbines	$Z_{k,t} = 6000\left(\frac{W_t}{\eta_t}\right)^{0.7} + 60W_t^{0.95}$	[94]
Storage tank	$Z_{k,st} = 4042V_T^{0.506}$	[76]
Cryogenic pump	$Z_{k,p} = 3540\dot{W}_P^{0.71}$	[76]
Evaporator	$Z_{k,e} = 130\left(\frac{A_E}{0.093}\right)^{0.78}$	[76]
Heaters	$Z_{k,h} = 130\left(\frac{A_H}{0.093}\right)^{0.78}$	[76]
Distillation column	$Z_{k,d} = Z_v + Z_t$	[40]
	$Z_v = 1780(l)^{0.87}(d)^{1.23}[2.86 + 1.694F_M(10.01 - 7.408lnP + 1.395(lnP)^2)]$	
	L - Length of the column, d - Diameter of the column	
	F_M - Material factor, P - Column mean pressure	
	$Z_t = (193.04 + 22.72(d) + 60.38(d)^2)[(F_{BM})(N_{act})(f_q)]$	
	F_{BM}=Bare-Module factor, N_{act} - Actual number of trays	
	f_q - Quantity factor	

3.4.1 Capital investment.

The total capital investment is established as the capital required to purchase and install the equipment, including also other costs. Table 3.5 presents the main mathematical functions to calculate the equipment cost along with its reference.

Every cost of the equipment must be modified to the cost index of 2021. That is, cost functions from Table 3.5 should be modified to the actual cost year. The cost indexes used in this study to update the cost function values are based on the Chemical Engineering Plant Cost Index (CEPCI) [205]. The Eq. 3.79 is applied to update the equipment costs [206, 40, 122].

$$\dot{Z}_{k,n} = \dot{Z}_{k,r}\left(\frac{I_{k,n}}{I_{k,r}}\right) \tag{3.79}$$

Where, $\dot{Z}_{k,n}$ and $\dot{Z}_{k,r}$ are the new updated cost rate and cost rate at the reference year expressed in $USD. $I_{k,n}$ and $I_{k,r}$ are the cost indexes at new and reference year, respectively. The CEPCI from February 2021 is set at 7.2 % higher than the corresponding figure from

Table 3.6 – Main cost elements for the CES systems ($USD) [12].

Cost item	Functions
1. Fixed capital investment (FCI)	
Purchased equipment cost (PEC)	$\sum Z_k$
Total direct cost (DC)	
Equipment installation	20 % of PEC
Piping	10 % of PEC
Instrumentation and control	6 % of PEC
Land	5 % of PEC
Civil, structural & architectural work	15 % of PEC
Service facilities	30 % of PEC
Total indirect cost (IC)	
Engineering & supervision	4 % of DC
Construction cost	15 % of DC
Contingencies	8 % of above sum
2. Other outlays (OL)	
Startup costs	5 % of FCI
Working capital	10 % of FCI
Cost of licensing, research & development	2 % of FCI
3. Total capital investment (TCI)	FCI+OL

2020, then CEPCI=639.1 for present year, knowing that for 2020 was set at 596.2 [205].

Table 3.6 describes the methodology used in this study to calculate the total capital investment for each alternative of CES system (operation mode). The fixed capital investment (FCI) is the sum of the updated equipment cost (PEC), and the direct (DC) and indirect (IC) costs. The direct cost elements are obtained by employing the purchased equipment cost (PEC) as a base of calculation. While the indirect cost uses the direct cost as a calculation basis. The total capital investment (TCI) is obtained as the sum of FCI and other outlays (OL).

3.4.2 Cash flow or annual revenue.

For each alternative, the net cash inflow (CF_n) is estimated as the amount of income acquired through selling the electricity and cooling load minus the operation and maintenance cost, charging electricity cost and the heat cost for air reheating. Eventually, the selling of a percentage of liquid air or nitrogen and oxygen can be another option of

income for every alternative if the use of cryogenic generators in small scale [15] become popular in the domestic market, and also considering the increasing demand of nitrogen and oxygen [165]. For this, the electricity generation and the cooling load for the external user are reduced, but the total income can be increased, improving the profitability of the CES systems. This option requires and additional investment, such as, air separation unit and auxiliaries [207, 208, 209]. In this study, it is considered to commercialize 20 % of the liquid air production (N_2 and O_2) in order to evaluate the economic feasibility of the three CES system alternatives. The cash inflows and outflows are respectively calculated by Eqs. 3.80 and 3.81. The annual net cash inflow is given by Eq. 3.82.

$$CF_{in} = \left(\dot{W}_n^{dis}\Delta\tau_{dis}E_{TP} + \dot{Q}_E\Delta\tau_{ne}C_C + M_lC_L\right)c_d365 \tag{3.80}$$

$$CF_{out} = \left(\dot{W}_n^{ch}\Delta\tau_{ch}E_{TO} + \dot{Q}_H\Delta\tau_{nh}C_H\right)c_d365 + OM \tag{3.81}$$

$$CF_n = CF_{in} - CF_{out} \tag{3.82}$$

where $\dot{W}_n^{dis}$ and $\dot{W}_n^{ch}$ represent the net power per cycle during discharging and charging processes, respectively; E_{TP} and E_{TO} are respectively the electricity tariff on peak and off-peak time; $\dot{Q}_E$ and $\dot{Q}_H$ are the rate of cooling load and waste heat for air reheating in every cycle, respectively; $\Delta\tau_n$ is the total time for cooling load generation (e) and waste heat consumption (h); C_C, C_H and C_L are the respective prices of cooling, waste heat and liquid air (or nitrogen and oxygen) whose values are given in Fig. 3.9; M_l depicts the amount of liquid air; c_d is the number of cycle per day; and OM is the annual operation and maintenance costs, which varies from 1.5 % to 3 % of the fixed capital cost [210].It has been assumed that every alternative operates 365 days in a year.

3.4.3 Net Present Value (NPV).

The NPV is a method frequently used to evaluate investment projects, it considers the time value of money and the net cash flow during the useful life of the project. The NPV is calculated with the following equation [211, 12].

$$NPV = \sum_{k=1}^{n} \frac{CF_k}{(1+i)^k} - TCI \tag{3.83}$$

where CF_k represents the net cash flow or annual revenue at the end of a generic $k-th$ year, i is the discount rate (i = 6 %) and n the span life of project. TCI is the Total Capital Investment estimated according to Table 3.6. For project selection the NPV must be positive and among different alternatives, the project with the highest NPV constitutes the priority.

3.4.4 Internal Rate of Return (IRR).

The IRR is the discount rate that makes the NPV of a project equal to zero [12]. For the investment to be attractive, the IRR must be greater than the discount rate.

$$\sum_{k=1}^{n} \frac{CF_k}{(1+IRR)^k} - TCI = 0 \tag{3.84}$$

3.4.5 Payback Period (PBP).

The PBP represents the time for the project or alternative of CES system to recover the initial investment (TCI) [163]. When the time value of money is taken into account, the dynamic payback period can be calculated by Eq. 3.85.

$$PBP = k + \frac{|NPV_k|}{CF_{k+1}} \tag{3.85}$$

Where, k is the last year when NPV is negative, $|NPV_k|$ is the absolute value at year k, and CF_{k+1} is the cash flow or annual revenue in y ear k+1.

3.4.6 Benefit to cost ratio (B/C).

The B/C ratio is a complement of the NPV method, and it represents the efficiency of a project [212, 213, 12]. It is desirable that B/C exceeds the unit, that is, the benefits of the project must be greater than the cost. Therefore, the project or alternative with the highest B/C must be the preference.

$$(B/C) = \frac{\sum_{k=1}^{n} \frac{CF_k}{(1+i)^k}}{TCI} \tag{3.86}$$

3.4.7 Levelized costs of products.

The levelized cost of storage liquid air (LCOL) can be calculated by adapting the traditional methodology to estimate the levelized cost of electricity (LCOE) [214, 215]. The LCOL for every operation mode is determined by Eq. 3.87, which is the ratio between the net levelized outlays and the levelized quantity of produced liquid air.

$$LCOL = \frac{TCI + \sum_{k=1}^{n} \frac{EC_{ch}}{(1+i)^k} + \sum_{k=1}^{n} \frac{OM}{(1+i)^k} + \sum_{k=1}^{n} \frac{HC_{ch}}{(1+i)^k} - \frac{S_v}{(1+i)^n}}{\sum_{k=1}^{n} \frac{M_l}{(1+i)^k}} \tag{3.87}$$

where EC_{ch} is the annual electricity charging costs, it can be deduced from Eq. 3.81 as $EC_{ch} = \dot{W}_n^{ch} \Delta\tau_{ch} E_{TO} c_d 365$; HC_{ch} represents the annual heat costs during charging process,

$HC_{ch} = \dot{Q}_H \Delta\tau_{nh} C_H c_d 365$; and M_l is the annual amount of produced liquid air, which is deduced by the mass balance equation in the cryogenic tank (Eq. 3.26). S_v represents the salvage value, which is assumed to be 5 % of TCI.

When it is required to compare several storage technologies with different investment costs and operation time, the levelized cost of storage results an useful comparison indicator. LCOS is defined as the levelized expenses (life-cycle cost) divided by the total amount of produced electricity [216, 217].

$$LCOS = \frac{TCI + \sum_{k=1}^{n} \frac{EC_{ch}}{(1+i)^k} + \sum_{k=1}^{n} \frac{OM}{(1+i)^k} + \sum_{k=1}^{n} \frac{HC_t}{(1+i)^k} - \frac{S_v}{(1+i)^n}}{\sum_{k=1}^{n} \frac{E_{dis}}{(1+i)^k}} \tag{3.88}$$

where E_{dis} is the annual electricity generation, which can be expressed as: $E_{dis} = \dot{W}_n^{dis} \Delta\tau_{dis} c_d 365$; HC_t depicts the annual total heat cost for air reheating, and is given by: $HC_t = \dot{Q}_H \Delta\tau_{nh} C_H c_d 365$.

Considering that all alternatives operate in cogeneration regime, the levelized cost of cogeneration (LCOC) is proposed for comparison among them. LCOC is expressed as the ratio of the levelized outlays over the sum of the life-time of electricity and cooling load generation.

$$LCOC = \frac{TCI + \sum_{k=1}^{n} \frac{EC_{ch}}{(1+i)^k} + \sum_{k=1}^{n} \frac{OM}{(1+i)^k} + \sum_{k=1}^{n} \frac{HC_t}{(1+i)^k} - \frac{S_v}{(1+i)^n}}{\sum_{k=1}^{n} \frac{E_{dis}}{(1+i)^k} + \sum_{k=1}^{n} \frac{Q_{E,a}}{(1+i)^k}} \tag{3.89}$$

where $Q_{E,a}$ represents the annual cooling load generation, and is expressed as $Q_{E,a} = \dot{Q}_E \Delta\tau_{ne} c_d 365$. In general, the levelized cost method can be used to assess the profitability of the technologies, considering that it provides information about the minimum price of product (electricity, cooling, heat, others) to break even along the life-time technology [116].

3.4.8 Uncertainty analysis.

The uncertainty (u_Y) of a certain parameter Y which is a function of independent variables $X_1, X_2, ..., X_n$, with a random variability, referred to their uncertainties, that is:

$$Y = f(X_1, X_2, ..., X_n) \tag{3.90}$$

can be estimated by Eq. 3.91 [218, 219].

$$u_Y = \sqrt{\left(\frac{\partial Y}{\partial X_1} u_{x_1}\right)^2 + \left(\frac{\partial Y}{\partial X_2} u_{x_2}\right)^2 + ... + \left(\frac{\partial Y}{\partial X_n} u_{x_n}\right)^2} \tag{3.91}$$

Where $u_{x_1}, u_{x_2}, u_{x_n}$ represent the uncertainties of the independent variables. The previous equation allows to quantify the propagation of the uncertainties of independent variables into the value of the calculated parameter.

The net present value (NPV) is considered an important economic parameter to evaluate the profitability of investment projects. Therefore, taking into account the relevance of this parameter for making decisions, the sources of uncertainty and their propagation in this indicator are assessed. The NPV depends on several parameters and indicators which normally carry a significant level of uncertainty. For example, capital costs, interest rate, O&M costs, cooling load price, and electricity tariffs are some of them. For this study, the electricity tariff on peak and off-peak time from 105 electrical energy distributors in Brazil were analyzed [164]. Consequently, the uncertainties of these two variables were quantified in order to assess their distribution in the NPV. Figure 3.15 illustrates the frequency histogram and probability function of the electricity tariff on peak time with mean (μ) of 0.2249 $\$/kWh$, standard deviation ($\sigma$) of 0.0537 $\$/kWh$ and range between the minimum and maximum values of 0.1076 - 0.4384 $\$/kWh$, respectively.

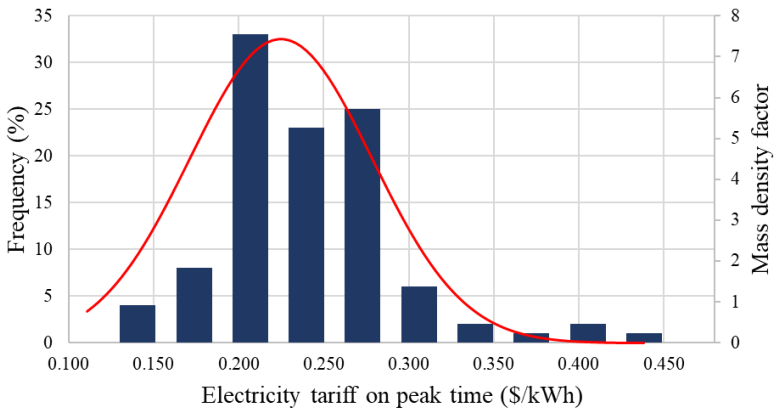

Figure 3.15 – Frequency histogram and probability function for the electricity tariff on peak time (Dollar trading on March, 22nd 2021. $\$USD$ 1.00 = $R\$$ 5.53).

The histogram for electricity tariff in off-peak time is shown in Fig. 3.16. For this, μ=0.0897 $\$/kWh$, σ=0.0133 $\$/kWh$, and range for minimum and maximum values of 0.0578 - 0.1410 $\$/kWh$, respectively.

The uncertainty analysis for operation modes A, B and C is carried out in EES software. The standard deviation for both the electricity tariff on peak and off-peak time are set as the input uncertainties to be propagated through the NPV (Eq. 3.83).

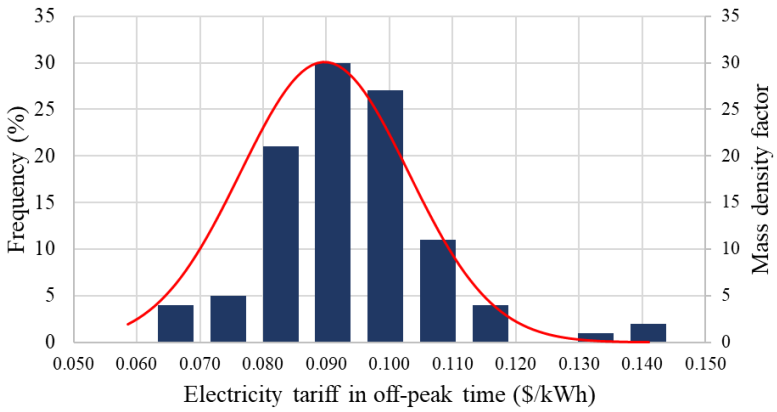

Figure 3.16 – Frequency histogram and probability function for the electricity tariff in off-peak time (Dollar trading on March, 22nd 2021. $\$USD$ 1.00 = $R\$$ 5.53).

4 Results and discussion.

The traditional mode of operating CES systems is based on the intermittent performance of the charging and discharging processes, which leads to low utilization of the cogeneration potential of this storage technology. Abdo [9] proposed the simultaneous operation of the charging and discharging processes, but did not demonstrate the thermodynamic viability of this transformation either quantitatively evaluate the main indexes and indicators. Moreover, no studies have previously examined the performance of cogeneration CES systems when charge and expansion sections operate simultaneously. Through the simultaneous operation of the charging and discharging processes in cogeneration CES systems, the efficiency, specific exergy consumption and other indexes and indicators can be significantly improved. Additionally, the method to store energy in the form of liquid air can be suitable to choose the storage capacity in order to meet the electricity and cooling demands. The simple layout of the cogeneration CES cycles (Figs. 3.3, 3.4 and 3.5) facilitates its integration to renewables to power the compressor and pump and also to use waste heat in the multi-expansion turbine. The last measure can contribute to increasing the power generation and the thermodynamic feasibility of the cogeneration CES system. In order to make clear the advantages of the simultaneous operation of the charging and discharging processes, four alternatives are compared. The first one, represented by Fig. 3.3, carries out both the charging and discharging processes simultaneously. The second one, name as option A and illustrated in Fig. 3.4, runs both the charging and discharging circuits separately. Option B represented by Fig. 3.5 operates with the simultaneous operation of the storage and release processes. Finally, option C also based on Fig. 3.5, but with the simultaneous operation of the liquefaction and discharge circuits for charging regime, whilst for discharging regime the liquefaction circuit remains out of service.

4.1 Mathematical model verification

.

In order to check and validate the accuracy of the obtained results and the modeling approach proposed for CES cogeneration system simulation, performance parameters, indexes, and indicators are compared with the corresponding results reported in [65, 9, 29, 7]. Figure 4.1 illustrates the influence of diverted air mass fraction on specific exergy consumption for $\varepsilon = 0.8$. As the curves of the present study and the Ref. [9] indicate, there is a good agreement between them and the results match with an deviation of the dispersion average of 5.8 %. Morgan *et al.* [65] and Sciacovelli *et al.* [70] evaluated the thermodynamic performance of a real CES pilot plant and found the specific work for the

liquefaction process in a range of about 0.50 and 0.67 kWh/kg_L. For this study, the same indicator is found to be 0.69 kWh/kg_L, which is 2.9 % higher than the upper limit of the referred studies. The air diverted through the expander in the Claude cycle must be closed to the optimal value in order to increase the performance of the liquefaction process. For this, Kreith [29] and Kerry [7] recommend, from practical studies, to use a fraction of 0.60 to 0.80. In this study, the results show that the optimal diverted air mass fraction is found to be between 0.66 and 0.72, which is in a great concordance with the experimental values of the aforementioned references. The match between the experimental evidences and the numerical prediction results of this study confirm the validity of the proposed mathematical model. Further results of the present investigation are compared throughout this section.

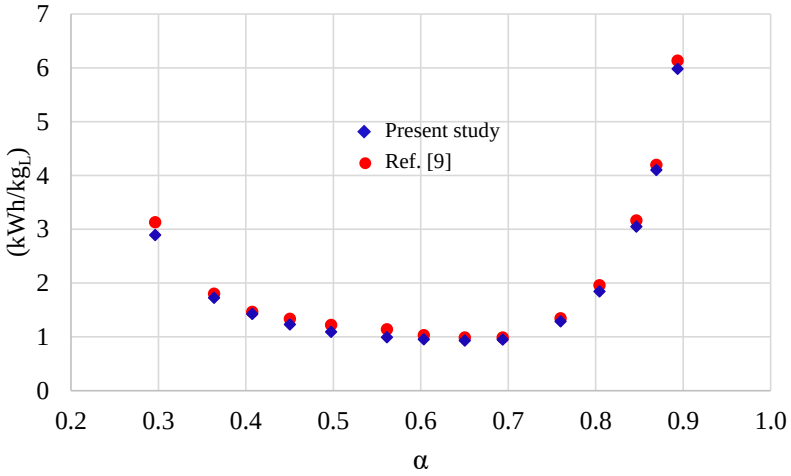

Figure 4.1 – Variation of the specific exergy consumption with diverted air mass fraction for $\varepsilon = 0.8$.

4.2 Liquid yield and charging time.

Figure 4.2 shows the effect of the diverted air mass fraction and effectiveness of the heat exchangers on specific liquid yield for the compressor pressure of 5.0 MPa. A linear trend can be observed, indicating that increasing the diverted fraction and effectiveness, proportionally increases the liquid yield up to values of diverted fraction ranged between 0.67 to 0.72, for the specified maximum and minimum values of effectiveness, respectively. For greater values of diverted air mass fraction, liquid yield shifts for a downward trend, almost becoming independent of effectiveness, which is led by Eq. 3.40, that is, a substantial increase in the diverted fraction produces a sharp decrease in the specific air liquid yield, on this point, the temperature drop experienced by stream 4-6 from Fig. 3.3 is not enough to keep the specific air liquid yield growing and, consequently, the even more reduced mass flow rate through the liquefaction circuit leads to an appreciable decrease of this indicator.

This result shows that, increasing diverted air fraction causes a reduction of air mass flow rate through the last two heat exchangers (HE-2 and HE-3), producing an even higher temperature drop (2-6, Figs. 3.3 and 3.5), ultimately becoming liquid (compressed liquid).

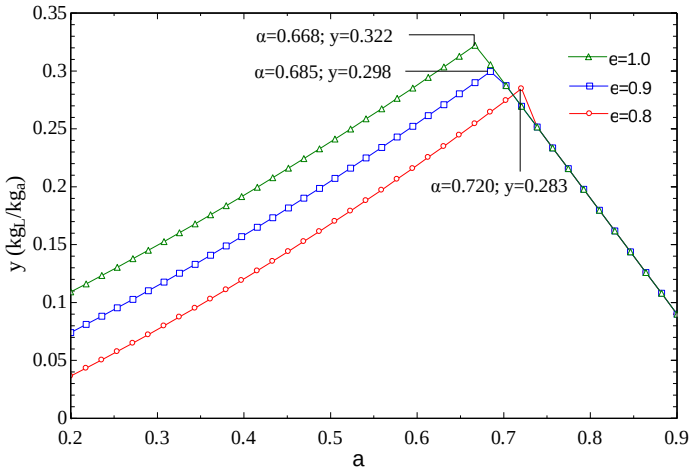

Figure 4.2 – Effect of diverted air mass fraction

and effectiveness of the heat exchangers on specific liquid yield during charging regime, considering a high pressure of 5.0 MPa (Fig. 3.3).

Results of Fig. 4.2 also emphasize the strong dependence of liquid yield on the heat exchangers effectiveness. For every 10 % of increasing effectiveness, liquid yield increases 0.026 kg_L/kg_a in average. For ε=1.0, the highest specific liquid yield is 0.322 kg_L/kg_a when the diverted air mass fraction reaches 0.662. The results presented in [9] show that the specific liquid yield for the CES system was 0.250 kg_L/kg_a, whilst in [140] was reported a value of 0.730 kg_L/kg_a. In other research [100], the authors evaluated a CES integrated to a single flash geothermal power plant and found a specific liquid yield of 0.585 kg_L/kg_a, considering adiabatic surface for the heat exchangers and ideal compression. While for hydrogen liquefaction, the research in [220] reported a total yield of 25.0 kg_L/kg_a.

Figure 4.3 displays, for operation modes B and C represented in Figure 3.5, the effect of diverted air mass fraction and effectiveness of the heat exchangers on specific liquid yield for an outlet compressor pressure of 5 MPa. The use of a double expansion turbine (Figure 3.5) produces an increase of liquid yield when compare to the single expansion turbine (Figure 3.4). This fact can be verified by the proportional relationship between specific air liquid yield and the power generation at T-1 from Eqs. 3.32, 3.33, 3.41, and 3.45. The increase in liquid yield (Δy) by the use of double expansion at T-1 (Fig. 3.5) is represented at the right side of Fig. 4.3. For ε=1.0, the maximum specific liquid yield is 0.412 kg_L/kg_a, which is 21.8 % higher than that of the CES system with expansion valve (Fig. 3.3). Additionally, the increase in liquid yield for every 10 % of increase effectiveness is almost 50 % higher than the result reported in Fig. 4.2. It is clear that turbine expansions (T-1 and T-2) are directly proportional to liquid yield (Eqs. 3.32 and 3.41) and produce a significant air temperature reduction (Fig. 3.8). These facts explain the higher proportion

of liquid yield for operation modes B and C respect to A, that is, the specific liquid yield for modes B and C is in between 16.2 % to 20 % higher than mode A.

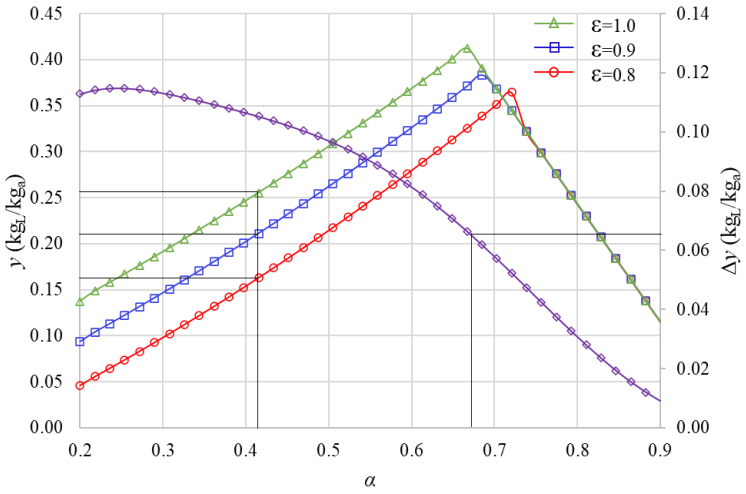

Figure 4.3 – Effect of diverted air mass fraction and effectiveness of the heat exchangers on specific liquid yield during charging regime for operation modes B and C.

The effect of outlet compressor pressure and effectiveness on liquid yield is illustrated in Fig. 4.4 for $\alpha = 0.60$. It can be seen that liquid yield rapidly increases with pressure and effectiveness up to approximately 4.0 MPa, at a rate ranged from 0.060 to 0.064 kg_L/kg_aMPa according to the effectiveness, beyond that point of pressure the slope reduces gradually at approximately constant rate of 0.011 kg_L/kg_aMPa, obtaining less liquid production for each unit of pressure increase. This behavior demonstrates that increasing compressor pressure is advantageous to the specific air liquid yield. But, the specific exergy consumption also goes up. Therefore, there is intermediate outlet compressor pressure that is more interesting for process. The increase in outlet compressor pressure produces an increase on the specific air liquid yield due to the increasing specific heat, and the earlier two phase formation at the second heat exchanger. During charging regime, the dislodgement of liquid level gradually increases (Fig. 3.13a), producing an increase in saturated vapor mass flow rate leaving from the cryogenic tank (state 8, Figs. 3.3-3.5), which leads to an intensification of the heat transfer conditions at the heat exchangers and the rise of liquid yield. As a result of the increase of compressor pressure, the power generation at the cryogenic turbine increases, especially at the first expansion section $(h_{13} - h_{14s})$, positively influencing the increase of liquid air production. It can be also observed that the isentropic efficiency of the turbine has a direct influence on liquid yield, thus when the expansions tend to be isentropic, more liquid air is obtained from the liquefaction process.

Figure 4.5 shows the influence of the heat exchanger effectiveness and outlet compressor pressure on charging time for $\dot{m}_c$=18.0 kg/s, α=0.60 and C_t=50 t. It is observed that charging time may become excessively high for low pressure values, leading

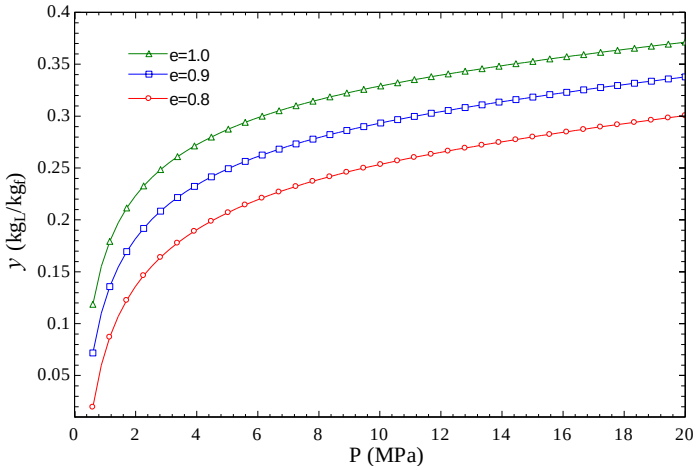

Figure 4.4 – Influence of compressor pressure and effectiveness of the heat exchangers on specific liquid yield during charging regime for α=0.60 (Fig. 3.3).

to inconvenient operating conditions for the cryogenic energy storage (CES) systems. The charging time becomes less sensitive for pressure values greater than 4.0 MPa, with an average reduction of 0.52 h/MPa considering $\varepsilon \geq$0.90.

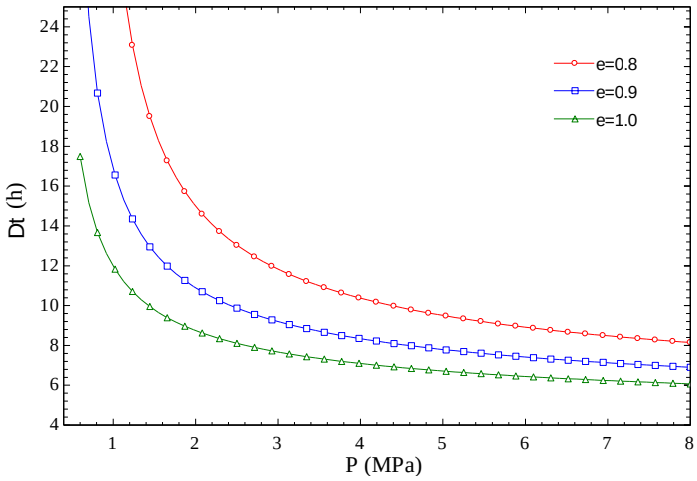

Figure 4.5 – Dependence of the charging time respect to compressor pressure and effectiveness of the heat exchangers, for $\dot{m}_c$=18.0 kg/s, α=0.60 and C_t=50 t (Fig. 3.3).

4.3 Exergy analysis.

Figure 4.6 shows the effect of heat exchanger effectiveness and outlet compressor pressure on exergy efficiency for charging regime. Increasing compressor pressure produces a positive effect on exergy efficiency up to certain values, from which efficiency slightly decreases. This can be understood from the fact that initially, the power consumption is low, which is motivated by the lower pressure values and the sustained increase in power

generation due to the increasing outlet compressor pressure. The exergy efficiency takes its maximum for pressure values $\leq$ 2.5 MPa, beyond that value, the power demand by the compression process results in higher proportion respect to power generation. The highest exergy efficiency for air liquefaction is 32.8 % when ideal heat transfer condition (ε=1.0) at the heat exchangers is considered. In Fig. 4.7 a higher exergy efficiency can be seen. The use of a cryogenic hydraulic turbine, considering its isentropic efficiency, (Fig. 3.5) instead of an expansion valve (Fig. 3.3) produces an increase in exergy efficiency of 24.7 %.

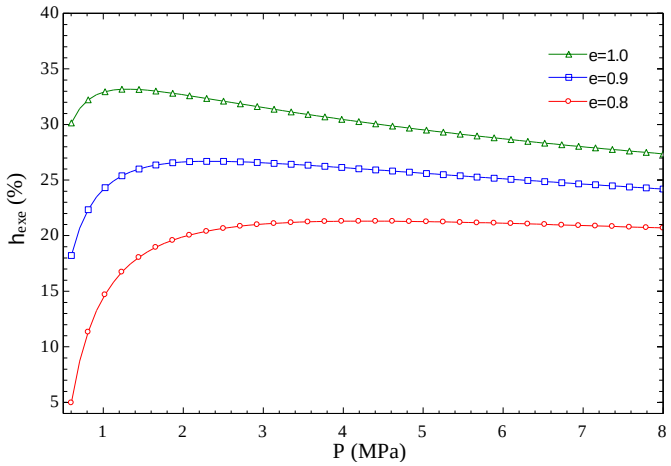

Figure 4.6 – Effect of compressor pressure and effectiveness of the heat exchangers on exergy efficiency during charging process, for $\dot{m}_c$=6.0 kg/s, α=0.60 and P_p=20.0 MPa (Fig. 3.3).

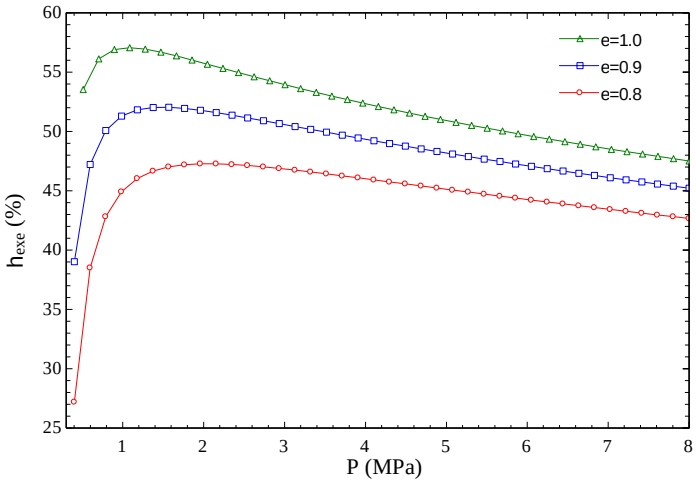

Figure 4.7 – Effect of compressor pressure and effectiveness of the heat exchangers on exergy efficiency for operation modes B and C during charging process, for $\dot{m}_c$=6.0 kg/s, α=0.60 and P_p=20.0 MPa.

The influence of the outlet pressure of the cryogenic pump and reheat temperature (T_r for turbine T-3, Fig. 3.3) on exergy efficiency during discharging process and $\dot{m}_p$=3.5 kg/s is shown in Fig. 4.8, while liquefaction section runs at 5.0 MPa of outlet

compressor pressure, α=0.60 and ε=0.95. For higher pressure and reheat temperature, the higher exergy efficiency is obtained. Every temperature curve increases logarithmically, producing a significant growth for pressure values less than 15.0 MPa, then exergy efficiency gradually increases with a lower slope. This result illustrates the significant increase in exergy efficiency when an external energy source at high temperature is available for power production. When waste heat is available at 500 K, the maximum exergy efficiency for discharging regime is 52.2 %, considering outlet pump pressure of 20.0 MPa. The result also suggests that for low outlet pump pressures the CES system produces more irreversibilities, pointing out a suitable range of outlet pressure of the cryogenic pump between 15 and 30 MPa. Another study [74] reported an exergy efficiency of 12.1 % for a air liquefaction cycle considering two stages of compression, this result was obtained considering a Claude cycle and similar operating conditions concerning the present study.

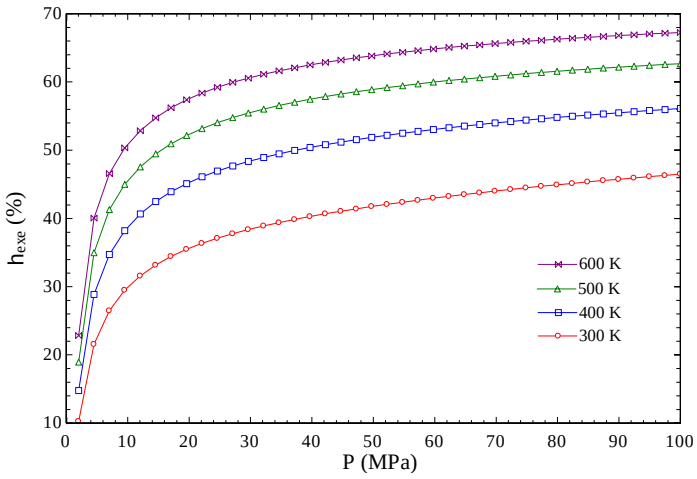

Figure 4.8 – Influence of pump pressure and inlet turbine temperature on exergy efficiency during discharging process, with compressor pressure of 5.0 MPa, α=0.60 and ε=0.95.

Variations in exergy efficiency for charging regime with air mass flow and heat exchanger effectiveness are shown in Fig. 4.9 for 5.0 MPa of outlet compressor pressure and α=0.60. The graph shows a sharp decrease in exergy efficiency with increasing air mass flow rate up to about 3.0 kg/s, after that, it reduces gradually for flow rates above 8.0 kg/s. This result suggests that for low air mass flow rate, any increase in air flow at low effectiveness represents a significant increase in irreversibilities, especially in the expansion valve, cryogenic turbine and compressor. Similarly, exergy efficiency presents a good behavior at very low air mass flow rate, however, the use of small air mass flow compromises the specific air liquid yield, the charging time and the exergy utilization factor, which negatively impacts the cycle performance during the discharging process. A similar trend is obtained when a cryogenic hydraulic turbine is used for liquefaction purposes (Fig. 4.10). However, the exergy efficiency is significantly higher for every effectiveness curve.

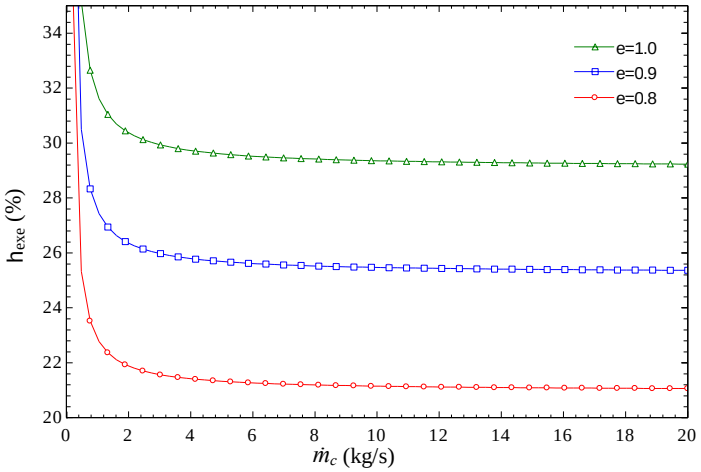

Figure 4.9 – Dependence of the exergy efficiency respect to air mass flow rate and effectiveness of the heat exchangers during charging process (Fig. 3.3).

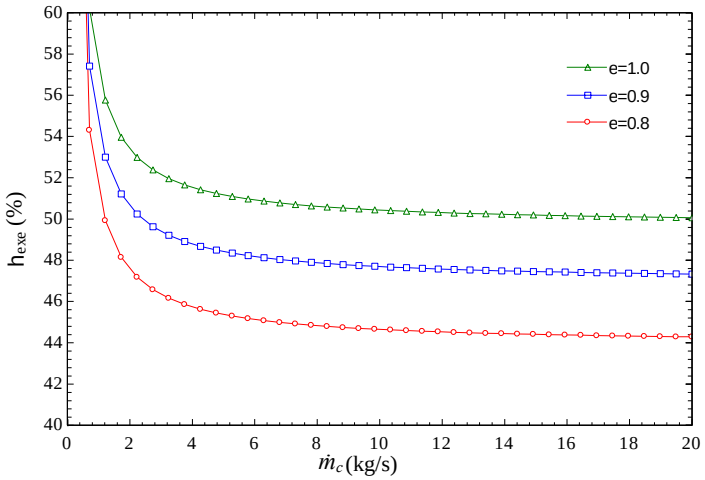

Figure 4.10 – Influence of the air mass flow rate and effectiveness of the heat exchangers on exergy efficiency during charging process for operation modes B and C (Fig. 3.5).

Based on data from Tables A.1 and A.2 from Appendix A, Figures 4.11 and 4.12 show a summary about the distribution of the exergy destruction of the cycle during charging and discharging regimes, respectively. As can be seen in Fig. 4.11, during charging regime, the components with the worst performance are the compressor and expansion valve, which carry 70.2 % of the total exergy destruction. Exergy destruction of all heat exchangers reached 17.6 %, which is higher than the cryogenic turbine (11.2 %). The isentropic efficiency of the turbines and the isothermal efficiency of the compressor were considered for calculation. Additionally, the effectiveness of the heat exchangers was set at 0.95.

For the discharging, the evaporator and the four-section expansion turbine contribute most to the total exergy destruction with 71.2 % as shown in Fig. 4.12. The

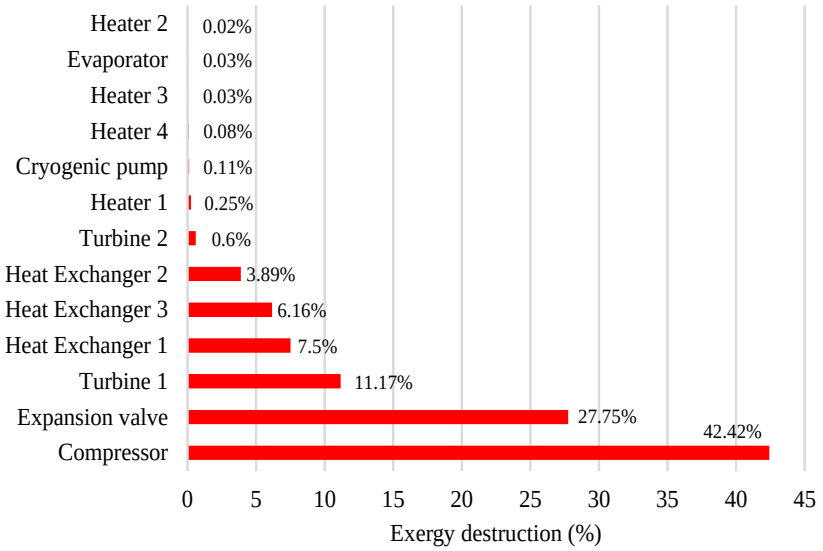

Figure 4.11 – Exergy destruction distribution for charging process, following the thermodynamic states given in Table A.1.

main reason of this result, for the heat exchangers, lies on the large temperature gradient between the streams and the surroundings, which increases the irreversibilities related to heat transfer under a finite temperature difference. In others studies, authors found the highest exergy destruction at the same components [156, 109]. Another research [58] points out that the worst thermodynamic behavior corresponded to the cryogenic turbine from the liquefaction section. Due to the high exergy destruction, the compression, expansion and cold transfer processes should be optimized in order to improve the cycle efficiency.

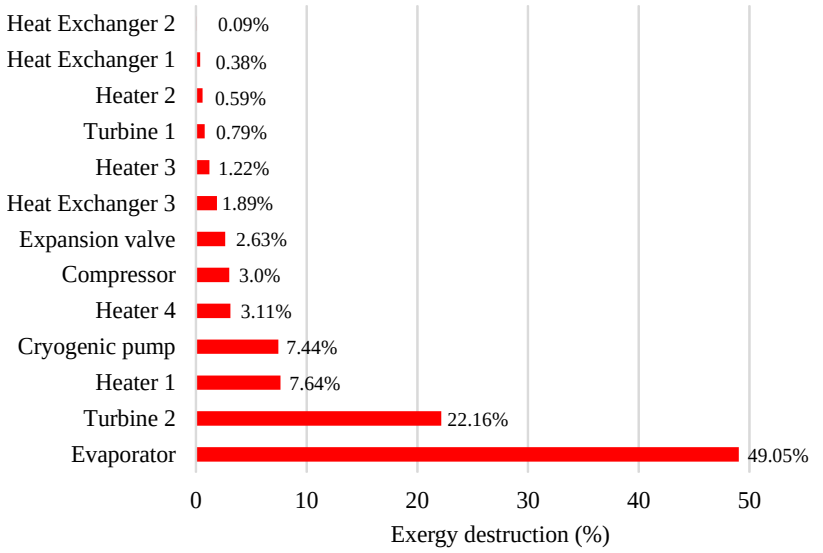

Figure 4.12 – Exergy destruction distribution for discharging process, following the thermodynamic states given in Table A.2.

As can be observed, for each operation mode in Fig. 4.13, the components with the worst thermodynamic performance are the compressor, heat exchangers and turbines, which carry with more than 96 % of the total exergy destruction. For the discharging process, the heaters, evaporator and expansion turbines contribute most to the total exergy destruction with more than 97 % as is shown in Fig. 4.14.

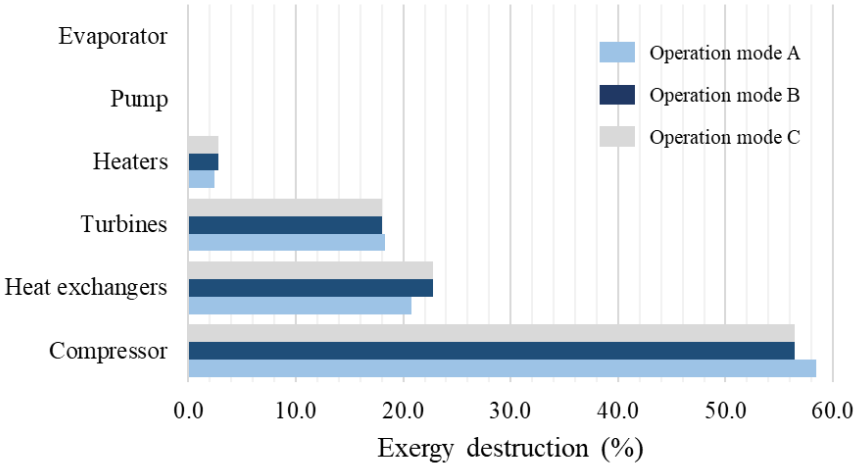

Figure 4.13 – Exergy destruction distribution for charging process.

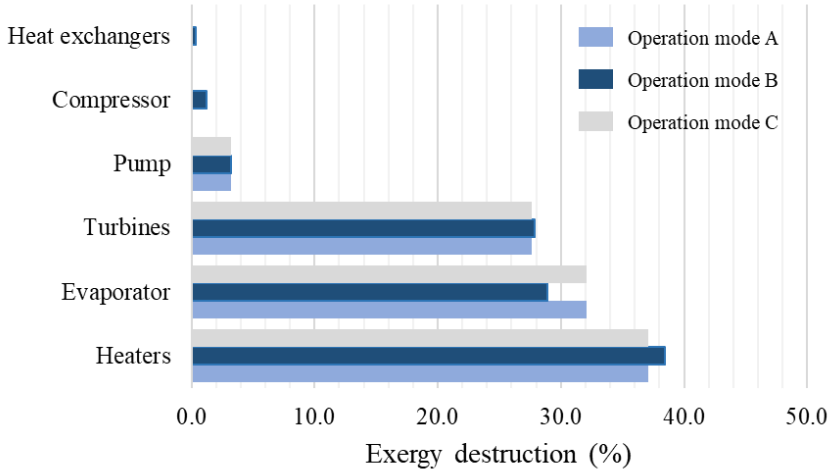

Figure 4.14 – Exergy destruction distribution for discharging process.

Table 4.1 lists a summary comparison of the exergy destruction proportion associated with each component for the CES systems. The irreversibility pattern of the present study, considering a whole cycle, is similar to other researches [159, 221]. It can be observed that compressor, heat exchanger, turbine and expansion valve subsystems carry the highest exergy destruction. When combustion devices are part of the CES system, for example, a hybrid CES plant, the combustion chamber results the most irreversible component [69]. For the heat exchanger component, the proportion of irreversibilities

between the present study (10.18 %) and the investigations listed in Table 4.1 presents a significant difference. One of the main reason of these differences lies on the consideration of a pressure drop through the heat exchangers [69, 159, 221, 222], for instance, in [159] the authors set a pressure drop through the heat exchanger of 50 kPa, this assumption, which is not considered in the present research, leads to an increase in irreversibilities due to the viscous effect of the fluid on the internal surface of the heat exchanger. Additionally, the use of high pressure (8-18 MPa) in the liquefaction section [69, 159] can bring to increase in irreversibilities how it was explained before in Fig.4.6. These results justify the growing trend of several researches at optimizing compressor, heat transfer and expansion processes [52, 96, 127]. The exergy analysis results for the cogeneration CES system illustrated in Fig. 3.3 are shown in Tables C.1 and C.2 from Appendix C for charging and discharging regimes, respectively. Similarly, for operation modes A, B and C, the exergy analysis results are presented in Tables C.3-C.8. The superiority of the simultaneous operation of the charging and discharging processes can be observed by analyzing these results. For instance, during the discharging regime, the operation mode B presents an exergy efficiency of 80.20 %, which is 1.3 % higher than that for operation mode A.

Table 4.1 – Comparison of the relative exergy destruction for different CES systems researches (%).

Component	Ref. [27]	Ref. [159]	Ref. [69]	Ref. [222]	Ref. [221]	Ref. [109]	This study
Compressor	22.00	21.43	9.00	16.20	25.21	21.80	23.30
Heat exchangers	28.00	20.31	38.00	37.70	26.22	22.70	10.18
Expansion valve	39.00	20.76	8.00	13.00	4.34	-	15.56
Turbines	6.00	16.51	5.00	3.10	25.01	25.40	17.19
Cryogenic pump	-	9.15	1.00	0.20	-	7.70	3.66
Evaporator	-	-	-	22.00	-	11.50	23.81
Cold storage	-	-	-	-	19.23	-	-
Combustor	-	-	39.00	11.90	-	-	-
Others components	5.00	11.84	-	17.80	-	10.90	6.29

4.4 Sensitivity analysis of performance indexes and indicators.

The influence of diverted air mass fraction and effectiveness on net specific exergy consumption is illustrated in Fig. 4.15, for the outlet compressor pressure of 5.0 MPa. The net specific exergy reaches its minimum value for α between 0.50 and 0.68, which is approximately 0.694 kWh/kg_L. Further increase of α reduces the air liquid production, increasing the specific exergy consumption (for $\alpha > 0.75$, Fig. 4.15). E. Borri *et al.* [74] modeled and optimized three air liquefaction plants and found for the Claude cycle a specific consumption between 0.72 and 0.73 kWh/kg_L, for diverted air mass fraction of

0.20 to 0.25 and discharge compressor pressure from 38 to 45 bar. Likewise, Abdo [9] and Chen *et al.* [140], in their researches, obtained 0.313 and 0.399 kWh/kg_L, respectively. While the first one assumed isentropic expansion at the cryogenic turbine and obtained overall efficiency greater than the unit for mass flow ratio $\geq$ 1.5 and α=0.60 to 0.80, in the second research the authors assumed adiabatic heat exchanger surface and did not consider the external source of heat to estimate the cycle efficiency. Another research [190] reported a specific energy consumption for a CES pilot plant of 0.730 kWh/kg_L without cold recycling.

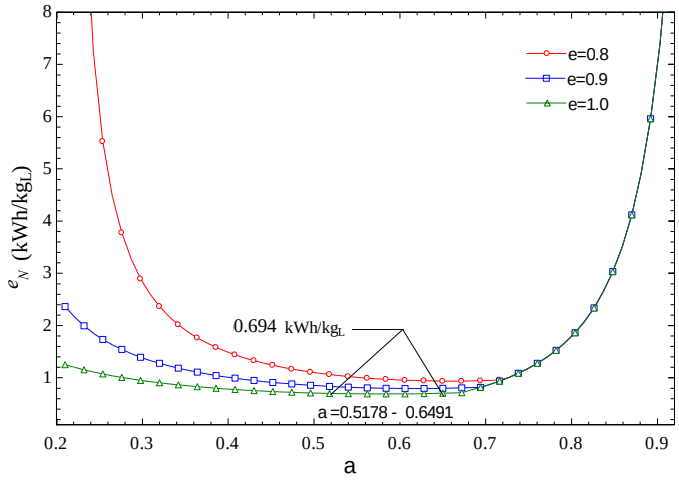

Figure 4.15 – Effect of diverted air mass fraction and effectiveness of the heat exchangers on specific exergy consumption during charging regime (Fig. 3.3).

The results presented in Fig. 4.16, for α=0.60, show that effectiveness of the heat exchangers and discharge compressor pressure are strongly related to the specific exergy consumption, especially for $P_c < 2.0$ MPa. Lower values of specific exergy consumption are observed in the pressure range from 1.2 MPa to 5.0 MPa. The lowest specific exergy consumption (0.956 kWh/kg_L) at ε=0.80 is obtained between 3.6 and 5.5 MPa, optimal values shift for lower pressure values, for instance, when ε=1.0, the optimum specific exergy consumption is 0.611 kWh/kg_L for a discharge pressure of 1.3 MPa. As the effectiveness of the heat exchangers increases from 0.80 to 0.90, the specific exergy consumption reduces in 0.179 kWh/kg_L at 4.0 MPa, while from 0.90 to 1.0, the reduction resulted in a contribution of 0.110 kWh/kg_L considering the same pressure value. When discharge pressure of 3.0 MPa is considered, the reduction of specific exergy consumption is a little higher, with values of 0.200 and 0.120 kWh/kg_L, respectively.

Figure 4.17 shows the effect of air mass flow and effectiveness on specific exergy consumption (for P_c = 5.0 MPa and α=0.60). After 5.0 kg/s, the specific exergy consumption tends to remain almost constant for every effectiveness value. In spite of the fact that the increase of air mass flow rate produces a rise of exergy destruction, these irreversibilities are compensated with the increase of power production at the cryogenic

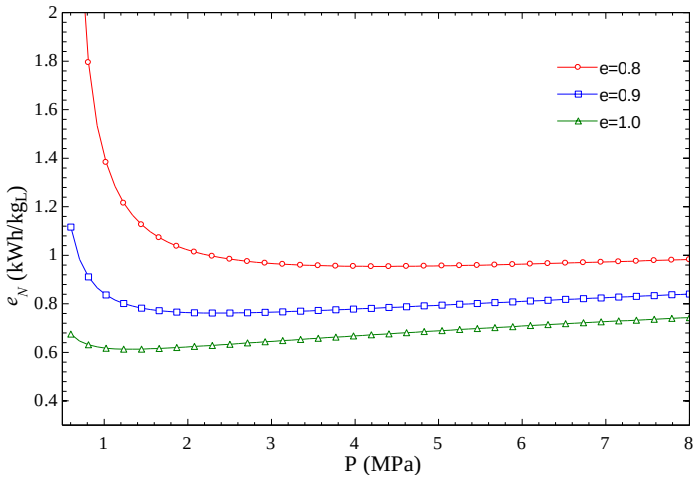

Figure 4.16 – Influence of compressor pressure and effectiveness of the heat exchangers on specific exergy consumption during charging regime (Fig. 3.3).

turbine. This explains the trend identified for the smooth section of the curves in Fig. 4.17. Additionally, for low air mass flow rate (< 1.0 kg/s) the CES system seems to perform with the lowest specific exergy consumption; however, the specific air liquid yield, the charging time and the exergy utilization factor are drastically affected. For instance, at low air mass flow rate, the air circulating through the liquefaction section would not be enough to stabilize the thermal inertia of the fixed heat transfer area in a short time, that is, the transient regime period would be extremely prolonged, which leads to increase the charging time and, consequently, to reduce the exergy utilization factor. In general, the trends of the curves suggest that it is possible to use a large air mass flow rate for liquefaction without a significant increase in specific exergy consumption.

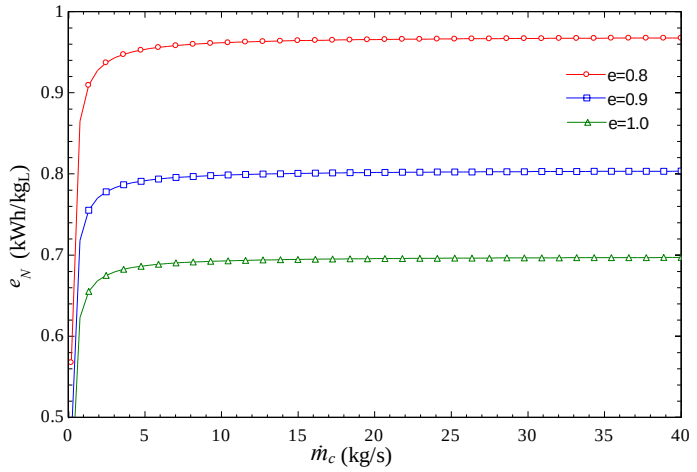

Figure 4.17 – Effect of air mass flow rate and effectiveness of the heat exchangers on specific exergy consumption during charging regime (Fig. 3.3).

Figure 4.18 depicts the influence of compressor pressure and effectiveness on

specific liquid yield and specific exergy consumption for α=0.60 and $\dot{m}_c$=6.0 kg/s. It can be observed that effectiveness must be higher than 0.43 to obtain liquid air at the cryogenic tank for compressor pressure of 5 MPa. The recommended effectiveness, for cryogenic heat exchangers, must be greater than 0.90 to get a more uniform difference temperature between the fluids [223]. For high effectiveness values specific exergy consumption becomes minimum and turns almost pressure independent. Furthermore, the growth in specific liquid yield due to the increase in pressure is reduced at every higher pressure level, suggesting the search of the optimal pressure to correlate energy required by compressor with specific liquid yield.

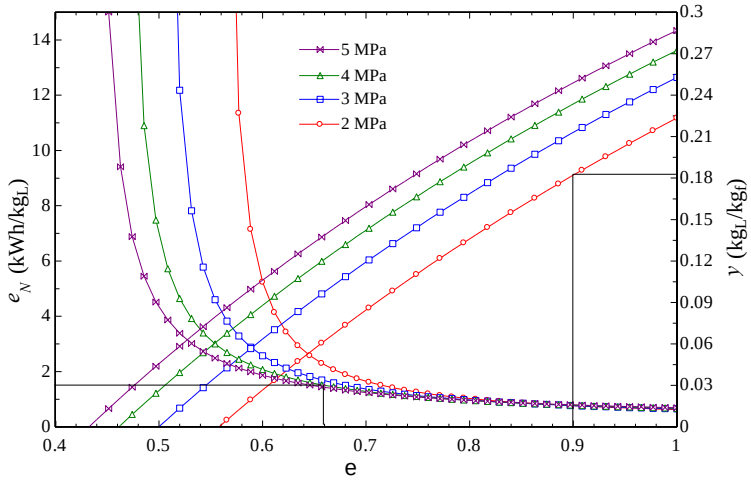

Figure 4.18 – Dependence of the net specific exergy consumption and liquid yield respect to effectiveness of the heat exchangers and compressor pressure (Fig. 3.3).

Figure 4.19 shows, for operation mode B, the effect of outlet compressor pressure and effectiveness of the heat exchangers on specific exergy consumption and liquid yield for α=0.6. It is observed that for high ε values specific exergy consumption becomes minimum. While for $\varepsilon < 0.80$, the lowest specific exergy consumption figures are registered for high outlet compressor pressure.

Figure 4.20 illustrates the behaviour of the specific exergy consumption for $\varepsilon \geq$0.92 where the indicator takes values from 0.410 kWh/kg_L to 0.506 kWh/kg_L. The minimum exergy required to produce the mass of liquid air is achieved for operation mode B, where the three turbines (T-1, T-2 and T-3) operate simultaneously reducing, even more than modes A and C, the power required by the compressor. For operation mode C, the indicator is slightly higher than mode B and for mode A, the difference is more significant, taking values for the same range of effectiveness from 0.513 kWh/kg_L to 0.609 kWh/kg_L. It must be also highlighted that the second expansion in T-1 (Fig. 3.5) improves the power production during charging process in 35.8 % and consequently reduces the compressor power consumption in 19.9 %.

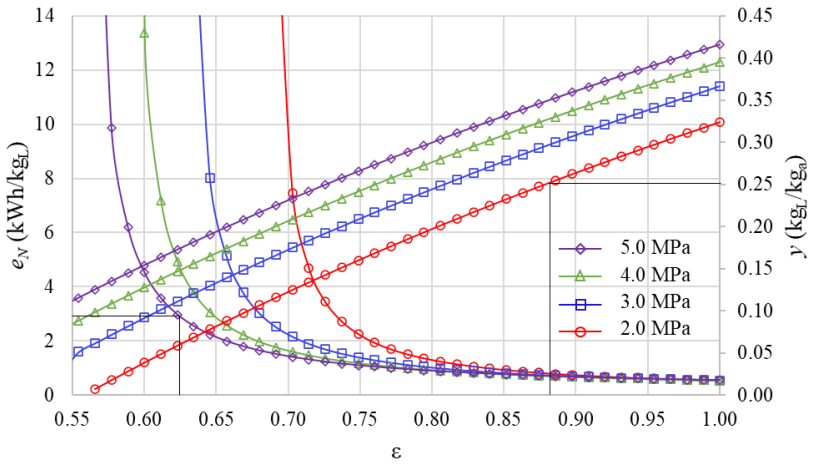

Figure 4.19 – Influence of compressor pressure and effectiveness of the heat exchangers on specific exergy consumption during charging regime, for α=0.6.

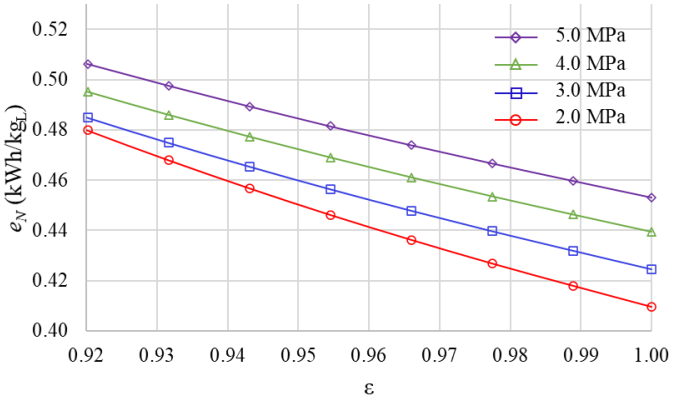

Figure 4.20 – Enlargement of the region for the overlapped curves in graph 4.19.

As shown in Fig. 4.21, for the case of CES cycle from Fig. 3.3, the increase of pump pressure and reheat temperature at the four sections expansion turbine produce a positive effect on exergy density. The optimal value at every temperature curve shifts to a higher pressure. At 20 MPa and between the temperature range considered the exergy density varies from 48.6 to 121.5 kWh/m^3, values much higher than the reported for compressed air energy storage (CAES) [78, 69], flywheel [217, 224], superconducting magnetic energy storage (SMES) [225, 226] and for the CES systems when carbon dioxide is used as cryogenic fluid [17, 50]. It is worthy to note that a larger exergy density also supposes a smaller reservoir for energy storage compared to the mentioned technologies. The considered heating temperatures are achievable by concentrating solar technologies [227], for instance, for Parabolic Trough Collector (PTC) the receiver outlet temperature can reach between 500 to 565 °C [228], for parabolic dish the fluid or gas can be heated to about 750 °C [229], and for solar tower the operating temperature can vary between 250 and 650 °C [230]. For a solar tower, the working thermal fluid can be heated at a high

temperature of more than 1500 °C [229].

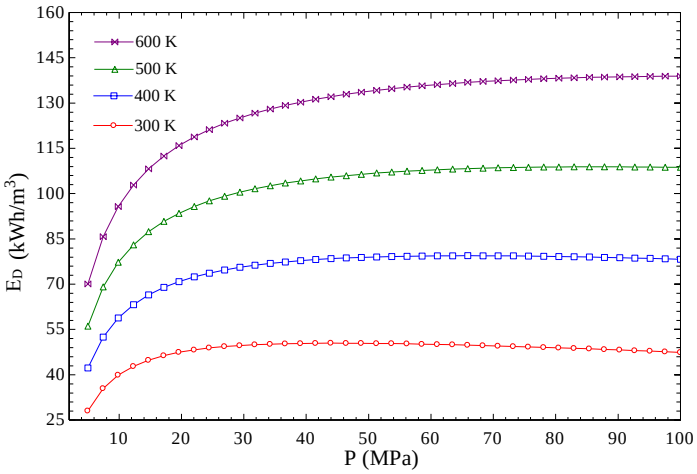

Figure 4.21 – Influence of pump pressure and turbine inlet temperature on exergy density during discharging process (Fig. 3.3).

In Fig. 4.22 it is shown the effect of pump pressure and reheat temperature at the four section expansion turbine on exergy density for operation modes A and C, which are represented by Figs. 3.4 and 3.5, respectively. The exergy density increases significantly with higher temperature and pressure up to approximately 20 MPa, after that, it increases gradually. This result suggests, according to the reheat temperature, that the maximum pump pressure, in order to achieve a suitable performance, lies between 20 MPa and 30 MPa. It can be also observed that for every temperature curve, the optimal value shifts to a higher pressure. On the right axis of the graph is represented the increase in exergy density respect to operation mode B. That is, the operation of the liquefaction section during discharging regime for mode B reduces the power generation and, consequently, the exergy density in the range of 15 kWh/m^3 to 24.2 kWh/m^3. For the considered temperature range (300 K - 600 K) and pump pressure of 20 MPa the exergy density varies from 54.7 kWh/m^3 to 133.5 kWh/m^3, which increased in approximately 9 % with respect to the values registered in Fig. 4.21.

During charging process, (for α=0.60, ε=0.95, P_c = 5.0 MPa, P_p = 20.0 MPa and T_r=400 K), the exergy efficiency drastically decreases in the course of the first hour, as indicated in Fig. 4.23. This initial behavior is highly influenced due to the increase in exergy destruction at compressor, turbines and expansion valve from Fig. 3.3. The exergy stored changes linearly with time and considering 50 t of cryogenic tank capacity, the total exergy stored is 10.31 MWh in a period of 6.81 h of charging time. For discharging process (Fig. 4.24), the rate of liquid exergy for power production is constant, that is why the exergy efficiency during exergy recovery remains the same (39.5 %) for a discharging time of 3.90 h.

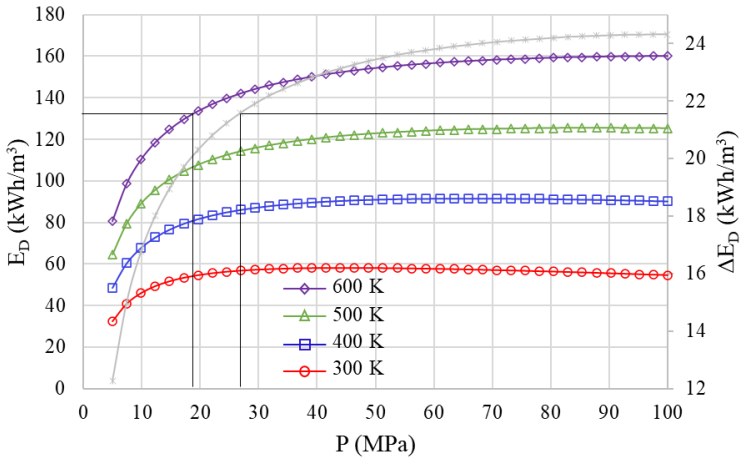

Figure 4.22 – Influence of pump outlet pressure and turbine inlet temperature on exergy density during discharging process for operation modes A and C.

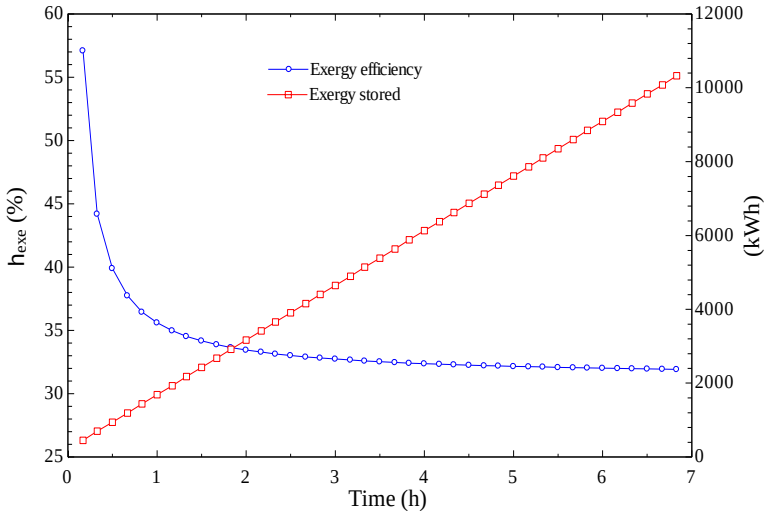

Figure 4.23 – Exergy efficiency and exergy stored at the cryogenic tank vs charging time.

The influence of diverted air mass fraction and reheat temperature in the four-section expansion turbine on round-trip efficiency (Eq. 3.70) is presented in Fig. 4.25, which corresponded to the CES cycle from Fig. 3.3 for $\varepsilon = 0.95$, $P_p = 20.0$ MPa, $\dot{m}_c = 12.0$ kg/s and $\dot{m}_p = 3.5$ kg/s. There is a clear maximum value at 0.64 of diverted air mass fraction with efficiency ranged between 7.9 and 30.2 % in the limits of the specified reheat temperature. The increase of α produces a higher power generation at the cryogenic turbine, which also rises the specific liquid yield (Fig. 4.2). Consequently, the improvement in the round-trip efficiency is highly benefited by the turbines power production. Further increase of α, beyond the optimum, affects the air liquid production due to the poor cooling performance at the heat exchangers, since less cold air coming from the cryogenic tank is sent back to the cold box, reducing the power output of the four-section expansion turbine, and therefore, the round-trip efficiency as well. The range of temperature set for

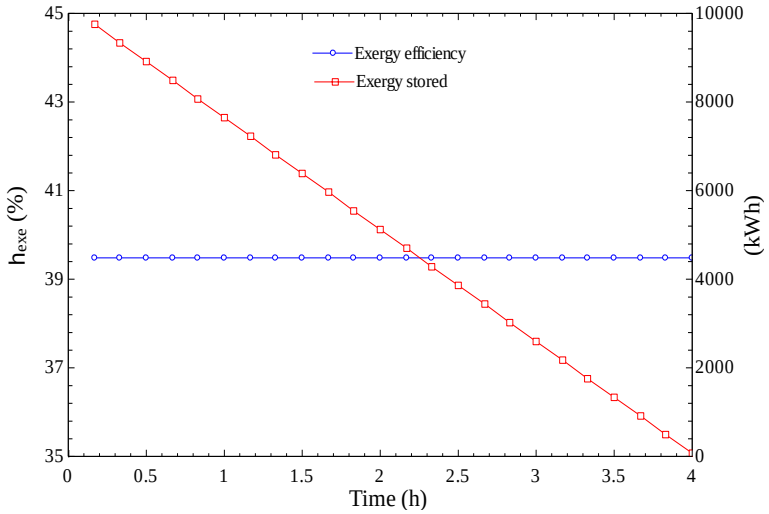

Figure 4.24 – Exergy efficiency and exergy stored at the cryogenic tank vs discharging time.

the sensitivity analysis of the round-trip efficiency was selected according to the available renewable energy technologies used for heating [229, 231].

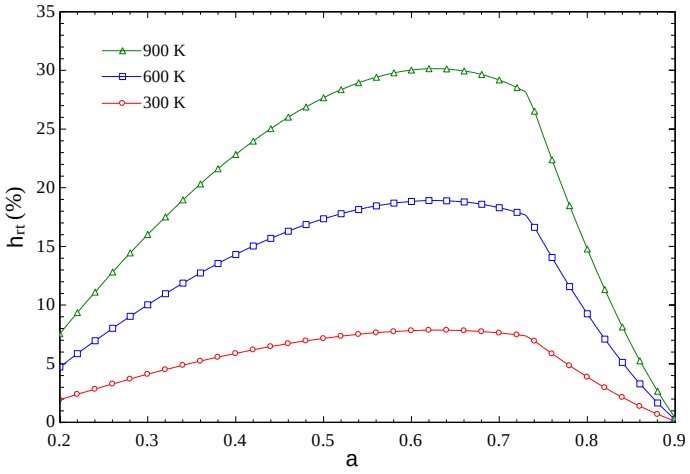

Figure 4.25 – Round-trip efficiency vs diverted air mass fraction and turbine inlet reheat temperature (Fig. 3.3).

As illustrated in Fig. 4.26, for a given reheat air temperature to the four-section expansion turbine, the round-trip efficiency increases with increasing compressor pressure, reaches an maximum, and then decreases with a further increase in pressure, advising that round trip efficiency is a function of charging pressure. The graph was plotted considering $\varepsilon = 0.95$, $\alpha = 0.60$, $P_p = 20.0$ MPa, $\dot{m}_c = 12.0$ kg/s and $\dot{m}_p = 3.5$ kg/s. The sudden increases of round-trip efficiency up to 1.6 MPa is leaded by both expansion turbines, the first one (cryogenic turbine) takes advantage of increase in pressure and the second one (four-section expansion turbine) of increase in reheat temperature (T_r). For further increases in pressure, larger compressor power consumption is obtained which leads to a

gradually reduction of the round-trip efficiency. The use of the two stages expansion turbine (T-1, Fig. 3.3) produces a 10.24 % reduction in power consumption during the charging process compared to the single-stage expansion turbine (T-1, Fig. 3.2) and the overall effect of the simultaneous operation of the expansion circuit with that of the liquefaction is a 19.91 % reduction in power consumption. That is, the CES system in Fig. 3.3 can be able to reduce the power consumption during charging process by almost a fifth. Those findings shown in Figs. 4.25 and 4.26 reveal that α, T_r and P_c have a significant effect on round-trip efficiency, which is also sensible to effectiveness of the heat exchangers, to outlet pump pressure and air mass flow rate for the liquefaction and expansion sections.

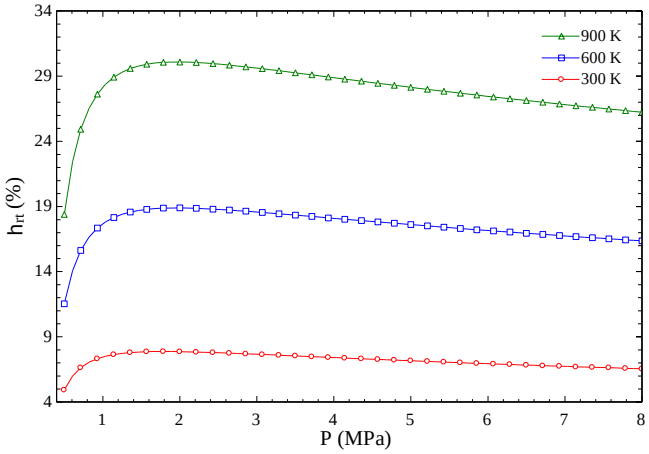

Figure 4.26 – Influence of compressor pressure and turbine inlet reheat temperature on round-trip efficiency (Fig. 3.3).

4.5 Cogeneration.

The round-trip efficiency accounting electrical power (Eq. 3.70) and considering cogeneration regime (Eq. 3.78) are evaluated for operation modes A, B and C as shown in Figs. 4.27, 4.28 and 4.29, respectively. For this, the charging and discharging times are considered the same, that is, $\Delta\tau_{ch}/\Delta\tau_{dis}$=1 [66, 99, 232]. For other analysis in this document, the time ratio ($\Delta\tau_{ch}/\Delta\tau_{dis}$) is estimated by Eqs. 3.46 and 3.47.

It should be noted that the highest electrical round-trip efficiency is achieved for operation mode C with 55.7 % as indicated in Fig. 4.29. When the electricity and cooling load are taken into account, the round trip efficiency reaches up to 98.6 %, the highest figure among the three options. The operation mode B has evident advantages with respect to mode A, it is observed that both the electrical and cogeneration round-trip efficiency are higher by 8.2 % and 16.1 %, respectively. The results point out that the simultaneous operation of the charging and discharging sections for CES systems using double expansion at the expander (T-1 from Fig. 3.5) can be feasible from thermodynamic point of view.

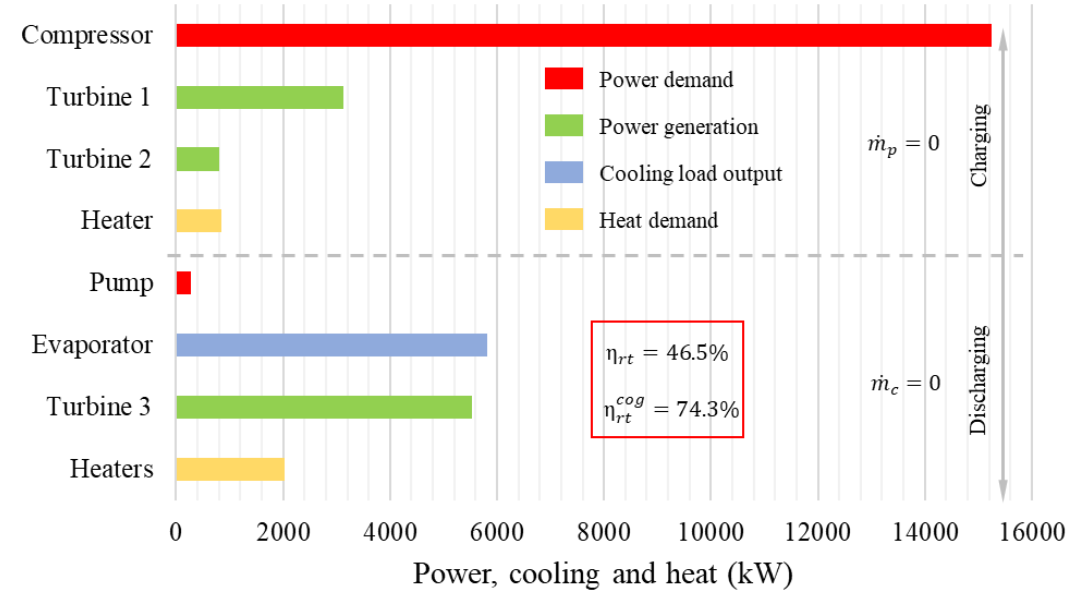

Figure 4.27 – Distribution of power, cooling and heat loads for operation mode A.

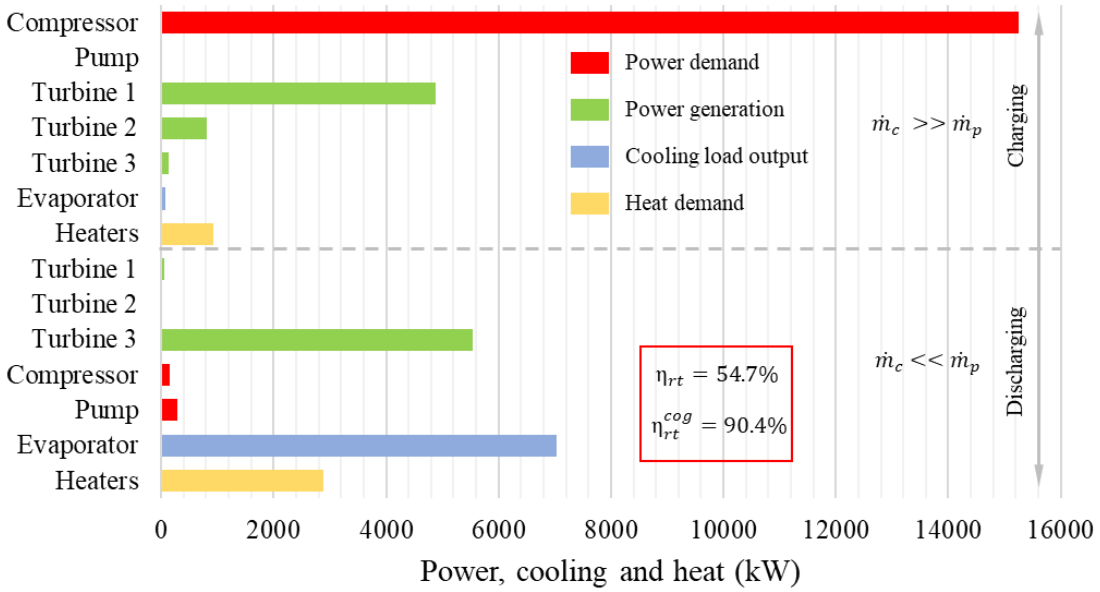

Figure 4.28 – Distribution of power, cooling and heat loads for operation mode B.

The variations of exergy utilization factor with ε and P_c are demonstrated in Fig. 4.30 from Fig. 3.3 for $\alpha = 0.60$, $P_p = 20.0$ MPa, $\dot{m}_c = 6.0$ kg/s, $\dot{m}_p = 0.1$ kg/s and $T_r = 400$ K during charging regime. E_xUF is benefited by increasing compressor pressure up to certain pressure value for every effectiveness curve. The result suggests that the power generated by the cryogenic turbine becomes initially determinant, further increase in pressure leads to an increase in the compressor power consumption in a higher proportion than the power generated by the turbine, affecting the cogeneration index. For ε=1.0, the

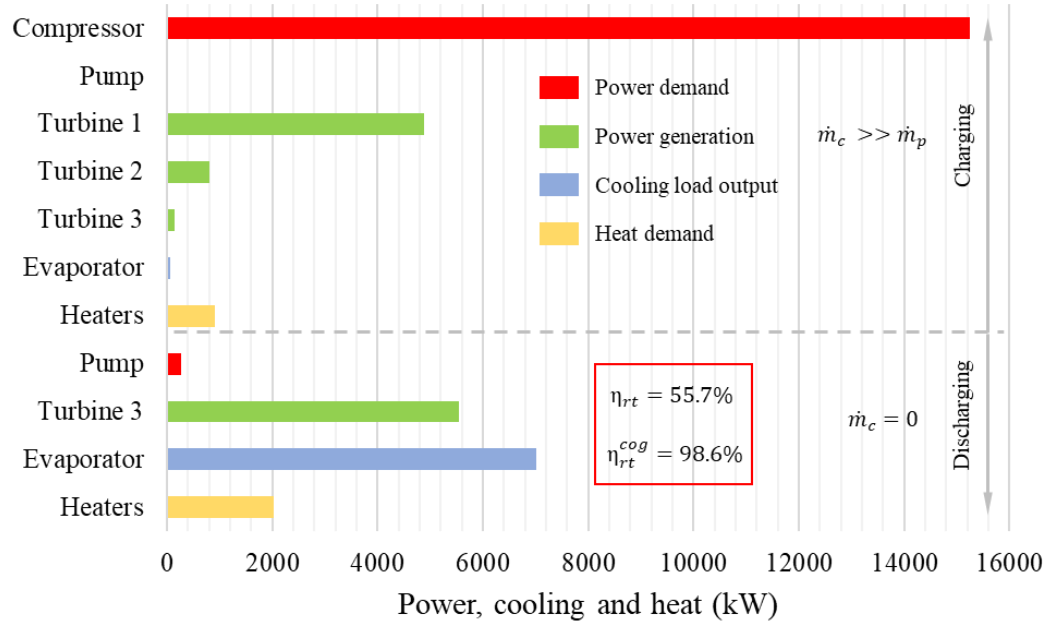

Figure 4.29 – Distribution of power, cooling and heat loads for operation mode C.

maximum E_xUF is 52.3 % at P_c=1.4 MPa, which is higher than the exergy efficiency (32.8 %, Fig. 4.6) for the base CES system, and even superior to what is reported in [9].

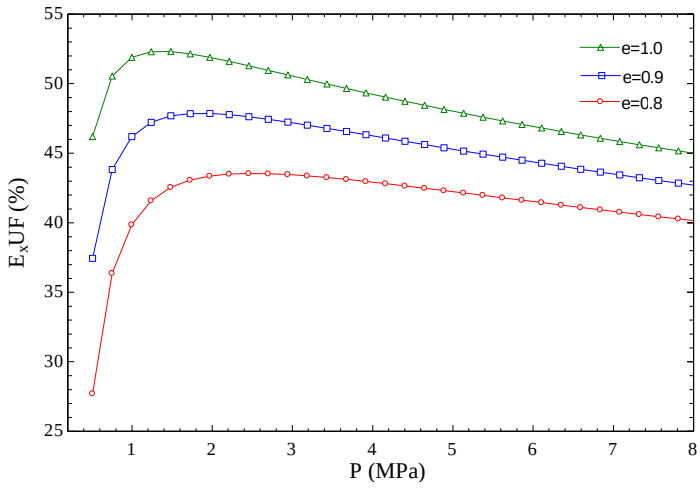

Figure 4.30 – Effect of compressor pressure and effectiveness of the heat exchangers on exergy utilization factor during the charging regime (Fig. 3.3).

The influence of compressor pressure and effectiveness of the heat exchangers on exergy utilization factor, for operation modes B and C (Fig. 3.5), is illustrated in Fig. 4.31 for $\alpha = 0.6$, $P_p = 20$ MPa, $\dot{m}_c = 36$ kg/s, $\dot{m}_p = 0.24$ kg/s and $T_r = 600$ K during charging regime. It is noticed from the figure that for each curve of effectiveness there is an optimum pressure where E_xUF is maximum. For ε=1.0, the maximum E_xUF is 64.1 % at P_c=1.48 MPa.

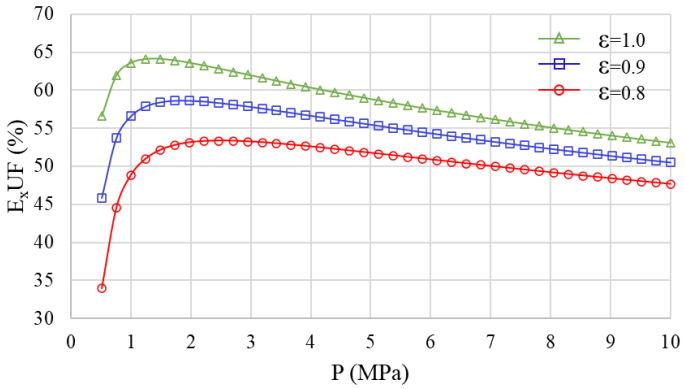

Figure 4.31 – Effect of compressor outlet pressure and effectiveness of the heat exchangers on exergy utilization factor during the charging regime (for operation modes B and C from Fig. 3.5).

Figure 4.32, from CES cycle of Fig. 3.3, illustrates the effect of air mass flow rate through the compressor and effectiveness of the heat exchangers on exergy utilization factor for $\alpha = 0.60$, $P_c = 5.0$ MPa, $P_p = 20.0$ MPa, $\dot{m}_p = 0.1$ kg/s and $T_r = 400$ K. It is clear a sharp increase of E_xUF up to 7.0 kg/s, beyond that value, the slope is drastically reduced and the factor increases at a lower rate, remaining almost steady for $\dot{m}_c > 30.0$ kg/s. This behavior is strongly influenced due to the increase in power production by the two-section expansion turbine and the exergy stored in the cryogenic tank, the further increase of air flow produces an increase in the power consumption by the compressor, turning smooth the curves for every effectiveness value. For every 10 % of increase in effectiveness, the exergy utilization factor rises as average 3.1 %.

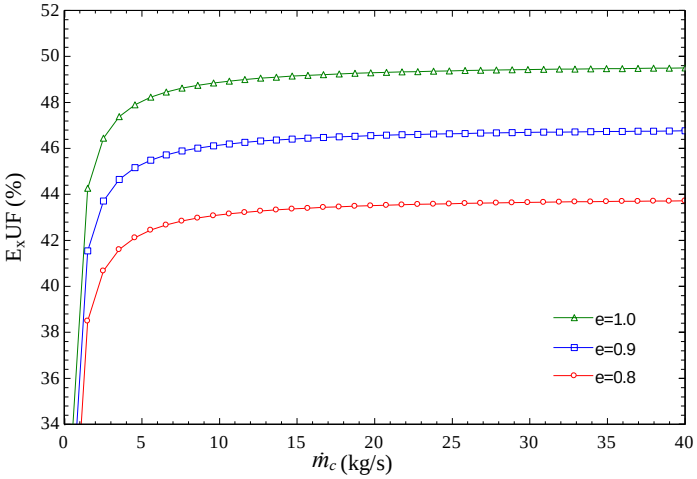

Figure 4.32 – Influence of air mass flow rate and effectiveness of the heat exchangers on exergy utilization factor during the charging regime (Fig. 3.3).

The increase of the inlet turbine temperature and pump pressure, during the discharging regime, produces a significant growth on E_xUF up to 15.0 MPa as shown in

Fig. 4.33 from CES cycle represented in Fig. 3.3. The graph is plotted for $\alpha = 0.60$, $\varepsilon = 0.95$, $P_c = 5.0$ MPa, $\dot{m}_p = 3.5$ kg/s and $\dot{m}_c = 0.4$ kg/s. There is an maximum E_xUF at each temperature curve, which moves for a higher pressure. Maximum values range from 60.4 to 79.0 % between the specified minimum and maximum temperature limits. The four-section expansion turbine produces the main contribution on this high values, which slightly reduces after their optimal due to the increase of power consumption by the cryogenic pump. At 20.0 MPa of pump pressure and $T_r = 400$ K, the E_xUF is 69.2 %, which is higher than the result obtained for the exergy efficiency (42.3 %, Fig. 4.8) of the base Claude cycle during discharging process at the same conditions. Tafone *et al.* [233] performed a technical and economic study for a CES system to cover the building cooling demand, and obtained an exergy efficiency of 67.0 % for the discharge process. In other research [105], authors compared a standalone CES system respect to an integrated CES with cooling and heating capabilities and found a favorable exergy efficiency of 53.7 % for the integrated CES.

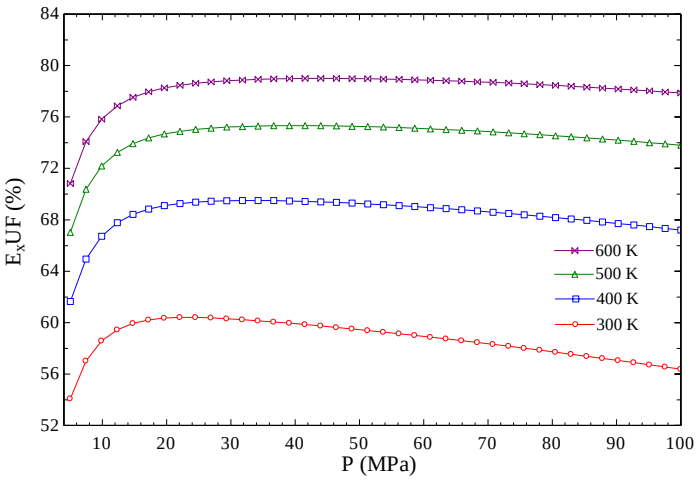

Figure 4.33 – Effect of pump pressure and turbine reheat inlet temperature on exergy utilization factor during the discharging process (Fig. 3.3).

For discharging process, all alternatives (A, B and C) operate in cogeneration regime. From the specified temperature curves in Fig. 4.34, the maximum values of E_xUF range from 68.8 % to 90.1 %. The E_xUF values, for operation mode B, are lower than the other two alternatives in a proportion range from 4.8 % to 5.4 % as a result of power consumption in the liquefaction section. The advantage of using a cryogenic hydraulic turbine instead of an expansion valve is evident when Figs. 4.33 and 4.34 are compared, which are referred to the CES cycles of Fig. 3.3, for the first case and Figs. 3.4 and 3.5 for the second one.

The influence of pump pressure and reheat temperature on electrical and thermal efficiency are illustrated in Fig. 4.35 for $\alpha = 0.60$, $\varepsilon = 0.95$, $P_c = 5.0$ MPa, $\dot{m}_p = 3.5$ kg/s and $\dot{m}_c = 0.4$ kg/s. The range of maximum values for electrical efficiency is stated from 54.6

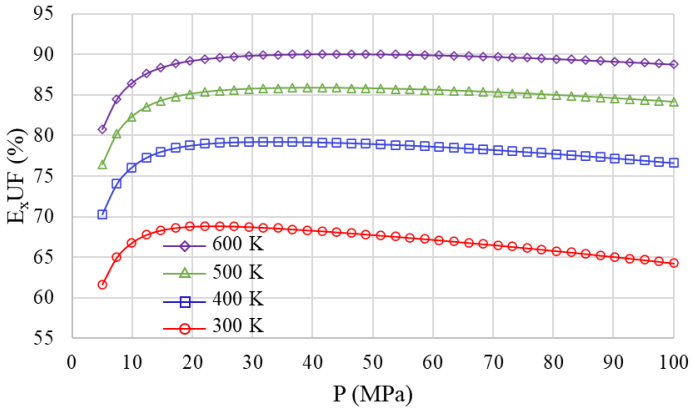

Figure 4.34 – Effect of pump discharge pressure and turbine inlet temperature on exergy utilization factor during the discharging process (operation modes A and C).

to 76.3 %, strongly influenced by the four-section expansion turbine. The difference between electrical and thermal efficiency points out power production as the main contributor for cogeneration process. A sudden increase in electrical efficiency up to 7.0 kg/s of air flow can be observed in Fig. 4.36, whilst thermal efficiency reduces. After that, both efficiencies remain almost steady.

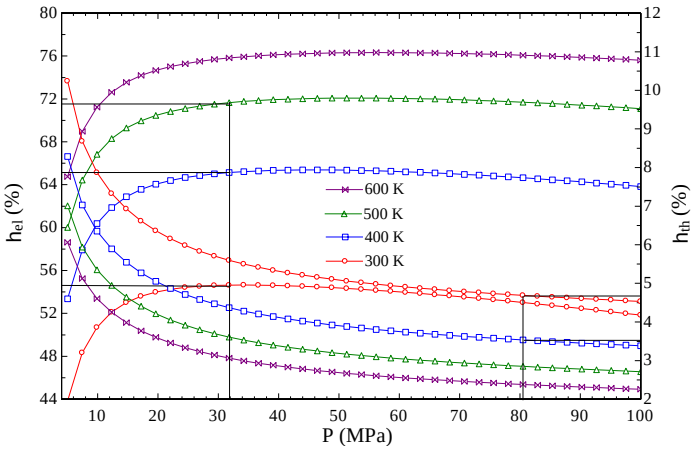

Figure 4.35 – Effect of pump pressure and inlet turbine temperature on electrical and thermal efficiency for discharging regime (Fig. 3.3).

Figures 4.37 and 4.38 illustrate the influence of diverted air mass fraction, discharge compressor pressure and reheat temperature on round-trip efficiency for cogeneration regime (Eqs. 3.76, 3.77 and 3.78). As shown in Fig. 4.37, the round-trip efficiency is highly benefited when waste heat at high temperature is available. It can be observed, that there is an maximum for every temperature curve, where the efficiency can attain values greater than 60 % for reheat temperature of 900 K. In Fig. 4.38, the optimal round-trip efficiency values shift for lower values of compressor discharge pressure. The advantages of

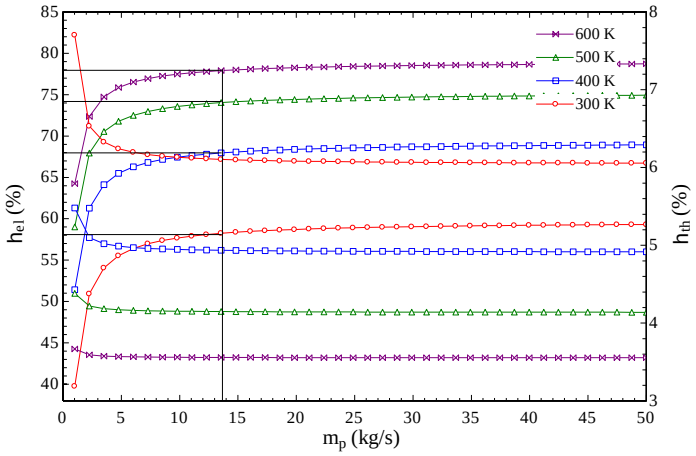

Figure 4.36 – Influence of liquid air mass flow rate and turbine inlet temperature on electrical and thermal efficiency for discharging regime (Fig. 3.3).

cogeneration can be clearly seen when Figures 4.25, 4.26, 4.37 and 4.38 are compared.

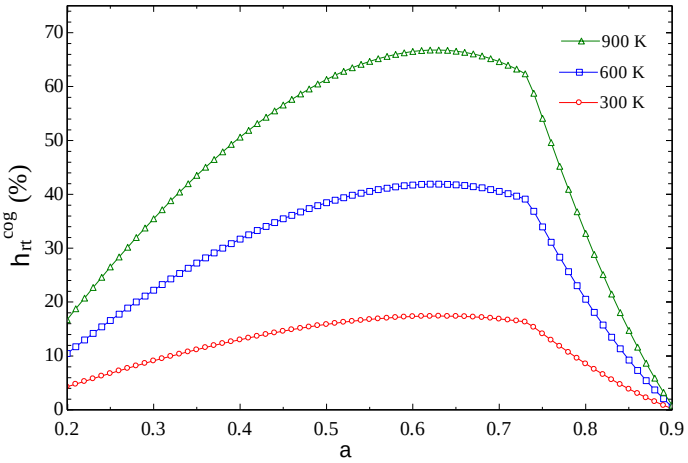

Figure 4.37 – Round-trip efficiency vs diverted air mass fraction and reheat turbine inlet temperature for cogeneration regime (Fig. 3.3).

The influence of diverted air mass fraction and operation modes on round-trip efficiency, for cogeneration regime, are presented in Fig. 4.39 for $\varepsilon = 0.95$, $P_p = 20$ MPa, $C_t = 200$ t and $T_r = 600$ K. It can be noticed that there is a clear maximum value of diverted air mass fraction for each operation mode. The optimum values of α for operation modes A, B and C are 0.63, 0.64 and 0.65, respectively. At these values, the respective round-trip efficiency figures are 38.5 %, 43.3 % and 46.8 %. The increase of α produces a higher power generation at the expander (T-1), which also rises the specific liquid yield (Fig. 4.3). Consequently, the improvement in the cogeneration round-trip efficiency is highly benefited by the power generation in the turbines. Further increase of α, beyond the maximum, affects the liquid air production due to the poor cooling performance at the heat exchangers, since less cold air coming from the cryogenic tank is sent back to the

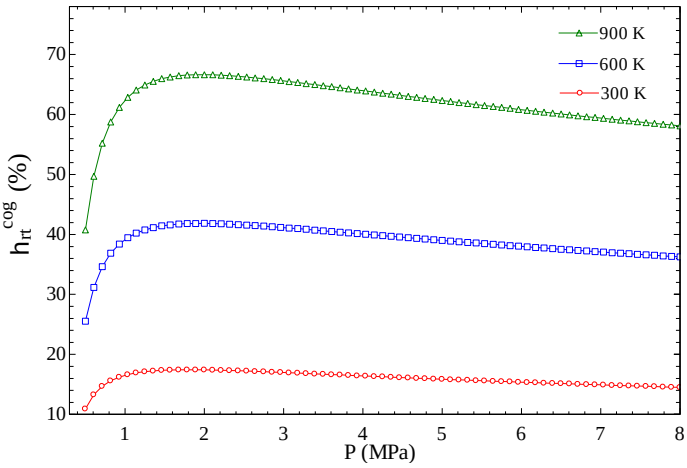

Figure 4.38 – Influence of compressor pressure and turbine inlet temperature on round-trip efficiency for cogeneration regime (Fig. 3.3).

cold box. This fact, reduces the power output of the four section expansion turbine during operation modes B and C, and therefore, the round-trip efficiency as well.

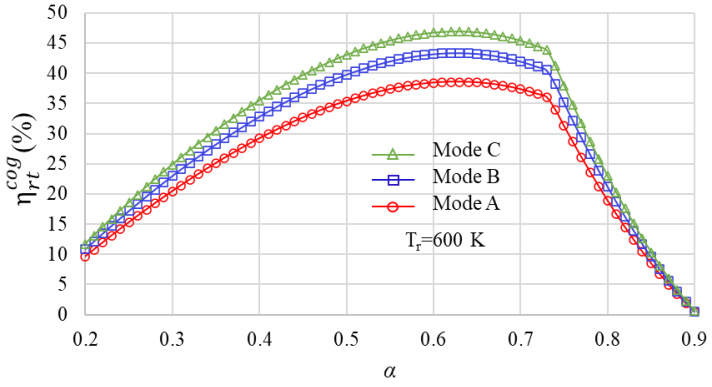

Figure 4.39 – Effect of diverted air mass fraction and operation modes on round trip efficiency for cogeneration regime at 600 K of reheat temperature.

As represented in Fig. 4.40, the cogeneration round-trip efficiency, for every operation mode, increases with increasing compressor discharge pressure, reaches an maximum, and then decreases with a further increase in pressure, advising that round trip efficiency is a function of the charging pressure. The graphic was plotted for $\varepsilon = 0.95$, $\alpha = 0.6$, $P_p = 20$ MPa, $C_t = 200$ t and $T_r = 600$ K. It is observed that the sudden increases of round-trip efficiency up to 1.57 MPa is leaded by both the expander (T-1) and cryogenic turbine (T-2). For operation modes B and C, the four section expansion turbine (T-3) also contribute for that initial increase of the efficiency. Then, further increase in pressure, brings to a greater compressor power consumption, which leads to a gradually reduction of the round-trip efficiency. Those findings shown in Figs. 4.39 and 4.40 reveal that α, T_r and P_c have a significant effect on cogeneration round-trip efficiency.

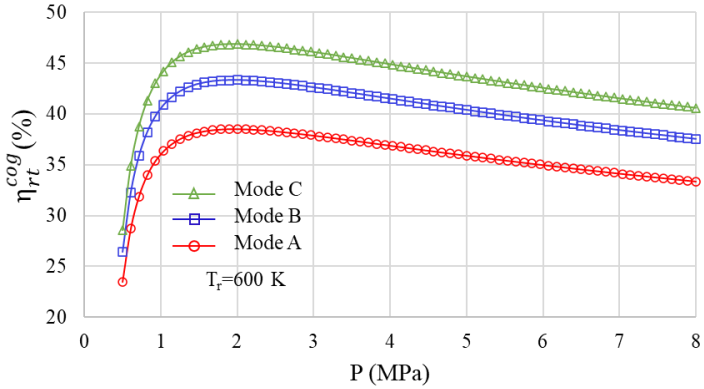

Figure 4.40 – Influence of compressor pressure and operation modes on round trip efficiency for cogeneration regime at 600 K of reheat temperature.

4.6 Optimization results.

For this research, the goal of thermodynamic optimization is to maximize specific liquid yield, exergy efficiency, exergy utilization factor, exergy density and round-trip efficiency, whilst specific exergy consumption must be minimized. A comparison between the base cycle represented in Fig. 3.2 (50 t storage capacity without multi-expansion) and optimum cases for 50, 100, 150 and 200 t (Fig. 3.3) are listed in Tables 4.2 and 4.3 for the charging and discharging regimes, respectively. The criteria for selecting the best option is based on the magnitude of the mains indexes and indicators, for instance, the lowest specific exergy consumption and the highest specific air liquid yield and efficiencies. It is observed that the benefit of producing both electrical and cooling exergy loads in CES systems is confirmed by comparing the exergy efficiency and the exergy utilization factor. For every storage capacity, the optimum E_xUF is about 20 % higher than η_{exe}. The optimal values of the recovered electrical exergy vary from 19.0 to 21.6 %, whilst for cogeneration, the electrical and cooling loads (round-trip efficiency) varies between 40.41 and 41.92 %.

In Appendix D, the results of thermodynamic optimization, for operation modes A, B and C, are listed in Tables D.1 and D.2. Referring to Table D.1, the CES systems with the operation modes B and C bring about the highest liquid air yield and the lowest specific exergy consumption. The specific liquid air yield for modes B and C is on average 16.1 % higher than operation mode A. Referring to Table D.2, the round-trip efficiency for the simultaneous operation of the charging and discharging regimes range from 39.14 % to 43.67 %, whilst for the separate operation of the aforementioned processes the round-trip efficiency varies from 34.3 % to 35.87 %.

Table 4.2 – Optimization results for charging regime for different capacities of the cryogenic tank.

Parameter	Unit	Base case	50 t	100 t	150 t	200 t
Specific liquid yield (y)	kg_L/kg_a	0.277	0.310	0.313	0.315	0.320
Diverted air mass fraction (α)	-	0.654	0.675	0.677	0.680	0.680
Effectiveness of the HE (ε)	-	0.96	0.97	0.97	0.97	0.98
Specific exergy consumed (e_n)	kWh/kg_L	0.812	0.764	0.754	0.751	0.744
Charging time ($\Delta\tau_{ch}$)	h	3.41	3.58	3.56	3.74	3.77
Exergy efficiency (η_{exe})	%	26.8	26.9	27.0	27.1	27.3
Exergy utilization factor (E_xUF)	%	-	50.1	50.7	51.0	51.1
Net electrical exergy consumed	MWh	41.78	37.15	72.48	108.05	142.29
Net exergy consumed (cogeneration)	MWh	-	28.63	57.80	102.52	141.55

Table 4.3 – Optimization results for discharging regime for different capacities of the cryogenic tank.

Parameter	Unit	Base case	50 t	100 t	150 t	200 t
Exergy density (E_D)	kWh/m^3	85.0	123.7	130.3	130.4	134.3
Electrical efficiency (η_{el})	%	-	81.0	82.7	82.7	83.1
Discharging time ($\Delta\tau_{ch}$)	h	3.29	1.37	1.35	1.38	1.37
Time ratio (r_t)	-	1.04	2.61	2.64	2.71	2.75
Exergy efficiency (η_{exe})	%	50.3	60.2	62.4	62.6	63.4
Exergy utilization factor (E_xUF)	%	-	85.2	86.0	86.2	86.3
Net electrical exergy generated	MWh	4.86	7.07	14.89	22.35	30.68
Net exergy generated (cogeneration)	MWh	-	11.57	23.70	42.57	59.34
Specific exergy generation	MWh/t	-	0.231	0.237	0.284	0.297
Round-trip efficiency	%	11.6	19.0	20.5	20.7	21.6
Round-trip efficiency (cogeneration)	%	-	40.4	41.0	41.5	41.9

4.7 Results of economic analysis.

In this section, the results about the economic feasibility of the three alternatives running under different operation modes are discussed. The optimum conditions corresponding to the thermodynamic evaluation are used to obtain the economic results. Additionally, the interest rate (i) considered for some analysis is 6 % when it is not specified. Fig. 4.41 shows the gross average annual revenue for life-cycle of each CES system as result of selling electricity and cooling load for different capacities of the cryogenic tank . For all operation modes, the annual revenue increases as the cryogenic tank capacity increases, according to a proportional relationship. Furthermore, for every capacity, mode C exhibits gross incomes (Eq. 3.80) higher than modes A and B in 2.1 % as average. As can be observed, for every alternative, the larger gross income is obtained from the sale of

electricity which represents about 91.9 % from the total.

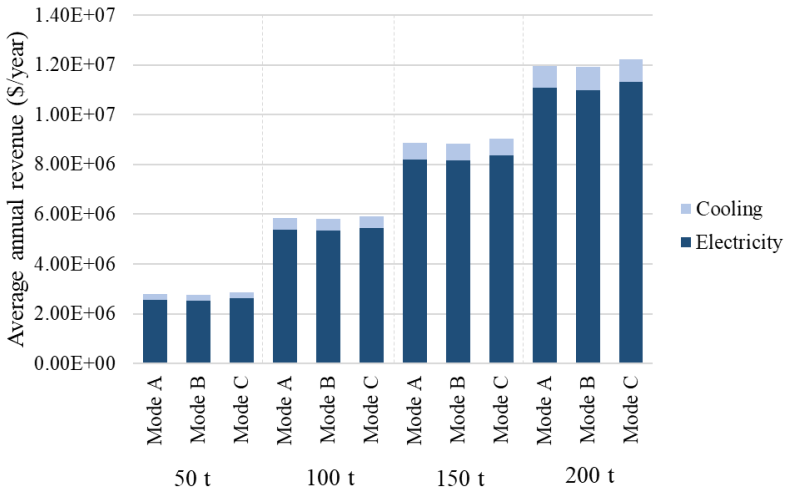

Figure 4.41 – Average annual revenue accounting for selling electricity and cooling load.

Figure 4.42 indicates as cryogenic tank capacity increases, the average annual revenue of every operation mode also increases. It is observed that operation modes B and C are more profitable than operation mode A. It suggests that the simultaneous operation of the charging and discharging processes (modes B and C) produces a significant reduction in power consumption by the compressor, which translates into a shortening in the cost of electricity. Additionally, as the specific liquid yield for modes B and C are higher than A, annual revenue for selling liquid air from these two alternatives are superior to mode A. These results point out that revenue does not only depend on the size or capacity of the cryogenic tank, therefore also depends on the simultaneity of operation of the charging and discharging cycles.

The effect of storage capacity on NPV for every operation mode is shown in Fig. 4.43 for reheat temperature of 600 K. The results indicate to achieve a favorable NPV, cryogenic tank capacity must be equal to or greater than 100 t for operation modes B and C. However, when liquid air is considered for selling (Fig. 4.44), the three operation modes (A, B and C) are profitable from a storage capacity of 100 t. It is clear that operation modes B and C are found to be significantly more profitable than operation mode A. These results reinforce the hypothesis about the economic viability in the simultaneous operation of the charging and discharging processes in CES systems in cogeneration regime. The uncertainty analysis is conducted to evaluate the impacts of the uncertainties of the electricity tariffs on the feasibility of every alternative through the NPV. It can be observed that the uncertainty for operation modes B and C are greater than that of operation mode A. For the highest storage capacity, the uncertainty for modes B and C are 12.5 and 13.2 %, respectively. These results suggest that these alternatives remain cost-effective

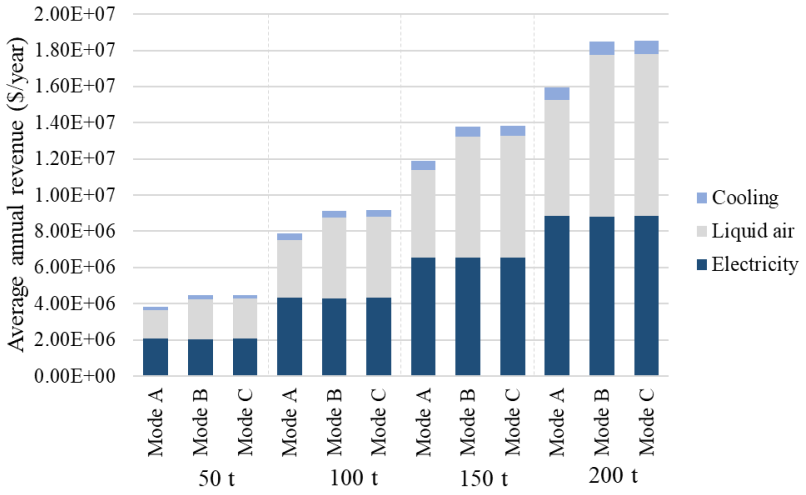

Figure 4.42 – Average annual revenue accounting for selling electricity, liquid air and cooling load.

for a scenario of uncertainties in electricity tariffs at peak and off-peak times of 81.2 and 18.8 %, respectively.

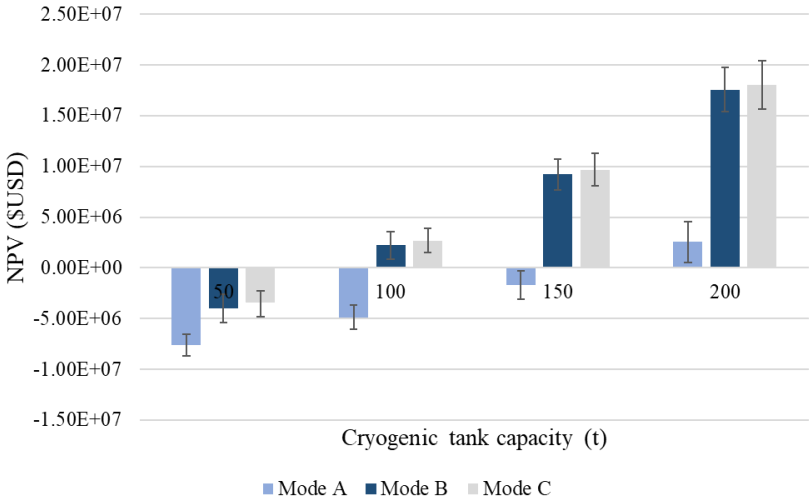

Figure 4.43 – Effect of cryogenic tank capacity on NPV for every operation mode accounting for selling electricity and cooling load.

The variation of NPV with respect to the interest rate is illustrated in Fig. 4.45 for a reheat air temperature and a cryogenic tank capacity of 600 K and 200 t, respectively. For every alternative, NPV sharply drops with the increase in the interest rate. The results suggest that the profitability of operation modes B and C can be obtained with a 2 % up to 8 % of interest rate. For further increase of the interest rate ($\geq$10 %), none of the alternatives can be profitable. The simultaneous performance of the charging and discharging cycles (modes B and C) show to be more profitable than the CES system (mode A) with the intermittent operation of the liquefaction and expansion processes. It is worth

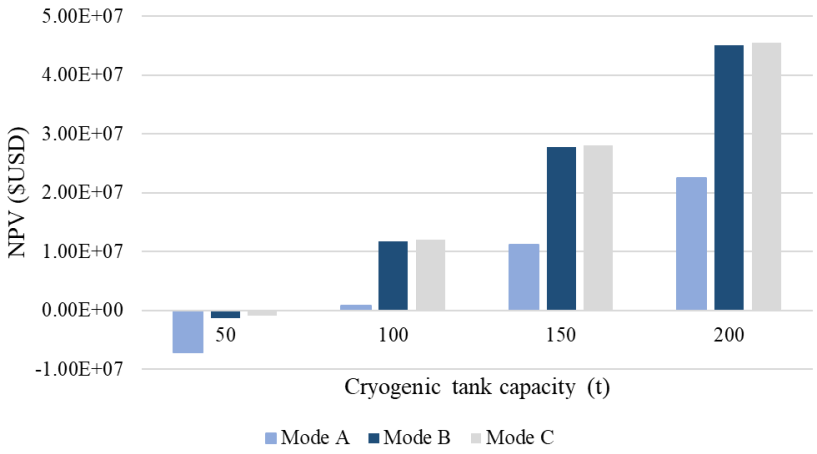

Figure 4.44 – Variation of NPV with cryogenic tank capacity for every operation mode accounting for selling electricity, liquid air and cooling load.

highlighting that NPV is highly sensitive to the interest rate in an inversely proportional relationship. In addition, the uncertainty analysis shows that the three alternatives continue to be feasible for an interest rate between 2 % and 4 %.

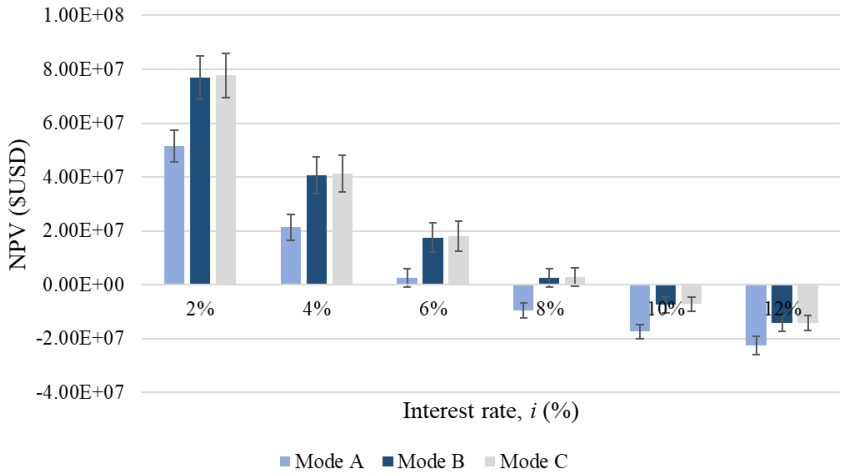

Figure 4.45 – Effect of interest rate on NPV for each operation mode accounting for selling electricity and cooling load.

The influence of reheat temperature on NPV is presented in Fig. 4.46 for an interest rate of 6 % and 200 t of storage capacity. It can be observed that, as the reheat temperature scales up, the NPV increases, with a better profitability for operation mode C, which increases from \$18.03 millions to \$36.94 millions for a reheat temperature increment of 100 K. In addition, all alternatives are profitable from reheat temperature of 600 K. However, for options B and C to be profitable at a reheat temperature of 500 K, the interest rate must be equal to or lower than 4 %. The variation of (B/C) with reheat temperature (Fig. 4.47) is directly related with the results of Fig. 4.46. Specifically, the

(B/C) values less than the unit correspond to the negative NPVs for reheat temperature of 400 K and 500 K. In other words, when the benefits dot not exceed the costs (B/C<1), the profitability of the projects is compromised. All these results indicate that the feasibility of the projects (operation modes A, B and C) strongly depends on the reheating temperature.

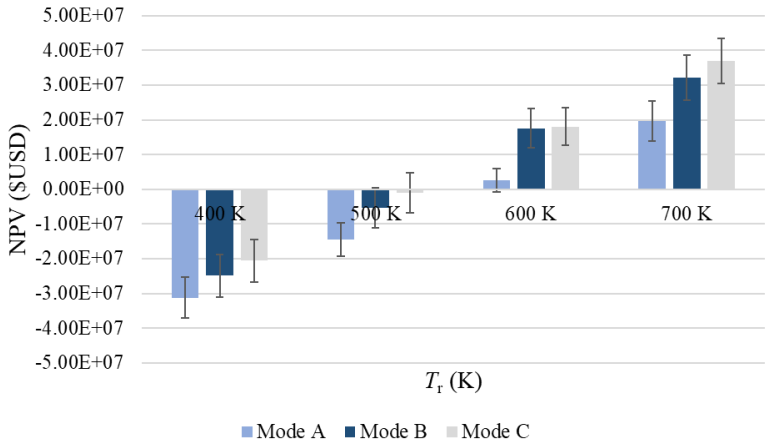

Figure 4.46 – Influence of reheat air temperature on NPV for every operation mode accounting for selling electricity and cooling load.

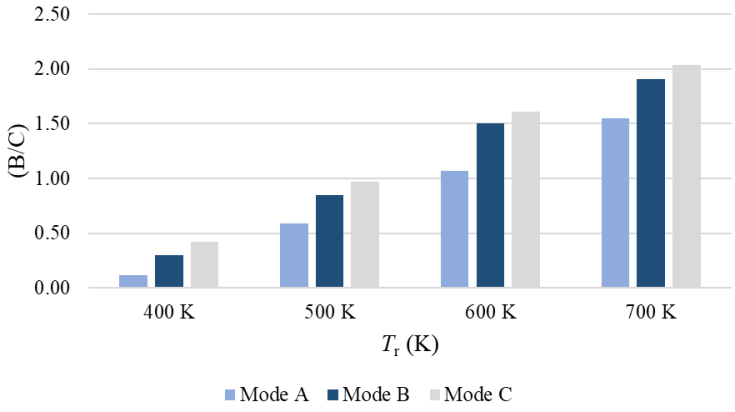

Figure 4.47 – Variation of benefit to cost ratio (B/C) with reheat temperature for every operation mode accounting for selling electricity and cooling load.

Figure 4.48 shows the variation of the payback period with the storage capacity for an interest rate of 6 % and a reheat temperature of 600 K. It is observed that, the higher the storage capacity the lower the payback period. The payback period for operation mode C is the lowest among the three alternatives. When the storage capacity varies from 50 t to 200 t, the payback period is shortened from 20.87 to 15.22 years for operation mode C. Moreover, operation mode B presented a payback period, for every storage capacity, slightly higher than alternative C, suggesting it is economically viable the simultaneous operation of the charging and discharging cycles when compared to the separate operation of the two cycles (operation mode A).

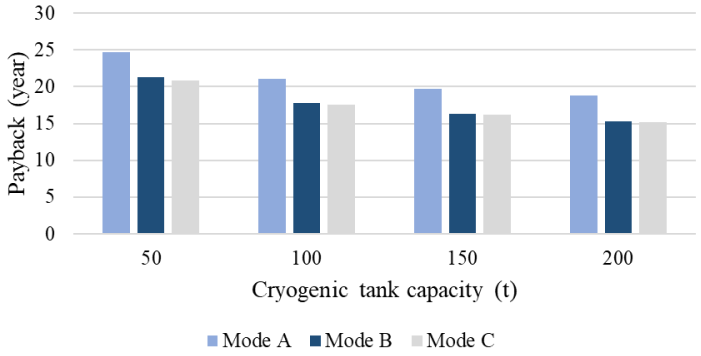

Figure 4.48 – Variation of payback period with cryogenic tank capacity for each operation mode accounting for selling electricity and cooling load.

Table 4.4 – Specific investment cost ($\$/kW$), IRR (%) and PBP (year) for different capacities of the cryogenic tank.

Cryogenic tank capacity	($\$/kW$)			(IRR, %)			(PBP, year)		
	A	B	C	A	B	C	A	B	C
50 t	1541.35	1301.39	1301.39	2.68	4.30	4.50	24.71	21.32	20.87
100 t	1165.46	991.99	991.99	4.82	6.53	6.64	21.05	17.78	17.60
150 t	1013.69	865.77	865.77	5.70	7.61	7.69	19.76	16.35	16.23
200 t	912.20	782.27	782.27	6.35	8.44	8.51	18.84	15.30	15.22

Table 4.4 shows the variation of the specific investment cost, IRR and PBP with respect to the storage capacity for each operation mode, assuming an interest rate of 6 % and reheat temperature of 600 K. It can be observed from Table 4.4 that for every storage capacity, the operation modes B and C are more profitable than mode A. For instance, the specific investment cost for operation mode A is about 15.5 % higher than that the other two alternatives. This result is due to the increase in available power when considering the simultaneous operation of the charging and discharging cycles. The internal rate of return (IRR) is favorable for operation mode C when it is compared to the other two alternatives. That is, the interest rate earned for mode C on the time-varying of the project life, for a storage capacity of 200 t, is 8.51 %, which is 24.4 % and 0.8 % superior to that of the operation modes A and B, respectively. For every indicator, the profitability increases when increasing the scale of the CES system, suggesting it is viable to design large cogeneration CES systems instead of small plant sizes.

The levelized cost of produced liquid air and specific exergy consumption as a function of the storage capacity for every operation mode are shown in Fig. 4.49 for an interest rate of 6 % and reheat temperature of 600 K. The LCOL for operation modes

B and C are significantly lower than mode A for each storage capacity. For the whole life of projects B and C the LCOL at 200 t are 6.95 and 6.82 $¢USD/kg_L$, respectively. Whilst for operation mode A, this indicator is as average 34.7 % higher than the other two options. These results are consistent with the specific exergy consumption, that is, for operation modes B and C the exergy required to produce the unit of liquid air is on average 0.4805 kWh/kg_L, which is 16.8 % lower than operation mode A. The operation of the liquefaction circuit during the discharge process for operating mode B (Fig. 3.5) generates additional expenses that lead to a higher cost of the final products, that is why the LCOL for alternative C is slightly lower than B. However, the operation mode B is superior to mode A and the complementary benefit in the simultaneous operation of the charging and discharging processes must be evaluated from the improvement of the thermal inertia of the CES system and its ability to perform an inversion process in a short time, that is, the transition from the charging to discharging process or vice versa. In this research, the thermal inertia and the effectiveness of the inversion process are not evaluated. From the observations earlier, it can be noticed that the specific investment cost and liquid yield are also determinants in the levelized cost of liquid air. Since operation modes B and C have a lower specific cost of investment and a higher liquid yield than A, the LCOL of these two options is more profitable, which produces a positive impact on the economic viability of the projects. In [215] the authors optimized a hydrogen liquefaction process integrated with LNG and found a levelized cost of hydrogen ranged from 2.97 $\$/kg_L$ to 5.46 $\$/kg_L$. For hydrogen, this result is appropriate considering its low boiling point (20.2 K), which leads to a high energy consumption during liquefaction process and, consequently, an increase of its levelized cost.

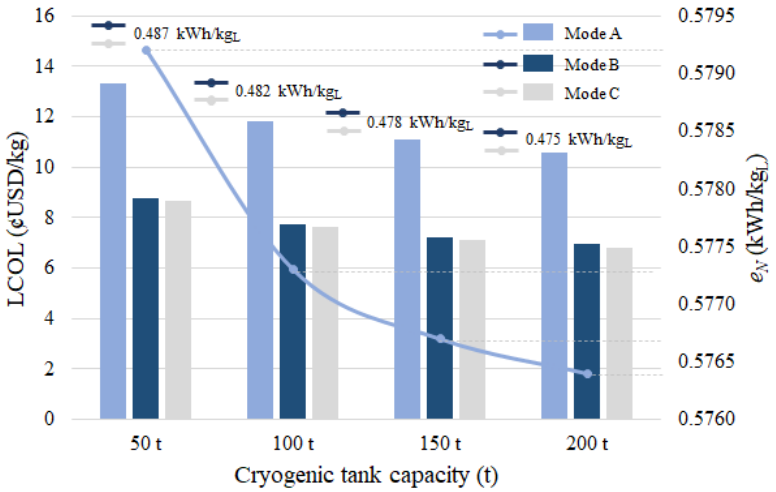

Figure 4.49 – Levelized cost of liquid air and specific exergy consumption as a function of cryogenic tank capacity for every operation mode.

Figures 4.50, 4.52 and 4.54 show, for operation modes A, B and C, respectively,

the trend of the LCOS as round-trip efficiency and electricity tariff in off-peak time vary. It is observed that the LCOS decreases significantly with increasing round-trip efficiency and decreasing the electricity tariff. Under these conditions, every alternative becomes more attractive. In addition, for higher electricity tariffs, the round-trip efficiency becomes relevant in order to keep down the levelized cost of storage. The minimum value of LCOS for operation modes A, B and C are 0.252 $\$/kWh$, 0.248 $\$/kWh$ and 0.236 $\$/kWh$, respectively. In [122] the authors compared liquid air energy storage (LAES for Claude cycle) and pumped thermal electricity storage (PTES) systems using a thermo-economic approach. The study showed that the average total LCOS for LAES and PTES systems were found to be 0.290 $\$/kWh$ and 0.380 $\$/kWh$, respectively for off-peak electricity price of 0.03 $\$/kWh$. Even though economic conditions vary from region to region, these results are respectively, as average, 15.5 % and 35.5 % higher than the results obtained in this study. The authors also found LAES more restricted to location due to energy cost and more vulnerable to market fluctuations of electricity costs. This scenario has matching points with respect to the Brazilian energy market, where the electricity price varies significantly among regions and throughout the year [234, 235]. This variability can affect the economic feasibility of the proposed CES systems, that is why higher round-trip efficiencies are required to make this technology cost-effective and more competitive.

Another study [119] presented a techno-economic comparative analysis of different hybrid CES systems and results shown that the adiabatic CES system integrated with the combustion of LNG and the CES waste heat recovery system exhibited a LCOS of 0.161 $€/kWh$ and 0.171 $€/kWh$, respectively. Kim et al. [92] studied a CES system integrated with LNG and combustion and found the LCOS ranging from 0.142 to 0.190 $\$/kWh$. It is evident that the integration of CES systems to other technologies significantly reduces the LCOS. For stand-alone CES systems this indicator can achieve 0.300 $\$/kWh$ [122] or depending on the round-trip efficiency and the scenario can be ranged from 0.191 $£/kWh$ to 0.590 $£/kWh$ for commercial CES plants [108].

The variation of the levelized cost of electricity and cooling (LCOC) with respect to cogeneration round-trip efficiency and electricity tariff in off-peak time for operation modes A, B and C are illustrated in Figs. 4.51, 4.53 and 4.55, respectively. For the lowest electricity tariff and the highest efficiency, the LCOC for operation modes A, B and C are 0.245 $\$/kWh$, 0.238 $\$/kWh$ and 0.231 $\$/kWh$, respectively. It is noticed that LCOC strongly depends on cogeneration round-trip efficiency. The existing literature on cogeneration CES systems are not abundant and only a few deal with economic issues. Tafone et al. [121] performed a comparative analysis between a stand-alone CES system and an integrated CES with organic Rankine cycle (CES-ORC). The study shown that the integrated system can achieve a LCOC in cogeneration regime of 0.437 $€/kWh$, whilst for the stand-alone CES system the indicator reached a value of about 0.480 $€/kWh$. Gao et al. [163] proposed a novel CES trigeneration system based on the liquid air energy storage.

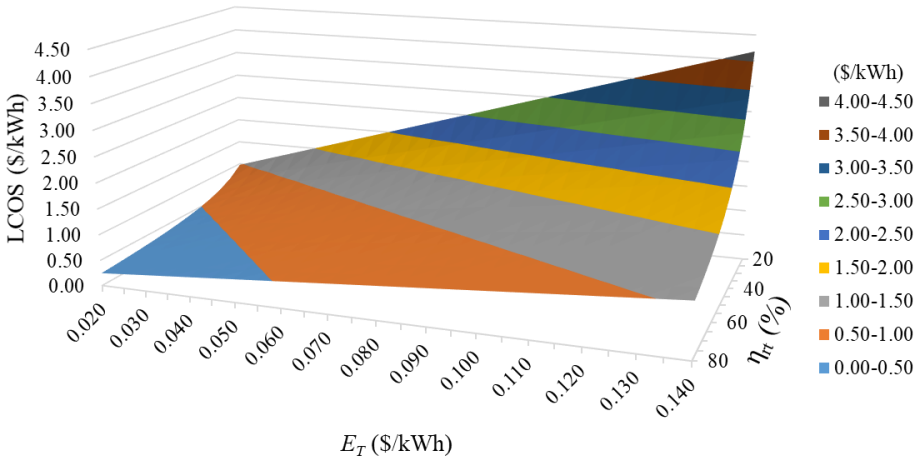

Figure 4.50 – Influence of electricity tariff in off-peak time and round-trip efficiency on levelized cost of electricity storage for operation mode A ($i = 6$ % and $c_y = 4$ $cycles/day$).

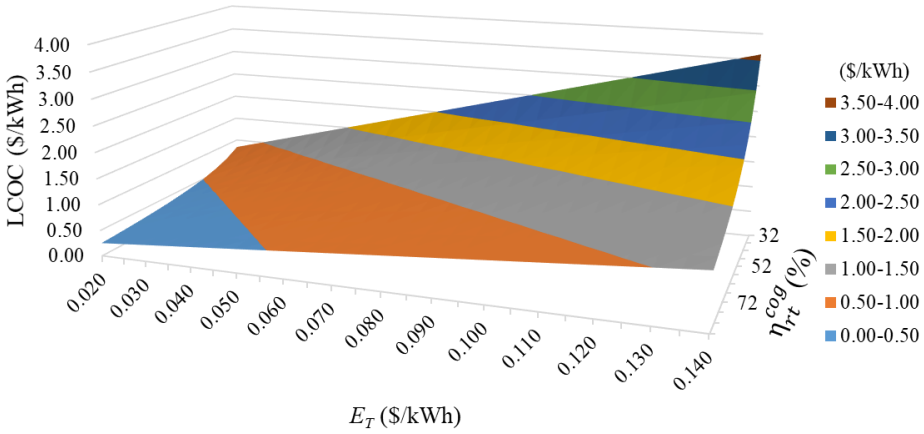

Figure 4.51 – Effect of electricity tariff in off-peak time and cogeneration round-trip efficiency on levelized cost of electricity and cooling for operation mode A ($i = 6$ % and $c_y = 4$ $cycles/day$).

According to the authors, the system is able to storage the off-peak electricity and supply the heating, cooling and power at the peak time. The study evaluated, among others aspects, the levelized cost of energy in five regions at different seasons and accounted values ranging from 0.110 $\$/kWh$ to 0.130 $\$/kWh$. In general, it is observed that levelized costs of energy are highly influenced by the technologies (stand-alone CES system or integrated CES system), electricity prices (off-peak and peak times), operation strategies, legislation to encourage the use of CES systems, heating and cooling loads prices and environmental conditions of the region.

The sensitivity analyses of the NPV for operation mode C are shown in Figs. 4.56

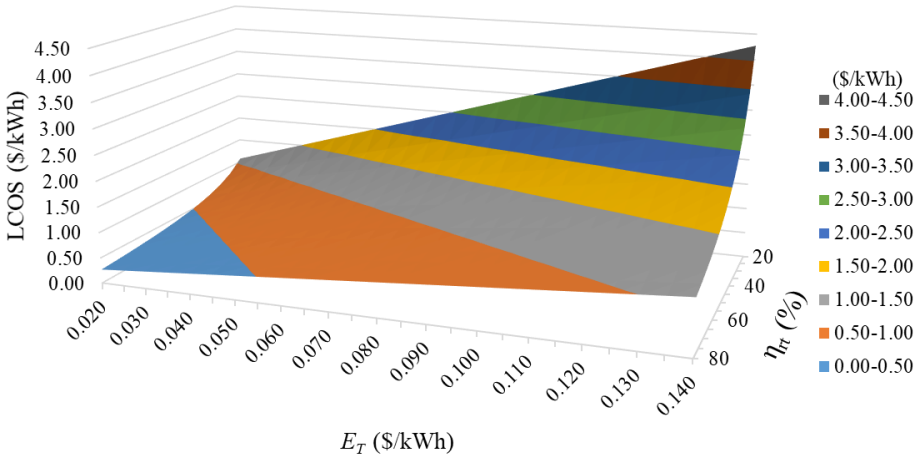

Figure 4.52 – Influence of electricity tariff in off-peak time and round-trip efficiency on levelized cost of electricity storage for operation mode B (i = 6 % and $c_y = 4\ cycles/day$).

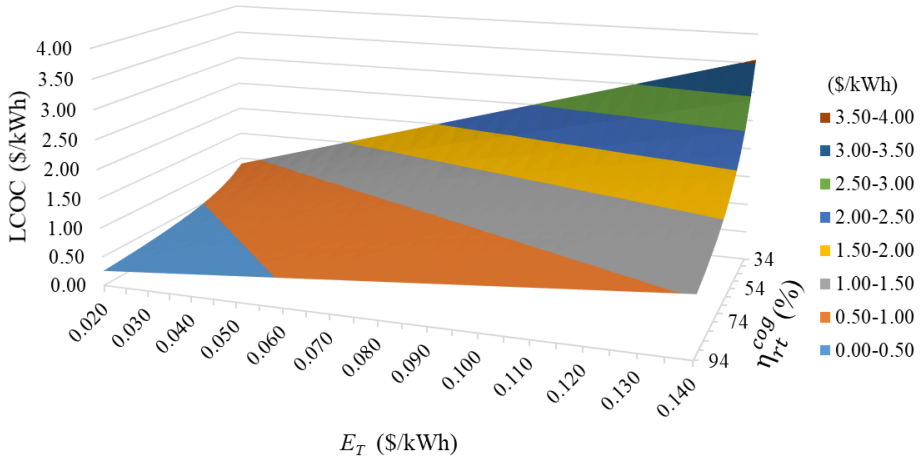

Figure 4.53 – Effect of electricity tariff in off-peak time and cogeneration round-trip efficiency on levelized cost of electricity and cooling for operation mode B ($i = 6$ % and $c_y = 4\ cycles/day$).

and 4.57. The analyses are performed by fixing a reference scenario which is given in Table 4.5 and changing the indexes and indicators by ±50 %. As Fig. 4.56 illustrates the NPV is highly sensitive to round-trip efficiencies, electricity tariffs, the economic life of the technology, interest rate and the number of cycles per year. It can be observed that the highest negative impact on NPV is accounted for the electrical round-trip efficiency. Similarly, the NPV is negative in reducing the cogeneration round-trip efficiency and the electricity tariff at peak time. The feasibility of the project is significantly positive when increasing efficiencies. For this, the NPV reaches values of $236 million and $225 million by increasing cogeneration round-trip efficiency and electrical round-trip efficiency, respectively. Moreover, the reduction of the electricity price at off-peak time is shown to have an

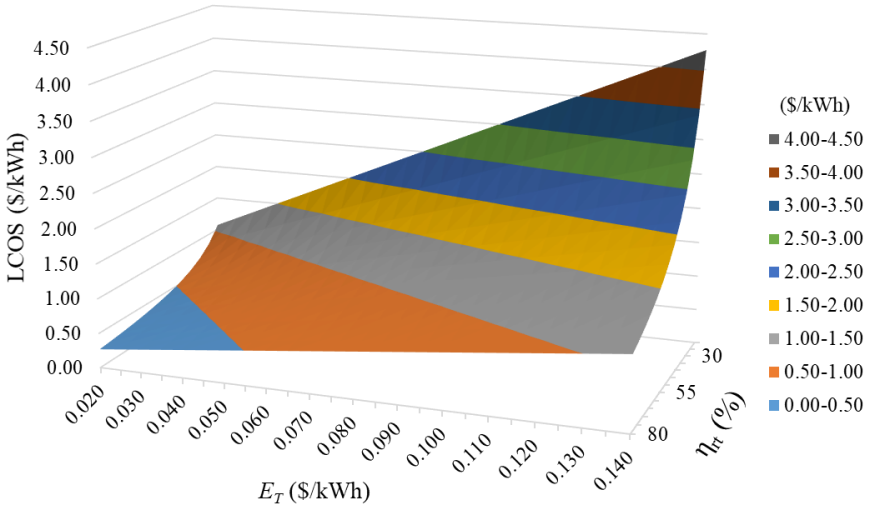

Figure 4.54 – Influence of electricity tariff in off-peak time and round-trip efficiency on levelized cost of electricity storage for operation mode C ($i = 6$ % and $c_y = 4$ *cycles/day*).

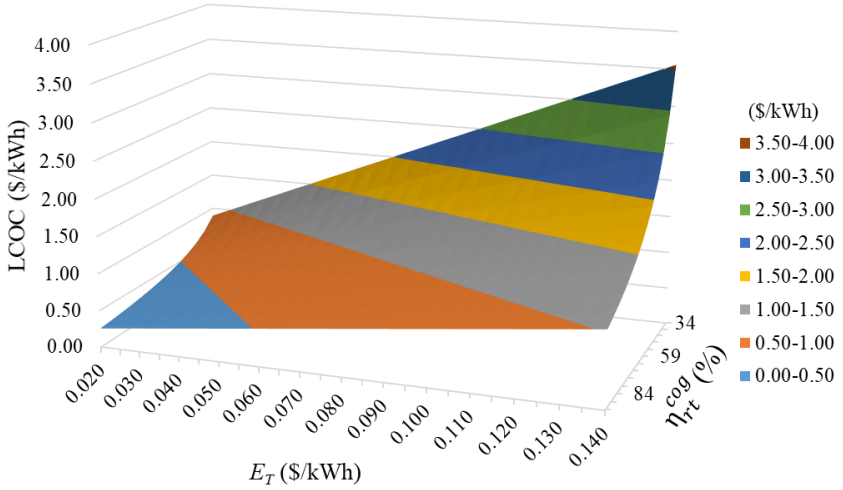

Figure 4.55 – Effect of electricity tariff in off-peak time and cogeneration round-trip efficiency on levelized cost of electricity and cooling for operation mode C ($i = 6$ % and $c_y = 4$ *cycles/day*).

appreciable impact, which produces a NPV of $150 million. Likewise, the interest rate has similar behavior, but the accumulated wealth in the useful life of the project is superior, that is, the NPV is $157 million. The meaningful variation in NPV due to the change in the economic life of the technology and the number of cycles per year suggests the continuous operation of the CES system in order to be profitable. This aspect reinforces the proposal on the simultaneous operation of the charging and discharging processes.

From Fig. 4.57 it can be seen that the NPV does not reach negative values when indexes and indicators change by ±50 %. The most impacting parameters on NPV are the

Table 4.5 – Indexes and indicators for the reference scenario.

Parameter	Unit	Value	Ref.
Economic life	year	30	[121, 109]
Cost of cooling load	$\$/kWh_{th}$	0.059	[163]
Cost of waste heat	$\$/kWh_{th}$	0.0098	[163]
Cost of liquid air	$\$/kg_L$	0.32	[165]
Electricity tariff on peak time	$\$/kWh_e$	0.2249	[164]
Electricity tariff off-peak time	$\$/kWh_e$	0.0897	[164]
Interest rate	%	6	[163]
Number of cycle per year	cycles/year	1460	-
Electrical round-trip efficiency	%	45.0	-
Cogeneration round-trip efficiency	%	62.6	-

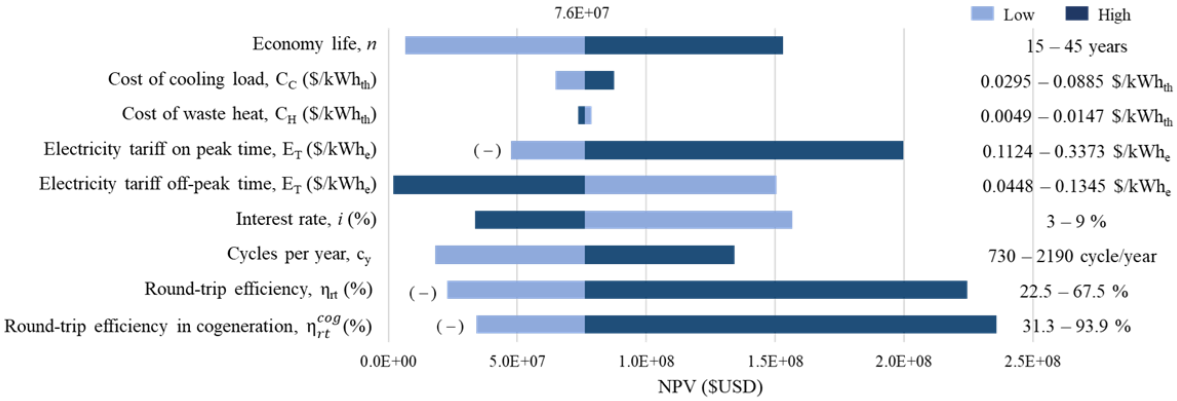

Figure 4.56 – Sensitivity analysis for the NPV varying the main parameters by ±50 % for operation mode C, accounting for selling electricity and cooling income.

round-trip efficiencies, interest rate, cost of liquid air, electricity price, economic life and number of cycles per year. The variation of the costs of the waste heat and cooling load do not have a great influence on the NPV.

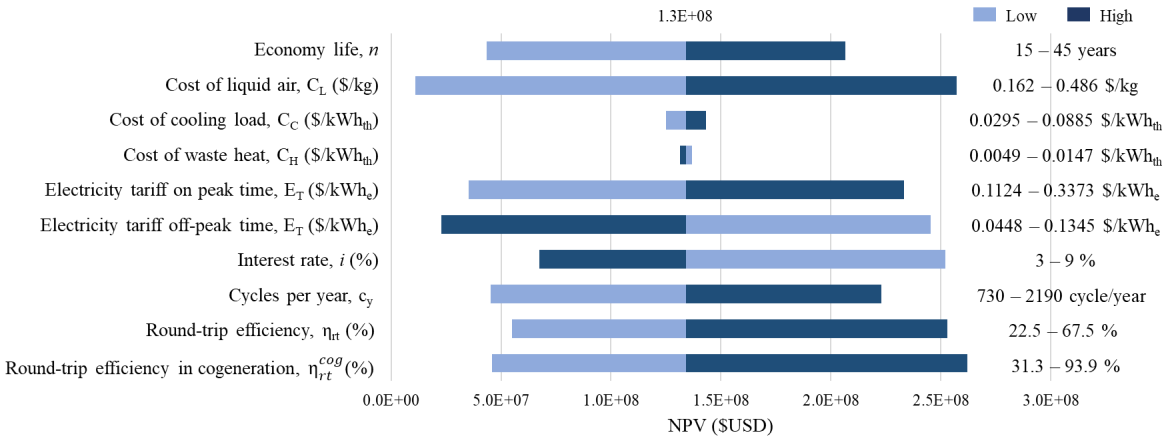

Figure 4.57 – Sensitivity analysis for the NPV varying the main parameters by ±50 % for operation mode C, accounting for selling electricity, liquid air and cooling income.

5 Conclusion, limitations and suggestions for further research

Cryogenic energy storage system is expected to play an important role in energy production in the coming years. This technology presents higher volumetric energy density than other storage technologies, long useful life (>30 years), and no geographical constraints. It is based on standard components that are easily found in the gas industry. It can also be integrated into the industry, power stations and in transport and service sectors. CES system can be used to optimize electricity bills by charging at off-peak hours or times of low prices and discharging during peak hours when prices are high. Another advantage is that it can contribute to power grid stability by responding to imbalances in electrical energy production and consumption. The low round-trip efficiency and the absence of deeply founded economic studies constitute the main limitations to spread this technology in the energy market.

This research aimed to enhance the thermodynamic and economic performance of CES systems through the simultaneous operation of the charging and discharging processes, implementation of cogeneration and their integration with an external energy source. An extensive literature review was carried out to identify the main knowledge gaps about the development of CES systems, which provided opportunities for scientific contribution. The layout of the baseline CES system was modified taking into account its operating constraints. In order to demonstrate the viability of the simultaneous operation of the storage and discharge regimes, four CES systems were evaluated and compared. A systematic mathematical model to describe and understand the optimal operation conditions of CES systems was developed. In addition, a sensitivity analysis and multi-objective optimization procedures were performed. Finally, an economic analysis of three alternatives of CES systems was carried out and the results were verified with the findings of other researches.

5.1 Conclusions.

1. The modeling results suggested that diverted air mass fraction, discharge compressor pressure and effectiveness of the heat exchangers significantly affect the liquefaction process. The maximum diverted air mass fraction was found in a range from 0.65 to 0.72. The modification of the layout of the baseline CES cycle, specifically, the application of two expansions in the turbine of the liquefaction section and the substitution of the expansion valve for a hydraulic cryogenic turbine contributed to

increase the specific liquid air yield from 0.250 kg_L/kg_a to 0.412 kg_L/kg_a. This result led to a significant reduction of the charging time, and consequently increased the number of cycles per year. The use of a hydraulic turbine instead of an expansion valve produced, on average, an increase of specific liquid air yield of 0.091 kg_L/kg_a. Additionally, the simultaneous operation of the charging and discharging processes was found a viable option to improve the liquefaction process, which provided a supplementary cooling load during both storage and discharge regimes.

2. With the use of multi-expansion turbines in the cogeneration CES system, the energy production during the discharging regime was increased in 45.5 %, whilst for charging regime the net energy consumed was reduced in 19.91 %. The simultaneous operation of the storage and discharge regimes also had a relevant contribution in these results, which led to reduce the specific exergy consumption from 0.695 kWh/kg_L to 0.410 kWh/kg_L for effectiveness of the heat exchanger >0.92. Moreover, the exergy density was highly benefited with this operation option and achieved an optimal value of 134.3 kWh/m^3 for a cryogenic tank capacity of 200 t, pump pressure of 20 MPa and reheat temperature of 600 K. This exergy density was higher than that reported for other storage technologies, such as CAES and SMES.

3. The integration of CES systems with waste heat sources and the implementation of cogeneration resulted in a significant improvement in round-trip efficiency. For the comparison of the three operation modes in the cogeneration regime, the round-trip efficiency for alternatives B and C achieved 40.3 and 43.7 %, respectively, which represented 4.4 and 7.8 % higher than that of operation mode A. The substitution of the expansion valve for a hydraulic turbine led to increasing the round-trip efficiency from 41.9 % to 46.8 %. Likewise, the round-trip efficiency in the cogeneration regime resulted in 50 % higher on average than that of accounting only for electrical energy. As shown in the discussion section, the round-trip efficiency for generating both electricity and cooling load could be ranged from 74.3 % to 98.6 % if the time ratio equals the unit. The exergy utilization factor, for operation mode C, reached a value of 89.2 % for waste heat temperature of 600 K and outlet pump pressure of 20 MPa. This factor value resulted in 4 % higher than that of the cogeneration CES cycle with expansion valve. Overall, the simultaneous operation of the charging and discharging processes was found a viable option to improve the round-trip efficiency of CES systems.

4. The economic profitability of CES systems was found to be highly sensitive to system scale, interest rate, electricity tariff, efficiency and waste heat temperature. The payback period for operation modes B and C reached 15.3 and 15.2 years, respectively for CES system scale of 200 t of cryogenic tank capacity, interest rate of 6 % and reheat air temperature of 600 K. These results were comparatively lower than the

payback period for alternative A, which achieved 18.8 years at the same conditions. A higher specific investment cost was found for operation mode A (912.2 $\$/kWh$) than operation modes B and C (782.2 $\$/kWh$) for the maximum storage capacity evaluated in this research. Likewise, the simultaneous operation of the charging and discharging processes was shown to have the highest IRR with values of 8.44 % and 8.51 % for operation modes B and C, respectively.

5. The operation modes B and C were found to be economically more feasible than operation mode A. With regard to the NPV, for a waste heat temperature of 600 K and an interest rate of 6 %, the operation modes B and C presented a positive NPV of $17.5 and $18.2 million, respectively. These results were higher on average than that of the operation mode A in 85.4 and 86.1 %, respectively. The NPV showed to be highly affected by interest rate, electricity tariff, round-trip efficiency, economic life of technology and the number of cycles per year when those parameters varied ±50 %. In general, the simultaneous operation of the storage and discharge processes showed its superiority compared to the separate performance of the two regimes.

6. The attractiveness of the CES systems were significantly improved when 20 % of liquid air production was considered as a marketable product. With this regard, the NPV for operation mode C rose from $76.1 million, considering electricity and cooling load as final products, to $134.1 million when liquid air was added in the commercialization program of the project. This shows the great potential of CES systems to enhance their economic viability when other final products can be considered. CES systems could supply liquid air to a cryogenset for electricity production, refrigerated trucks for transporting food and hybrid vehicles. These represent some examples of the wide market that CES systems have. The LCOL for operation modes B and C, considering interest rate of 6 % and waste heat temperature of 600 K, were found to be 6.95 and 6.82 $¢/kg_L$, respectively. While operation mode A achieved a LCOL of 10.57 $¢/kg_L$. That is, the specific cost of liquid air at which it must be sold to break even over the useful life of the project was significantly lower for the simultaneous operation of the storage and discharge processes. In general, the results corroborate the thermodynamic and economic feasibility of operating the storage and discharge processes simultaneously in cogeneration CES systems.

5.2 Limitations of this research.

1. Despite verification the model and results with other investigations, this study was developed through theoretical fundamentals. The processes of compression, heat transfer, storage and expansion in the liquefaction section require experimental studies to characterize the inversion process during the transition of one regime

to another in order to deeply survey the simultaneity of the storage and discharge processes.

2. With the exception of the cryogenic tank, all components of the CES systems were simulated under steady-state conditions. The application of the simultaneity of the storage and discharge processes, the off-design operation, start up and shut down for CES systems imply the variation in time of the working fluid mass flow rate, the operative parameters and consequently the fluid properties. Therefore, in order to improve the accuracy of the results, a dynamic simulation research should be undertaken.

3. In this research, the pressure drop through the pipe lines and equipments was neglected. However, the thermodynamic and economic results of CES systems may significantly be modified when pressure changes through the whole cycle. Consequently, the pressure drop should be considered for further studies to improve the prediction of the CES systems performance.

4. For the economic analysis, the electricity tariff was the only cost uncertainty considered. In fact, other sources of uncertainty, such as maintenance cost, interest rate and cost of liquid air should be included in an economic optimization study. These uncertainties may influence the economic feasibility of CES systems. Additionally, the uncertainty analysis should be also extended to the thermodynamic mathematical modeling in order to verify the amplitude of variation of the main indexes and indicators as a result of the sources of uncertainties.

5.3 Suggestions for further research.

Despite the positive results obtained in this research, more studies are required to evaluate and optimize CES systems and make possible their introduction in the energy market. Taking into account the main findings and limitations of this study, the following research activities can be addressed.

1. Experimental investigations of the main processes involved in the liquefaction section is required, i.e. compression, heat transfer, expansion and storage. The integration of these processes to assess the simultaneity of the storage and discharge regimes is highly important. In addition, these experiments could be used to validate the performance of CES systems. In this case, the compression process must be evaluated for partial load, variable discharge pressure, and different inlet air temperatures in order to describe the compressor's performance. At the same time, the validation of a mathematical model to predict the heat transferred from the surroundings to the heat exchangers and the effectiveness will be required considering different types

of arrangements, materials, and the non-uniformity of fluid temperatures. Under this condition, it is recommended to evaluate the cryogenic turbines performance, computing power generation, and efficiency. The study in the storage tank should be aimed at quantifying the heat transferred from the environment and its thermal inertia to verify the response speed during the inversion process, that is, from the charging regime to discharging and vice versa.

2. Dynamic simulation of the whole CES system involving compressor, cryogenic tank, heat exchanger, and cryogenic turbines. The integration of CES technology with renewable energy sources, which are intermittent and unpredictable, especially solar and wind, supported by dynamic study, may contribute to improving the understanding of the impacts of CES systems on the electrical network. Likewise, the simultaneity of the storage and discharge processes could be more deeply studied.

3. Assessment of the integration of CES systems with organic Rankine cycle (ORC), refrigeration cycles, LNG terminal, renewables technologies and CHP plants. The integration of CES systems with other technologies may significantly improve their thermodynamic and economic feasibility. A further improvement could be implemented on the evaluated CES systems if the first expanded stream from T-1 is drawn in to the second heat exchanger (HE-2) instead of releasing the cold exergy to the environment. Furthermore, environmental and life cycle analysis could also be assessed with the integration of CES systems.

4. Economic analysis and optimization to assess the feasibility of CES systems, accounting for multiple sources of revenue and the main uncertainties. The costs of equipment, operation, maintenance, electricity, and others vary significantly in different regions and future markets, that is why a precise procedure should be required to update all relevant information in order to reduce the uncertainties.

Bibliography

[1] BP p.l.c. 2018 bp energy outlook. 2018.

[2] XOM: Exxon Mobil. 2018 outlook for energy: A view to 2040. February, 2018.

[3] European Association for Storage of Energy (EASE). Liquid air energy storage. https://ease-storage.eu/wp-content/uploads/2016/07/EASE_TD_Mechanical_LAES.pdf/, 2016. [Accessed: 12-08-2018].

[4] Peter Taylor, Ronan Bolton, Dave Stone, Xiao-Ping Zhang, Chris Martin, and Paul Upham. Pathways for energy storage in the uk. *Report for the centre for low carbon futures, York*, 2012.

[5] Emiliano Borri, Alessio Tafone, Alessandro Romagnoli, and Gabriele Comodi. A review on liquid air energy storage: History, state of the art and recent developments. *Renewable and Sustainable Energy Reviews*, 137:110572, 2021.

[6] Jacob W Leachman, Richard T Jacobsen, Eric W Lemmon, and Steven G Penoncello. *Thermodynamic properties of cryogenic fluids*. Springer, 2017.

[7] Frank G Kerry. *Industrial gas handbook: gas separation and purification*. CRC press, 2007.

[8] Frank Kreith. *CRC Handbook of Thermal Engineering*. CRC press LLC, 1999.

[9] R. F. Abdo. *Performance evaluation of liquid air energy storage and generation using Linde, Claude and Collins liquefaction cycles*. MSc dissertation in mechanical engineering, Federal University of Minas Gerais, Brazil, 2015.

[10] Rodrigo F Abdo, Hugo TC Pedro, Ricardo NN Koury, Luiz Machado, Carlos FM Coimbra, and Matheus P Porto. Performance evaluation of various cryogenic energy storage systems. *Energy*, 90:1024–1032, 2015.

[11] A Krauss, A Bar-Cohen, and AA Wative. Mechanical engineer's handbook: energy and power. 2006.

[12] Adrian Bejan, George Tsatsaronis, Michael Moran, et al. *Thermal design and optimization*. John Wiley & Sons, 1996.

[13] International Energy Agency (IEA). *Key world energy statistics*. International Energy Agency Paris, 2020.

[14] Empresa de Pesquisa Energética (EPE). *Balanço Energetico Nacional 2019*. Ministerio de Minas e Energia (MME), Brasil, 2019.

[15] David Strahan. *Liquid air technologies: a guide to the potential*. Centre for Low Carbon Futures, 2013.

[16] Daniel Weisser and Raquel S Garcia. Instantaneous wind energy penetration in isolated electricity grids: concepts and review. *Renewable energy*, 30(8):1299–1308, 2005.

[17] M. Wang, P. Zhao, Y. Wu, and Y. Dai. Performance analysis of a novel energy storage system based on liquid carbon dioxide. *Applied Thermal Engineering*, 91:812–823, 2015.

[18] Ceyhun Yilmaz and Onder Kaska. Performance analysis and optimization of a hydrogen liquefaction system assisted by geothermal absorption precooling refrigeration cycle. *International Journal of Hydrogen Energy*, 43(44):20203–20213, 2018.

[19] Shahram Derakhshan and Mohammadreza Khosravian. Exergy optimization of a novel combination of a liquid air energy storage system and a parabolic trough solar collector power plant. *Journal of Energy Resources Technology*, 141(8), 2019.

[20] Shafiqur Rehman, Luai M Al-Hadhrami, and Md Mahbub Alam. Pumped hydro energy storage system: A technological review. *Renewable and Sustainable Energy Reviews*, 44:586–598, 2015.

[21] B. Ameel, C. T'Joen, K. De Kerpel, P. De Jaeger, H. Huisseune, M. Van Belleghem, and M. De Paepe. Thermodynamic analysis of energy storage with a liquid air rankine cycle. *Applied Thermal Engineering*, 52(1):130–140, 2013.

[22] AD Prasad, Kamal Jain, and Ajay Gairola. Pumped storage hydropower plants environmental impacts using geomatics techniques: an overview. *International Journal of Computer Applications*, 81(14), 2013.

[23] International Renewable Energy Agency (IRENA). Electricity storage and renewables: Costs and markets to 2030. *Report Abu Dhabi*, 2017.

[24] O Teller, JP Nicolai, M Lafoz, D Laing, R Tamme, A Schroeder Pederson, M Andersson, C Folke, C Bourdil, M Conte, et al. Joint ease/eera recommendations for a european energy storage technology development roadmap towards 2030. *Brussels, Belgium: European Association for Storage of Energy (EASE) and European Energy Research Alliance (EERA)*, 2013.

[25] Rohan Dutta, Parthasarathi Ghosh, and Kanchan Chowdhury. Process configuration of liquid-nitrogen energy storage system (less) for maximum turnaround efficiency. *Cryogenics*, 88:132–142, 2017.

[26] Tong Zhang, Laijun Chen, Xuelin Zhang, Shengwei Mei, Xiaodai Xue, and Yuan Zhou. Thermodynamic analysis of a novel hybrid liquid air energy storage system based on the utilization of lng cold energy. *Energy*, 155:641–650, 2018.

[27] Sarah Hamdy, Tatiana Morosuk, and George Tsatsaronis. Cryogenics-based energy storage: Evaluation of cold exergy recovery cycles. *Energy*, 138:1069–1080, 2017.

[28] Majid Aasadnia and Mehdi Mehrpooya. Large-scale liquid hydrogen production methods and approaches: a review. *Applied Energy*, 212:57–83, 2018.

[29] Frank Kreith and Raj P Chhabra. *CRC Handbook of Thermal Engineering*. CRC press, 2017.

[30] Wolfgang Foerg. History of cryogenics: the epoch of the pioneers from the beginning to the year 1911. *International journal of refrigeration*, 25(3):283–292, 2002.

[31] Adriano Sciacovelli, Daniel Smith, Helena Navarro, Yongliang Li, and Yulong Ding. Liquid air energy storage–operation and performance of the first pilot plant in the world. In *Proceedings of ECOS 2016-the 29th international conference on efficiency, cost, optimization, simulation and environmental impact of energy systems, portoroz, Slovenia*, 2016.

[32] Mathew Aneke and Meihong Wang. Energy storage technologies and real life applications–a state of the art review. *Applied Energy*, 179:350–377, 2016.

[33] RB Stewart and KD Timmerhaus. The correlation of thermodynamic properties of cryogenic fluids. In *Advances in Cryogenic Engineering*, pages 20–27. Springer, 1964.

[34] Klaus D Timmerhaus and Thomas M Flynn. Properties of cryogenic fluids. In *Cryogenic Process Engineering*, pages 13–38. Springer, 1989.

[35] Richard T Jacobsen, Steven G Penoncello, and Eric W Lemmon. Thermodynamic properties of cryogenic fluids. In *Thermodynamic Properties of Cryogenic Fluids*, pages 31–287. Springer, 1997.

[36] Eric W Lemmon and Richard T Jacobsen. Viscosity and thermal conductivity equations for nitrogen, oxygen, argon, and air. *International journal of thermophysics*, 25(1):21–69, 2004.

[37] Randall F Barron and Gregory F Nellis. *Cryogenic Heat Transfer*. CRC press Taylor Francis Group, 2nd edition, 2017.

[38] Mostafa Abolala, Kiana Peyvandi, Farshad Varaminian, and Seyed Majid Hashemianzadeh. A comprehensive description of single-phase and vle properties of cryogenic fluids using molecular-based equations of state. *Fluid phase equilibria*, 494:143–160, 2019.

[39] Klaus D Timmerhaus and Thomas M Flynn. *Cryogenic Process Engineering*. Springer Science & Business Media, 2013.

[40] James R Couper, W Roy Penney, and James R Fair. *Chemical Process Equipment-Selection and Design (Revised 3rd Edition)*. Gulf Professional Publishing, 2012.

[41] Farshad Kalavani, Behnam Mohammadi-Ivatloo, and Kazem Zare. Optimal stochastic scheduling of cryogenic energy storage with wind power in the presence of a demand response program. *Renewable Energy*, 130:268–280, 2019.

[42] Christopher Winnefeld, Thomas Kadyk, Boris Bensmann, Ulrike Krewer, and Richard Hanke-Rauschenbach. Modelling and designing cryogenic hydrogen tanks for future aircraft applications. *Energies*, 11(1):105, 2018.

[43] P. Wojcieszak, J. Poliński, and M. Chorowski. Investigation of a working fluid for cryogenic energy storage systems. *Materials Science and Engineering*, 278:1–8, 2017.

[44] Desmond Winterbone and Ali Turan. *Advanced thermodynamics for engineers*. Butterworth-Heinemann, 2015.

[45] M Akhurst, I Arbon, M Ayres, N Brandon, R Bruges, S Cooper, Y Ding, T Evison, N Goode, P Grünewald, et al. Liquid air in the energy and transport systems: Opportunities for industry and innovation in the uk. 2013.

[46] Adrian Bejan. *Advanced engineering thermodynamics*. John Wiley & Sons, 2016.

[47] Kenneth Wark. *Advanced thermodynamics for engineers*. McGraw-Hill New York, 1995.

[48] Jan Szargut and Ireneusz Szczygiel. Utilization of the cryogenic exergy of liquid natural gas (lng) for the production of electricity. *Energy*, 34(7):827–837, 2009.

[49] Bahram Ghorbani, Mehdi Mehrpooya, Mohammad-Hossein Hamedi, and Majid Amidpour. Exergoeconomic analysis of integrated natural gas liquids (ngl) and liquefied natural gas (lng) processes. *Applied Thermal Engineering*, 113:1483–1495, 2017.

[50] Y. Zhang, K. Yang, H. Hong, and J. Zhong, X.and Xu. Thermodynamic analysis of a novel energy storage system with carbon dioxide as working fluid. *Renewable Energy*, 99:682–697, 2016.

[51] CR Baker and RL Shaner. A study of the efficiency of hydrogen liquefaction. *International Journal of Hydrogen Energy*, 3(3):321–334, 1978.

[52] TK Nandi and S Sarangi. Performance and optimization of hydrogen liquefaction cycles. *International journal of hydrogen energy*, 18(2):131–139, 1993.

[53] Abdalqader Ahmad, Raya Al-Dadah, and Saad Mahmoud. Liquid nitrogen energy storage for air conditioning and power generation in domestic applications. *Energy conversion and management*, 128:34–43, 2016.

[54] MD Atrey. Thermodynamic analysis of collins helium liquefaction cycle. *Cryogenics*, 38(12):1199–1206, 1998.

[55] Rijo Jacob Thomas, Parthasarathi Ghosh, and Kanchan Chowdhury. Exergy analysis of helium liquefaction systems based on modified claude cycle with two-expanders. *Cryogenics*, 51(6):287–294, 2011.

[56] Arpan Kundu and Kanchan Chowdhury. Evaluating performance of mixed mode multistage helium plants for design and off-design conditions by exergy analysis. *International Journal of Refrigeration*, 38:46–57, 2014.

[57] Khalil M Khalil, Abdalqader Ahmad, Saad Mahmoud, and RK Al-Dadah. Liquid air/nitrogen energy storage and power generation system for micro-grid applications. *Journal of cleaner production*, 164:606–617, 2017.

[58] G. L. Guizzi, M. Manno, L. M. Tolomei, and R. M. Vitali. Thermodynamic analysis of a liquid air energy storage system. *Energy*, 93:1639–1647, 2015.

[59] Thomas Flynn. *Cryogenic engineering, revised and expanded*. CRC Press, 2005.

[60] Yvonne Lim, Mushtak Al-Atabi, and Richard A Williams. Liquid air as an energy storage: a review. *Journal of Engineering Science and Technology*, 11(4):496–515, 2016.

[61] SC Collins. A helium cryostat. *Review of Scientific Instruments*, 18(3):157–167, 1947.

[62] Sarah Hamdy, Francisco Moser, Tatiana Morosuk, and George Tsatsaronis. Exergy-based and economic evaluation of liquefaction processes for cryogenics energy storage. *Energies*, 12(3):493, 2019.

[63] EM Smith. Storage of electrical energy using supercritical liquid air. *Proceedings of the Institution of Mechanical Engineers*, 191(1):289–298, 1977.

[64] Haisheng Chen, Yulong Ding, Toby Peters, and Ferdinand Berger. Energy storage and generation, November 19 2009. US Patent App. 12/280,739.

[65] Robert Morgan, Stuart Nelmes, Emma Gibson, and Gareth Brett. Liquid air energy storage–analysis and first results from a pilot scale demonstration plant. *Applied energy*, 137:845–853, 2015.

[66] Xiaodong Peng, Xiaohui She, Chuan Li, Yimo Luo, Tongtong Zhang, Yongliang Li, and Yulong Ding. Liquid air energy storage flexibly coupled with lng regasification for improving air liquefaction. *Applied Energy*, 250:1190–1201, 2019.

[67] XD Xue, SX Wang, XL Zhang, C Cui, LB Chen, Y Zhou, and JJ Wang. Thermodynamic analysis of a novel liquid air energy storage system. *Physics procedia*, 67:733–738, 2015.

[68] Lars Hüttermann and Roland Span. Influence of the heat capacity of the storage material on the efficiency of thermal regenerators in liquid air energy storage systems. *Energy*, 174:236–245, 2019.

[69] Piotr Krawczyk, Łukasz Szabłowski, Sotirios Karellas, Emmanuel Kakaras, and Krzysztof Badyda. Comparative thermodynamic analysis of compressed air and liquid air energy storage systems. *Energy*, 142:46–54, 2018.

[70] Adriano Sciacovelli, A Vecchi, and Y Ding. Liquid air energy storage (laes) with packed bed cold thermal storage–from component to system level performance through dynamic modelling. *Applied Energy*, 190:84–98, 2017.

[71] Rijo Jacob Thomas, Parthasarathi Ghosh, and Kanchan Chowdhury. Exergy analysis of helium liquefaction systems based on modified claude cycle with two-expanders. *Cryogenics*, 51(6):287–294, 2011.

[72] YP Du and YL Ding. Feasibility of small-scale cold energy storage (ces) through carbon dioxide based rankine cycle. *Journal of Energy Storage*, 6:40–49, 2016.

[73] Rijo Jacob Thomas, Parthasarathi Ghosh, and Kanchan Chowdhury. Role of heat exchangers in helium liquefaction cycles: Simulation studies using collins cycle. *Fusion Engineering and Design*, 87(1):39–46, 2012.

[74] E Borri, Alessio Tafone, A Romagnoli, and G Comodi. A preliminary study on the optimal configuration and operating range of a "microgrid scale" air liquefaction plant for liquid air energy storage. *Energy Conversion and Management*, 143:275–285, 2017.

[75] Mirhadi S Sadaghiani and Mehdi Mehrpooya. Introducing and energy analysis of a novel cryogenic hydrogen liquefaction process configuration. *International Journal of Hydrogen Energy*, 42(9):6033–6050, 2017.

[76] Yongliang Li. *Cryogen based energy storage: process modelling and optimisation*. PhD thesis, University of Leeds, 2011.

[77] Piotr Krawczyk, Łukasz Szabłowski, Krzysztof Badyda, Sotirios Karellas, and Emmanuel Kakaras. Impact of selected parameters on performance of the adiabatic liquid air energy storage system. *Journal of Power Technologies*, 96(4), 2016.

[78] Hao Peng, Xuekun Shan, Yu Yang, and Xiang Ling. A study on performance of a liquid air energy storage system with packed bed units. *Applied Energy*, 211:126–135, 2018.

[79] Alessio Tafone, Alessandro Romagnoli, Emiliano Borri, and Gabriele Comodi. New parametric performance maps for a novel sizing and selection methodology of a liquid air energy storage system. *Applied Energy*, 250:1641–1656, 2019.

[80] Mengjuan Xu, Pan Zhao, Yaowu Huo, Jianming Han, Jiangfeng Wang, and Yiping Dai. Thermodynamic analysis of a novel liquid carbon dioxide energy storage system and comparison to a liquid air energy storage system. *Journal of Cleaner Production*, 242:118437, 2020.

[81] Wenxu Sun, Xu Liu, Xuqing Yang, Xiaohu Yang, and Zhan Liu. Design and thermodynamic performance analysis of a new liquid carbon dioxide energy storage system with low pressure stores. *Energy Conversion and Management*, 239:114227, 2021.

[82] Marco Antonelli, Stefano Barsali, Umberto Desideri, Romano Giglioli, Fabrizio Paganucci, and Gianluca Pasini. Liquid air energy storage: Potential and challenges of hybrid power plants. *Applied energy*, 194:522–529, 2017.

[83] Huan Guo, Yujie Xu, Haisheng Chen, Cong Guo, and Wei Qin. Thermodynamic analytical solution and exergy analysis for supercritical compressed air energy storage system. *Applied Energy*, 199:96–106, 2017.

[84] Majid Asadnia and Mehdi Mehrpooya. A novel hydrogen liquefaction process configuration with combined mixed refrigerant systems. *International Journal of Hydrogen Energy*, 42(23):15564–15585, 2017.

[85] Xiaohui She, Xiaodong Peng, Binjian Nie, Guanghui Leng, Xiaosong Zhang, Likui Weng, Lige Tong, Lifang Zheng, Li Wang, and Yulong Ding. Enhancement of round trip efficiency of liquid air energy storage through effective utilization of heat of compression. *Applied Energy*, 206:1632–1642, 2017.

[86] X. Peng, X. She, Y. Li, and Y. Ding. Thermodynamic analysis of liquid air energy storage integrated with a serial system of organic rankine and absorption refrigeration cycles driven by compression heat. *Energy Procedia*, 142:3440–3446, 2017.

[87] Yongliang Li, Xiang Wang, Yi Jin, and Yulong Ding. An integrated solar-cryogen hybrid power system. *Renewable energy*, 37(1):76–81, 2012.

[88] Mehmet Kanoglu, Ceyhun Yilmaz, and Aysegul Abusoglu. Geothermal energy use in absorption precooling for claude hydrogen liquefaction cycle. *international journal of hydrogen energy*, 41(26):11185–11200, 2016.

[89] Jianyong Wang, Jiangfeng Wang, Yiping Dai, and Pan Zhao. Thermodynamic analysis and optimization of a transcritical co2 geothermal power generation system based on the cold energy utilization of lng. *Applied Thermal Engineering*, 70(1):531–540, 2014.

[90] Inkyu Lee, Jinwoo Park, and Il Moon. Conceptual design and exergy analysis of combined cryogenic energy storage and lng regasification processes: cold and power integration. *Energy*, 140:106–115, 2017.

[91] Feier Xue, Yu Chen, and Yonglin Ju. Design and optimization of a novel cryogenic rankine power generation system employing binary and ternary mixtures as working fluids based on the cold exergy utilization of liquefied natural gas (lng). *Energy*, 138:706–720, 2017.

[92] Juwon Kim, Yeelyong Noh, and Daejun Chang. Storage system for distributed-energy generation using liquid air combined with liquefied natural gas. *Applied Energy*, 212:1417–1432, 2018.

[93] Paweł Dorosz, Paweł Wojcieszak, and Ziemowit Malecha. Exergetic analysis, optimization and comparison of lng cold exergy recovery systems for transportation. *Entropy*, 20(1):59, 2018.

[94] Yongliang Li, Hui Cao, Shuhao Wang, Yi Jin, Dacheng Li, Xiang Wang, and Yulong Ding. Load shifting of nuclear power plants using cryogenic energy storage technology. *Applied Energy*, 113:1710–1716, 2014.

[95] Bharath Kantharaj, Seamus Garvey, and Andrew Pimm. Compressed air energy storage with liquid air capacity extension. *Applied energy*, 157:152–164, 2015.

[96] Pau Farres-Antunez, Haobai Xue, and Alexander J White. Thermodynamic analysis and optimisation of a combined liquid air and pumped thermal energy storage cycle. *Journal of Energy Storage*, 18:90–102, 2018.

[97] Alessio Tafone, Emiliano Borri, Gabriele Comodi, Martijn van den Broek, and Alessandro Romagnoli. Liquid air energy storage performance enhancement by means of organic rankine cycle and absorption chiller. *Applied Energy*, 228:1810–1821, 2018.

[98] Stefano Barsali, Alessio Ciambellotti, Romano Giglioli, Fabrizio Paganucci, and Gianluca Pasini. Hybrid power plant for energy storage and peak shaving by liquefied oxygen and natural gas. *Applied Energy*, 228:33–41, 2018.

[99] Xiaohui She, Tongtong Zhang, Lin Cong, Xiaodong Peng, Chuan Li, Yimo Luo, and Yulong Ding. Flexible integration of liquid air energy storage with liquefied natural gas regasification for power generation enhancement. *Applied Energy*, 251:113355, 2019.

[100] Tugberk Hakan Cetin, Mehmet Kanoglu, and Neslihan Yanikomer. Cryogenic energy storage powered by geothermal energy. *Geothermics*, 77:34–40, 2019.

[101] Inkyu Lee and Fengqi You. Systems design and analysis of liquid air energy storage from liquefied natural gas cold energy. *Applied Energy*, 242:168–180, 2019.

[102] Stefano Briola, Roberto Gabbrielli, and Antonio Delgado. Energy and economic performance assessment of the novel integration of an advanced configuration of liquid air energy storage plant with an existing large-scale natural gas combined cycle. *Energy Conversion and Management*, 205:112434, 2020.

[103] Meng Qi, Jinwoo Park, Jeongdong Kim, Inkyu Lee, and Il Moon. Advanced integration of lng regasification power plant with liquid air energy storage: Enhancements in flexibility, safety, and power generation. *Applied Energy*, 269:115049, 2020.

[104] Armin Ebrahimi, Bahram Ghorbani, Fatemeh Skandarzadeh, and Masoud Ziabasharhagh. Introducing a novel liquid air cryogenic energy storage system using phase change material, solar parabolic trough collectors, and kalina power cycle (process integration, pinch, and exergy analyses). *Energy Conversion and Management*, 228:113653, 2021.

[105] Maan Al-Zareer, Ibrahim Dincer, and Marc A Rosen. Analysis and assessment of novel liquid air energy storage system with district heating and cooling capabilities. *Energy*, 141:792–802, 2017.

[106] Gabriele Comodi, Francesco Carducci, Jia Yin Sze, Nagarajan Balamurugan, and Alessandro Romagnoli. Storing energy for cooling demand management in tropical climates: A techno-economic comparison between different energy storage technologies. *Energy*, 121:676–694, 2017.

[107] Andrea Vecchi, Yongliang Li, Pierluigi Mancarella, and Adriano Sciacovelli. Multi-energy liquid air energy storage: A novel solution for flexible operation of districts with thermal networks. *Energy Conversion and Management*, 238:114161, 2021.

[108] Chunping Xie, Yongliang Li, Yulong Ding, and Jonathan Radcliffe. Evaluating levelized cost of storage (lcos) based on price arbitrage operations: with liquid air energy storage (laes) as an example. *Energy Procedia*, 158:4852–4860, 2019.

[109] Xipeng Lin, Liang Wang, Ningning Xie, Guoyue Li, and Haisheng Chen. Thermodynamic analysis of the cascaded packed bed cryogenic storage based supercritical air energy storage system. *Energy Procedia*, 158:5079–5085, 2019.

[110] Andrew J Pimm, Seamus D Garvey, and Bharath Kantharaj. Economic analysis of a hybrid energy storage system based on liquid air and compressed air. *Journal of energy storage*, 4:24–35, 2015.

[111] Andrea Vecchi, Yongliang Li, Pierluigi Mancarella, and Adriano Sciacovelli. Integrated techno-economic assessment of liquid air energy storage (laes) under off-design conditions: Links between provision of market services and thermodynamic performance. *Applied Energy*, 262:114589, 2020.

[112] Stefano Mazzoni, S Ooi, Alessio Tafone, E Borri, G Comodi, and Alessandro Romagnoli. Liquid air energy storage as a polygeneration system to solve the unit commitment and economic dispatch problems in micro-grids applications. *Energy Procedia*, 158:5026–5033, 2019.

[113] Zhaozhao Gao, Wei Ji, Luna Guo, Xiaoyu Fan, and Junjie Wang. Thermo-economic analysis of the integrated bidirectional peak shaving system consisted by liquid air energy storage and combined cycle power plant. *Energy Conversion and Management*, 234:113945, 2021.

[114] MT Syed, SA Sherif, TN Veziroglu, and John W Sheffield. An economic analysis of three hydrogen liquefaction systems. *International Journal of Hydrogen Energy*, 23(7):565–576, 1998.

[115] Hoseyn Sayyaadi and M Babaelahi. Thermoeconomic optimization of a cryogenic refrigeration cycle for re-liquefaction of the lng boil-off gas. *international journal of refrigeration*, 33(6):1197–1207, 2010.

[116] Oliver Schmidt, Sylvain Melchior, Adam Hawkes, and Iain Staffell. Projecting the future levelized cost of electricity storage technologies. *Joule*, 3(1):81–100, 2019.

[117] Manasseh Obi, Shauna M Jensen, Jennifer B Ferris, and Robert B Bass. Calculation of levelized costs of electricity for various electrical energy storage systems. *Renewable and Sustainable Energy Reviews*, 67:908–920, 2017.

[118] Aldo Orioli and Alessandra Di Gangi. The recent change in the italian policies for photovoltaics: Effects on the payback period and levelized cost of electricity of grid-

connected photovoltaic systems installed in urban contexts. *Energy*, 93:1989–2005, 2015.

[119] Sarah Hamdy, Tatiana Morosuk, and George Tsatsaronis. Exergetic and economic assessment of integrated cryogenic energy storage systems. *Cryogenics*, 99:39–50, 2019.

[120] Mathieu Legrand, Luis Miguel Rodríguez-Antón, Carmen Martinez-Arevalo, and Fernando Gutiérrez-Martín. Integration of liquid air energy storage into the spanish power grid. *Energy*, 187:115965, 2019.

[121] Alessio Tafone, Yulong Ding, Yongliang Li, Chunping Xie, and Alessandro Romagnoli. Levelised cost of storage (lcos) analysis of liquid air energy storage system integrated with organic rankine cycle. *Energy*, 198:117275, 2020.

[122] Solomos Georgiou, Nilay Shah, and Christos N Markides. A thermo-economic analysis and comparison of pumped-thermal and liquid-air electricity storage systems. *Applied Energy*, 226:1119–1133, 2018.

[123] Ceyhun Yilmaz. A case study: Exergoeconomic analysis and genetic algorithm optimization of performance of a hydrogen liquefaction cycle assisted by geothermal absorption precooling cycle. *Renewable Energy*, 128:68–80, 2018.

[124] Ceyhun Yilmaz and Onder Kaska. Performance analysis and optimization of a hydrogen liquefaction system assisted by geothermal absorption precooling refrigeration cycle. *International Journal of Hydrogen Energy*, 2018.

[125] Önder Kaşka, Ceyhun Yılmaz, Onur Bor, and Nehir Tokgöz. The performance assessment of a combined organic rankine-vapor compression refrigeration cycle aided hydrogen liquefaction. *International Journal of Hydrogen Energy*, 2018.

[126] EPE Empresa de Pesquisa Energética. Empresa de pesquisa energética. 2019c. *Terminais de Regaseificação de GNL no Brasil- Panorama dos Principais Projetos. Disponível em:< http://www. epe. gov. br/sites-pt/publicacoes-dadosabertos/publicacoes/PublicacoesArquivos/publicacao-412/Nota% 20T% C3% A9cnica*, 2019.

[127] Inkyu Lee, Jinwoo Park, Fengqi You, and Il Moon. A novel cryogenic energy storage system with lng direct expansion regasification: Design, energy optimization, and exergy analysis. *Energy*, 173:691–705, 2019.

[128] Bao Ha. Cryogenic nitrogen generator with bottom reboiler and nitrogen expander, June 23 1992. US Patent 5,123,946.

[129] M Atsumi. Liquid air storage gas turbine power generation system. *Japan Patent JPH08149722A*, 1996.

[130] Harumi Wakana, Koichi Chino, and Osamu Yokomizo. Cold heat-reused air liquefaction/vaporization and storage gas turbine electric power system, June 28 2001. US Patent App. 09/765,338.

[131] K Chino, Y Nishiura, Y Noguchi, and O Yokomizo. Energy storaging type gas turbine power generating system. *Japan Patent JP3460433B2*, 2003.

[132] Mark A. Shirk, Gary A. Storck, and Wesley W. Weigel. Cryogenic cogeneration system, 14 2005. US Patent 10/961,942.

[133] Claire Williamson. Cryogenic propulsion system, November 3 2006. GB Patent App. 0621972.9.

[134] Haisheng Chen, Yulong Ding, Toby Peters, and Ferdinand Berger. Method of storing energy and a cryogenic energy storage system, 30 2007. GB Patent App. PCT/GB2007/000667.

[135] David Vandor. System and method for liquid air production, power storage and power release, 18 2011. US Patent App. 12/127,520.

[136] R Morgan, S Nelmes, N Castellucci, and G Brett. Method and apparatus for power storage. *Patent: WO2014/006426*, 2013.

[137] Charles Cook and William Lear. Cryogenic power extraction, 27 2015. US Patent App. 61/942,998.

[138] Alexander Alekseev. Process and system for storing and recovering energy, 14 2015. DE Patent App. 14001926.6.

[139] Matheus Porto, Luiz Machado, and Rodrigo Abdo. MÉtodo e dispositivo de armazenamento e geraÇÃo de energia por lÍquido criogÊnico, e usos, 15 2016. BR Patente App. 10 2016 005698 5.

[140] Haisheng Chen, Yulong Ding, Toby Peters, and Ferdinand Berger. Method of storing energy and a cryogenic energy storage system, June 23 2016. US Patent App. 15/053,840.

[141] Haisheng Chen, Chunqing Tan, Jia Liu, Yujie Xu, and Zheng Yang. Sistema de almacenamiento de energía con aire supercrítico, 2 2016. ES Patent App. 2 572 657 T3.

[142] Joseph Naumovitz and Martin Kibili. Cold storage methods, 9 2017. US Patent App. 14/818,921.

[143] Robert Morgan, Stuart Nelmes, Nicola Castellucci, and Stephen Gareth Brett. Method and apparatus for power storage, February 13 2018. US Patent 9,890,712.

[144] Yulong Ding, Xiaohui She, Xiaodong Peng, Binjian Nie, Lin Cong, and Zhu Jiang. An integrated liquid air energy storage and battery system for black start and frequency regulation of power grids, February 3 2018. China Patent App. 201710491478.2.

[145] Xiaohui She, Yulong Ding, Xiaodong Peng, Likui Weng, Binjian Nie, Jiuliang Chen, Lin Cong, and Guanghui Leng. A device and method for enhancing round trip efficiency of liquid air energy storage system, February 3 2018. China Patent App. 201710491411.9.

[146] John D Upperman and Ralph Greenberg. System and method for liquid air energy storage, December 17 2019. US Patent 10,508,596.

[147] William M. Conlon. Liquid air power and storage, July 17 2019. GB Patent App. EP 3 090 198 B1.

[148] John D Upperman and Ralph Greenberg. System and method for liquid air energy storage, June 23 2020. US Patent 10,690,013.

[149] William M. Conlon. High pressure liquid air power and storage, November 18 2020. GB Patent App. EP 3 365 536 B1.

[150] Stanislav Sinatov. Method for liquid air and gas energy storage, 8 2020. US Patent App. 16/109,884.

[151] William M. Conlon. Cryogenic combined cycle power plant, July 6 2021. US Patent App. 16/458,831.

[152] Barry Taylor. *Guide for the use of the International System of Units (SI): The metric system*. DIANE Publishing, 1995.

[153] Jeswin Joseph, Gagan Agrawal, Deepak Kumar Agarwal, JC Pisharady, and S Sunil Kumar. Effect of insulation thickness on pressure evolution and thermal stratification in a cryogenic tank. *Applied Thermal Engineering*, 111:1629–1639, 2017.

[154] Ho-Myung Chang, Hye Su Lim, and Kun Hyung Choe. Thermodynamic design of natural gas liquefaction cycles for offshore application. *Cryogenics*, 63:114–121, 2014.

[155] Sarah Hamdy, Francisco Moser, Tatiana Morosuk, and George Tsatsaronis. Exergy-based and economic evaluation of liquefaction processes for cryogenics energy storage. *Energies*, 12(3):493, 2019.

[156] Yunus Emre Yuksel, Murat Ozturk, and Ibrahim Dincer. Analysis and performance assessment of a combined geothermal power-based hydrogen production and liquefaction system. *International Journal of Hydrogen Energy*, 43(22):10268–10280, 2018.

[157] Tonguç Gökçeer, Gökmen Demirkaya, and Ricardo Vasquez Padilla. Thermoeconomic analysis of liquid air energy storage system. In *ASME 2017 11th International Conference on Energy Sustainability collocated with the ASME 2017 Power Conference Joint With ICOPE-17, the ASME 2017 15th International Conference on Fuel Cell Science, Engineering and Technology, and the ASME 2017 Nuclear Forum*. American Society of Mechanical Engineers Digital Collection, 2017.

[158] Wayne Lawrence Staats. *Analysis of a supercritical hydrogen liquefaction cycle*. PhD thesis, Massachusetts Institute of Technology, 2008.

[159] He Qing, Wang Lijian, Zhou Qian, Lu Chang, Du Dongmei, and Liu Wenyi. Thermodynamic analysis and optimization of liquefied air energy storage system. *Energy*, 173:162–173, 2019.

[160] Gareth Brett and Matthew Barnett. The application of liquid air energy storage for large scale long duration solutions to grid balancing. In *EPJ Web of Conferences*, volume 79, page 03002. EDP Sciences, 2014.

[161] Standard Atmosphere. International organization for standardization. *ISO*, 2533:1975, 1975.

[162] Chen Wang, Nevzat Akkurt, Xiaosong Zhang, Yimo Luo, and Xiaohui She. Techno-economic analyses of multi-functional liquid air energy storage for power generation, oxygen production and heating. *Applied Energy*, 275:115392, 2020.

[163] Zhaozhao Gao, Luna Guo, Wei Ji, Hao Xu, Baolin An, and Junjie Wang. Thermodynamic and economic analysis of a trigeneration system based on liquid air energy storage under different operating modes. *Energy Conversion and Management*, 221:113184, 2020.

[164] ANEEL. agência nacional de energia elétrica. https://www.aneel.gov.br/ranking-das-tarifas/. [Accessed: 22-3-2021].

[165] CRIOMEC. distribuidora de nitrogênio liquido. https://www.criomec.com.br/. [Accessed: 26-3-2021].

[166] Kuppan Thulukkanam. *Heat Exchanger Design Handbook*. CRC press, 2013.

[167] Yun-Ho Cho and Ho-Myung Chang. An effectiveness-ntu method for triple-passage counterflow heat exchangers. *KSME Journal*, 7(3):282–289, 1993.

[168] Darrell D Aulds and Randall F Barron. Three-fluid heat exchanger effectiveness. *International Journal of Heat and Mass Transfer*, 10(10):1457–1462, 1967.

[169] Jiyuan Tu, Guan Heng Yeoh, and Chaoqun Liu. *Computational fluid dynamics: a practical approach*. Butterworth-Heinemann, 2018.

[170] Guan Heng Yeoh and Jiyuan Tu. *Computational techniques for multiphase flows*. Butterworth-Heinemann, 2019.

[171] Prabhat Kumar Gupta, PK Kush, and Ashesh Tiwari. Design and optimization of coil finned-tube heat exchangers for cryogenic applications. *Cryogenics*, 47(5-6):322–332, 2007.

[172] Ho-Myung Chang, Hye Su Lim, and Kun Hyung Choe. Effect of multi-stream heat exchanger on performance of natural gas liquefaction with mixed refrigerant. *Cryogenics*, 52:642–647, 2012.

[173] Towhid Parikhani, Towhid Gholizadeh, Hadi Ghaebi, Seyed Mohammad Sattari Sadat, and Mehrdad Sarabi. Exergoeconomic optimization of a novel multigeneration system driven by geothermal heat source and liquefied natural gas cold energy recovery. *Journal of cleaner production*, 209:550–571, 2019.

[174] Hadi Rostamzadeh, Hadi Ghaebi, Shahram Vosoughi, and Javad Jannatkhah. Thermodynamic and thermoeconomic analysis and optimization of a novel dual-loop power/refrigeration cycle. *Applied Thermal Engineering*, 138:1–17, 2018.

[175] Peng Liu, Gequn Shu, Hua Tian, and Xuan Wang. Engine load effects on the energy and exergy performance of a medium cycle/organic rankine cycle for exhaust waste heat recovery. *Entropy*, 20(2):137, 2018.

[176] Tadeusz Jozef Kotas. *The exergy method of thermal plant analysis*. Elsevier, 2013.

[177] Tatiana Morosuk and George Tsatsaronis. Splitting physical exergy: Theory and application. *Energy*, 167:698–707, 2019.

[178] Antonio Piacentino and Fabio Cardona. Scope-oriented thermoeconomic analysis of energy systems. part i: Looking for a non-postulated cost accounting for the dissipative devices of a vapour compression chiller. is it feasible? *Applied energy*, 87(3):943–956, 2010.

[179] Qinghua Yu, Wenji Song, Bushra Al-Duri, Yan Zhang, Danmei Xie, Yulong Ding, and Yongliang Li. Theoretical analysis for heat exchange performance of transcritical nitrogen evaporator used for liquid air energy storage. *Applied Thermal Engineering*, 2018.

[180] Ramesh K Shah and Dusan P Sekulic. *Fundamentals of heat exchanger design*. John Wiley & Sons, 2003.

[181] ZY Guo, XB Liu, WQ Tao, and RK Shah. Effectiveness–thermal resistance method for heat exchanger design and analysis. *International Journal of Heat and Mass Transfer*, 53(13-14):2877–2884, 2010.

[182] A. B. Lourenço. *Uma abordagem termoeconômica sistemática para modelagem de ciclos termodinâmicos*. PhD tese de doutorado, Universidade Federal do ABC. Santo André, Brasil, 2016.

[183] Jan Szargut, David R Morris, and Frank R Steward. Exergy analysis of thermal, chemical, and metallurgical processes. 1987.

[184] William Z Black and James G Hartley. Thermodynamics. si version, 1991.

[185] Michael J Moran, Howard N Shapiro, Daisie D Boettner, and Margaret B Bailey. *Fundamentals of engineering thermodynamics*. John Wiley & Sons, 2010.

[186] KamW Li. *Applied thermodynamics: availability method and energy conversion*. Routledge, 2018.

[187] Silvio de Oliveira. Exergy, exergy costing, and renewability analysis of energy conversion processes. In *Exergy*, pages 5–53. Springer, 2013.

[188] Adrian Bejan and Eden Mamut. *Thermodynamic optimization of complex energy systems*, volume 69. Springer Science & Business Media, 2012.

[189] Xiaodong Peng. *Liquid air energy storage: process optimization and performance enhancement*. PhD thesis, University of Birmingham, 2018.

[190] A Sciacovelli, D Smith, ME Navarro, A Vecchi, X Peng, Y Li, J Radcliffe, and Y Ding. Performance analysis and detailed experimental results of the first liquid air energy storage plant in the world. *Journal of Energy Resources Technology*, 140(2), 2018.

[191] J.H. Horlock. *Cogeneration—Combined Heat and Power (CHP): Thermodynamics and Economics*. Malabar, Florida: Krieger Publishing Company, 1997.

[192] Marco F Torchio. Energy-exergy, environmental and economic criteria in combined heat and power (chp) plants: indexes for the evaluation of the cogeneration potential. *Energies*, 6(5):2686–2708, 2013.

[193] Manojkumar Ramteke and Santosh K Gupta. Multi-objective genetic algorithm and simulated annealing with the jumping gene adaptations. In *MULTI-OBJECTIVE*

OPTIMIZATION: Techniques and Application in Chemical Engineering, pages 93–133. World Scientific, 2017.

[194] Gade Pandu Rangaiah. *Multi-objective optimization: techniques and applications in chemical engineering*, volume 1. World Scientific, 2009.

[195] Jiangfeng Wang, Zhixin Sun, Yiping Dai, and Shaolin Ma. Parametric optimization design for supercritical co2 power cycle using genetic algorithm and artificial neural network. *Applied Energy*, 87(4):1317–1324, 2010.

[196] Seyed Mostafa Safdarnejad, John D Hedengren, and Larry L Baxter. Dynamic optimization of a hybrid system of energy-storing cryogenic carbon capture and a baseline power generation unit. *Applied Energy*, 172:66–79, 2016.

[197] SMS Mahmoudi and AR Ghavimi. Thermoeconomic analysis and multi objective optimization of a molten carbonate fuel cell–supercritical carbon dioxide–organic rankin cycle integrated power system using liquefied natural gas as heat sink. *Applied Thermal Engineering*, 107:1219–1232, 2016.

[198] Mitsuo Gen and Runwei Cheng. *Genetic algorithms and engineering optimization*, volume 7. John Wiley & Sons, 2000.

[199] SN Sivanandam and SN Deepa. Genetic algorithm optimization problems. In *Introduction to Genetic Algorithms*, pages 165–209. Springer, 2008.

[200] Ibrahim Dincer, Marc A Rosen, and Pouria Ahmadi. *Optimization of energy systems*. Wiley Online Library, 2017.

[201] Roberto Carapellucci and Lorena Giordano. A comparison between exergetic and economic criteria for optimizing the heat recovery steam generators of gas-steam power plants. *Energy*, 58:458–472, 2013.

[202] Pouria Ahmadi and Ibrahim Dincer. Exergoenvironmental analysis and optimization of a cogeneration plant system using multimodal genetic algorithm (mga). *Energy*, 35(12):5161–5172, 2010.

[203] Runwei Cheng. *Genetic algorithms and engineering optimization*. Wiley-Interscience, 2000.

[204] Randy L Haupt, Sue Ellen Haupt, and Sue Ellen Haupt. *Practical genetic algorithms*, volume 2. Wiley New York, 1998.

[205] Jenkins Scott. Economic indicators: CEPCI. chemical engineering essentials for the cpi professional. https://www.chemengonline.com/2021-cepci-updates-february-prelim-and-january-final/. [Accessed: 25-3-2021].

[206] Mahdi Moghimi, Mohammadali Emadi, Pouria Ahmadi, and Hesam Moghadasi. 4e analysis and multi-objective optimization of a cchp cycle based on gas turbine and ejector refrigeration. *Applied Thermal Engineering*, 141:516–530, 2018.

[207] Mehdi Mehrpooya and Masood Jalali Zonouz. Analysis of an integrated cryogenic air separation unit, oxy-combustion carbon dioxide power cycle and liquefied natural gas regasification process by exergoeconomic method. *Energy conversion and management*, 139:245–259, 2017.

[208] Armin Ebrahimi and Masoud Ziabasharhagh. Optimal design and integration of a cryogenic air separation unit (asu) with liquefied natural gas (lng) as heat sink, thermodynamic and economic analyses. *Energy*, 126:868–885, 2017.

[209] Xiufen He, Yunong Liu, Ali Rehman, and Li Wang. A novel air separation unit with energy storage and generation and its energy efficiency and economy analysis. *Applied Energy*, 281:115976, 2021.

[210] Chunping Xie, Yan Hong, Yulong Ding, Yongliang Li, and Jonathan Radcliffe. An economic feasibility assessment of decoupled energy storage in the uk: With liquid air energy storage as a case study. *Applied Energy*, 225:244–257, 2018.

[211] Tung Au and Thomas P Au. *Engineering Economics for Capital Investment Analysis.* 1983.

[212] Chan S Park. *Fundamentals of Engineering Economics. Chan S. Park.* Pearson Education, 2012.

[213] John Vail Farr and Isaac Faber. *Engineering Economics of Life Cycle Cost Analysis.* CRC Press, 2019.

[214] Ehsan Baniasadi. Concurrent hydrogen and water production from brine water based on solar spectrum splitting: process design and thermoeconomic analysis. *Renewable Energy*, 102:50–64, 2017.

[215] Ju-Eon Bae, Supaporn Wilailak, Jae-Hyeon Yang, Dong-Yeol Yun, Umer Zahid, and Chul-Jin Lee. Multi-objective optimization of hydrogen liquefaction process integrated with liquefied natural gas system. *Energy Conversion and Management*, 231:113835, 2021.

[216] Chun Sing Lai and Malcolm D McCulloch. Levelized cost of electricity for solar photovoltaic and electrical energy storage. *Applied energy*, 190:191–203, 2017.

[217] B. Zakeri and S. Syri. Electrical energy storage systems: A comparative life cycle cost analysis. *Renewable and Sustainable Energy Reviews*, 42:569–596, 2015.

[218] Barry N Taylor, Chris E Kuyatt, et al. Guidelines for evaluating and expressing the uncertainty of nist measurement results. 1994.

[219] Jack Philip Holman. *Experimental methods for engineers*. 2001.

[220] Anwar Hammad and Ibrahim Dincer. Analysis and assessment of an advanced hydrogen liquefaction system. *International Journal of Hydrogen Energy*, 43(2):1139–1151, 2018.

[221] Zhan Liu, Bin Liu, Jianzhang Guo, Xuan Xin, and Xiaohu Yang. Conventional and advanced exergy analysis of a novel transcritical compressed carbon dioxide energy storage system. *Energy Conversion and Management*, 198:111807, 2019.

[222] Ali Rehman, Muhammad Abdul Qyyum, Kinza Qadeer, Fatima Zakir, Yulong Ding, Moonyong Lee, and Li Wang. Integrated biomethane liquefaction using exergy from the discharging end of a liquid air energy storage system. *Applied Energy*, 260:114260, 2020.

[223] Evan P Sheehan. *Development of a High-Effectiveness Cryogenic Stacked Slotted Plate Heat Exchanger*. The University of Wisconsin-Madison, 2019.

[224] Turgut M Gür. Review of electrical energy storage technologies, materials and systems: challenges and prospects for large-scale grid storage. *Energy & Environmental Science*, 11(10):2696–2767, 2018.

[225] Helder Lopes Ferreira, Raquel Garde, Gianluca Fulli, Wil Kling, and Joao Pecas Lopes. Characterisation of electrical energy storage technologies. *Energy*, 53:288–298, 2013.

[226] Gaurav Vyas and Raja Sekhar Dondapati. Superconducting magnetic energy storage (smes). In *High-Temperature Superconducting Devices for Energy Applications*, pages 85–140. CRC Press, 2020.

[227] Md Tasbirul Islam, Nazmul Huda, AB Abdullah, and R Saidur. A comprehensive review of state-of-the-art concentrating solar power (csp) technologies: Current status and research trends. *Renewable and Sustainable Energy Reviews*, 91:987–1018, 2018.

[228] RP Merchán, MJ Santos, A Medina, and A Calvo Hernández. High temperature central tower plants for concentrated solar power: 2021 overview. *Renewable and Sustainable Energy Reviews*, page 111828, 2021.

[229] Amita Ummadisingu and MS Soni. Concentrating solar power–technology, potential and policy in india. *Renewable and sustainable energy reviews*, 15(9):5169–5175, 2011.

[230] Sarada Kuravi, Jamie Trahan, D Yogi Goswami, Muhammad M Rahman, and Elias K Stefanakos. Thermal energy storage technologies and systems for concentrating solar power plants. *Progress in Energy and Combustion Science*, 39(4):285–319, 2013.

[231] AZ Hafez, AM Attia, HS Eltwab, AO ElKousy, AA Afifi, AG AbdElhamid, AN AbdElqader, SE K Fateen, KA El-Metwally, A Soliman, et al. Design analysis of solar parabolic trough thermal collectors. *Renewable and Sustainable Energy Reviews*, 82:1215–1260, 2018.

[232] Rohan Dutta and Pavitra Sandilya. Improvement potential of cryogenic energy storage systems by process modifications and heat integration. *Energy*, 221:119841, 2021.

[233] Alessio Tafone, Alessandro Romagnoli, Yongliang Li, Emiliano Borri, and Gabriele Comodi. Techno-economic analysis of a liquid air energy storage (laes) for cooling application in hot climates. *Energy Procedia*, 105:4450–4457, 2017.

[234] Agencia Nacional de Energia Elétrica (ANEEL). Cálculo tarifário e metodologias. https://www.aneel.gov.br/calculo-tarifario-e-metodologia/, 2016. [Accessed: 22-06-2021].

[235] Rodrigo Corrêa da Silva, Ismael de Marchi Neto, and Stephan Silva Seifert. Electricity supply security and the future role of renewable energy sources in brazil. *Renewable and Sustainable Energy Reviews*, 59:328–341, 2016.

Appendix

APPENDIX A – Thermodynamic properties.

Table A.1 – Thermodynamics properties and parameters for charging regime.

No	$\dot{m}$	T	P	v	h	s	u	e_x	x
	(kg/s)	(K)	(MPa)	(m^3/kg)	(kJ/kg)	(kJ/kgK)	(kJ/Kg)	(kJ/Kg)	-
1	6.0	298.15	0.1	0.8440	298.2	6.858	212.8	0.00	
2	6.0	298.15	5.0	0.0169	287.5	5.707	202.9	332.47	
3	6.0	221.10	5.0	0.0118	200.6	5.369	141.7	346.35	
4	2.4	221.10	5.0	0.0118	200.6	5.369	141.7	346.35	
5	2.4	174.70	5.0	0.0081	139.4	5.056	98.9	378.47	
6	2.4	120.20	5.0	0.0015	-37.9	3.808	-45.5	574.53	
7	2.4	80.12	0.1	0.0944	-37.9	4.078	-47.9	492.20	0.4292
8	1.5	81.75	0.1	0.2225	78.7	5.538	56.2	174.06	
9	1.5	118.60	0.1	0.3317	117.3	5.928	83.63	96.40	
10	5.1	144.50	0.1	0.4065	143.6	6.129	102.4	62.83	
11	5.1	196.30	0.1	0.5546	195.9	6.438	139.7	22.92	
12	5.1	288.10	0.1	0.8158	288.3	6.824	205.5	0.24	
13	3.6	221.10	5.0	0.0118	200.6	5.369	141.7	346.35	
14	3.6	136.70	1.0	0.0359	126.4	5.369	90.5	272.15	
15	3.6	298.15	1.0	0.0853	298.4	6.202	211.0	195.79	
16	3.6	155.35	0.1	0.4377	154.6	6.202	110.3	51.98	
17	0.1	78.95	0.1	0.0011	-126.1	2.978	-126.2	732.52	
18	0.1	83.55	20.0	0.2223	-103.3	2.982	56.2	754.13	
19	0.1	130.10	20.0	0.0014	-17.6	3.796	-45.7	597.14	
20	0.1	170.20	20.0	0.0019	60.5	4.319	22.7	519.30	
21	0.1	210.15	20.0	0.0027	135.4	4.716	82.2	475.84	
22	0.1	290.00	20.0	0.0043	252.9	5.193	167.8	451.12	
23	0.1	400.00	20.0	0.0062	385.6	5.583	261.9	467.54	
24	0.1	368.10	15.0	0.0073	352.2	5.583	242.0	434.14	
25	0.1	400.00	15.0	0.0080	388.3	5.677	267.6	442.21	
26	0.1	355.45	10.0	0.0104	342.9	5.677	238.9	396.82	
27	0.1	400.00	10.0	0.0118	391.8	5.807	273.6	406.96	
28	0.1	327.10	5.0	0.0188	318.8	5.807	225.0	333.96	
29	0.1	400.00	5.0	0.0232	396.1	6.020	279.9	347.75	
30	0.1	129.75	0.1	0.3642	128.7	6.020	91.8	80.35	
31	0.1	285.8	0.1	0.8093	285.9	6.816	203.9	0.27	

Table A.2 – Thermodynamics properties and parameters for discharging regime.

No	$\dot{m}$ (kg/s)	T (K)	P (MPa)	v (m^3/kg)	h (kJ/kg)	s (kJ/kgK)	u (kJ/Kg)	e_x (kJ/Kg)	x -
1	0.4	298.15	0.1	0.8440	298.2	6.858	212.8	0.00	
2	0.4	298.15	5.0	0.0169	287.5	5.707	202.9	332.47	
3	0.4	220.70	5.0	0.0118	200.2	5.367	141.4	346.54	
4	0.2	220.70	5.0	0.0118	200.2	5.367	141.4	346.54	
5	0.2	170.20	5.0	0.0077	132.3	5.015	94.0	383.59	
6	0.2	128.10	5.0	0.0017	-16.8	3.978	-25.3	543.80	
7	0.2	80.41	0.1	0.1191	-16.8	4.344	-28.9	434.74	0.5334
8	0.1	81.75	0.1	0.2022	78.7	5.538	39.7	174.10	
9	0.1	118.60	0.1	0.3317	117.3	5.928	83.67	96.40	
10	0.3	143.10	0.1	0.4024	142.2	6.119	101.4	64.40	
11	0.3	196.30	0.1	0.5548	195.9	6.438	139.7	22.92	
12	0.3	288.00	0.1	0.8157	288.2	6.824	205.5	0.14	
13	0.2	220.70	5.0	0.0118	200.2	5.367	141.4	346.54	
14	0.2	136.45	1.0	0.0358	126.2	5.367	90.4	272.54	
15	0.2	298.15	1.0	0.0859	298.4	6.202	212.5	195.79	
16	0.2	155.35	0.1	0.4377	154.6	6.202	110.3	51.99	
17	3.5	78.95	0.1	0.0011	-126.1	2.978	-126.2	732.52	
18	3.5	83.55	20.0	0.2223	-103.3	2.982	56.2	754.13	
19	3.5	85.00	20.0	0.0011	-100.8	3.012	-123.2	747.68	
22	3.5	298.15	20.0	0.0044	263.4	5.229	175.3	450.89	
23	3.5	400.00	20.0	0.0062	385.6	5.583	261.9	467.54	
24	3.5	368.05	15.0	0.0073	352.2	5.583	242.0	434.14	
25	3.5	400.00	15.0	0.0080	388.3	5.677	267.6	442.21	
26	3.5	355.45	10.0	0.0104	342.9	5.677	238.9	396.82	
27	3.5	400.00	10.0	0.0118	391.8	5.807	273.6	406.96	
28	3.5	327.05	5.0	0.0188	318.8	5.807	225.0	333.96	
29	3.5	400.00	5.0	0.0232	396.1	6.020	279.9	347.75	
30	3.5	129.85	0.1	0.3642	128.7	6.020	91.8	80.35	
31	3.5	285.8	0.1	0.8093	285.9	6.816	203.9	0.27	

APPENDIX B – Summary of modeling equations.

Table B.1 – Mass, energy and exergy balance equations for modeling and optimization.

Component	Mass balance equations	Energy balance equations	Exergy balance equations
Compressor	$\dot{m}_1 = \dot{m}_2$	$-\dot{W}_c = \frac{\dot{m}_c[T_1(s_1-s_2)-(h_1-h_2)]}{\eta_c}$	$\dot{E}_{xD} = \dot{W}_c - \dot{m}_2(e_{x2}-e_{x1}) - \left(1-\frac{T_0}{T_i}\right)\dot{Q}_C$
Heat exchanger 1	$\dot{m}_2 = \dot{m}_3, \dot{m}_{11} = \dot{m}_{12}, \dot{m}_{20} = \dot{m}_{21}$	$\dot{m}_h(h_{h,i}-h_{h,o}) = \dot{m}_{in}(h_{in,o}-h_{in,i})$ $+\dot{m}_c(h_{c,o}-h_{c,i}) - \dot{Q}_{0,1}$	$(1-\varepsilon_1)\left(\frac{T_0}{T_m}-1\right)\dot{Q}_{a,1} - \dot{E}_{xD} = \dot{m}_{in}[(h_{12}-h_{11}) - T_0(s_{12}-s_{11})]$ $+\dot{m}_h[(h_3-h_2) - T_0(s_3-s_2)] - \dot{m}_c[(h_{21}-h_{20}) - T_0(s_{21}-s_{20})]$
Heat exchanger 2	$\dot{m}_4 = \dot{m}_5, \dot{m}_{10} = \dot{m}_{11}, \dot{m}_{19} = \dot{m}_{20}$	$\dot{m}_h(h_{h,i}-h_{h,o}) = \dot{m}_{in}(h_{in,o}-h_{in,i})$ $+\dot{m}_c(h_{c,o}-h_{c,i}) - \dot{Q}_{0,2}$	$(1-\varepsilon_2)\left(\frac{T_0}{T_m}-1\right)\dot{Q}_{a,2} - \dot{E}_{xD} = \dot{m}_{in}[(h_{11}-h_{10}) - T_0(s_{11}-s_{10})]$ $+\dot{m}_h[(h_5-h_4) - T_0(s_5-s_4)] - \dot{m}_c[(h_{20}-h_{19}) - T_0(s_{20}-s_{19})]$
Heat exchanger 3	$\dot{m}_5 = \dot{m}_6, \dot{m}_8 = \dot{m}_9, \dot{m}_{18} = \dot{m}_{19}$	$\dot{m}_h(h_{h,i}-h_{h,o}) = \dot{m}_{in}(h_{in,o}-h_{in,i})$ $+\dot{m}_c(h_{c,o}-h_{c,i}) - \dot{Q}_{0,3}$	$(1-\varepsilon_3)\left(\frac{T_0}{T_m}-1\right)\dot{Q}_{a,3} - \dot{E}_{xD} = \dot{m}_{in}[(h_9-h_8) - T_0(s_9-s_8)]$ $+\dot{m}_h[(h_6-h_5) - T_0(s_6-s_5)] - \dot{m}_c[(h_{19}-h_{18}) - T_0(s_{19}-s_{18})]$
Turbine 1	$\dot{m}_{13} = \dot{m}_{14} = \dot{m}_{15} = \dot{m}_{16}$	$\dot{W}_{t1} = \dot{m}_{13}[(h_{13}-h_{14s}) + (h_{15}-h_{16s})]\eta_t$	$\dot{E}_{xD} = \dot{m}_{13}[(e_{x13}-e_{x14}) + (e_{x15}-e_{x16})] - \dot{W}_{t1}$
Turbine 2	$\dot{m}_6 = \dot{m}_7$	$\dot{W}_{t2} = \dot{m}_6[(h_6-h_{7s})]\eta_t$	$\dot{E}_{xD} = \dot{m}_6[(e_{x6}-e_{x7})] - \dot{W}_{t2}$
Turbine 3	$\dot{m}_{23} = ... = \dot{m}_{30}$	$\dot{W}_{t3} = \dot{m}_{23}[(h_{23}-h_{24s}) + (h_{25}-h_{26s})$ $+(h_{27}-h_{28s}) + (h_{29}-h_{30s})]\eta_t$	$\dot{E}_{xD} = \dot{m}_{23}[(e_{x23}-e_{x24}) + (e_{x25}-e_{x26}) + (e_{x27}-e_{x28})$ $+(e_{x29}-e_{x30})] - \dot{W}_{t2}$
Expansion valve	$\dot{m}_6 = \dot{m}_7$	$h_6 = h_7$	$-\dot{E}_{xD} = (1-\alpha)\dot{m}_c[(u_7-u_6) + (p_7\upsilon_7 - p_6\upsilon_6) - T_0(s_7-s_6)]$
Cryogenic tank	$\frac{dm}{dt} = [(1-\alpha)y\dot{m}_c - \dot{m}_p](1-\rho_g\upsilon_l)$	$\frac{dU}{dt} = [(1-\alpha)y\dot{m}_c - \dot{m}_p]u_l - (1-\alpha)\dot{m}_c u_g\gamma$	$\frac{dEx}{dt} = [(1-\alpha)y\dot{m}_c - \dot{m}_p](e_{xl} - \rho_g\upsilon_l e_{xg})$
Cryogenic pump	$\dot{m}_{17} = \dot{m}_{18}$	$\dot{W}_p = \frac{\dot{m}_p(h_{18}-h_{17})}{\eta_p}$	$\dot{E}_{xD} = \dot{W}_p + \dot{m}_p(e_{x17}-e_{x18})$
Evaporator	$\dot{m}_{21} = \dot{m}_{22} = \dot{m}_{30} = \dot{m}_{31}$	$\dot{Q}_E = \dot{m}_p[(h_{22}-h_{21}) + (h_{31}-h_{30})]$	$\dot{E}_{xD} = T_0\left[\dot{m}_p[(s_{22}-s_{21}) + (s_{31}-s_{30})] - \frac{\dot{Q}_E}{T_w}\right]$
Heater 1	$\dot{m}_{22} = \dot{m}_{23}$	$\dot{Q}_{H1} = \dot{m}_{22}(h_{23}-h_{22})$	$\dot{E}_{xD} = \dot{Q}_{H1}\left(1-\frac{T_0}{T_{23}}\right) + \dot{m}_{22}(e_{x22}-e_{x23})$
Heater 2	$\dot{m}_{24} = \dot{m}_{25}$	$\dot{Q}_{H2} = \dot{m}_{24}(h_{25}-h_{24})$	$\dot{E}_{xD} = \dot{Q}_{H2}\left(1-\frac{T_0}{T_{25}}\right) + \dot{m}_{24}(e_{x24}-e_{x25})$
Heater 3	$\dot{m}_{26} = \dot{m}_{27}$	$\dot{Q}_{H3} = \dot{m}_{26}(h_{27}-h_{26})$	$\dot{E}_{xD} = \dot{Q}_{H3}\left(1-\frac{T_0}{T_{27}}\right) + \dot{m}_{26}(e_{x26}-e_{x27})$
Heater 4	$\dot{m}_{28} = \dot{m}_{29}$	$\dot{Q}_{H4} = \dot{m}_{28}(h_{29}-h_{28})$	$\dot{E}_{xD} = \dot{Q}_{H4}\left(1-\frac{T_0}{T_{29}}\right) + \dot{m}_{28}(e_{x28}-e_{x29})$
Heater 5	$\dot{m}_{14} = \dot{m}_{15}$	$\dot{Q}_{H5} = \dot{m}_{14}(h_{15}-h_{14})$	$\dot{E}_{xD} = \dot{Q}_{H5}\left(\frac{T_0}{T_m}-1\right) + \dot{m}_{14}(e_{x14}-e_{x15})$

APPENDIX C – Exergy performance results for the components.

Table C.1 – Exergy performance results for CES system components for charging regime.

Components	$\dot{E}_{xF}$ (kW)	$\dot{E}_{xP}$ (kW)	$\dot{E}_{xD}$ (kW)	$y^*_{D,k}$ (%)	$y_{D,k}$ (%)	η_{exe} (%)
Compressor	2292.90	1994.82	298.08	42.05	5.0178	87.00
Heat exchanger 1	1134.22	1081.53	52.69	7.43	0.8870	95.35
Heat exchanger 2	402.37	375.04	27.33	3.86	0.4601	93.21
Heat exchanger 3	796.13	752.85	43.28	6.11	0.7286	94.56
Turbine 1	784.8	706.32	78.48	11.07	1.3211	90.00
Turbine 3	41.92	37.73	4.19	0.59	0.0705	90.00
Expansion valve	200.32	5.36	194.96	27.51	3.2819	2.68
Cryogenic pump	2.92	2.16	0.76	0.11	0.0128	73.97
Evaporator	2.47	2.26	0.21	0.03	0.0035	91.50
Heater 1	3.38	1.64	1.74	0.25	0.0293	48.52
Heater 2	0.92	0.81	0.11	0.02	0.0019	88.04
Heater 3	1.25	1.01	0.24	0.03	0.0040	80.80
Heater 4	1.97	1.38	0.59	0.08	0.0099	70.05
Heater 5	274.89	268.74	6.15	0.87	0.1035	97.76
Total	5940.46	5231.65	708.81	100.00	11.9319	88.07

Table C.2 – Exergy performance results for CES system components for discharging regime.

Components	$\dot{E}_{xF}$ (kW)	$\dot{E}_{xP}$ (kW)	$\dot{E}_{xD}$ (kW)	$y^*_{D,k}$ (%)	$y_{D,k}$ (%)	η_{exe} (%)
Compressor	152.86	132.99	19.87	2.99	0.6043	87.00
Heat exchanger 1	76.02	73.51	2.51	0.38	0.0763	96.70
Heat exchanger 2	27.43	26.83	0.6	0.09	0.0182	97.81
Heat exchanger 3	81.27	68.77	12.5	1.88	0.3802	84.62
Turbine 1	52.27	47.04	5.23	0.79	0.1591	89.99
Turbine 3	1467.20	1320.48	146.72	22.10	4.4621	90.00
Expansion valve	18.00	0.57	17.43	2.63	0.5301	3.17
Cryogenic pump	102.31	53.07	49.24	7.42	1.4975	51.87
Evaporator	1038.79	714.00	324.79	48.92	9.8777	68.73
Heater 1	108.90	58.29	50.61	7.62	1.5392	53.53
Heater 2	32.17	28.26	3.91	0.59	0.1189	87.85
Heater 3	43.58	35.49	8.09	1.22	0.2460	81.44
Heater 4	68.89	48.28	20.61	3.10	0.6268	70.08
Heater 5	18.42	16.56	1.86	0.28	0.0566	89.90
Total	3288.11	2624.14	663.97	100.00	20.1931	79.81

Table C.3 – Exergy performance results for CES system components in operating mode A for charging regime.

Components	$\dot{E}_{xF}$ (kW)	$\dot{E}_{xP}$ (kW)	$\dot{E}_{xD}$ (kW)	$y^*_{D,k}$ (%)	$y_{D,k}$ (%)	η_{exe} (%)
Compressor	2292.90	1994.82	298.08	56.25	5.1782	87.00
Heat exchanger 1	1134.22	1081.53	52.69	9.94	0.9153	95.35
Heat exchanger 2	402.37	375.04	27.33	5.16	0.4748	93.21
Heat exchanger 3	796.13	752.85	43.28	8.17	0.7519	94.56
Turbine 1	784.8	706.32	78.48	14.81	1.3633	90.00
Turbine 2	71.13	47.23	23.9	4.51	0.4152	66.40
Heater 5	274.89	268.74	6.15	1.16	0.1068	97.76
Total	5756.44	5226.53	529.91	100.00	9.2055	90.79

Table C.4 – Exergy performance results for CES system components in operating mode A for discharging regime.

Components	$\dot{E}_{xF}$ (kW)	$\dot{E}_{xP}$ (kW)	$\dot{E}_{xD}$ (kW)	$y^*_{D,k}$ (%)	$y_{D,k}$ (%)	η_{exe} (%)
Turbine 3	1467.20	1320.48	146.72	24.29	5.1268	90.00
Cryogenic pump	102.31	53.07	49.24	8.15	1.7206	51.87
Evaporator	1038.79	714.00	324.79	53.78	11.3490	68.73
Heater 1	108.90	58.29	50.61	8.38	1.7684	53.53
Heater 2	32.17	28.26	3.91	0.65	0.1366	87.85
Heater 3	43.58	35.49	8.09	1.34	0.2827	81.44
Heater 4	68.89	48.28	20.61	3.41	0.7202	70.08
Total	2861.84	2257.87	603.97	100.00	21.1043	78.90

Table C.5 – Exergy performance results for CES system components in operating mode B for charging regime.

Components	$\dot{E}_{xF}$ (kW)	$\dot{E}_{xP}$ (kW)	$\dot{E}_{xD}$ (kW)	$y^*_{D,k}$ (%)	$y_{D,k}$ (%)	η_{exe} (%)
Compressor	2292.90	1994.82	298.08	55.43	5.1293	87.00
Heat exchanger 1	1134.22	1081.53	52.69	9.80	0.9067	95.35
Heat exchanger 2	402.37	375.04	27.33	5.08	0.4703	93.21
Heat exchanger 3	796.13	752.85	43.28	8.05	0.7448	94.56
Turbine 1	784.8	706.32	78.48	14.59	1.3505	90.00
Turbine 2	71.13	47.23	23.90	4.44	0.4113	66.40
Turbine 3	41.92	37.73	4.19	0.78	0.0721	90.00
Cryogenic pump	2.92	2.16	0.76	0.14	0.0131	73.97
Evaporator	2.47	2.26	0.21	0.04	0.0036	91.50
Heater 1	3.38	1.64	1.74	0.32	0.0299	48.52
Heater 2	0.92	0.81	0.11	0.02	0.0019	88.04
Heater 3	1.25	1.01	0.24	0.04	0.0041	80.80
Heater 4	1.97	1.38	0.59	0.11	0.0102	70.05
Heater 5	274.89	268.74	6.15	1.14	0.1058	97.76
Total	5811.27	5273.52	537.75	100.00	9.2536	90.75

Table C.6 – Exergy performance results for CES system components in operating mode B for discharging regime.

Components	$\dot{E}_{xF}$ (kW)	$\dot{E}_{xP}$ (kW)	$\dot{E}_{xD}$ (kW)	$y^*_{D,k}$ (%)	$y_{D,k}$ (%)	η_{exe} (%)
Compressor	152.86	132.99	19.87	3.06	0.6065	87.00
Heat exchanger 1	76.02	73.51	2.51	0.39	0.0766	96.70
Heat exchanger 2	27.43	26.83	0.6	0.09	0.0183	97.81
Heat exchanger 3	81.27	68.77	12.5	1.93	0.3816	84.62
Turbine 1	52.27	47.04	5.23	0.81	0.1596	89.99
Turbine 2	5.92	3.94	1.98	0.31	0.0604	66.55
Turbine 3	1467.20	1320.48	146.72	22.62	4.4786	90.00
Cryogenic pump	102.31	53.07	49.24	7.59	1.5030	51.87
Evaporator	1038.79	714.00	324.79	50.08	9.9141	68.73
Heater 1	108.90	58.29	50.61	7.80	1.5449	53.53
Heater 2	32.17	28.26	3.91	0.60	0.1194	87.85
Heater 3	43.58	35.49	8.09	1.25	0.2469	81.44
Heater 4	68.89	48.28	20.61	3.18	0.6291	70.08
Heater 5	18.42	16.56	1.86	0.29	0.0568	89.90
Total	3276.03	2627.51	648.52	100.00	19.7959	80.20

Table C.7 – Exergy performance results for CES system components in operating mode C for charging regime.

Components	$\dot{E}_{xF}$ (kW)	$\dot{E}_{xP}$ (kW)	$\dot{E}_{xD}$ (kW)	$y^*_{D,k}$ (%)	$y_{D,k}$ (%)	η_{exe} (%)
Compressor	2292.90	1994.82	298.08	55.43	5.1293	87.00
Heat exchanger 1	1134.22	1081.53	52.69	9.80	0.9067	95.35
Heat exchanger 2	402.37	375.04	27.33	5.08	0.4703	93.21
Heat exchanger 3	796.13	752.85	43.28	8.05	0.7448	94.56
Turbine 1	784.8	706.32	78.48	14.59	1.3505	90.00
Turbine 2	71.13	47.23	23.90	4.44	0.4113	66.40
Turbine 3	41.92	37.73	4.19	0.78	0.0721	90.00
Cryogenic pump	2.92	2.16	0.76	0.14	0.0131	73.97
Evaporator	2.47	2.26	0.21	0.04	0.0036	91.50
Heater 1	3.38	1.64	1.74	0.32	0.0299	48.52
Heater 2	0.92	0.81	0.11	0.02	0.0019	88.04
Heater 3	1.25	1.01	0.24	0.04	0.0041	80.80
Heater 4	1.97	1.38	0.59	0.11	0.0102	70.05
Heater 5	274.89	268.74	6.15	1.14	0.1058	97.76
Total	5811.27	5273.52	537.75	100.00	9.2536	90.75

Table C.8 – Exergy performance results for CES system components in operating mode C for discharging regime.

Components	$\dot{E}_{xF}$ (kW)	$\dot{E}_{xP}$ (kW)	$\dot{E}_{xD}$ (kW)	$y^*_{D,k}$ (%)	$y_{D,k}$ (%)	η_{exe} (%)
Turbine 3	1467.20	1320.48	146.72	24.29	5.1268	90.00
Cryogenic pump	102.31	53.07	49.24	8.15	1.7206	51.87
Evaporator	1038.79	714.00	324.79	53.78	11.3490	68.73
Heater 1	108.90	58.29	50.61	8.38	1.7684	53.53
Heater 2	32.17	28.26	3.91	0.65	0.1366	87.85
Heater 3	43.58	35.49	8.09	1.34	0.2827	81.44
Heater 4	68.89	48.28	20.61	3.41	0.7202	70.08
Total	2861.84	2257.87	603.97	100.00	21.1043	78.90

APPENDIX D – Optimization results.

Table D.1 – Optimization results for charging regime for different capacities of the cryogenic tank.

Parameter	50 t			100 t			150 t			200 t		
	A	B	C	A	B	C	A	B	C	A	B	C
Specific liquid yield (y), kg_L/kg_a	0.341	0.404	0.404	0.343	0.409	0.409	0.345	0.411	0.411	0.347	0.412	0.412
Diverted air mass fraction (α)	0.643	0.664	0.661	0.644	0.667	0.665	0.646	0.671	0.668	0.651	0.678	0.670
Specific exergy consumption (e_N), kWh/kg_L	0.579	0.486	0.481	0.577	0.482	0.479	0.576	0.478	0.474	0.575	0.477	0.472
Air reheating temperature (T_r), K	-	597.7	598.6	-	598.4	599.1	-	599.6	598.5	-	598.2	599.8
Exergy utilization factor (E_xUF), %	-	57.12	57.89	-	57.68	58.32	-	57.96	58.91	-	58.09	59.42
Net electrical exergy consumed, MWh	46.48	36.48	38.80	87.01	78.69	80.13	134.12	112.57	111.43	172.43	142.75	143.65
Net exergy consumed (cogeneration), MWh	37.46	42.99	39.91	68.66	66.91	63.80	124.73	117.03	109.91	185.03	169.63	159.93

Table D.2 – Optimization results for discharging regime for different capacities of the cryogenic tank.

Parameter	50 t			100 t			150 t			200 t		
	A	B	C	A	B	C	A	B	C	A	B	C
Exergy density (E_D), kWh/m^3	133.2	127.4	133.2	133.6	128.3	133.6	134.02	128.87	134.02	134.3	129.34	134.3
Air reheating temperature (T_r), K	598.6	598.8	599.6	596.5	597.5	598.2	599.1	598.4	599.6	597.9	598.8	599.2
Exergy utilization factor (E_xUF), %	88.23	85.14	88.23	88.78	85.56	88.78	89.01	85.92	89.01	89.21	86.10	89.21
Net electrical exergy generated, MWh	7.93	8.11	8.89	15.21	17.88	18.64	23.86	25.97	26.31	31.28	33.42	34.29
Net exergy generated (cogeneration), MWh	12.85	16.83	17.12	23.97	26.69	27.46	44.23	46.94	47.58	66.37	68.41	69.84
Round-trip efficiency (electrical), %	17.06	22.23	22.91	17.48	22.72	23.26	17.79	23.07	23.61	18.14	23.41	23.87
Round-trip efficiency (cogeneration), %	34.3	39.14	42.89	34.91	39.89	43.04	35.46	40.11	43.29	35.87	40.33	43.67